FUNCTIONAL CONSEQUENCES OF TOP-DOWN ANTICIPATORY MODULATION OF PRIMARY VISUAL CORTEX

by

Craig G. Richter

A Dissertation Submitted to the Faculty of

The Charles E. Schmidt College of Science

in Partial Fulfillment of the Requirements for the Degree of

Doctor of Philosophy

Florida Atlantic University

Boca Raton, Florida

December 2009

FUNCTIONAL CONSEQUENCES OF TOP-DOWN ANTICIPATORY MODULATION OF PRIMARY VISUAL CORTEX

by

Craig G. Richter

This dissertation was prepared under the direction of the candidate's dissertation advisor, Dr. Steven L. Bressler, Program in Complex Systems and Brain Sciences, and has been approved by the members of his supervisory committee. It was submitted to the faculty of the Charles E. Schmidt College of Science and was accepted in partial fulfillment of the requirements for the degree of Doctor of Philosophy.

SUPERVISORY COMMITTEE:

Steven L. Bressler, Ph.D.
Dissertation Advisor

Mingzhou Ding, Ph.D.

Howard S. Hock, Ph.D.

Viktor K. Jirsa, Ph.D.

J. A. Scott Kelso, Ph.D.

Janet Blanks, Ph.D.
Director, Program in Complex Systems and Brain Sciences

Gary W. Perry, Ph.D.
Dean, The Charles E. Schmidt College of Science

Barry T. Rosson, Ph.D.
Dean, Graduate College

November 10, 2009
Date

ACKNOWLEDGEMENTS

Firstly, I would like to thank my advisor Dr. Steven Bressler for his tremendous mentorship. Many years ago we embarked on what turned out to be an a fascinating and fruitful scientific adventure. During this time I gained the abilities required by a scientist, and also found a dear friend. Thank you Steve. I would also like to thank the members of my committee: Dr. Mingzhou Ding, Dr. Howard Hock, Dr. Viktor Jirsa and Dr. Scott Kelso, for their dedication and their wisdom and to thank all of the faculty and students of the Center for Complex Systems and Brain Sciences for their friendship and knowledge, and our administrative staff for making it all possible.

Finally, I'd like to thank my friends and family for their unwavering support.

ABSTRACT

Author:	Craig G. Richter
Title:	Functional Consequences of Top-down Anticipatory Modulation of Primary Visual Cortex
Institution:	Florida Atlantic University
Dissertation Advisor:	Dr. Steven L. Bressler
Degree:	Doctor of Philosophy
Year:	2009

It is well established that anticipation of the arrival of an expected stimulus is accompanied by rich ongoing oscillatory neurodynamics, which span and link large areas of cortex. An intriguing possibility is that these dynamic interactions may convey knowledge that is embodied by large-scale neurocognitive networks from higher level regions of multi-model cortex to lower level primary sensory areas. In the current study, using autoregressive spectral analysis, we establish that during the anticipatory phase of a visual discrimination task there are rich patterns of coherent interaction between various levels of the ventral visual hierarchy across the frequency spectrum of 8 - 90 Hz. Using spectral Granger causality we determined that a subset of these interactions carry beta frequency (14 - 30 Hz) top-down influences from higher level visual regions V4 and TEO to primary visual cortex. We investigated the functional significance of these top-down interactions by correlating the magnitude of the anticipatory signals with the amplitude of the visual evoked potential that was elicited by stimulus processing. We found that in one third of the extrastriate-striate pairs, tested in three monkeys, the amplitude of the visual evoked response is well predicted by the magnitude of pre-stimulus coherent

top-down anticipatory influences. To investigate the dynamics of the coherent and top-down Granger causal interactions we analyzed the relationship between coherence and top-down Granger causality with stimulus onset asynchrony. This analysis revealed that in an abundance of cases the magnitudes of the coherent interactions and top-down directional influences scaled with the length of time that had elapsed before stimulus onset. Together these results reveal a complex network of coherent and top-down directional interactions that predict the amplitude of early components of the visual evoked potential in primary visual cortex and vary in strength on the basis of the length of the stimulus onset.

FUNCTIONAL CONSEQUENCES OF TOP-DOWN ANTICIPATORY MODULATION OF PRIMARY VISUAL CORTEX

LIST OF TABLES

LIST OF FIGURES

CHAPTER 1

INTRODUCTION

"Dans les champs de l'observation le hasard ne favorise que les esprits préparés."
"In the field of observation chance favors the prepared mind."

- Louis Pasteur

This quote by Pasteur regards the practice of scientific observation, but the sentiment is equally pertinent to all manners of observation. As Pasteur indicates, chance pervades all acts of observation. Events rarely occur exactly as expected. They most often unfold in a probabilistic fashion and thus according to chance. So then what comprises the *prepared mind*? As implied by the quotation, this must be a system which can anticipate probabilistic occurrences, and recognize novel events. Such an ability conveys a survival advantage to organisms that is in proportion to their capacity to forecast events and identify unforeseen circumstances; thus there is strong evolutionary pressure for enhancement of the skill of prediction.

At the psychological level, prediction, anticipation, and expectancy are modes of top-down processing. Exactly how this activity is implemented neurobiologically remains an outstanding question in cognitive neuroscience, but it is believed to involve the top-down modulation of activity in lower level sensory regions by high level transmodal networks that integrate multimodal sensory input, memory, executive activity, attention, motivation

and emotion. The recognition that top-down neuronal modulation is a critical determinant of cortical function has dramatically increased over the last decade, fueled by increased experimental investigation of top-down activity, the construction of theoretical models of large-scale brain function that are critically dependent on feedback processing (Lee and Mumford, 2003; Mumford, 1992; Ullman, 1995), and the development of a new breed of computational models that capitalize on the increased computational power provided by the inclusion of feedback and recurrent processing (Deco and Rolls, 2005; Spratling, 2002). This advancement is paralleled by work in philosophy and cognitive science where the realization that the brain is not a passive stimulus-driven system, but rather actively interacts with the body and environment in a goal-oriented and adaptive fashion, has called for re-conceptualization of the brain as embodied and situated (Varela et al., 1993). This view posits an intimate relationship between cognition and action in two critical ways: (1) that perception always occurs within the context of action, and (2) that the act of perception itself is akin to action. Just as tactile perceptual acts involve the manipulation of objects, visual perception also involves active processes that manipulate visual input so as to arrive at a coherent interpretation of sensory input (Noë, 2004). William James anticipated this sentiment by the year 1890, when he wrote:

> The highest and most elaborated mental products are filtered from the data chosen by the faculty next beneath, out of the mass offered by the faculty below that, which mass in turn was sifted from a still larger amount of yet simpler material, and so on. The mind, in short, works on the data it receives very much as a sculptor works on his block of stone. In a sense the statue stood there from eternity. But there were a thousand different ones beside it, and the sculptor alone is to thank for having extricated this one from the rest (James, 1950, p. 288).

James choice of the words: choosing, filtering and sifting, is particularly telling. They

portray an active and constructive search for meaning. Here we see a conceptualization of perception where perceptual processes are active, and in this sense akin to a process of sculpting. In James' view, each successive level in the perceptual hierarchy actively selects from the perceptual products offered by the subordinate level. This view lay dormant for nearly a century while thinking in psychology and neuroscience was largely dominated by reflex theory; a theory which was largely based on the work of Pavlov and Sherrington. Reflex theory, and the many contemporary theories that it has inspired, views hierarchical processing as a passive stimulus-driven feedforward system. In such a scheme higher-level regions in the hierarchy perform rote operations upon inputs from lower levels in a reflex arc from stimulus to response. This forms a serial feedforward chain, which does not require feedback from higher to lower levels (Bressler, 1995). Unlike the constructive process of sculpting, this process is analogous to a cascade of toppling dominoes. According to James, the perceptual act is not a division of labor where each successive processing level performs its function and passes the results to the next level like an assembly line. In his view higher levels must actively engage lower levels and in this way sculpt the perceptual product. Such a view may put too much emphasis on higher-level cortical regions and risk taking 'a loan on intelligence' (Dennett, 1971), but it functions as a healthy alternative view to that of pure serial feedforward processing. Indeed, based on these considerations, a more moderate view is now emerging that posits that sensory percepts are actively constructed via the dynamic interplay of sensory stimulation with task specific brain states (Gilbert and Sigman, 2007). These states comprise contextually specific intrinsic cortical and sub-cortical dynamics that are rich in knowledge - anticipating and predicting future states of the environment in an online fashion (Engel et al., 2001). States of anticipation, such as these, require modification of the activity of more peripheral sensory regions so that stimulus energy is dealt with in the most adaptive manner. Thus states of knowledge in the brain may exert top-down influences on lower level

sensory structures and modify the behavior of the lower level structural elements. This has even been shown to occur at the level of single neurons in V1 (Li et al., 2004), where a change in task without modification of the visual stimulus resulted in a dramatic change in the response of single V1 neurons. This result demonstrates that even single neurons in the early visual system are not dedicated processors with static input output relationships, but rather that they are dynamic information processors that are highly sensitive to contextual modulation via their interaction with other neurons. Thus despite identical input to the brain, a single neuron may respond in a dramatically different way due to the contextual modulation it receives via its interactions as a component of the large-scale network that is the brain. Such a result demands the significant rethinking of how neurons and networks function that is currently afoot.

The goal of this dissertation is to examine the neural dynamics between higher and lower level visual regions during a period when the organism is anticipating the impending events of a visual discrimination task; to quantify interdependent states of coordination between distributed cortical areas, identifying patterns of top-down constraint; and to demonstrate the functional consequences of this constraint on subsequent stimulus processing.

CHAPTER 2

BRAIN STATES, CORTICAL COORDINATION AND NEUROCOGNITIVE NETWORKS

The term *brain state* may be misleading in that it might invoke a conception of a static, unchanging and rigid structure; whereas here it is intended to portray a state of coordination between neuronal populations of the brain. States of coordination are consistent spatio-temporal patterns of interaction that are exhibited by transiently interdependent brain areas. They are dynamic, evolving with task and behavior by establishing new interactions between previously uninvolved areas, while current couplings may weaken and dissipate (Bressler and Kelso, 2001; Kelso, 1995). Thus, in this context, a brain state is a coordinated entity that consists of elements adaptively integrated to fit the current demands upon the organism. In the realm of cognition, the proposed entity that underlies this type of activity is the neurocognitive network (Bressler, 2008; Mesulam, 1998).

States of cortical coordination span a graded architecture that, towards the periphery, is hierarchical and unimodal in nature, and which feeds into an increasingly heterarchical transmodal architecture at higher levels (Fuster, 2003; Mesulam, 1998). In the following two sections I wish to sketch the theoretical and experimental developments in the understanding of 1) structure: the cortical architecture that supports the construction and

maintenance of neurocognitive networks, and 2) dynamics: the functional interactions that play out within the structural architecture and how these dynamics may support states of expectation, anticipation and prediction.

2.1 Structure: From the historical to a modern perspective

2.1.1 Localizationism versus globalism

The debate

The modern understanding of cortical function draws much of its current form as a result of an important debate in the history of neuroscience: localizationism versus globalism. The resolution of these conflicting views ultimately relied on a reformulation of the notion of function, and resulted in a revamped understanding of the functional role played by the cerebral cortex (Luria, 1973; Luria, 1980).

The crux of the debate is this: do distinct regions of the cortical sheet perform specific functions, or are cortical functions properties of the entire cortical mass acting *in toto*? The stance of localizationism is that cortical functions - using function in the sense derived from the faculty psychology that was dominant at the time - are located in circumscribed regions of the cortex. In contrast, the globalist or holistic approach purports that cortical functions are distributed throughout the entire cortical mass and do not inhabit specific regions of cortex.

The roots of cerebral localizationism can be traced at least as far back as Galen in the second century, but an appropriate starting point can be found in Franz Joseph Gall's contribution to physiognomy. Physiognomy as a discipline held that personality, or mental faculties can be determined from aspects of the body, such as posture, movement,

facial features and body structure (Jahnke, 1997). Gall in collaboration with his student Johann Gasper Spurzheim formulated an extension of physiognomy that would become known as phrenology. In the practice of phrenology, bumps or depressions on the skull are used to infer the level of development of a psychological trait. By comparing the bumps of the skull with an atlas of extremely dubious validity, the phrenologist claimed to be able to assess the mental capabilities and personality traits of an individual (Hergenhahn, 2001). Though this claim would remain contentious and ultimately be regarded as false, the assertion of the existence of functionally specialized regions of cortex would remain an influential development in the understanding of the relationship between the psychological properties of the mind and the organization of the brain.

The clinical research of Paul Broca added tangible neurophysiological evidence to the claims of the phrenologists via his observations of a patient known as Tan, since ”Tan, tan”, was the only verbalization of which he was capable, aside from a French expletive phrase. Broca (1861) observed that despite his inability to produce language, his ability to comprehend it was fully intact. After the patient's death Broca determined from autopsy of his brain that Tan possessed a severe lesion in the third frontal convolution of the left cerebral hemisphere, which he later confirmed in a second patient (Herrnstein and Boring, 1965). Broca had thus demonstrated that damage to a circumscribed area of the brain could lead to a very specific cognitive deficit, while sparring other highly related cognitive abilities.

Shortly after Broca's discovery, Carl Wernicke (1874) contributed to the localizationist approach when he described cases where lesions of the posterior third of the left superior temporal gyrus resulted in the loss of the comprehension of speech while sparing speech production, though the speech was often rapid, possessing the proper meter and tone of regular speech, but was mostly incomprehensible and paraphasic (Geschwind, 1970).

In concert with the work of Wernicke and Broca, a slew of functional locations would be discovered in the late nineteenth century; a period which Luria (1973) dubbed the *splendid seventies*. Luria designated the practitioners of this period *narrow localizationists* and balked at the results of this pursuit on the basis that the results were over-generalized, lacking sufficient investigation of the symptoms exhibited by the patient. This period resulted in the preponderance of increasingly detailed functional maps which failed to accomplish the goal of scientific inquiry: the discovery of common principles that explain and link phenomena.

Localizationism was a very dominant view in the history of neurology, but suffered attack at many points by proponents of the globalist approach. Pierre Flourens was an early opponent of localizationism. His ablasion experiments on birds led him to the opposite view of the phrenologists. Flourens observed recovery of function shortly following experimental lesions. This led him to conclude that cortical functions could not be solely attributed to circumscribed areas, since they could re-emerge following destruction of the attributed area. He had observed cortical plasticity. Friedrich Goltz continued these investigations with ablation work on dogs. He also concluded that since considerable destruction of motor cortex and even decortication did not abolish motor function that stance of strict localizationism could not be correct (Kolb and Wishaw, 1996). Karl Lashley furthered this holistic understanding with his attempts to localize the *mental engram* of associative memory. During this search he was unable, following hundreds of lesion experiments, to obliterate a complex learned association. He concluded that the degree of loss of function is proportional to the extent of the damage, rather than to the specific site of damage. He termed this the principle of mass action. His second conclusion was based on his observations of recovery of function following ablation. He interpreted this result as indicative of the multifunctionality of the brain, insomuch as cortical tissue can take on new functions after damage, and can perhaps perform any function that is already

performed by another cortical area. This was his principle of equipotentiality (Lashley, 1950). Lashley's work, and that of the previous antilocalizationists led to a view that the cortex functioned as a homogeneous structure, a view which resonated with the then very influential school of Gestalt psychology. Unfortunately, like the Gestalt principle of psychophysical isomorphism (Köhler, 1970), the globalists appealed to quasi-mystical conceptions and exotic physics to explain the holistic function of the brain that they were proposing (Luria, 1980). Ultimately, psychophysical isomorphism and pure globalism were ultimately shown to be incorrect.

Thesis, antithesis, synthesis

In the midst of the dialectic between the localizationists and the globalists, synthesis was emerging. Many researchers and theorists were instrumental in the development of this synthesis, but the ideas of few were as prescient as those of John Hughlings-Jackson. Jackson's conception of the brain was very advanced for the period, and his ideas are much more influential to modern theory than they were during his lifetime (Kolb and Wishaw, 1996). Jackson offered the concept of a functional hierarchy, where functions exist in a simple form at the low level of the spinal cord and brainstem, in a more complex form at the middle level of the motor and sensory regions, and finally at their most complex level, which he believed resided in the frontal lobes (Luria, 1980). Thus the same function spanned multiple levels, each with more elaborate complexity. In general, hierarchical functional organization is a system where more complex functions are built out of and control functional elements that are responsible for lower component functions. In this way behavioral complexity emerges in the same way organic complexity emerges during evolution - via the novel coordination and elaboration of existing structures, which gives rise to complex systems of functional interrelationships. Jackson attributed the loss of function due to cortical damage, and the concurrent loss of behavioral complexity, as

regression to lower levels of functional organization, since the higher level of organization, which imposed order on the lower, had been destroyed. Jackson's conception of functional hierarchies would prove critical to modern theory by rectifying many of the contentious points debated by the localizationists and globalists, though it would remain underappreciated many years after its introduction.

A second important development that led to the modern view of cortical organization is evident when we revisit Wernicke's 1873 analysis of aphasia. Wernicke postulated a system of language comprehension and production that depended upon the flow of information from posterior (Wernicke's area) to frontal (Broca's area) locations on the cerebral convexity. Wernicke suggested that disconnection of these areas results in conduction aphasia. Geschwind (1970) would revive and expand upon this idea creating a model of language comprehension and production that was capable of explaining various psychological and behavioral deficits that occur based on the disconnection of different components of the system. Geschwind's focus on disconnection syndromes put focus on the importance of connectivity. The Wernicke-Geschwind model is ultimately connectionist, in that the overall functioning of the system is intimately linked to the connection topology of the elements. Though Wernicke's original network was composed of only two elements, he had postulated a unidirectional network of distributed localized areas, and had ascribed the dependence of fluent language production on their intact connectivity. The Wernicke-Geschwind model is now conceived as overly simple due to its feed-forward serial nature (Ojemann, 1991), but it contributed fundamentally to the current understanding that cortical function is dependent on the interaction of distributed local areas, and that the disturbance of these interactions leads to distinct cognitive deficits.

Together, the concepts of functional hierarchical organization, and distributed processing by interacting localized cortical areas, helped fuel the growth of the network view of cortical function (Bressler, 2008; Fuster, 2003). The network approach overcomes the

shortcomings of narrow localizationism by postulating that localized areas interact over distances and mutually influence the activities of one another. The functional character of the network emerges as a result of the intrinsic dynamics of the local areas involved, and the influences of each area on the others via their interactions. Thus the network view proposes a system of cortical organization that is both local and global, since localized networks are embedded in larger distributed networks that may span the entire cortical sheet and subcortical structures.

2.1.2 Function redefined

The emergence of the network view displaced the faculty view of function which posited that the mechanisms contained within specific regions of tissue were solely responsible for the performance of specialized functions (Luria, 1973; Luria, 1980). In tandem with the emergence of the concept of biological networks, the notion of function itself also underwent considerable evolution.

John Dewey's (1896) criticism of the reflex arc represented an important departure from the compartmentalized view of function that the mechanistic reflex arc traditionally inspires. Dewey pointed out that the components of the reflex arc are not autonomous entities which serially process environmental events from stimulus to response, but that they comprise a distinct pattern of coordination (Dewey, 1896). The elements of the coordinated system are collectively organized to achieve a specific goal - they are *purposive*. He claimed that when the system is decomposed into its component elements this purposiveness is lost, which causes the reason for their specific coordination to be no longer evident. Respiration is an act that involves a vast number of intricately networked elements, the function of which is to bring oxygen into the blood, and dispel of carbon dioxide that results from cellular metabolism. It is this function that justifies the intricate network of coordinated elements that subserve it. Breathing considered alone

is quite devoid of function, since it is not clear what role the inhalation and exhalation of gases and the dynamics of the process may play without understanding the role that the gas exchange plays in the larger context of cellular metabolism. When breathing is considered in the broader context of respiration it becomes possible to understand how the rate of breathing is coupled to the rate of oxygen consumption and carbon dioxide production by cellular metabolism. Such an argument demonstrates that biological networks are adaptive coordinated structures that serve the internal and external demands of the organism.

A second important contribution that follows from the ideas of Dewey is that the component parts that subserve a function need not be constant. In order to achieve a particular function, a vast number of different elements may be recruited. The task is invariant, and the result is invariant, but the mechanism used to achieve the result is highly variable. Luria (1973/1980) and Kelso (1995) both refer to the work of the Bernstein school in illustrating this fact. Faced with the massively high-dimensional demands of motor coordination, Bernstein was convinced that the individual function of specific motor cells or groups could not code for the huge space of coordinated actions that are produced by organisms, or be responsible for the incredible flexibility in the motor repertoire, which allows specific actions to be achieved under a vast number of environmental circumstances. The specific problem was that the degrees of freedom manifested by the motor acts were too high to be managed by the neural system as it was conceived of at the time. Like Jackson, Bernstein envisioned a dynamic structure with linkages between elements at multiple hierarchical levels. To perform the motor act, specific elements are dynamically linked on the basis of the particular act to be performed leading to far greater degrees of freedom which can be controlled by the same system of finite elements. In fact, the linkage of motor elements into functional systems may reduce the degrees of freedom tremendously so that far fewer parameters are left which require explicit control (Kelso, 1995). This indi-

cates that the functional elements of the motor act cannot be traced to individual localized regions of the brain, which perform discrete motor behaviors, but rather that the motor act consists of a dynamic structure of neurons, brain areas, bodily effectors, sensors and environmental variables that are coupled to achieve a specific function. Such a system is a synergy (Kelso, 1995). Synergies consist of dynamic couplings between elements that exist to perform a specific function or task. They are flexible in their constituents, which often change based on internal and external constraints. Kelso et al. (1984) provided an excellent example of a functional synergy by spontaneously perturbing the jaw while a speaker attempted to speak various words. Incredibly. the motor system compensated immediately, so that the word was properly spoken despite the destruction of degrees of freedom that were normally recruited to perform the task. The system had spontaneously reconfigured the coordination of its components so as to compensate for the loss of functionality of the jaw induced by the perturbation.

The application of the principles of synergetics (Haken, 1978), in combination with the tools of non-linear dynamics has led to the establishment of the field of coordination dynamics (Kelso, 1991; Schöner and Kelso, 1988). Coordination dynamics seeks to discover the control parameters that govern the behavior of high-dimensional complex systems, and to study the nature and evolution of self-organized patterns of coordination between synergetic elements. The unit of analysis is the dynamic pattern, and thus coordination dynamics is not constrained to a particular level of analysis (Kelso, 1991). This freedom makes coordination dynamics a powerful framework to study functional systems, which exist simultaneously at multiple levels of description.

Based on the previous considerations: if a functional specialization is to be assigned to a muscle, organ, or a region of cortical tissue, then this specialization needs to be regarded in the greater context of its membership in a functional dynamic structure. If the component is destroyed, this may or may not alter or abolish the functional properties

of the system, which will depend on the ability of the system to reorganize around the missing or malfunctioning component. This reconceptualization of function has helped to displace the reflex arc as the fundamental functional unit of brain function and pave the way for the modern notion of the biological network, which is a distributed dynamic structure, which emerges under distinct functional demands. In this scheme the *fundamental units* of adaptive function are not neurons, muscles, or any *part* in general. They are dynamic functional networks, which may exist at many spatial and temporal scales, span multiple levels of analysis, and consist of variegated components spanning brain, body and world. Most importantly: the precise composition and pattern of coordination of the system depends on the functional context in which the network is operating.

2.1.3 The nerve cell assembly

States of cortical coordination span multiple levels of analysis in the brain, from the microscopic level of interactions between individual neurons, to the macroscopic domain at which large-scale cortical networks exist. Early theories of network formation began with work at the level of individual neurons by Donald Hebb and Friedrick Hayek (Hayek, 1952; Hebb, 1949). They both postulated a mechanism of association between neurons that is known as Hebbian learning. The mechanism describes a process whereby synaptic strength is increased between neurons that are coactive within a short temporal window (Hebb, 1949). Hebb theorized that during development this mechanism gives rise to strongly connected networks of neurons that he termed nerve-cell assemblies, and that the activation of these assemblies was the substrate of perception, cognition and action. Activation of one or a few members of the cell assembly could cause activation of the entire assembly, comprising the perception of the relationships between the temporally coincident sensory activation that caused its creation. Via this relational code, elements of a cell assembly may function as components of innumerable other cell as-

sembles and provide for an infinite space of associational possibilities due to the massive number of neurons that compose the brain (Fuster, 2008). Pioneering work over the last two decades spearheaded by the seminal work of Gray et al. (1989) has demonstrated that cell assemblies may be identified via transient synchronization of action potentials between groups of neurons. These patterns of neuronal synchronization have been shown to follow Gestalt rules of perceptual organization, and thus code for relationships between perceptual objects as Hebb had intuited.

2.1.4 Large-scale neurocognitive networks: Cortical columns, local cortical area networks and large-scale cortical networks

The understanding of the precise structure of the neural networks postulated by Hebb and Hayek has relied on advancements yielded by a number of important experimental results and theoretical positions in the neurosciences, which have given rise to a detailed view of the microscopic, mesoscopic and macroscopic organization of cortical networks.

At the microscopic level of the neural circuit, the cortical sheet is organized as into six cortical layers, or laminae, much like an onion. The laminae are populated by a variety of different cell types, specific to each layer, and have distinct internal anatomical connectivity with specific patterns of input and output to other areas. Neuronal assemblies are organized in columnar structures that are oriented perpendicularly to the cortical surface. Minicolumns, consisting of 80 - 100 densely interconnected neurons, form cortical macrocolumns, which consist of 50 - 80 minicolumns bound together by short-range horizontal connections (Mountcastle, 1998; Mountcastle, 2003). Macrocolumns range from 300 to 500 micrometers in diameter. The neurons within each macrocolumn display similar response properties and manifest a distinct change in tuning at the border that is shared with neighboring columns (Mountcastle, 1957; Mountcastle, 1997; Powell and Mountcastle, 1959). Networks of macrocolumns, which share common connectivity

with other brain areas, define local cortical area networks (Bressler and Tognoli, 2006). Local cortical area networks have been delineated structurally by cytoarchitectonic methods (Brodmann, 1909), which identify common cellular makeup to differentiate cortical areas, and tracing methods, which reveal regions with common input and output patterning (Felleman and Van Essen, 1991). Functional imaging methods, such as fMRI, PET, and optical imaging, reveal local cortical area networks as circumscribed regions of cortex that are activated by specific experimental manipulations (Bressler and Tognoli, 2006; Mesulam, 1990). Together, structural and functional methods reveal areas of cortex with similar structural composition, anatomical connectivity and functional specificity, which define them as a local cortical area network.

Neurocognitive networks are coordinated assemblies of local cortical area networks linked by cortico-cortical, cortico-thalamo-cortical, and connectivity with subcortical structures. These large-scale cortical networks may traverse long distances in the brain and are hypothesized to govern cognition and action by facilitating communication between distributed local cortical area networks (Bressler and Tognoli, 2006; Bressler, 2008; Fuster, 2003; Fuster, 2006; Mesulam, 1990). Neurocognitive networks are dynamic structures proposed to underlie cognitive function, and as such, may consist of vast arrays of different elements depending on the specific cognitive task at hand.

2.1.5 Hierarchy and heterarchy

The structure of a neurocognitive network is dynamic and task specific, yet its overall structure is largely determined by the brain's complex pattern of anatomical connectivity. The overall connectivity pattern of the brain is certainly not all-to-all. Within the visual system, amongst a large collection of local cortical areas that were tested for connectivity, only 40 percent of areas have been found to be connected (Felleman and Van Essen, 1991). In fact, the cerebral cortex has a highly specific pattern of connectivity, which is

likely a major determinant of cognitive function, and consequently constrains the possible coordination dynamics (Bressler, 1996; Sporns and Kötter, 2004). The precise pattern of connectivity is governed by both phylogenetic factors that govern the development of the organism in a species-specific manner, and ontogenetic factors, which interact with the phylogenetically determined structure during the lifetime of the organism; modifying, establishing and destroying anatomical connections (Bressler and Tognoli, 2006).

Common patterns of cortical connectivity are found between cortical areas and consist of three main types of laminar relations, which correspond with distinct patterns of connectivity: lateral, ascending/feedforward and descending/feedback. In addition to these different types of anatomical connectivity, the cortex shows unique patterns of convergence and divergence, which is a key factor to how the cortex integrates and disseminates information throughout its structure (Freeman, 1975). Convergent inputs may arrive at a target cell from a number of different neurons in one or many cortical areas, and so, convergent inputs originating from one area will carry a strong influence from that area on to others, whereas convergent inputs from many different areas will bring diverse information from those areas to the target cell or region, which will then integrate this input. Divergence refers to the pattern of axonal projections that emanate from a neuron or area. Divergent projections reach many different locations within and across different areas. Through divergent connectivity the activities of single neurons and circuits are broadcast to many other different cortical areas.

Through the careful tracing of anatomical connectivity, sensory and motor regions can be assigned hierarchical levels that roughly progress from the sensorium and motor interface through the higher cortical levels (Felleman and Van Essen, 1991). Across the progression from primary to secondary to tertiary cortex, which corresponds with a progression from heterotypical cortex to homotypical cortex (Luria, 1980; Mountcastle, 1998), the roughly hierarchical scheme gives way to a heterarchical pattern of or-

ganization where cortical connectivity dictates a circulation of activity rather than a hierarchical progression (Fuster, 2003). This corresponds to a change in the functional specialization of cortical areas, with heterotypical cortex showing cellular specialization by the enhancement of certain cortical laminae. This enhancement is likely responsible for enhancing specific types of connectivity with other areas and subserves specialized sensory and motor functions (Mountcastle, 1998). Conversely, homotypical cortex shows a uniform laminar profile tangential to the cortical surface, which is suggestive of a common functional role. Heterotypic cortex supports unimodal processing streams that converge in homotypical transmodal association cortex within the frontal, temporal and parietal lobes. These association areas are thought to control the global aspects of cognitive acts, and house the most abstract aspects of cognitive processing (Mesulam, 1990; Mesulam, 1998). Due to the divergent nature of connectivity in the cerebral cortex, high-level transmodal association areas provide for global connectivity between the unimodal sensory and executive streams. This allows for the establishment of global networks that may span multiple unimodal streams and subcortical structures. Figure 2.1 illustrates a neurocognitive network that spans the auditory and visual unimodal streams, frontal, parietal and temporal transmodal association cortex, and subcortical structures. In this scheme high-level transmodal networks are not isolated from the hierarchical unimodal streams, but in fact bind them together and unite them with additional networks (Fuster, 2003; Mesulam, 1998).

Despite the hierarchical nature of heterotypic unimodal areas, sensory processing is by no means constrained to a serial feedforward mode of successive elaboration that is characteristic of classical feedforward artificial neural networks. Due to extensive lateral connectivity, areas within a hierarchical level may communicate between one another, and with higher-level areas via feedforward connectivity. Additionally, higher-level areas may communicate with lower level areas via feedback connections (Barbas and Rempel-

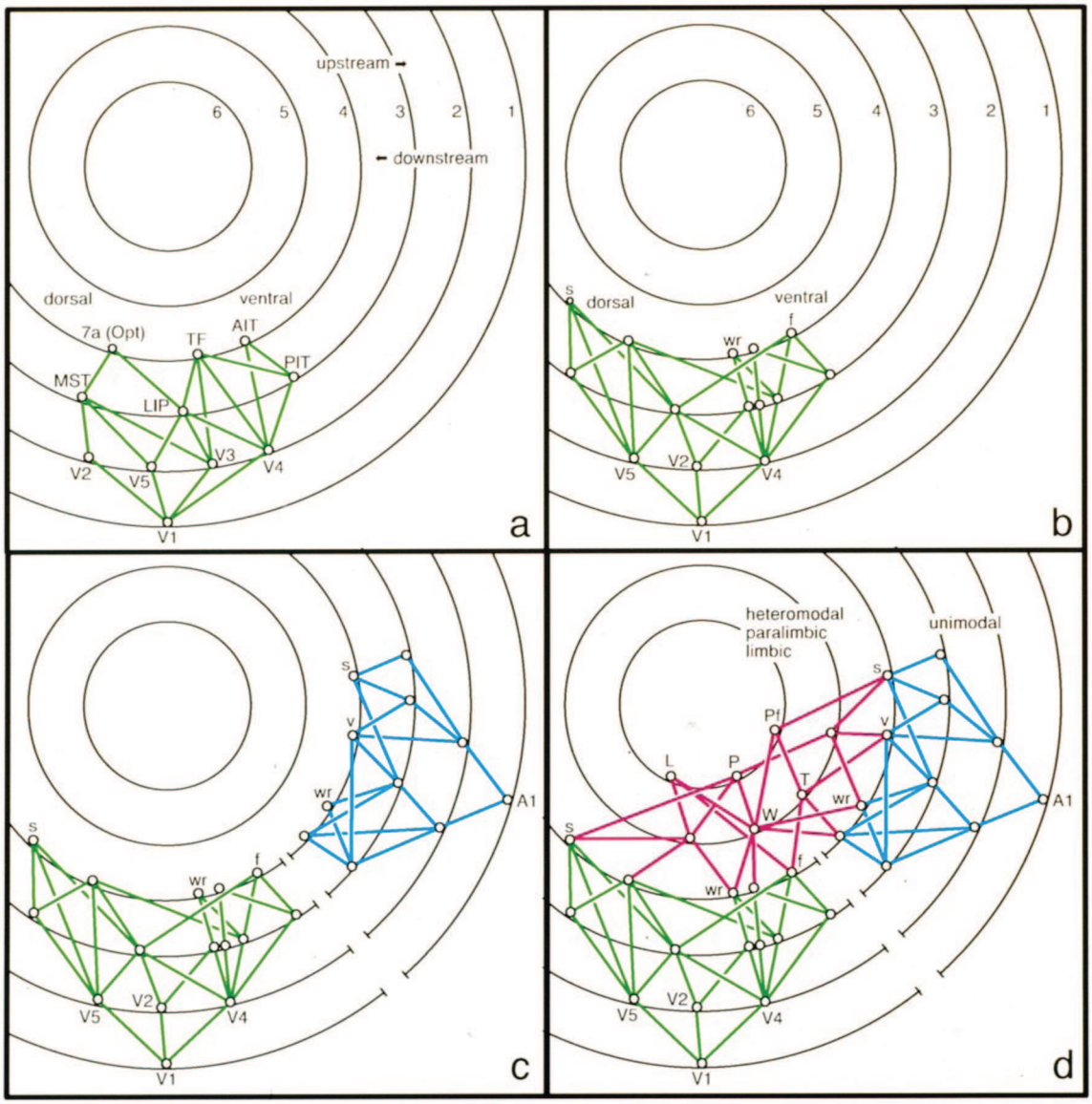

Figure 2.1: A graphical illustration from Mesulam (1998) of a hierarchically integrated auditory-visual neurocognitive network

Clower, 1997; Mountcastle, 1998; Mumford, 1992). Thus despite the roughly hierarchical structure of cortical areas, processing may procceed in parallel, distributed within and across hierarchical levels. This architecture provides a dynamic processing architecture that can support dynamic interactions between areas and across levels, and rich recurrent processing (Bressler, 1995; Lamme et al., 1998; Roelfsema et al., 2000).

The establishment of the hierarchical nature of sensory processing was highly influenced by the meta-analysis of Felleman and Van Essen (1991). Using extensive data from numerous tract tracing studies, they hierarchically organized many areas within occipital, temporal, parietal and frontal cortex. Using an algorithm, the cortical areas were sorted on the basis of the connectivity pattern share with other areas. Cortical areas that shared extensive lateral connectivity were classified at the same hierarchical level. It must be noted that some disagreement has arisen regarding the nature of the algorithm employed by Felleman and Van Essen (1991) (Van Essen and Felleman, 1996; Hilgetag et al., 1996), but that alternative algorithms also rely on sorting based on ascending, descending and lateral connectivity. It seems to be agreed that a precise hierarchy may not be achievable, but that the visual system is at least quasi-hierarchical, which refers to a structure of largely hierarchical organization with some departures from the hierarchical scheme. A similar understanding of the frontal executive system as a quasi-hierarchy has recently been advanced (Badre and D'Esposito, 2009).

Lateral connectivity is characterized by neurons which originate in both supragranular and infragranular cell layers, and terminate upon all layers of the target population. Such connectivity is common across the large region of V1, and is believed to play an important role in figure-ground segregation (Lamme, 1995). The supragranular layers II/III of V1 and the infragranular layer V exhibit large numbers of horizontal fibers that connect cells with similar orientation tuning, at distances of several millimeters (Gilbert and Wiesel, 1989; Rockland and Lund, 1983). These lateral connections are prime candidates

for carrying contextual information from different regions of the visual field. Lateral connectivity between areas V4 and MT, which are categorized at the same hierarchical level may unify motion and shape processing at corresponding positions in the visual field.

Subordinate and superordinate levels are determined by patterns of ascending and decending connectivity. Ascending connections originate most prolifically from the supragranular layers, with fewer connections emanating from infragranular layers. These connections terminate in the input layer IV of target areas (Mountcastle, 1998; Rockland and Pandya, 1979). These connections play the role of carrying information from the senses through the ascending hierarchy of cortical areas, or in the motor domain, they carry information from higher-level motor control regions through the motor hierarchy to the primary motor cortex. Connectivity is reciprocal between a vast number of cortical areas with feedforward connections carrying information from area A to area B, and feedback connections relaying information in the reverse direction. Feedback connections are characterized by connectivity to target areas that emanates predominately from the infragranular layers and to a lesser extent the supragranular layers. They synapse above and below layer IV. A majority of feedback connections target layer I, which is suggestive of a controlling or modulatory role, rather than driving the activity in the area (Budd, 1998; Mountcastle, 1998). Feedforward inputs typically reach layer II and III pyramidal cells via their basal dendrites, while feedback inputs are processed by the apical dendrites. This pattern of stimulation of cortical pyramidal cells suggests that the feedforward connectivity plays a driving role, since postsynaptic potentials (PSPs) are larger and more spatially constrained on the basal dendrites, than those generated at the apical dendrites (Rockland, 1998). It has been suggested that the apical and basal dendrites may function as separate dendritic compartments since the activity from the apical dendrites is integrated before transmission to the soma (Larkum et al., 1999). The small protracted PSPs generated on the apical dendrites in contrast to those on the basal dendrites, in combination with their

different patterns of PSP integration suggests that these two types of input may subserve different mechanisms. This is consistent with the view that feedback connectivity provides a modulatory input, while feedforward input is largely responsible for the neuron's response (Hupé et al., 1998; Spratling, 2002; Spratling and Johnson, 2004).

To summarize, the anatomical architecture of the cerebral cortex provides for a rich interplay of information between cortical areas. Though this flexible architecture provides for rich connectivity between diverse cortical areas, the architecture is constrained by varying patterns of convergence and divergence, and precise interlaminar relations, which give rise to a specific global structure of communication. This structure is determined by phylogenetic and ontogentic factors, and is a major determinant of the structure and function of neurocognitive networks, and thus the nature of cognition and consciousness at large.

2.2 Dynamics

2.2.1 Synchronization, cortical oscillations, and neurocognitive networks

The classical view of neuronal communication is known as rate coding, whereby the signaling between two neurons is mitigated by an increase of the firing rate of the presynaptic cell, which increases the frequency of postsynaptic potentials (PSPs) in the dendritic arbour of the target cell, and thus the probability of the postsynaptic cell firing (Singer, 1993). Research in the last two decades has supplemented this view with a complementary mechanism based on precise timing between the spike trains of multiple neurons. In fact, recent studies have indicated that increases in firing rate may not under all conditions lead to enhanced firing probability in the post-synaptic cell, and that specific cellular mechanism seem to be tuned to give rise to sharper postsynaptic depolarizations in response to temporally coincident inputs (Azouz and Gray, 2000; Azouz and Gray, 2003; Tsodyks and Markram, 1997).

Correlation between spike trains of pairs of individual neurons is a ubiquitous phenomenon found throughout the nervous system, the study of which was initially suggested as an effective means to study synaptic connectivity (Gerstein and Perkel, 1969). Early observations revealed correlations between neurons in area V1. These correlations occurred between neurons with similar tuning properties when mutually stimulated by a preferred stimulus (Ts'o et al., 1986).

Spike timing correlations have been linked to cognitive operations as an economical and flexible solution to the problems of feature integration and perceptual grouping, which are both instances of the binding problem (von der Malsburg, 1981; von der Malsburg and Schneider, 1986; Milner, 1974; Treisman and Gelade, 1980). Evidence for

this putative role of coordinated spike timing has shown that correlations between action potentials in visual neurons within a cortical column, in different columns, and even interhemispherically (Gray, 1999), increases for visual stimuli that follow Gestalt rules of perceptual organization, such as *good continuation* (Engel et al., 1991; Engel et al., 1991; Engel et al., 1991; Gray et al., 1989; Koffka, 1935; Singer et al., 1997). The phenomenon of neuronal synchronization has now been demonstrated to play functional roles in motor behavior (Baker et al., 1999; Riehle et al., 1997), somatosensation (Steinmetz et al., 2000), sensorimotor integration (Fetz et al., 2000), olfaction (Wehr and Laurent, 1996), memory (Chrobak and Buzsáki, 1996; Whittington et al., 1997), attentional selection (Fries et al., 2001; Niebur et al., 2002), and sleep (Steriade, 1999).

An important property of synchronized spike activity observed by Gray et al. (1989) was that statistically, the synchronized spikes are periodic, having a tendency to occur at frequencies in the gamma band (30-50 Hz). Additionally, coincident spikes were found to occur at the negative trough of the simultaneously recorded local field potential (LFP). Local field potentials are fluctuations in voltage that result from the summation of extracellular dendritic currents across pyramidal cells generated by excitatory (EPSPs) and inhibitory post-synaptic potentials (IPSPs) (Elul, 1971; Speckman and Elger, 1999). It is important to note that synchronous spiking does not occur on every cycle of the oscillation, but exhibits cycle skipping (Singer, 1999), which is when a recorded neuron is silent on the great majority of cycles. This sparse firing pattern is too low to effectively transmit information on the sub-second timescale that cognition operates, thus assemblies of synchronized neurons are required: neuronal ensembles, which are groups of synchronously active nearby neurons that cooperatively transmit information to other cortical areas (Grinvald et al., 2003). As a result of their synchronization, and convergent connectivity to other cortical areas, neuronal ensembles give rise to pulse probability waves. These waves allow effective communication to other neuronal ensembles, despite

the sparse firing nature of the individual neuronal components of the assembly (Bressler et al., 2007). The output of an individual member of an assembly is divergent in that its axonal terminations share synapses with those from neurons in many different cortical areas. In this way a neuronal ensembles may coordinate with a vast number of other cortical areas.

The axonal firing characteristics, or pulse mode activity, of the neuronal ensemble are reflected in measurements of multi-unit activity (MUA), which is a record of spike activity within the vicinity of a sharp electrode; while the dendritic, or wave mode, component can be measured invasively by the LFP, which results from summed extracellular dendritic currents across the ensemble (Bressler, 1995). Together, MUA and the LFP index the degree of synchronization of the pulse mode output of the ensemble and the synchronization of the wave mode input to the ensemble, respectively.

The electroencephalogram (EEG) is also a measure of summed extracellular dendritic currents, but is an average over a larger spatial area than the LFP. Magnetoencephalography (MEG) measures the summation of intracellular currents within pyramidal cells, but also integrates activity over a much larger area than the LFP. Both these measures reflect the synchronized activity of neuronal ensembles, but result from integration over larger areas of the cortical sheet, and as a result, a greater number of neuronal ensembles contribute to the activity recorded from a given sensor. Thus the power spectrum derived from a single sensor reflects the level of intraareal phase synchronization of the cortical activity being recorded, while the coherence spectrum resulting from two sensors reveals the consistency of interareal phase locking between the cortical generators measured independently by the two sensors. The level of granularity resolved by measurements of neuronal ensemble activity is dependent on the spatial scale at which cortical activity can be localized, which makes the LFP an excellent index of neurocognitive network interactions, though EEG and MEG often can survey a larger spatial area overall due to the

technical difficulty of implanting LFP electrodes at high density over large spatial areas of cortex. Overall, the study of synchronization of neuronal ensembles via unit activity, MUA, LFP, EEG and MEG, offers an important window through which to study the relationship between large-scale cortical network activity and cognition. The successful establishment of the nature of this relationship is what defines the constitutive elements, the functional relationships between the elements, and the cognitive significance of a particular neurocognitive network.

Cortical oscillations are grouped as slow (0.3-7 Hz), medium, (8-13 Hz), fast (14-30 Hz) and very fast (>30 Hz). These ranges correspond to the delta and theta, alpha, beta, and gamma frequency ranges, respectively (Niedermeyer, 1999). For the purposes of this work, the discussion of the functional correlates of cortical rhythms will be limited to the medium, through very fast: the alpha, beta and gamma frequency ranges.

Neurocognitive networks may consist of neuronal ensembles expressing interrelated ongoing activity at multiple frequencies, spanning the full frequency spectrum (Bressler et al., 1993; Bressler and Tognoli, 2006). This ongoing activity often shows distinct patterns of temporal evolution when perturbed by a stimulus that are manifested as periods of event related synchronization (ERS) and desynchronization (ERD) within different frequency bands (Pfurtscheller and Lopes da Silva, 1999; Tallon-Baudry, 2003). This activity is reflected by temporal changes in the power, and/or coherence spectra of electrophysiological recordings from before, during, and after the introduction of the stimulus. It has been theorized that the specific frequency of the interaction between neuronal ensembles may be due to the spatial extent of the network, with larger networks exhibiting slower oscillations (Nunez, 2000). Modeling work based on hippocampal slice preparations also supports this idea, showing that beta band oscillations can support synchronization over axonal conduction delays greater than 10 ms (Kopell et al., 2000). Thus gamma band activity may be particularly suited for local processing,

while long-range interactions may be best subserved by slower oscillations. Indeed it has been demonstrated that interactions between distant cortical areas supporting diverse functional roles integrate at frequencies within the beta (Roelfsema et al., 1997; von Stein et al., 1999), and alpha bands (von Stein and Sarnthein, 2000).

Beta and gamma frequency activity (fast oscillations) have been suggested to play important roles in cognitive functioning (Singer, 1993), while alpha band power has often been attributed to cortical idling, and therefore was not thought to contribute positively to cognitive operations. More recent work points to an important cognitive role of the alpha band during the anticipation of visual stimuli (Capotosto et al., 2009). These studies show a decrease in alpha band power prior to stimulus onset in areas contralateral to the cued/attended location (Rihs et al., 2009; Sauseng et al., 2005; Wyart and Tallon-Baudry, 2009), while alpha power increases for areas responsive to the unattended location (Rihs et al., 2007; Worden et al., 2000). This activity is thought to suppress the input of objects in the unattended visual hemifield, while enhancing processing of objects in the attended location. Other work points to the role of alpha band synchronization during mental imagery (von Stein and Sarnthein, 2000). Thus alpha band synchronization may comprise a powerful mechanism of top-down control over visual processing and contribute to other top-down operations such as mental imagery.

Fast cortical oscillations have been linked to a host of sensory and cognitive phenomena. Beta band oscillations are known to play an important role in vision (Bekisz and Wróbel, 2003; Bressler et al., 2007), motor output (Baker et al., 1999; Farmer, 1998; Salmelin and Hari, 1994; Sanes and Donoghue, 1993), somatosensation (Cheron et al., 2007), sensorimotor integration (Alegre et al., 2004; Brovelli et al., 2002; Brovelli et al., 2004; Jensen et al., 2005; Roelfsema et al., 1997; Zhang et al., 2008), visuomotor integration (Classen et al., 1998; Liang et al., 2002), audition (Kayser and Logothetis, 2009), olfaction (Cenier et al., 2009; Fontanini and Bower, 2006; Jung et al., 2006), facial recog-

nition (Ozgören et al., 2005), attention (Buia and Tiesinga, 2008; Gómez et al., 2006; Gross et al., 2004; Wróbel, 2000), expectation (Gómez et al., 2004), memory (Düzel et al., 2003; Tallon-Baudry et al., 1999), language (Nikolaev et al., 2001), consciousness (Gaillard et al., 2009; Kranczioch et al., 2007), and has been implicated in pathological states such as Parkinson's disease (Bronte-Stewart et al., 2009). Symptoms of Parkinson's disease may be a manifestation of pathological activity in the beta band between sensorimotor networks and subcortical structures such as the basal ganglia (Brown et al., 2001; Courtemanche et al., 2003; Mallet et al., 2008). The body of literature concerning gamma oscillations is exceedingly large (see Engel et al., 1997; Singer, 1993; Singer and Gray, 1995; Singer, 1999; König and Engel, 1995 for reviews). Unlike beta oscillations, gamma oscillations are believed to be most well suited for local processing; that is, on spatial scales seven millimeters or less (Gray, 1999; Kopell et al., 2000; von Stein and Sarnthein, 2000), yet there are numerous studies that show gamma band synchronization between areas that far exceed this range (Melloni et al., 2007; Rodriguez et al., 1999). A debate is currently underway due to the demonstration that long-distance gamma band synchronization results as an ocular artifact of miniature saccades (Melloni et al., 2009a; Melloni et al., 2009b; Yuval-Greenberg et al., 2008). This artifact should only affect scalp EEG and to a much lesser extent, intracranial EEG. In defense of the stance that the establishment of long-range interareal gamma synchronization is a cognitive phenomenon, the research presented herein finds interareal gamma synchronization between electrodes in excess of seven millimeters. Based on the bipolar electrode design used to collect this data, which provides a high degree of spatial resolution, and thus very precise localization of signal generators and suppression of distant signals, it is very unlikely that this effect could be due to ocular artifact (Bressler et al., 1993). It must be noted that the size of the gamma coherence peaks is significantly smaller than that of those found for the beta range, which is consistent with the proposal that synchronization

drops off with distance, and that lower frequency oscillations may maintain the integrity of synchronization at greater conduction delays.

In summary, neurocognitive networks are composed of synchronized neuronal ensembles that make up local cortical area networks. The composition of the neuronal ensembles is very flexible and is based on anatomical connectivity, the intrinsic dynamics of the ensemble components and the properties of afferent stimulation upon the ensemble, which determines precise patterns of spike timing across the ensemble. Linkages between neuronal ensembles form local cortical area networks, which may coordinate over longer distances in the alpha, beta and gamma frequency ranges based on top-down influences, such as attention, anticipation and task constraints, in combination the with bottom-up influence of feedforward stimulation. Local cortical area networks may coordinate at multiple frequencies simultaneously with the precise topography of coordinated areas and the frequencies at which they are interacting acting as a major determinant of the function of a specific neurocognitive network.

2.2.2 Neural context, spatial coherence and metastability as determinants of neurocognitive network dynamics

In keeping with the reconceptualization of function outlined by Luria (1973) and Kelso (1995), a region of cortical tissue is not solely responsible for its functional character but rather is a cooperating part of a larger functional whole, or synergy, which derives its functional nature from the pattern of cooperative couplings with other brain regions, the body and the environment. Additionally it is known that the functional role of a cortical area is to a great extent determined by its pattern of afferent connectivity (Mountcastle, 1998). The cortical area emerges as a highly plastic and multifunctional unit. More recent theorizing and experimentation have demonstrated that this plasticity of function is even greater since the effective connectivity of afferent input to a cortical area is highly

dependent on the spike timing between afferent volleys. This means that the effect that one area exerts upon another can change dramatically based on the current pattern of spatially synchronized activity that they share (Bressler et al., 2007; Fries, 2005).

Cortical areas exist in a state of integration∼segregation, where their behavior may be constrained by influences from other cortical areas, and thus be integrated, while expressing autonomy (segregation) that derives from the intrinsic dynamics of the area that result from the specific architecture and synaptic weights of the area's cortical circuit, and its afferent anatomical connectivity (Kelso and Engstrøm, 2008). Bressler and McIntosh (2007) outline a dynamic neural environment where the specific functional nature of a cortical area results from the dense reciprocal connectivity and reentrant dynamics between areas (Tononi et al., 1992). The areas to which a local area is directly connected are termed its *connection set* (Bressler, 2002; Bressler and McIntosh, 2007), or *connectional fingerprint* (Passingham et al., 2002), and are the main determinants of the area's function. Reciprocal connectivity and reentrant dynamics allow elements of a connection set to modulate one another. This interactive modulation between the nodes of the neurocognitive network causes the emergence of a functional topology (Bressler, 1995). The impact of the local processing environment upon a neural element, which consists of the modulatory influences of the other areas comprising its connection set is defined as its *neural context* (Bressler et al., 2007). The consequence of neural context is that the functional behavior of the area is greatly affected by the pattern of input from members of its connection set, and thus a given area may express multifunctionality, with its specific functional properties defined by the current neural context in which it operates (Bressler and Tognoli, 2006). Experimental and theoretical work has demonstrated how the functional properties of a neural element may profoundly change based on the specific input from other cortical areas, which is hypothesized to occur via interactions that are lateral, and thus exist at the same hierarchical

level, and feedback connections from higher level regions (Gilbert, 1998; Lee et al., 2003; Li et al., 2004). Bressler and McIntosh (2007) differentiate between neural context, which operates only at the level of the brain, and situational context, which results from contingencies in the internal milieu and external environment. The specific elements and their spatial configuration that construct a sensory scene, or the social relationships that exist between a group of individuals with which an organism is interacting, are examples of situational context. It has been well demonstrated that the contents of a visual scene have a large impact on the local processing of V1 neurons via lateral connectivity, which represents a case of neural context generated by the specific situational context (Zipser et al., 1996). Bressler and McIntosh (2007) postulate that through the convergence of the activity of local networks, a global cortical context may emerge which reflects the situational context, and thus gives rise to a neurocognitive network capable of governing meaningful cognition and action (Bressler, 2004; Bressler and McIntosh, 2007; Bressler, 2007).

Neural context is implemented via effective connections between the target area, and the transmitting areas of the connection set. Effective connectivity is defined as connections that carry a causal influence from one area to another. This differs from the study of functional connectivity, which is identified by correlated activity between areas that is often signified by their co-activation, as is typically studied with fMRI (Friston, 1994; Friston, 2002; McIntosh, 2000). Neural context is hypothesized to shift on the millisecond to second time-scale of cognition, which implies that changes in effective connectivity are too rapid to depend upon the modification of synaptic weights. This indicates that any candidate mechanism must possess features that allow effective connections to change on this fast time-scale. One candidate mechanism is the formation of spatial patterns of phase coherence, which form via the interactions between the members of the connection set, and interact with the spatial patterns generated by the local network ele-

ments (Bressler, 2004; Bressler and McIntosh, 2007; Singer, 1994). Such a mechanism would increase the efficacy of afferent activity to target populations. This is achieved due to the high degree of intra and interareal synchronization between the transmitter populations and the resulting synchronization of their convergent afferent volleys (Bressler, 2004). Synchronized input to target cells is hypothesized to generate larger EPSPs on the dendritic membrane due to the increased probability of the summation of individual EPSPs. This results in greater membrane depolarization, and a greater probability of triggering an action potential (Niebur et al., 2002). A related view has been advanced by Fries (2005), which he terms the communication-though-coherence (CTC) hypothesis. Here coherent oscillations within both the sending and the receiving neuronal groups are of prime importance. The coherent oscillations function as *windows* for communication, so that not only are afferent volleys synchronized due to the mechanism mentioned above, but the voltage of the dendritic membranes of the neurons of the receiving group are also oscillating at the coherent frequency. Fries proposes that relative phase differences between the coherent oscillations of the interareal neuronal groups are precisely timed, on a sub-cycle order of tens of milliseconds, so that afferent volleys leave the transmitting group at the excitability peak of the wave, and arrive at the target neurons at their respective peak depolarization. In this regime the receiving neurons should act as coincidence detectors (König et al., 1996). The conduction delay is compensated for by a shift in relative phase. This shift should increase as conduction delays increase. Interestingly, it has been found that axonal conduction velocities may be adjusted via different patterns of myelination such that axon pulses arrive near simultaneity despite large differences in conduction distances (Salami et al., 2003). Such a mechanism may play a vital role in ensuring the precise spike timing that the CTC hypothesis requires. Gregoriou et al. (2009) recently demonstrated that the relative phase values of coherent alpha, beta and gamma oscillations between V4 and the frontal eye fields (FEF) all corresponded to a fixed time

shift of 8-12 milliseconds, a value that is near the expected range for the conduction delay between these regions (Nowak and Bullier, 1997). This suggests that relative phase values are adjusted to match the conduction delay, and thus to facilitate communication between the regions by optimizing the transmission and receipt of synchronized activity.

A relatively new method of studying effective interactions between coherent groups is Granger causality (Granger, 1969). The concept of Granger causality originated from the work of Norber Wiener (Wiener, 1956). Wiener proposed that if information generated by one source can be used to improve the prediction of future events of another source, than that source can be considered causal to the first. Granger formalized this concept in the framework of autoregressive models. Using Granger causality, interactions between coherent groups of neurons can be decomposed into three terms: Granger causality from A to B, Granger causality from B to A, and instantaneous causality. Instantaneous causality can be conceived of as causal influence that is simultaneously affecting both A and B, from a third, perhaps unknown, or unmeasured source (Ding et al., 2006). Geweke (1982) extended Granger causality to the frequency domain, so that at a given frequency the magnitude of Granger causality represents the ratio of the spectral power at a given source predicted by past measurements of another source to the amount of power predicted by its own past. To date, spectral Granger causal analysis has been applied to electrophysiological recordings by a number of researchers (Bernasconi et al., 2000; Bressler and Richter, 2009; Bressler et al., 2007; Brovelli et al., 2004; Gregoriou et al., 2009; Kaminski et al., 2001; Salazar et al., 2004).

Another principle that is thought to govern the coordination between neuronal groups is metastability (Friston, 1997; Fingelkurts and Fingelkurts, 2004; Kelso, 1995). As discussed, the members of neurocognitive networks: neuronal ensembles, exhibit the coexisting propensities to integrate and segregate. Due to these complementary tendencies, these networks exhibit intermittency (Bressler and Kelso, 2001; Bressler, 2002). Inter-

mittency refers to short-lived epochs of coordination that occur between components of the neurocognitive network that are interspersed with longer periods during which interdependency is low. Metastable systems are devoid of attractors, yet the *ghosts* of these attractors exist such that the system still possesses a tendency to dwell near these regions of phase space, which for this discussion represent states of coherent oscillation (Kelso, 1995). This property of metastable dynamics ensures that metastable systems cannot become stuck in any particular basin of attraction, but more importantly, it allows the components of the system to explore large areas of the landscape of potential coordination patterns. Thus a neuronal group may couple with another for a short period of time exhibiting interdependence with that group, but this coordination may break down as the tendency for autonomy increases. The neuronal group may then operate in a more autonomous fashion for a period of time, before re-establishing interdependence with the same or a different neuronal group. In this way a probably infinite number of coordinated states may exist in the brain. This is especially apparent when one extends the above bivariate example to the massively multivariate reality that is the brain. Thus the concept of multistability governs the creation, transient existence, and destruction of neurocognitive networks in the brain, and suggests that through deformations in the attractor landscape of the metastable brain, the creation of specific neurocognitive networks may be favored, which subserve the current cognitive and environmental demands of the organism.

CHAPTER 3

VISUAL ANTICIPATORY NETWORK: EVIDENCE FOR TOP-DOWN MODULATION

3.1 Introduction

Top-down and bottom-up activity differ in that top-down activity is not directly evoked by environmental events, but rather guides neural processing and subsequent behavior by embodying states such as knowledge, expectation, attention and goal-orientation (Engel et al., 2001; Gilbert and Sigman, 2007). Such states dynamically interact with bottom-up sensory stimulation, which is inherently unpredictable due to the vast complexity of the environment, and thus, top-down activity may reduce this uncertainty by guiding the brain to states of expectation and prediction. This is likely achieved via the dynamic co-ordination of specific local area networks that form large-scale neurocognitive networks.

Within neurocognitive networks, effective influences may propagate from higher-level coordinated regions to lower-level sensory regions of the network. Such a mechanism has been proposed to explain experimental results in visual area V1 (Motter, 1993; Roelfsema et al., 1998; Zipser et al., 1996). These top-down influences may function to alter the local intrinsic dynamic of target areas, or enforce particular modes of coordination within and between local cortical area networks (Bressler, 2004; Bressler and McIn-

tosh, 2007). Top-down influences are rich sources of neural context, and may function to synchronize neural and situational context by conveying task specific information to sensory regions (Bressler and McIntosh, 2007). Such a system is embodied by the concept of inferential constraint (Bressler, 2004; Bressler and McIntosh, 2007). Bressler (2004) hypothesizes that in the context of an expected impending visual stimulus, higher-level areas may impose predictions on lower level target areas in the form of spatial coherence, where high levels of spatial coherence signal a higher level of prediction and concurrent higher levels of constraint over the target population. In agreement with the CTC hypothesis (Fries, 2005), higher levels of spatial coherence may lead to an increase in communication between the areas, and may cause modification of the response properties of the target area, and facilitated processing of the stimulus (Bressler, 2004). Such a mechanism may provide for knowledge of the impending stimulus to be deployed from higher-level regions to lower level regions in a manner specific to the expected stimulus. Bressler and Richter (2009) propose that expectancy results from the parallel dynamics of knowledge retrieval and perceptual processes that occur within neurocognitive networks so that knowledge of the past, present and future may be simultaneously embodied in these large-scale networks (Ingvar, 1985). In the context of vision, a neurocognitive network is be hypothesized to span the unimodal visual stream and the transmodal networks of the temporal, parietal and frontal lobes, which is in agreement with evidence that has shown that prefrontal and posterior parietal cortex exert top-down influences on sensory areas during the anticipation of sensory events. (Corbetta et al., 2008; Corbetta and Shulman, 2002).

Recent evidence has implicated synchronized activity between distributed neuronal assemblies in the mediation of top-down effects in the visual system (Bernasconi et al., 2000; Siegel et al., 2000), particularly in anticipation of an expected visual stimulus (Engel et al., 2001; Liang et al., 2002; Düzel et al., 2005; von Stein et al., 2000;

Salazar et al., 2004).

The present study observed lfp data from several monkeys during an interval that preceded the delivery of an expected visual stimulus. Based on the previous considerations the presence of a neurocognitive network is hypothesized that is defined on the basis of coherent functional interdependencies, and effective interdependencies, quantified by Granger causality, that occur between visual network areas that span the unimodal ventral stream, and early transmodal areas of inferotemporal cortex. It is specifically hypothesized that the network will be rich in top-down oscillatory interactions, which we propose carry inferential constraint to primary visual cortex during anticipation.

3.2 Methods

3.2.1 Recording

Bipolar Teflon-coated platinum-iridium microelectrodes of 0.125 millimeter diameter were used to record surface-to-depth (2.5 mm tip separation) LFPs from three adult rhesus macaque (*Macaca mulatta*) monkeys (GE, LU and TI) from up to 16 cortical sites in the hemisphere contralateral to the dominant hand. The electrode positions were verified in one monkey (GE) by both postmortem visual inspection, and magnetic resonance imaging, (for further details see Ledberg et al., 2007). The surface and depth signals from each recording electrode were differentially recorded using a Grass model P511J amplifier, band-passed filtered (-6 dB at 1 and 100 Hz, 6 dB per octave falloff) and digitized at 200 Hz. Differential recording of the transcortical potential reduced the common contributions to the two bipolar electrode tips by more than 10000 times, excluding propagated fields from more than a few millimeters away and localizing activity to the tissue between the tips of the bipolar electrode. All experiments were performed at the Laboratory of Neuropsychology at the National Institute for Mental Health. Animal care was in accordance with institutional guidelines at the time. Surgical methods were as described by Bressler et al. (1993), and Ledberg et al. (2007).

The data analyzed in this report were recorded during multiple daily sessions spanning several months and have not been analyzed previously, though other sessions from the same animals have been used in multiple studies by our group (Bressler et al., 1993; Bressler and Nakamura, 1993; Bressler, 1995; Bressler, 1996; Bressler et al., 1999; Brovelli et al., 2004; Ledberg et al., 2007; Liang et al., 2002; Zhang et al., 2008). One session was recorded from each monkey per day with a typical recording session composed of 1000 trials. The current study employed 18, 19 and 16 sessions; comprising 10178, 8276

and 8943 correct trials (go or no-go); from GE, LU and TI, respectively.

3.2.2 Task

The monkeys were trained to perform a go/no-go visual pattern discrimination task. They performed at a level of at least 80 percent correct during all sessions selected for analysis. Each trial was initiated when the monkey engaged a lever with the dominant hand. Once the lever was depressed and maintained in the depressed position, the trial sequence and data acquisition commenced. After initiation of the trial by the lever press, there was a random period of 200 - 1215 milliseconds before the appearance of the visual stimulus. The visual stimulus was displayed for 100 milliseconds after which the monkey had a 400 millisecond period to respond. Responses consisted of a go response (release of the lever) or a no-go response (maintenance of the lever press). Correct go responses were followed by a water reward. The monkey typically initiated the next trial on the order of a second after the response to the previous trial.

The response of go versus no-go was dependent on the categorization of four visual stimulus patterns into two groups: lines and diamonds. The stimuli were displayed on a screen 57 cm from the monkeys head. Each of the four visual stimuli consisted of four solid white dots (0.9 degrees visual angle per side), with two of the dots arranged diagonally on opposite corners of an outer square (six degrees visual angle), and the other two dots arranged diagonally on the opposite corners of an inner square (two degrees visual angle). Line stimuli were designated as patterns where the dots on the outer and inner squares were slanted in the same direction, while diamond stimuli had outer and inner dots slanted in opposing directions. The design of the stimulus ensured that categorization could not be completed by observing any single dot, and that the total area, contrast, edge length, and brightness were constant across all stimulus types. Each of the stimulus types occurred equiprobably throughout each session. Go and no-go response contingen-

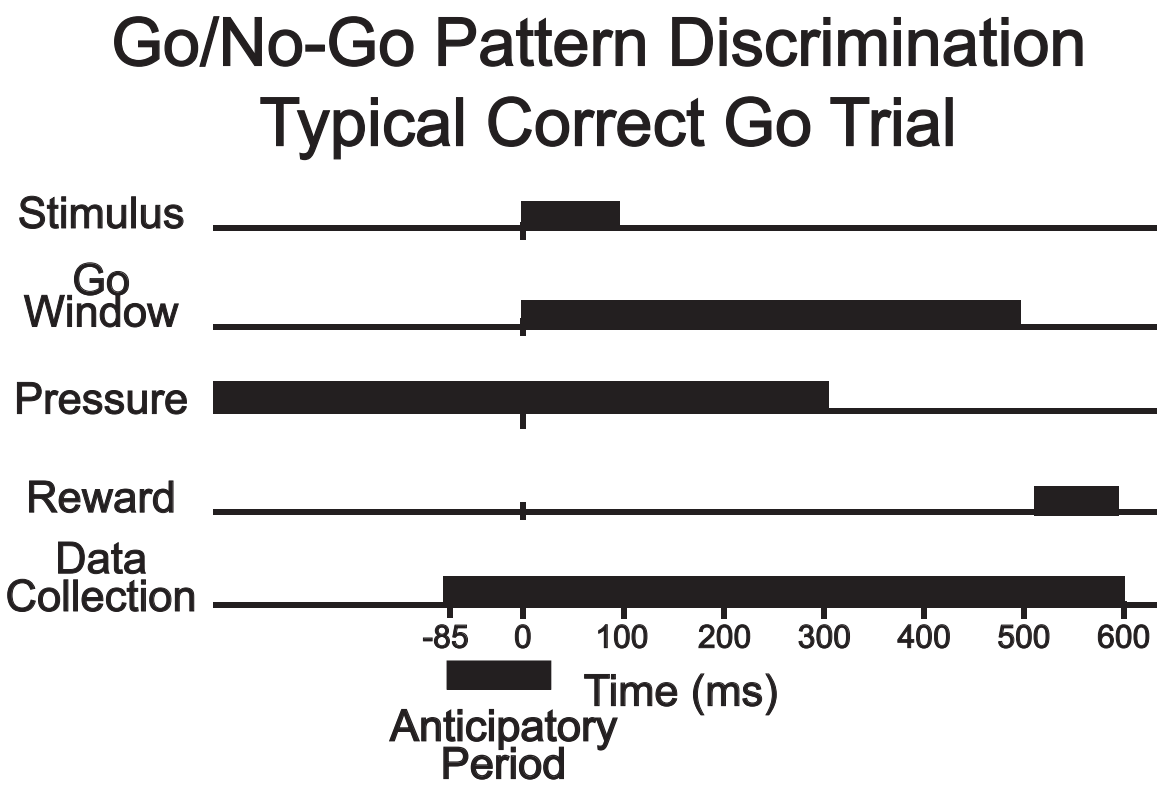

Figure 3.1: Task timeline for a typical go trial. The anticipatory period (pre-stimulus period) spans 85 milliseconds before stimulus onset to 25 milliseconds after stimulus onset.

cies were assigned randomly to the line and diamond stimulus categories at the beginning of each session, i.e. in the line-go condition, the monkey released the lever if a line stimulus is shown on the display, and maintained pressure if a diamond stimulus was shown. In the diamond-go condition, the lever was released for diamond stimuli and maintained for the line stimuli. Figure 3.1 shows the time-course of a go trial. The no-go trials differed in that the pressure had to be maintained until the end of the trial period. No reward was given for correct no-go trials.

3.2.3 Data preprocessing

The data segment analyzed in this study began 85 milliseconds before the visual stimulus onset, and extended to 515 milliseconds after stimulus onset. For the purpose of

the present study, recording sites were chosen that lay in the ventral visual stream. Electrodes recordings from areas corresponding to V1, V4, and temporal occipital area (TEO) were analyzed. In the following discussion, recording sites posterior to the lunate sulcus, corresponding to V1, have been designated as striate cortex, while sites lying anterior to the lunate sulcus (V4) and in inferotemporal cortex (TEO) are designated as extrastriate cortex. Recordings from LU consisted of four electrodes, three in striate cortex and one in area TEO. Recordings from GE consisted of three striate recording sites, and three extrastriate recording sites. Of the three extrastriate sites, two lay in area V4, while one recorded from TEO. Recording from TI was from two electrodes in striate cortex, and three extrastriate electrodes. Two of the extrastriate electrodes lay in area V4, with the remaining electrode recording from TEO. Prior to statistical analysis trials from the selected recording sites were subjected to artifact rejection. Trials with large variance were rejected to remove muscle and eye movement contamination. Line noise was removed via a multitaper filter (Mitra and Pesaran, 1999), followed by the rejection of trials with incorrect responses.

3.2.4 Assessment of behavioral performance within and across sessions

To quantify changes in the monkey's performance of the task within each session, the temporally ordered trials from each session were divided into 15 equally sized bins. The percentage of trials that were correctly performed was calculated for each bin number. The average of these percentages was then computed over the sessions producing a set of 15 bins that assessed the average evolution of the monkeys performance within a session. The performance percentages were then tested for linear correlation between performance and bin number to determine if the monkey's performance changed during the session in a systematic way.

To determine if the monkeys performance of the task changed across the ensemble of recording sessions, the percentage of correct trials was calculated for each recording session. Theses values were arranged in the temporal order in which the sessions were recorded, and were tested for linear correlation between performance and session to determine if the monkeys performance systematically changed from session to session.

3.2.5 Measuring coherence and Granger causality

We performed autoregressive (AR) spectral analysis on a 110 millisecond (22 point) pre-stimulus window. The pre-stimulus period spanned 85 milliseconds before the stimulus onset to 25 milliseconds post stimulus onset. The interval was selected based on inspection of the visual event related potentials (VERPs) from the striate sites of each monkey. It was determined that neuronal activity elicited by the stimulus was absent during this period (Ledberg et al., 2007). Prior to AR modeling each trial was subjected to linear detrending. To ensure that each trial of LFP data could be considered a realization of a zero-mean stochastic process, as required by the AR modeling procedure, the ensemble average was subtracted from each trial for each recording site included in the model (Ding et al., 2000). The Akaike Information Criterion (AIC) was used to determine the model order of the AR model, but was found to monotonically decrease with increasing model order. The model order of 10 used for the AR model was determined to be optimal as described by Brovelli et al. (2004). An AR model was then computed for each session. Bivariate AR models were constructed for the p channels of LFP data recorded from each monkey at time t, and are denoted by $X_t = (x_{1t}, x_{2t}, ..., x_{pt})^T$, where T stands for matrix transposition. Bivariate AR models were constructed for all site pairs k and l. The bivariate AR model of order m describes the data as:

$$\sum_{k=0}^{m} A_k X_{t-k} = E_t, \tag{3.1}$$

where E is a temporally uncorrelated white noise vector with covariance matrix Σ, A_k are p x p coefficient matrices ($p = 2$), and $A_0 = I$.

The coefficient matrices were obtained by solving the multivariate YuleWalker equations (of size mp^2) using the Levinson, Wiggins, and Robinson algorithm (Ding et al., 2000). From the coefficient matrices, the transfer function of the system was computed as:

$$H(\omega) = \left(\sum_{k=0}^{m} A_k e^{-2\pi i k \omega} \right)^{-1}. \tag{3.2}$$

The spectral matrix is then derived from the transfer function and noise covariance matrix as:

$$S(\omega) = H(\omega) \Sigma H^*(\omega), \tag{3.3}$$

where the asterisk denotes matrix transposition and complex conjugation.

Coherence spectral estimates are derived from the spectral matrix for all site pairs, k and l, as:

$$C_{kl}(\omega) = \frac{\left| S_{kl}(\omega)^2 \right|}{\left[S_{kk}(\omega) S_{ll}(\omega) \right]}, \tag{3.4}$$

where $S_{lk}(\omega)$ is the cross spectrum of the pair, and $S_{ll}(\omega)$ and $S_{kk}(\omega)$ are the individual power spectra. The value of coherence is a normalized quantity from 0 to 1, with a value of 1 indicating maximum linear interdependence and 0 indicating no linear interdependence.

Granger causality spectral estimates are computed for all site pairs, k and l, according to a modification of Geweke's (Ding et al., 2006; Geweke, 1982) formulation as:

$$I_{k\to l}(\omega) = \frac{\left(\sum_{kk} - \frac{\sum_{lk}^2}{\sum_{ll}}\right)|H_{lk}(\omega)|^2}{|S_{ll}(\omega)|} \tag{3.5}$$

and

$$I_{l\to k}(\omega) = \frac{\left(\sum_{ll} - \frac{\sum_{kl}^2}{\sum_{kk}}\right)|H_{kl}(\omega)|^2}{|S_{kk}(\omega)|}, \tag{3.6}$$

where Σ_{kk}, Σ_{ll}, Σ_{lk} and Σ_{kl} are elements of the covariance matrix Σ of the noise vector of the bivariate model, and S_{kk} and S_{ll} are power spectra of sites k and l, respectively. In the above modification of Geweke's formulation (Geweke, 1982), the Granger causality at frequency ω is expressed as the fraction of the total power at that frequency at one site that can be explained by the causal influence from the other site. The value ranges from 0, representing no causal influence from the other site, to 1, representing total casual influence from the other site.

Using these bivariate AR models power, coherence, relative phase and Granger causality spectra were computed for each striate-extrastriate pair, for each session from each monkey. We then identified all peaks between 8 and 90 Hz in each spectrum using in-house software. The software searched for local maxima in the spectrum, and then evaluated the curvature at each maximum using the second order difference. The curvatures were thresholded to reject peaks that were exceedingly shallow, and likely spurious. Additionally, peaks falling between 58 and 63 Hz were not tabulated due to the possibility that they were a result of residual line noise contamination that was not removed by the multitaper filter. Figure 3.2 illustrates the power, coherence, and Granger causality spectra for one striate-extrastriate pair in monkey GE.

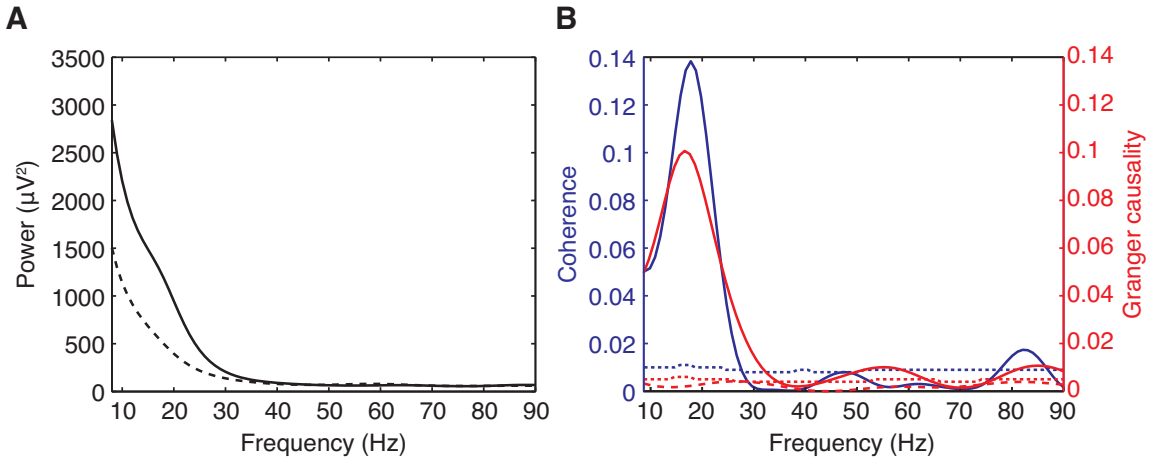

Figure 3.2: (A) Examples of power spectra from an extrastriate (solid line) and striate site (dotted line). (B) Examples of a striate-extrastriate coherence spectrum (blue), and striate-extrastriate Granger causality spectra in both directions. Top-down Granger causality is denoted by the solid red line, while bottom-up Granger causality is denoted by the dashed red line. These spectra are derived from the pre-stimulus anticipatory time period in monkey GE. Dotted lines indicate the $p < .05$ significance thresholds that were determined by randomization testing. The coherence and the top-down Granger causality spectra show large peaks at 16 and 17 Hz respectively, that were determined to be significant at $p < .05$.

3.2.6 Statistical Analysis

Each detected coherence or Granger causality spectral peak was tested for significance by comparison with a respective coherence or Granger causality randomization distribution at the same frequency created by trial permutation. The trial permutation method consisted of the generation of randomization distributions for each site pair from each monkey. These distributions were constructed by 1 000 000 independent random permutations of the trial order of a set of 1000 trials randomly selected from the entire set of sessions. For each random permutation, a bivariate AR model was constructed, and coherence or Granger causality spectra were computed, for each site pair. The random rearrangement of the trial order for each site, that is the basis of this process, disrupted the temporal interdependencies existing between the LFPs of those sites, while leaving all other statistical aspects of the data intact. Significance thresholds were derived from the resulting randomization distributions of coherence or Granger causality values for each site pair (Edgington, 1995). The significance thresholds were corrected for multiple comparisons by Dunn's method (Dunn, 1961) in each monkey by the total number of spectral peaks detected over all site pairs and sessions. The corrected significance ($p < .05$) thresholds of coherence and Granger causality are displayed as dotted lines for the example shown in Figure 3.2.

By comparison with these significance thresholds, peaks in the coherence and Granger causality spectra from each session that were significantly greater than the corrected threshold ($p < .05$, corrected) were tabulated. Distributions of significant ($p < 0.05$, corrected) mean peak coherence (Fig. 3.5) and Granger causality (Fig. 3.6) were plotted as a function of frequency, averaged over all pairs and sessions. To facilitate the analysis of differences in the spatial patterning of coherent and directional activity across the frequency spectrum, the full 8 - 90 Hz range was divided into four frequency ranges: alpha (8 - 13 Hz), beta (14 - 30 Hz), low gamma (31 - 58 Hz), and high gamma (63 - 90 Hz).

Network graphs of the mean coherence and Granger Causality interactions over each session for each pair were then constructed for each of the four frequency bands for the three monkeys (Figures 3.7, 3.8 , and 3.9).

3.3 Results

3.3.1 Assessment of behavioral performance within and across sessions

Correlation of the percentage correct (performance) for the 15 bins of trials equally spaced over each session, with time (temporal epoch) did not reveal any significant correlations, (see Figure 3.3). Thus behavioral performance did not significantly change within the recording sessions.

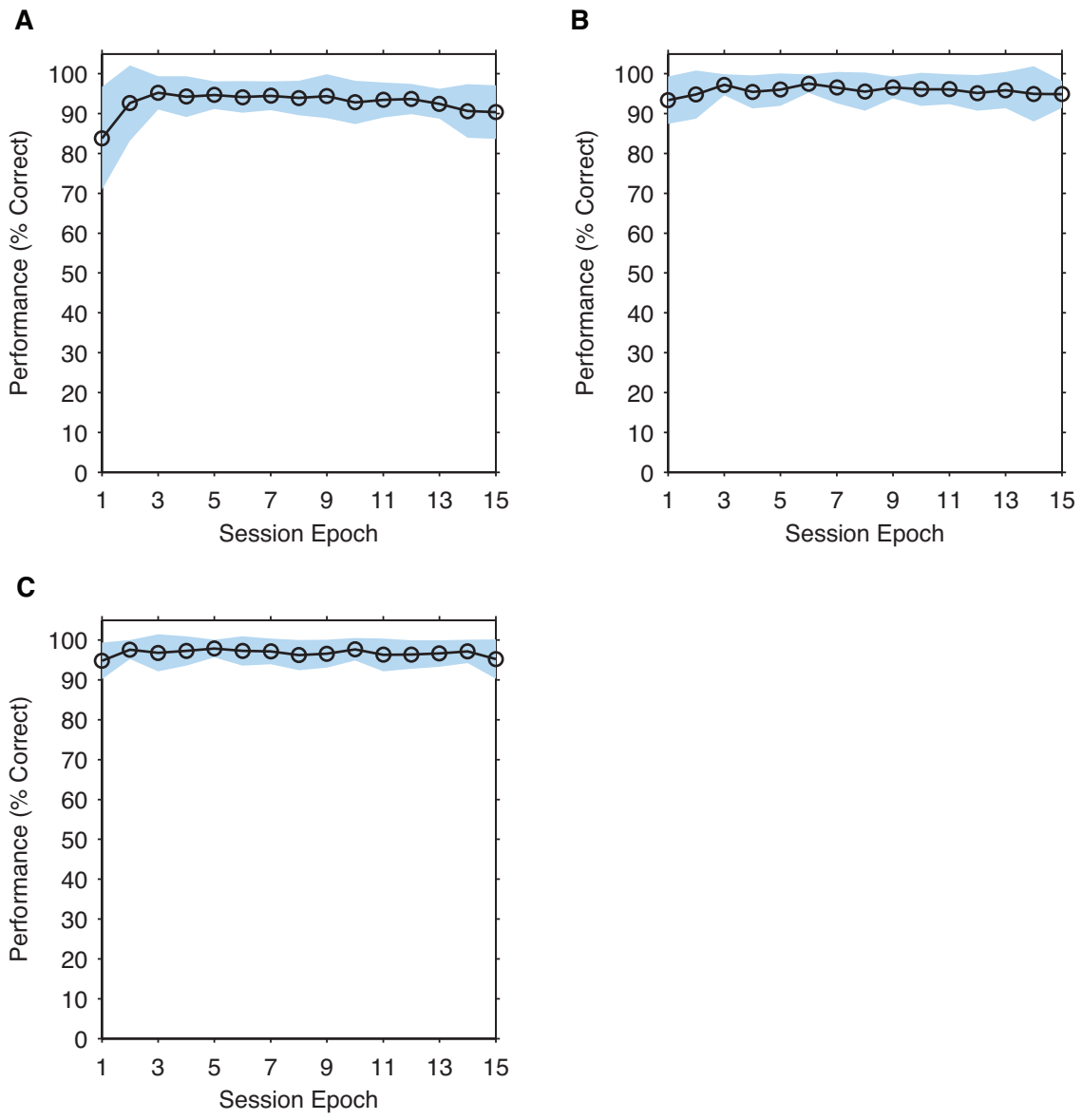

Figure 3.3: Correlation of performance and session epoch displaying the mean percentage correct for 15 bins equally spaced across the temporally ordered ensemble of trials from each session. None of the correlations were significant. (A) GE, ($\rho(13) = -0.37, p < 0.17$, uncorrected); (B) LU, ($\rho(13) = -0.06, p < 0.82$, uncorrected); (C) TI, ($\rho(13) = -0.26, p < 0.34$, uncorrected). Blue shaded regions indicate $+/-1$ standard deviation of the mean.

Correlation between behavioral performance and session was significantly correlated for monkey LU (Figure 3.4 B), showing an increase in performance across the recording sessions. GE and TI did not show a significant correlation between performance and

recording session (Figure 3.4 A,C). The positive correlation in LU (Figure Figure 3.4 B) shows an improvement in behavioral performance over the course of the recording sessions that may be indicative of learning.

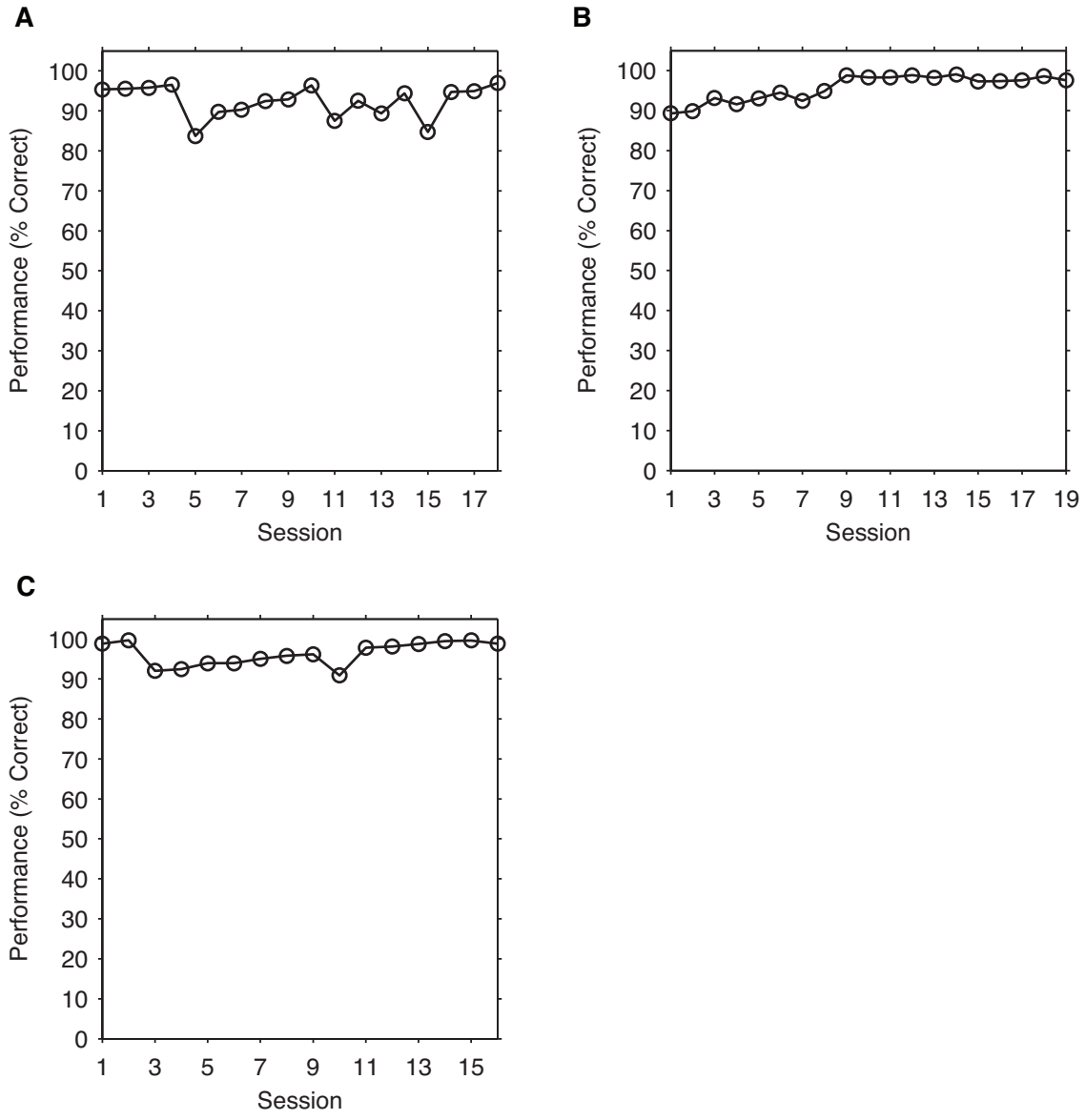

Figure 3.4: Correlation of performance and recording session displaying the mean percentage correct for each of the sessions ordered by the recording sequence. The correlation was significant for monkey LU (B) ($\rho(17) = 0.70, p < 0.003$, corrected). The correlation was not significant for monkeys GE (A) ($\rho(16) = -0.09, p < 0.74$, uncorrected) or TI (C) ($\rho(14) = 0.33, p < 0.22$, uncorrected).

3.3.2 Distributions of significant peak coherence and Granger causality

Power, coherence, relative phase and Granger causality spectra were computed for every session for each of the three monkeys. Peaks were identified in these spectra as representing narrow-band concentrations of rhythmic activity. The distribution of significant peak coherence over all pairs and sessions is shown for each monkey, and averaged across monkeys, in Figure 3.5, A-D. Visual inspection of these distributions revealed a concentration of coherence spanning the alpha and beta bands, in all three monkeys and the average of the three, with a more broad concentration across the gamma band.

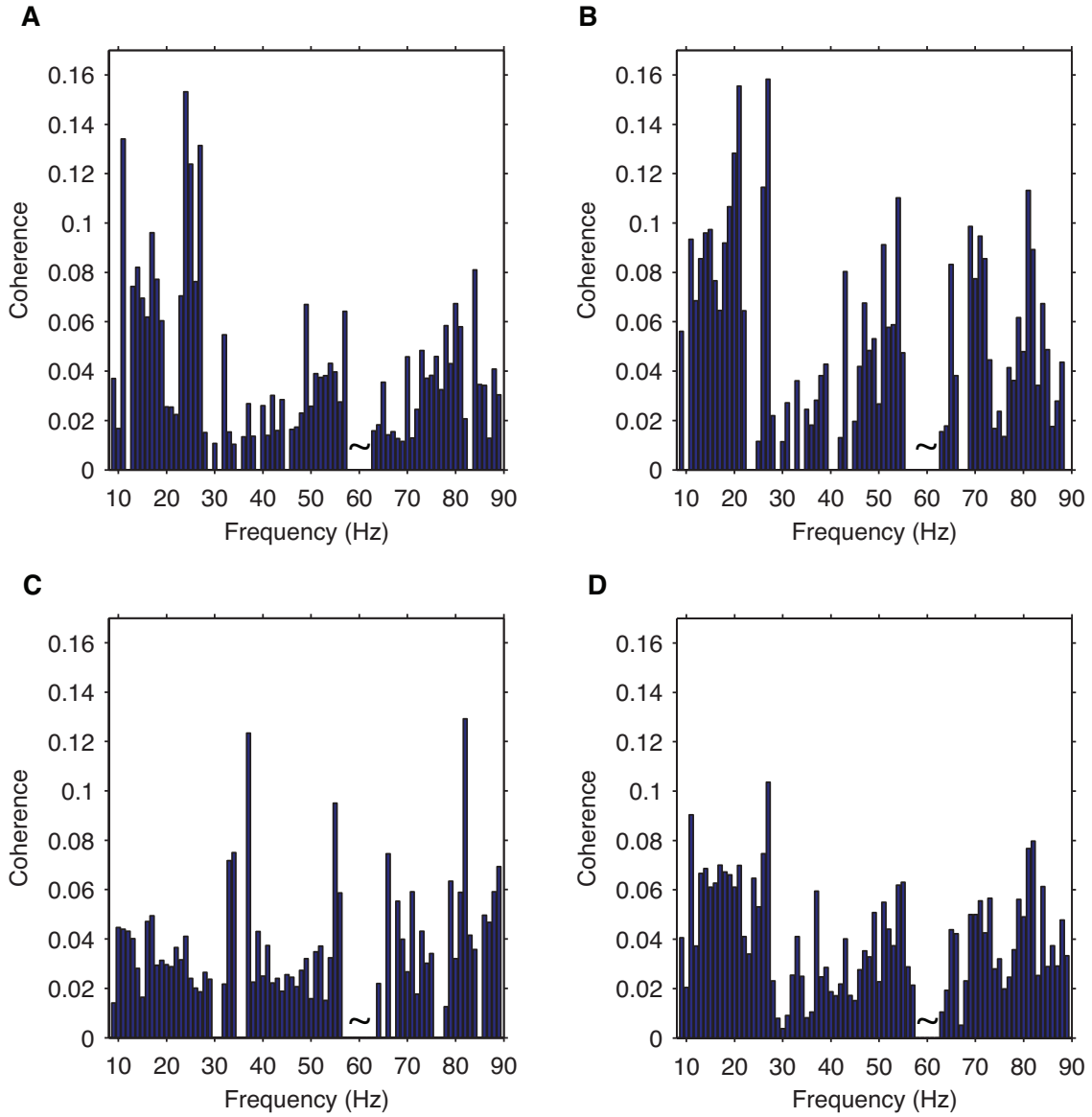

Figure 3.5: Distributions significant mean peak coherence from 8 - 90 Hz. The alternating current symbol denotes the 58 - 63 Hz window where peaks were not tabulated. (A) GE, (B) LU, (C) TI, (D) the average of the three distributions.

Figure 3.6 illustrates the distribution of significant mean peak Granger Causality, averaged over each pair and session for each monkey, in addition to these values averaged across the three monkeys. Qualitatively the distributions show two concentrations of Granger Causality in both the top-down and bottom-up directions occurring below 30 Hz, with a broad distribution occurring above 30 Hz. GE and TI (Figure 3.6 A and C),

show a predominance of top-down over bottom-up Granger causality, whereas the directional effects appear more balanced for LU (Figure 3.6, B) in the alpha and beta bands. None of the monkeys show clear directional effects in the gamma band, though there are small frequency regions of 5-10 Hz that show a large difference between the top-down and bottom-up directions. The mean of Figure 3.6: A, B, and C, shown in Figure 3.6 D, displays a predominance top-down over bottom-up Granger causality in the alpha and beta bands, whereas activity in the gamma band does no show a strong qualitative bias in either direction, except for a predominance of bottom-up activity near 50 Hz.

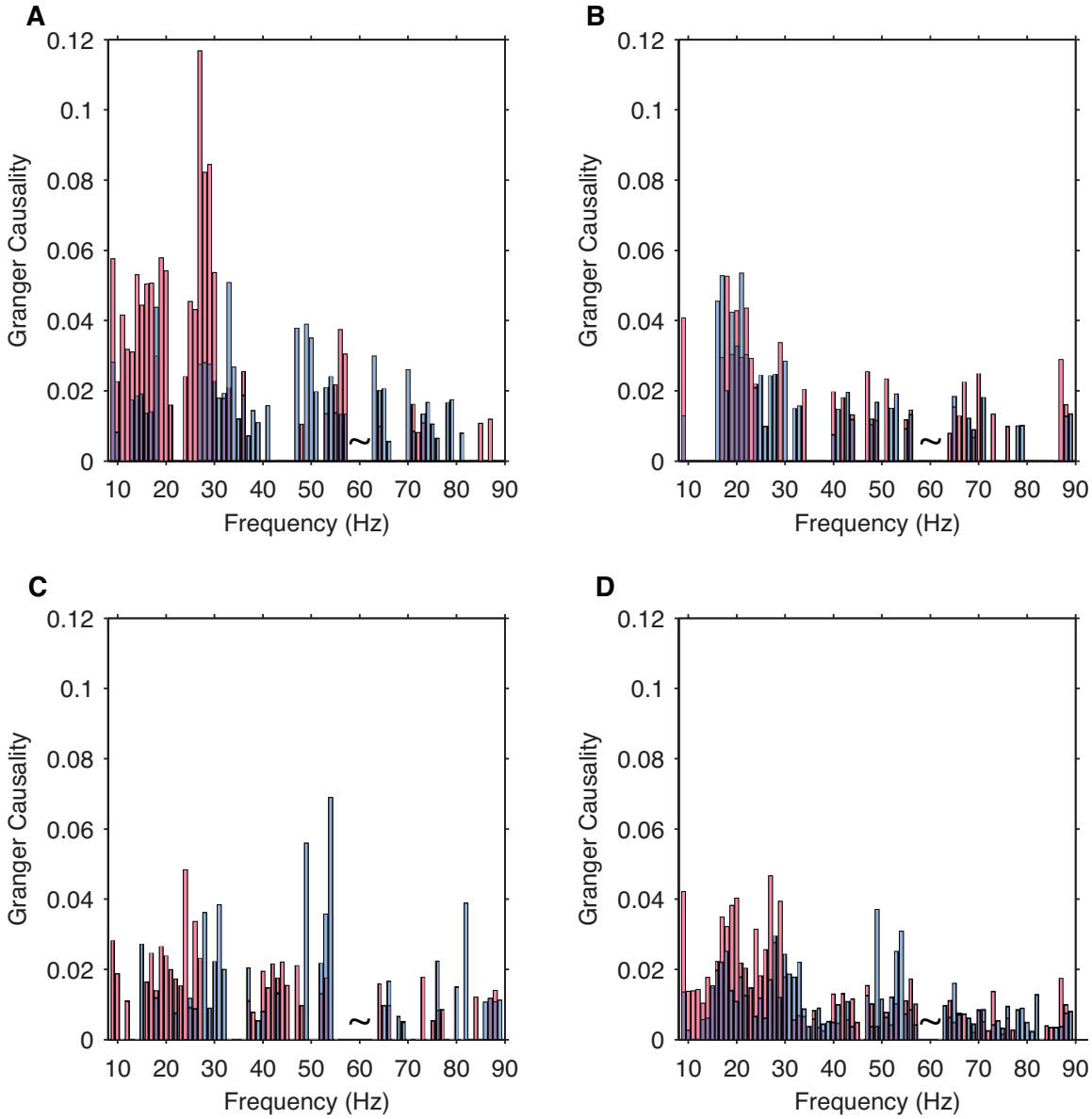

Figure 3.6: Distributions significant mean Granger Causality from 8 - 90 Hz. The alternating current symbol denotes the 58 - 63 Hz window where peaks were not tabulated. Peaks in the top-down direction are pink, while those in the bottom direction are blue. (A) GE, (B) LU, (C) TI, (D) the average of the three distributions.

Based on the results shown in Figures 3.5 and 3.6, it is apparent that there are coherent and Granger causal interactions occurring across the entire 8 - 90 Hz spectrum, and in both directions of interaction, yet the alpha and beta bands show a predominance of top-down directional activity in GE and TI, and the overall average.

3.3.3 Power, coherence, and Granger causality spectra within each frequency band

Table 3.1 tabulates the power spectral peaks that were identified from a total of eight striate sites (three in LU, three in GE, and two in TI) and seven extrastriate sites (one in LU, three in GE, and three in TI) from the total of 53 sessions. The table details the number of sessions exhibiting one or more power spectral peaks for each pair and frequency band for each monkey.

It is apparent from Table 3.1 that the number of power spectral peaks across the four frequency bands increases with frequency for each monkey, and the overall average. The alpha band shows no power spectra peaks in any of the monkeys, while the beta band shows an overall average less than one. This indicates a broadband process since the power spectra of the individual channels tend to follow a $1/f$ distribution as is shown in Figure 3.2. The low gamma and high gamma ranges show much a much higher incidence of peaks since the spectral profile is quite flat over this range, and more likely to show local maxima.

Coherence and Granger causality spectra were computed for all 18 extrastriate-striate pairs of sites in each monkey (three in LU, nine in GE, and six in TI). The significance of each peak was assessed using the randomization procedure described above. Table 3.2 details the number of sessions exhibiting one or more coherence and Granger Causality peaks over pairs and frequency bands, for each monkey.

The results shown in Table 3.2 differ quite markedly from those in Table 3.1. Like Table 3.1, the alpha band shows very few coherence peaks on average in each monkey, and in the overall average, but the beta band shows a large number of coherence peaks. The incidence of significant coherence peaks in the beta range is larger or on par with low and high gamma in each of the monkeys and on average. The incidence of significant

Table 3.1: Counts of the number of sessions that exhibited one or more power spectral peaks over the alpha, beta, low gamma, and high gamma ranges for each recording site

Monkey	Channel	Power				Sessions
		α	β	γ1	γ2	
GE	1	0	0	11	18	18
	2	0	0	5	14	
	3	0	0	4	12	
	4	0	2	8	14	
	5	0	0	5	12	
	6	0	0	8	16	
		M				
		0	0.33	6.83	14.33	
LU	2	0	2	7	14	19
	3	0	4	9	19	
	10	0	0	8	19	
	11	0	1	7	19	
		M				
		0	1.75	7.75	17.75	
TI	1	0	0	0	0	16
	2	0	0	1	7	
	3	0	3	0	0	
	8	0	0	0	0	
	9	0	0	4	7	
		M				
		0	0.6	1	2.8	
		M (over monkeys)				17.67
		0	0.80	5.13	11.40	

Table 3.2: Counts of the number of sessions that exhibited one or more significant coherence and Granger causality peaks over the alpha , beta, low gamma, and high gamma ranges for each striate-extrastriate pair.

Monkey	Pair		Coherence				TD Granger Causality				BU Granger Causality				Sessions
	E	S	α	β	γ1	γ2	α	β	γ1	γ2	α	β	γ1	γ2	
GE	4	1	0	14	17	17	0	16	5	1	0	0	9	9	18
	4	2	0	10	6	6	0	6	1	1	2	0	2	1	
	4	3	2	7	5	4	0	2	1	0	0	4	1	0	
	5	1	3	15	14	15	1	17	1	1	0	5	8	6	
	5	2	1	14	4	5	4	13	0	0	0	1	2	0	
	5	3	1	17	3	4	1	17	0	1	1	1	0	0	
	6	1	0	15	9	11	5	13	1	2	0	3	6	2	
	6	2	1	8	16	17	1	7	2	1	0	7	9	2	
	6	3	0	10	6	3	0	4	0	0	0	4	0	0	
								M							
			0.89	12.22	8.89	9.11	1.33	10.56	1.22	0.78	0.33	2.78	4.11	2.22	
LU	3	2	3	12	14	15	0	10	5	6	1	8	4	5	19
	3	10	2	12	16	14	0	8	3	1	1	6	5	3	
	3	11	0	19	14	15	1	11	7	7	0	16	7	3	
								M							
			1.67	14.33	14.67	14.67	0.33	9.67	5.00	4.67	0.67	10.00	5.33	3.67	
TI	2	1	2	10	13	12	0	6	2	1	0	4	1	4	16
	2	8	1	13	8	12	1	2	4	2	0	3	0	2	
	3	1	0	16	8	11	2	11	7	3	0	2	8	4	
	3	8	1	13	8	11	0	10	4	1	0	3	2	3	
	9	1	2	2	5	6	3	0	0	2	0	0	0	0	
	9	8	6	9	7	12	3	5	1	4	0	1	2	1	
								M							
			2.00	10.50	8.17	10.67	1.50	5.67	3.00	2.17	0.00	2.17	2.17	2.33	
								M (over monkeys)							17.67
			1.52	12.35	10.58	11.48	1.05	8.63	3.07	2.54	0.33	4.98	3.87	2.74	

Granger causality peaks in the top-down direction shows the beta range to have nearly double the number of instances than the other three bands in each monkey individually, and on average. This pattern is not as pervasive in the bottom-up direction where overall the beta range shows nominally more peaks than low and high gamma ranges, while all three show more peaks than the alpha range.

3.3.4 Network Graphs of spatial distributions of coherence and Granger causality relationships between each pair over the alpha, beta, low gamma, and high gamma frequency ranges

Figures 3.7, 3.8 and 3.9 break down the coherence and Granger causality peaks by pair and frequency band showing the mean magnitude over session as the thickness of the bar or arrow respectively. In monkey GE (Figure 3.7), the mean magnitude, like the mean incidence, shown in Table 3.2, of coherence is the largest in the beta band. The alpha, low and high gamma bands show nominal levels of coherence, though the low and high gamma bands do exhibit appreciable coherence between pairs (5-1) and (6-2). The top-down Granger causality results are similar to the coherence results in the beta band, with large top-down Granger causality values. These top-down influences are complemented by significantly smaller bottom-up influences. The alpha band shows a preponderance of top-down values, with only one small bottom-up influence. The low and high gamma bands show similar patterns of Granger causality, which appears to be dominated by bottom-up influences.

Like monkey GE, monkey LU (Figure 3.8) shows the strongest coherence in the beta band, with nominal levels of coherence in the alpha band. Also like GE, LU shows a similar pattern of coherence in the low and high gamma bands. LU's top-down Granger causality, like GE's, is also highest in the beta band, and favors the top-down direction two to one. The alpha band does not show a clear dominance of either direction overall, with all of the values of a very small magnitude. Like GE, the low and high gamma ranges show similar spatial configurations of Granger causality in addition to similar yet small magnitudes.

Monkey TI (Figure 3.9) exhibits very small coherence magnitudes in the alpha band and very similar patterns of interaction and magnitude for the beta, low gamma and high

gamma bands. Like GE and LU, Granger causality magnitudes are largest in the beta band. The largest magnitudes are in the top-down direction. The alpha band shows only top-down influences, while the low and high gamma bands show influences in both directions. One pair of interest is pair (3-1), which shows a top-down influence in the alpha and beta ranges, with the beta range exhibiting a fairly large magnitude influence, while the low and high gamma ranges show a bottom-up influence for this pair. A difference like this may indicate different roles for the four frequency bands, with alpha and beta involved in modulatory feedback mechanisms, and the gamma band operating in a feed-forward mode.

Overall the spatial maps indicate that the four frequency bands demonstrate rich dynamics of coherence and Granger causality indicating the presence of phase synchronized networks with directional influences. The beta band appears to exhibit the strongest of these dynamics, overall, with strong top-down influences predominating between most pairs. This may indicate a proprietary role for the beta band during the pre-stimulus period.

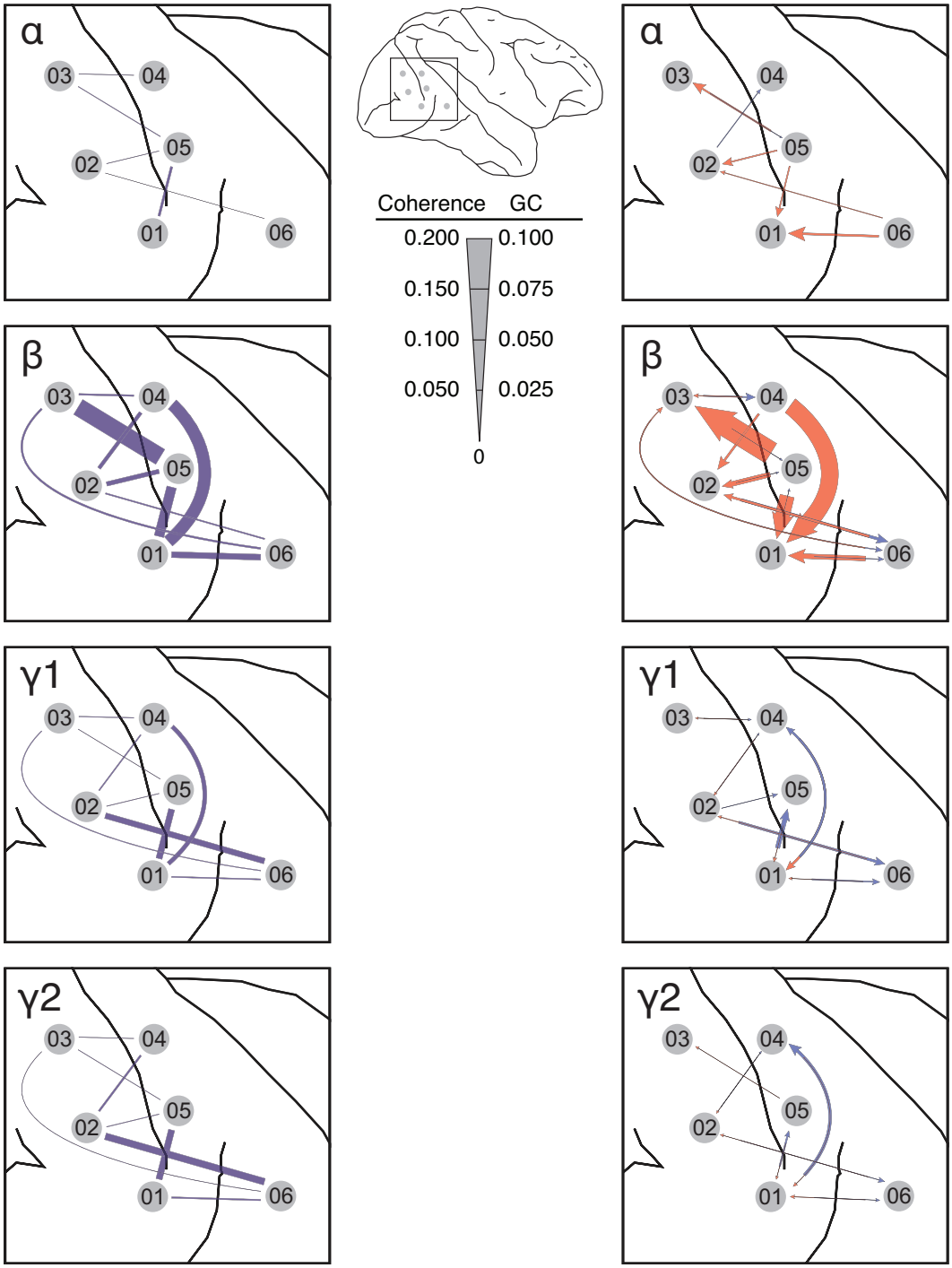

Figure 3.7: Significant mean peak coherence (left panel) and Granger causality (right panel) for the alpha (α), beta (β), low gamma ($\gamma 1$) and high gamma ($\gamma 2$) ranges for each striate-extrastriate pair for monkey GE. Red arrows represent top-down Granger causality, while blue arrows are based on the bottom-up spectra. The thickness of the lines indicates the magnitude of the coherence and Granger causality.

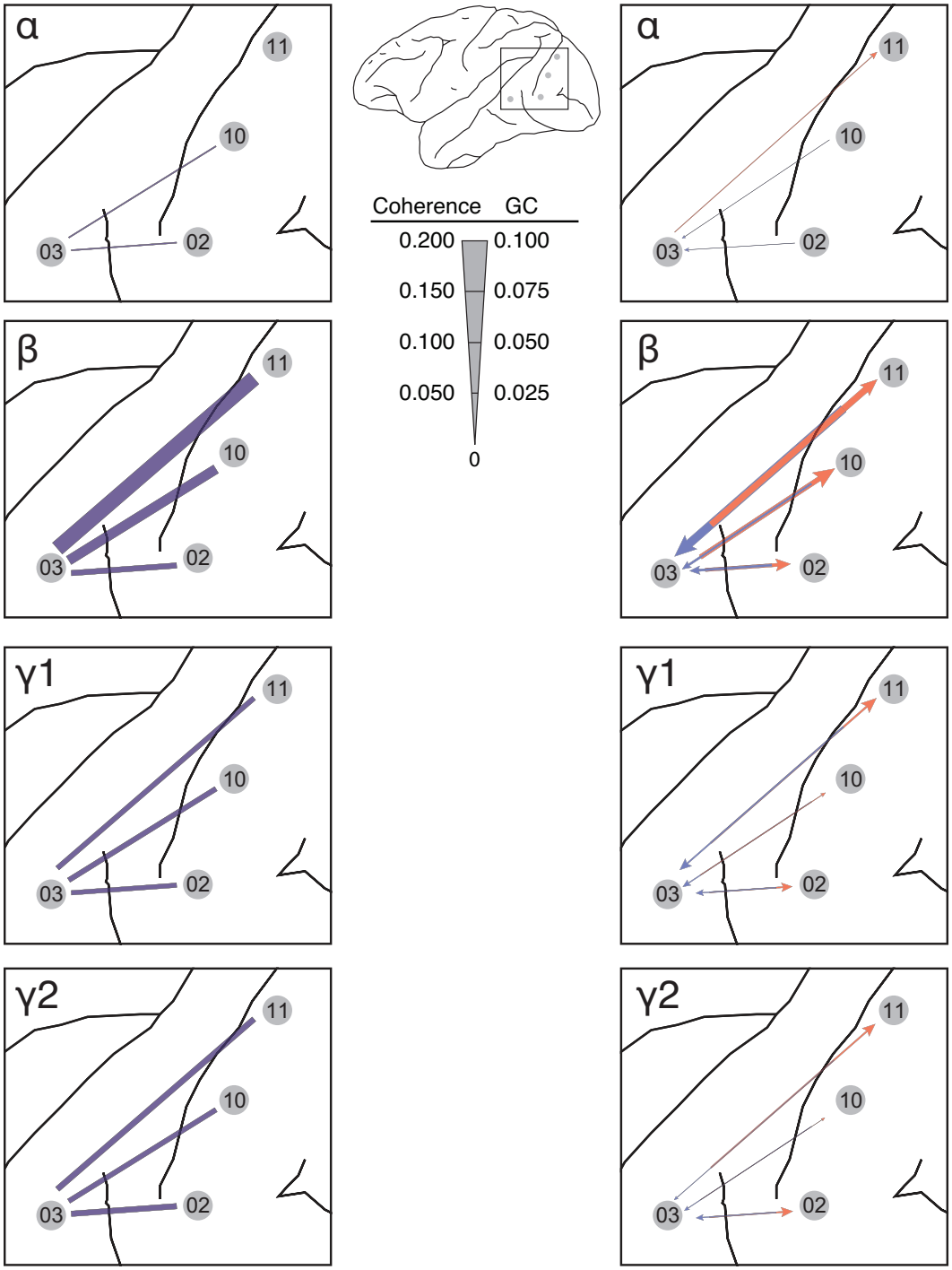

Figure 3.8: Significant mean peak coherence (left panel) and Granger causality (right panel) for the alpha (α), beta (β), low gamma ($\gamma 1$) and high gamma ($\gamma 2$) ranges for each striate-extrastriate pair for monkey LU. Red arrows represent top-down Granger causality, while blue arrows are based on the bottom-up spectra. The thickness of the lines indicates the magnitude of the coherence and Granger causality.

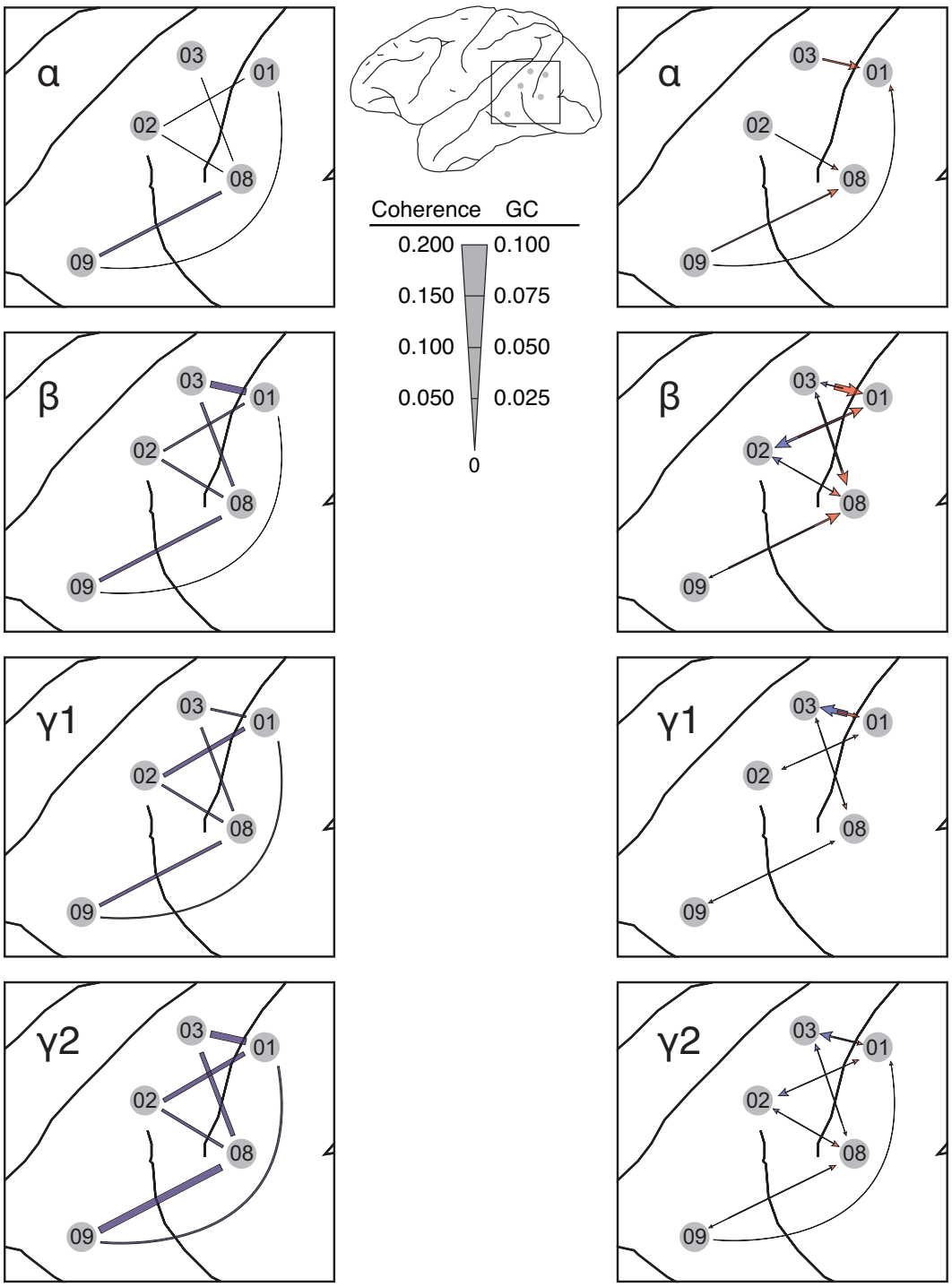

Figure 3.9: Significant mean peak coherence (left panel) and Granger causality (right panel) for the alpha (α), beta (β), low gamma ($\gamma 1$) and high gamma ($\gamma 2$) ranges for each striate-extrastriate pair for monkey TI. Red arrows represent top-down Granger causality, while blue arrows are based on the bottom-up spectra. The thickness of the lines indicates the magnitude of the coherence and Granger causality.

3.4 Discussion

The behavioral results indicate a very stable level of performance both within session and across sessions, with the exception of monkey LU showing a slight increase in performance over the recording session. Generally, there is a homogeneous high level of performance across the sessions and monkeys.

The distributions shown in Figures 3.5 and 3.6 indicate the presence of phase-locked directional oscillatory activity across the frequency spectrum of 8 - 90 Hz. The coherence spectra show a concentration of peaks in the alpha and beta range, with a more broad distribution of peaks through the low and high gamma ranges. A directional effect is present that is larger in the top-down direction for the alpha and beta bands in monkeys GE and TI, in addition to the overall average. The low and high gamma bands do not show a clear predominance in either direction. Tables 3.1 and 3.2 demonstrate that despite a near $1/f$ power spectral distribution (see Figure 3.2), the beta band shows a clear predominance of peaks in the coherence and Granger causality spectra. The dominance of the incidence of beta band Granger causality is most evident in the top-down direction. This result is mirrored in Figures 3.7, 3.8 and 3.9, where the beta band shows the strongest coherence interactions in monkeys GE and LU, and the strongest Granger causality interactions in all three monkeys. Thus the incidence of significant peaks, and the mean magnitude of these peaks calculated over the sessions are both large in the beta band. The predominance of beta band activity may be linked to the spatial scale of centimeters that separate the recording sites, and that the recording sites lie in different visual regions. As discussed in section 2.2.1, gamma oscillations often predominate at a local scale of less than seven millimeters, and link activity in regions with similar tuning properties (Gray, 1999; Kopell et al., 2000; von Stein et al., 2000). This seems to be evident from Table 3.1, where power peaks predominate in the gamma range. Power is a measure of local synchroniza-

tion and thus indexes the degree of phase synchronization in the population measured by the electrode[1]. The local power appears more broadband in the alpha and beta bands (see Figure 3.2), yet the interareal coupling is large for the beta band as evidenced from the high incidence of coherence and Granger causality peaks shown in Table 3.2, and the large magnitude of the coherence and Granger causality peaks between pairs, shown in Figures 3.7, 3.8 and 3.9. These patterns of coherent interaction and top-down directional influences may be signatures of enhanced communication between specific visual regions (Fries, 2005) that is occurring during the pre-stimulus period. This activity may comprise a neurocognitive network that is predicting forthcoming stimuli, or forming inferences that may impact the processing of the subsequent visual stimulus (Engel et al., 2001; Bressler, 2004)

In summary, the current analysis demonstrates that during the pre-stimulus period of a visual discrimination task, rich inter and intraareal dynamics exist within the ventral visual stream while the monkey anticipates the visual stimulus. The dynamics demonstrate intraareal phase-locking that is most consistent in the gamma band, while interareal phase-locking is most consistent in the beta band, and is also the largest in magnitude. Beta band interareal coupling also shows distinct instances of large magnitude top-down influences that are larger than bottom-up influences. In conclusion, the evidence suggests the existence of a phase-locked anticipatory neurocognitive network operating at multiple frequencies. The presence of such a network during a period of anticipation suggests that the interactions between ongoing neural activity play an important role in subsequent processing of the visual stimulus. The functional significance of the dynamics of this anticipatory neurocognitive network are unknown and will be the focus of the following study.

[1]It must be noted, as discussed in section 2.2.1, interdependence is present in the gamma band, though of small magnitude, but between a large number of sites, which supports the stance of Melloni et al. (2009b)

CHAPTER 4

FUNCTIONAL ROLE OF TOP-DOWN MODULATION: ERP GAIN CONTROL

4.1 Introduction

A number of studies have demonstrated that quantitative aspects of ongoing neural activity, that precedes stimulus processing, are significantly correlated with both neural activity elicited by a subsequent stimulus (Arieli et al., 1995; Arieli et al., 1996; Ergenoglu et al., 2004; Grinvald et al., 2003; Leopold and Logothetis, 2003) and a number of behavioral variables (van Dijk et al., 2008; Hanslmayr et al., 2005; Hanslmayr et al., 2007; Wyart and Tallon-Baudry, 2009). Many studies have pointed to the alpha rhythm as disruptive to subsequent stimulus processing. These results show patterns where ongoing alpha activity is decreased in attended locations and increased in unattended locations (Rihs et al., 2007; Rihs et al., 2009; Sauseng et al., 2005). Beta rhythms have been suggested to play a similar role in movement suppression in the motor system (van Wijk et al., 2009), though increases in beta frequency amplitude have been linked to decreases in reaction time during the processing of multisensory stimuli (Senkowski et al., 2006). Other studies have linked enhanced pre-stimulus gamma-band oscillations to perception (Wyart and Tallon-Baudry, 2009) and response time (Gonzalez Andino et al., 2005). Based on the large body

of literature concerning ongoing oscillations that precede stimulus processing, a consensus is emerging that slow oscillations may function to attenuate stimulus processing and perception, whereas fast cortical oscillations (>13 Hz) may facilitate stimulus processing and perception (Hanslmayr et al., 2007), with different rhythms acting at different spatial scales (von Stein and Sarnthein, 2000).

The precise mechanism by which ongoing oscillations modulate stimulus processing has remained highly debated, but much emphasis has been put on the effect of ongoing oscillations on the generation of the ERP. One influential theory holds that the ERP is the result of phase resetting of ongoing oscillations by stimulation, and that the superposition of the phase reset oscillations result in the ERP waveform (Makeig et al., 2002; Klimesch et al., 2007). An opposing theory states that the ERP results from the averaging of an evoked neuronal population response (Shah et al., 2004). A common feature of the ERP that both theories must explain is the relationship between ongoing neural activity and aspects of the ERP waveform such as the amplitude of ERP components. One aspect of ongoing activity in relationship to the ERP that has received little attention is the contribution of interdependent activity between visual regions to the generation of the ERP. As the previous study in Chapter 3 demonstrated: pre-stimulus ongoing activity recorded from distributed sites in the ventral visual stream shows distinct interdependencies revealed by coherent interactions and directional influences at multiple frequency bands. Based on the highly recurrent nature of visual cortex (Lamme et al., 1998), it is likely that the ERP waveform is dependent on precise interactions between distributed visual regions, and thus on their interdependencies. As previously discussed in section 2.2.1: specific patterns of coherence may facilitate communication between distributed processing regions. Thus particular patterns and magnitudes of coherent ongoing oscillations and directional influences may impact the ERP waveform generated by subsequent stimulus processing. This enhanced communication may function to sensitize primary visual cor-

tex so that feedforward stimulus processing is enhanced, or it may increase distributed processing of feedforward inputs giving rise to an enhanced ERP waveform.

One proposed function of top-down modulation is as a component of a gain control mechanism that increases the sensitivity of the targeted neuronal ensemble to stimulus-driven input, and leads to an amplified evoked response (Hillyard and Anllo-Vento, 1998; Hillyard et al., 1998). Alternatively, a sustained bias signal emanating from extrastriate cortex may increase baseline activity in striate cortex and thus enhance subsequent stimulus related activity without enhancing sensitivity to specific stimuli in striate cortex (Luck et al., 1997; Desimone and Duncan, 1995; Martìnez et al., 1999; Murray, 2008).

Von Stein et al. (2000, 2000a) have suggested that ongoing oscillatory synchronization underlies top-down internally generated constraints such as expectation. The beta band, in particular, has been specifically implicated in mediating top-down interactions via long-range synchronization (Liang et al., 2002; Wróbel et al., 1994; Wróbel, 2000). This would suggest that beta band top-down directed influences may have a particularly salient effect on stimulus processing, and thus, on the ERP waveform.

The current study seeks to test the hypothesis that interdependencies between visual regions, within specific frequency bands, contribute to the modulation of the amplitude of the visual ERP (VERP) waveform. Furthermore, it is proposed that beta band top-down anticipatory influences specifically modulate VERP amplitude.

4.2 Methods

4.2.1 Recording

The recording methodology used for this experiment was the same as described in section 3.2.1.

4.2.2 Task

The task used for this experiment was the same as described in section 3.2.2.

4.2.3 Data preprocessing

Data was preprocessed as described in section 3.2.3 with the exception that an additional 110 millisecond period of data was analyzed, which spanned 35 - 145 milliseconds post stimulus onset. This region of the trial contained the early components of the VERP and was subject to the same preprocessing procedures described in section 3.2.3.

4.2.4 Single-trial amplitude estimation

Single-trial early VERP amplitudes were estimated in a 110 millisecond window between 35 milliseconds and 145 milliseconds post-stimulus for each striate site using a template matching procedure (Woody, 1967). Before the application of the template matching procedure, a number of preprocessing steps were performed in addition to those mentioned in sections 3.2.3 and 4.2.3. First, the LFP data from each session were subjected to grand variance normalization. This process resulted in a variance of unity for the concatenation of all trials from each channel of each session. This step was performed to limit differences in VERP magnitude between sessions that could be due to differences in gain between the channels. Each trial was then baseline corrected by subtracting the mean of

the pre-stimulus period (-85 - 0 milliseconds) from all points of the trial. The data were then spline interpolated to a resolution of 1000 Hz. To improve the signal-to-noise ratio of the VERPs, the data were then low pass filtered using a Hamming-windowed Finite Impulse Response filter (-6db at 39 Hz, 140 db per octave falloff).

The template matching procedure consisted of a process whereby the latency τ^r and amplitude α^r of the *r*th trial's VERP waveform $Z^r(k)$ were obtained with respect to a template VERP waveform $E(k)$, where k is the sample index. By computing the Pearson correlation between each VERP waveform $Z^r(k)$, of trial r, and the template $E(k)$, at one sample lags of $+/-$ 25% of the waveform's length, the lag at which the two waveforms exhibit maximal correlation was determined. This lag is the estimated latency τ^r of the VERP waveform with respect to the template. By aligning the template $E(k)$ and single-trial VERP waveform $Z^r(k)$ by the estimated latency τ^r, an amplitude estimate of the single-trial VERP waveform may be derived relative to the template. Single-trial VERP amplitude estimates α^r were obtained for each of the *r*th trials, adapted from (Truccolo et al., 2002), and were computed as:

$$\alpha^r = \frac{\langle Z^r(k)E(k+\tau^r)\rangle_k}{\langle E(k)^2\rangle_k}. \tag{4.1}$$

This measure is bounded by 0 and infinity, excluding cases where the single-trial and template waveforms and inverted, and represents the scalar value by which each point of the latency adjusted template waveform must be multiplied to match the amplitude of the single-trial VERP waveform, as expressed in equation 4.2.

$$Z^r(k) = \alpha^r E(k+\tau^r). \tag{4.2}$$

When the template waveform and the estimated waveform have equal amplitude $\alpha^r = 1$.

In order to reject spurious estimates, matches where the maximum correlation coeffi-

cient between the template and the estimated VERP was below $r = 0.60$ were discarded. Since the α values for each single-trial VERP of each channel were required to be relative to the same template, this dictated that they be matched to a template of equal amplitude. This can be achieved by matching each trial to a template that is the average of the ensemble of all trials, over all stimulus types from all sessions, but this will cause a significant decrease in the correlation between the single trial VERPs and the template due to loss of variability in the VERP waveshape that is specific to the session and stimulus type. To overcome this problem, we took the approach of deriving α estimates for the grand stimulus type averages (the average over all trials, over all sessions, for each of the four stimulus types) with respect to the grand average (the average over all trials, from all sessions and stimulus types). Using these four α estimates, we then rescaled each of the four stimulus type grand averages by division by α so that each of the four stimulus type averages were of the same amplitude as the grand average VERP waveform. To correct for differences in the stimulus type ensemble averages across sessions, this process was repeated where the session specific stimulus type ensemble averages were matched to the four rescaled grand stimulus type averages and rescaled so that each of the four stimulus type averages from each session were of the same amplitude, both across and between sessions. These rescaled stimulus type averages were then used as the templates for the estimation of single-trial VERP amplitudes. Single trial amplitude estimates were then obtained for each striate channel of each monkey within the interval of 35 - 145 milliseconds. The start of this interval was chosen to capture the earliest onset of stimulus processing, while the end was based on the previously described temporal separation between stimulus and response processing (Ledberg et al., 2007). An example of the template matching procedure is shown in Figure 4.1.

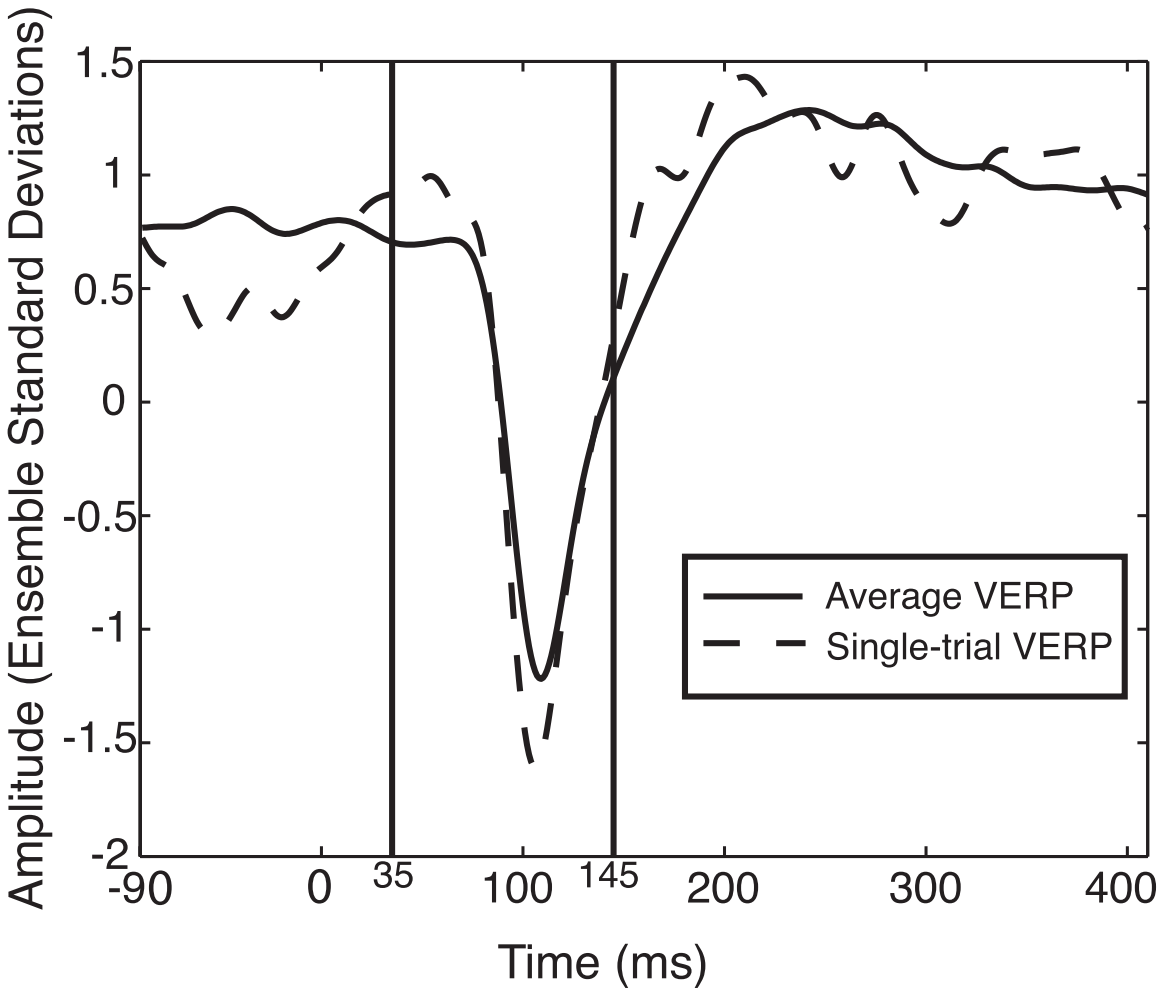

Figure 4.1: A representative single-trial VERP (dashed line) from a recording site in primary visual cortex (V1) is shown superimposed on the average VERP (solid line) computed over an ensemble of trials from the same site. The average VERP is the template for template matching procedure. The vertical lines mark the boundaries of the time period used for template matching. The amplitude of the single-trial VERP is 32% greater than that of the average VERP, and precedes it by 3 milliseconds.

4.2.5 Trial subensembles

Single-trial VERP amplitude estimates were obtained for each LFP trial for each striate site, and then ordered by magnitude. This resulted in a list of trials for each striate site ordered by estimated VERP amplitude. Each list was divided into 400-trial subensembles, overlapped by 75%. The value of 400 trials per subensemble was chosen as an acceptable

trade-off between maximizing the number of subensembles while providing enough trials per subensemble to produce a stable AR model. Figure 4.2 shows an example of the resulting subensembles for GE striate channel three, colored by the VERP mean amplitude scaling factor. The smooth gradation of VERP amplitude between 35 - 145 milliseconds, and the smooth gradation in color demonstrates the accuracy of the template matching procedure.

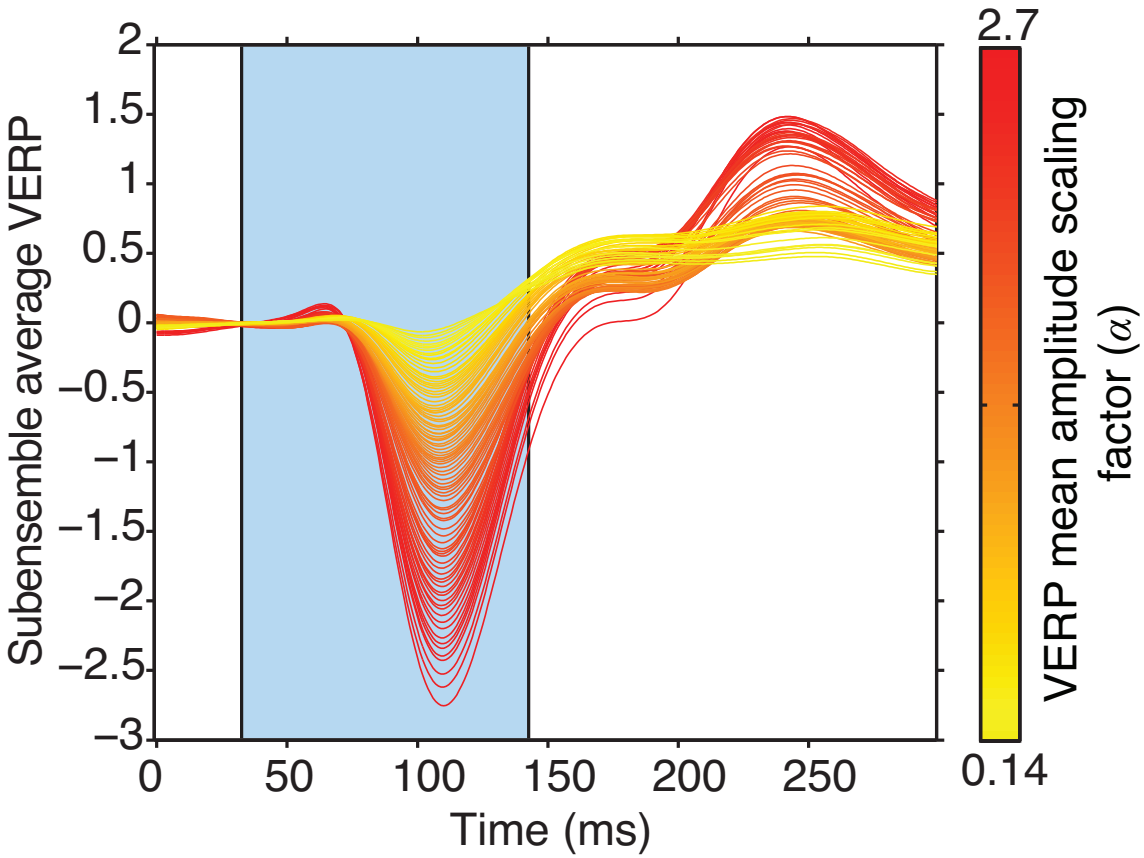

Figure 4.2: Subensemble result for GE striate channel 3. Each line denotes the VERP for one subensemble and is colored according to the mean of the amplitude estimates (α) from each single-trial that contributed to the subensemble.

4.2.6 Correlation of pre-stimulus coherence and Granger causality with post-stimulus VERP amplitude

For each subensemble of trials, we computed peak coherence, Granger causality, in both directions, and the relative phase for each striate-extrastriate pair over the alpha, beta, low gamma and high gamma frequency ranges (as defined in Chapter 3) as the local spectral maximum, employing the same AR preprocessing stages and parameters described in section 3.2.5. These peaks were thresholded for significance using the same randomization distribution and multiple comparisons correction as described in section 3.2.6. Relative phase values were calculated at the frequency that corresponded with the significant peak coherence. A Spearman rank correlation coefficient was then computed between the magnitude of the significant peaks in the Granger causality and coherence spectra, and the mean VERP amplitude estimates of the corresponding subensembles. The correlation was computed separately for Granger causality in both the top-down and bottom-up directions. The correlation p-values were corrected for multiple comparisons using Dunn's method (Dunn, 1961).

4.2.7 Assessment of single-trial VERP estimates within and across sessions

To assess variation in the VERP estimates within sessions, each session was divided into 15 bins containing an equal number of trials, in the order that they were recorded. The single-trial VERP amplitude estimates for each trial, within each bin, were averaged for each of the striate recording sites. These 15 values from each session were then averaged and Spearman correlation was performed between the averaged VERP amplitude estimates and bin number to assess if the single trial VERP amplitude estimates were systematically changing over session.

To assess variation in the VERP estimates across the sessions, the VERP estimates were averaged for each striate recording site for each session and then ordered in the temporal succession in which the sessions were recorded. Spearman correlation was performed between the averaged VERP amplitude and the order in which the sessions were recorded to assess any systematic change in the VERP amplitude over the recording period.

4.3 Results

4.3.1 Correlation analysis

For each site pair, 400 trial subensembles were created that were ordered by the single-trial striate VERP amplitude. A Spearman rank correlation was then computed between the pre-stimulus alpha, beta, low gamma and high gamma significant peak coherence and the post-stimulus (35 - 145 milliseconds) striate VERP mean amplitude scaling factor from each subensemble. This process was repeated with top-down Granger causality, and bottom-up Granger causality spectra for each of the four frequency bands. The correlation results for coherence and mean VERP amplitude are tabulated in Tables 4.1 - 4.4, while those for Granger causality are tabulated in Tables 4.5 - 4.8. Figures 4.3 through 4.5 show spectral and correlation results for pairs in the alpha band with subsensemble coherence or Granger causality values that are correlated with the mean VERP amplitude. Figures 4.6 through 4.14 show this for pairs in the beta band, Figures 4.15 through 4.18 for the low gamma band and Figures 4.19 through 4.21 for the high gamma band.

Correlation analysis of subsensemble coherence and mean VERP amplitude

In the alpha range (Table 4.1), two of the 18 pairs showed a significant correlation between subensemble coherence and the mean VERP amplitude scaling factor. In LU (pair 3-11, Figure 4.4) the correlation was negative between subsensemble coherence and mean VERP amplitude. This indicates that stronger coherence resulted in a decrease in the subsequent VERP amplitude, while in monkey TI, the correlation was positive (pair 9-8, Figure 4.5) indicating that increased pre-stimulus coherence in the alpha band results in a larger VERP. The beta range (Table 4.2) showed an impressive number of significant correlations between pre-stimulus coherence and the VERP amplitude. Seven of the 18

pairs showed a significant positive correlation, with four of these results in GE (pairs 5-1 Figure 4.6, 5-2 Figure 4.7, 5-3 Figure 4.8, and 6-3 Figure 4.10) and three in LU (pairs 3-2 Figure 4.11, 3-10, Figure 4.12 and 3-11 Figure 4.13). The low gamma band (Table 4.3) also showed a large number of significant correlations between coherence and VERP amplitude. Four of the 18 pairs showed a significant correlation, with LU (pair 3-11 Figure 4.15) exhibiting one significant negative correlation and TI exhibiting two positive correlations (pairs 2-8 Figure 4.16, and 3-1 Figure 4.17) and one negative correlation (pair 3-8 Figure 4.18). The high gamma band (Table 4.4) possessed three significant correlations with each monkey exhibiting one significant correlation, which was negative in GE (pair 6-2 Figure 4.19) and LU (pair 3-10 Figure 4.20) and positive in TI (pair 3-1 Figure 4.21).

Overall the four frequency bands show interesting patterns of correlation between pre-stimulus coherence and mean VERP amplitude. Interestingly the beta band was the only frequency band to consistently show positive correlations, while the other three bands revealed mixed results suggesting that coherent activity in these bands may facilitate or attenuate the subsequent VERP depending on the particular pair considered. In contrast, the beta band correlations consistently showed an amplifying effect on the VERP.

Correlation analysis of subsensemble Granger causality and mean VERP amplitude

The Granger causality results show a pattern of top-down influence that is completely absent in the bottom-up direction in all pairs and frequency ranges, and is abundant in the beta band. Correlation of top-down Granger causality and mean VERP amplitude is present in only one case in the alpha band, with no significant correlations in either the low or high gamma bands. The alpha band Granger causality revealed one significant negative correlation in GE (pair 6-2 Figure 4.3) between top-down alpha band Granger causality and mean VERP amplitude. In the beta band, of the nine extrastriate-striate pairs in GE,

three pairs showed a significant positive correlation between top-down Granger causality and mean VERP amplitude (pairs 5-1 Figure 4.6, 5-3 Figure 4.8, and 6-1 Figure 4.9). Two of three extrastriate-striate pairs in LU also showed a significant positive correlation between top-down Granger causality and mean VERP amplitude (pairs 3-10 Figure 4.12, and 3-11 Figure 4.13), and one of six pairs showed the same result in TI (pair 3-1 Figure 4.14). Overall, six of the 18 pairs from the three monkeys showed a positive correlation between top-down beta band Granger causality and mean subensemble VERP amplitude. Of these six pairs, four were also positively correlated with coherence. This confluence between the coherence and Granger causality results did not occur for any of the other frequency bands. As stated previously, the low and high gamma bands did not show any significant correlations between Granger causality and VERP amplitude, and overall of the frequency bands there were no significant correlations between VERP amplitude and bottom-up Granger causality.

Table 4.1: Correlation results of subsensemble peak coherence versus subensemble mean VERP amplitude, and subsensemble coherence statistics for the alpha band.

Monkey	Pair		ρ	Coherence f (Hz)		Coherence	
	E	S		*M*	*SD*	*M*	*SD*
GE	4	1	-.60	11.00	2.45	.046	0.016
	4	2	.00	12.00	0.71	.022	0.009
	4	3	-.70	10.40	1.34	.033	0.007
	5	1	.10	12.75	0.46	.074	0.013
	5	2	-.07	10.11	1.81	.043	0.018
	5	3	-.14	8.00	0.00	.059	0.011
	6	1	1.00	12.67	0.58	.037	0.009
	6	2	.35	9.00	1.47	.022	0.007
	6	3	-.55	8.89	1.62	.024	0.007
LU	3	2	.39	11.57	1.51	.026	0.009
	3	10	.41	9.22	1.42	.106	0.033
	3	11	-.86*	8.00	0.00	.113	0.032
TI	2	1	-.20	11.25	1.50	.016	0.004
	2	8	.21	12.71	0.49	.023	0.006
	3	1	1.00	10.00	0.00	.016	0.000
	3	8	.50	12.13	0.99	.019	0.004
	9	1	-.37	11.56	1.33	.018	0.005
	9	8	.45*	11.05	1.81	.060	0.022

* $p < 0.05$. ** $p < 0.01$. *** $p << 0.001$, corrected

Table 4.2: Correlation results of subsensemble peak coherence versus subensemble mean VERP amplitude, and subsensemble coherence statistics for the beta band.

Monkey	Pair		ρ	Coherence f (Hz)		Coherence	
	E	S		*M*	*SD*	*M*	*SD*
GE	4	1	-.39	26.36	3.30	0.055	0.023
	4	2	-.50	21.54	3.13	0.029	0.010
	4	3	-.71	21.13	2.17	0.044	0.011
	5	1	.53***	15.38	1.09	0.095	0.028
	5	2	.34*	17.74	2.07	0.037	0.015
	5	3	.37**	17.59	1.30	0.129	0.039
	6	1	.17	17.28	1.55	0.053	0.019
	6	2	.08	19.32	1.69	0.020	0.007
	6	3	.69***	19.00	2.10	0.025	0.008
LU	3	2	.58**	18.78	3.05	0.031	0.013
	3	10	.52***	19.40	3.82	0.079	0.027
	3	11	.47***	19.26	1.39	0.149	0.059
TI	2	1	-.03	23.53	3.03	0.024	0.009
	2	8	-.06	23.50	4.32	0.023	0.008
	3	1	.23	21.30	1.65	0.050	0.021
	3	8	-.06	23.94	3.23	0.027	0.010
	9	1	-.26	22.00	4.29	0.023	0.004
	9	8	.02	20.36	5.48	0.041	0.017

* $p < 0.05$. ** $p < 0.01$. *** $p \ll 0.001$, corrected

Table 4.3: Correlation results of subsensemble peak coherence versus subensemble mean VERP amplitude, and subsensemble coherence statistics for the low gamma band.

Monkey	Pair		ρ	Coherence f (Hz)		Coherence	
	E	S		*M*	*SD*	*M*	*SD*
GE	4	1	-.02	52.54	3.51	0.031	0.011
	4	2	-.42	46.50	7.62	0.024	0.007
	4	3	-1.00	43.00	11.31	0.033	0.006
	5	1	-.33	53.35	5.24	0.043	0.012
	5	2	-.57	49.71	6.94	0.019	0.008
	5	3	.25	44.40	5.44	0.018	0.005
	6	1	-.03	45.56	8.59	0.020	0.006
	6	2	.13	46.59	6.72	0.038	0.013
	6	3	.39	46.56	5.64	0.017	0.004
LU	3	2	0.02	49.48	5.43	0.027	0.011
	3	10	-0.30	47.37	5.53	0.030	0.011
	3	11	-0.49**	44.38	7.47	0.018	0.006
TI	2	1	.32	48.21	5.72	0.038	0.013
	2	8	.51**	48.63	4.37	0.021	0.009
	3	1	.53**	46.36	6.70	0.026	0.014
	3	8	-.55***	44.52	5.97	0.021	0.006
	9	1	-.02	52.54	3.51	0.031	0.011
	9	8	-.42	46.50	7.62	0.024	0.007

* $p < 0.05$. ** $p < 0.01$. *** $p << 0.001$, corrected

Table 4.4: Correlation results of subsensemble peak coherence versus subensemble mean VERP amplitude estimate, and subsensemble coherence statistics for the high gamma band.

Monkey	Pair		ρ	Coherence f (Hz)		Coherence	
	E	S		*M*	*SD*	*M*	*SD*
GE	4	1	.45	76.31	2.85	0.044	0.013
	4	2	-.46	74.00	1.93	0.026	0.006
	4	3	1.00	89.50	0.71	0.023	0.007
	5	1	-.29	77.17	8.37	0.040	0.012
	5	2	.07	73.00	7.35	0.019	0.004
	5	3	.17	78.05	7.90	0.018	0.004
	6	1	-.21	83.19	6.68	0.018	0.004
	6	2	-.34**	81.06	6.47	0.039	0.014
	6	3	.12	83.54	5.70	0.016	0.003
LU	3	2	-.26	76.79	6.25	0.032	0.011
	3	10	-.44***	76.56	7.07	0.037	0.019
	3	11	.31	77.09	7.28	0.018	0.005
TI	2	1	.23	79.18	7.13	0.038	0.013
	2	8	-.01	77.58	8.75	0.019	0.006
	3	1	0.75***	82.70	6.28	0.050	0.027
	3	8	-0.25	77.21	8.81	0.031	0.013
	9	1	0.11	81.92	5.02	0.016	0.003
	9	8	0.01	77.46	7.90	0.062	0.014

* $p < 0.05$. ** $p < 0.01$. *** $p << 0.001$, corrected

Table 4.5: Correlation results of subsensemble peak Granger causality versus subensemble mean VERP amplitude, and subsensemble Granger causality statistics for the alpha band.

Monkey	Pair		Top-down					Bottom-up				
				GC f (Hz)		GC			GC f (Hz)		GC	
	E	S	ρ	*M*	*SD*	*M*	*SD*	ρ	*M*	*SD*	*M*	*SD*
GE	4	1	-.30	10.12	1.32	0.028	0.013	-	-	-	-	-
	4	2	-1.00	12.00	1.41	0.013	0.005	.60	11.50	1.29	0.013	0.004
	4	3	-	-	-	-	-	.40	12.00	1.41	0.022	0.006
	5	1	-	-	-	-	-	.50	12.00	1.00	0.024	0.005
	5	2	-.14	10.85	1.64	0.023	0.010	.06	9.45	1.69	0.014	0.004
	5	3	-1.00	13.00	0.00	0.092	0.007	-1.00	11.50	2.12	0.024	0.010
	6	1	.50	12.20	0.84	0.022	0.003	-	-	-	-	-
	6	2	-.79**	10.93	1.79	0.015	0.004	-	8.00	0.00	0.015	0.000
	6	3	1.00	10.00	2.83	0.017	0.010	-1.00	13.00	0.00	0.019	0.003
LU	3	2	-	-	-	-	-	-.50	8.00	0.00	0.012	0.001
	3	10	-	12.00	0.00	0.048	0.000	-	8.00	0.00	0.032	0.000
	3	11	.36	9.50	1.57	0.055	0.023	-	-	-	-	-
TI	2	1	1.00	8.67	0.58	0.020	0.005	.71	9.17	2.04	0.024	0.006
	2	8	-	-	-	-	-	-1.00	8.50	0.71	0.012	0.000
	3	1	-.40	8.25	0.50	0.025	0.004	-	-	-	-	-
	3	8	-	-	-	-	-	-	-	-	-	-
	9	1	-.70	10.80	1.64	0.014	0.005	-	-	-	-	-
	9	8	-	13.00	0.00	0.013	0.000	-	9.00	0.00	0.013	0.000

* $p < 0.05$. ** $p < 0.01$. *** $p << 0.001$, corrected

Table 4.6: Correlation results of subsensemble peak Granger causality versus subensemble mean VERP amplitude, and subsensemble Granger causality statistics for the beta band.

Monkey	Pair		Top-down					Bottom-up				
				GC f (Hz)		GC			GC f (Hz)		GC	
	E	S	ρ	*M*	*SD*	*M*	*SD*	ρ	*M*	*SD*	*M*	*SD*
GE	4	1	-.28	27.44	2.57	0.026	0.006	-	-	-	-	-
	4	2	-	21.00	0.00	0.014	0.000	-	-	-	-	-
	4	3	-.50	22.33	3.21	0.019	0.003	-	16.00	0.00	0.018	0.000
	5	1	.52***	17.55	1.38	0.054	0.022	-.38	22.06	6.16	0.035	0.013
	5	2	-.06	15.53	1.21	0.030	0.010	.80	28.50	0.58	0.015	0.002
	5	3	.58***	15.39	0.91	0.085	0.026	-.76	19.55	5.99	0.019	0.005
	6	1	.41*	16.09	1.81	0.027	0.012	-.24	28.36	1.28	0.014	0.005
	6	2	-.14	16.68	2.83	0.020	0.007	-.12	29.37	0.97	0.017	0.005
	6	3	.71	16.40	1.17	0.014	0.005	-.86	15.14	0.90	0.013	0.002
LU	3	2	-.32	22.86	1.95	0.012	0.004	1.00	21.67	0.58	0.011	0.003
	3	10	.60***	19.09	2.76	0.033	0.014	.09	24.03	2.17	0.018	0.005
	3	11	.54**	21.17	2.92	0.052	0.020	.20	22.67	2.13	0.039	0.014
TI	2	1	.19	20.94	6.20	0.013	0.005	.13	18.83	3.477	0.013	0.004
	2	8	.29	18.14	2.41	0.013	0.001	-.50	24.40	1.517	0.008	0.001
	3	1	.55***	19.98	1.90	0.034	0.011	.25	26.86	1.800	0.012	0.004
	3	8	-.15	22.00	2.00	0.011	0.004	.21	25.00	2.268	0.008	0.002
	9	1	-	14.00	0.00	0.012	0.000	.18	20.57	1.988	0.011	0.002
	9	8	.24	19.45	4.14	0.016	0.005	.60	23.20	2.049	0.011	0.002

* $p < 0.05$. ** $p < 0.01$. *** $p << 0.001$, corrected

Table 4.7: Correlation results of subsensemble peak Granger causality versus subensemble mean VERP amplitude, and subsensemble Granger causality statistics for the low gamma band.

Monkey	Pair		Top-down					Bottom-up				
				GC f (Hz)		GC			GC f (Hz)		GC	
	E	S	ρ	*M*	*SD*	*M*	*SD*	ρ	*M*	*SD*	*M*	*SD*
GE	4	1	-.11	32.13	1.68	0.023	0.009	-.54	51.14	2.79	0.017	0.005
	4	2	-	-	-	-	-	1.00	49.50	10.61	0.015	0.004
	4	3	-	-	-	-	-	-	-	-	-	-
	5	1	-.30	52.60	2.30	0.012	0.003	-.36	48.93	7.38	0.023	0.006
	5	2	-1.00	47.00	8.49	0.014	0.002	-.66	52.17	9.95	0.009	0.002
	5	3	.70	49.20	5.89	0.015	0.006	-	-	-	-	-
	6	1	.00	50.25	2.22	0.010	0.002	-.31	52.75	5.95	0.009	0.002
	6	2	-.28	37.75	7.53	0.016	0.003	-.04	46.17	11.41	0.013	0.005
	6	3	-	-	-	-	-	-	-	-	-	-
LU	3	2	-.14	44.86	2.27	0.016	0.005	-	-	-	-	-
	3	10	-	47.00	0.00	0.011	0.000	-1.00	49.00	1.15	0.010	0.004
	3	11	.30	44.78	7.43	0.014	0.006	-.18	53.08	2.75	0.014	0.005
TI	2	1	-.50	41.33	0.58	0.010	0.002	.32	44.17	1.85	0.014	0.003
	2	8	-	-	-	-	-	-	-	-	-	-
	3	1	.06	42.12	2.56	0.019	0.007	.41	49.17	4.26	0.021	0.007
	3	8	-	-	-	-	-	-	39.00	0.00	0.015	0.000
	9	1	-	-	-	-	-	-	-	-	-	-
	9	8	-.02	49.73	4.62	0.019	0.005	-	-	-	-	-

* $p < 0.05$. ** $p < 0.01$. *** $p << 0.001$, corrected

Table 4.8: Correlation results of subsensemble peak Granger causality versus subensemble mean VERP amplitude, and subsensemble Granger causality statistics for the high gamma band.

Monkey	Pair		Top-down					Bottom-up				
				GC f (Hz)		GC			GC f (Hz)		GC	
	E	S	ρ	*M*	*SD*	*M*	*SD*	ρ	*M*	*SD*	*M*	*SD*
GE	4	1	-	67.00	0.00	0.021	0.000	-	-	-	-	-
	4	2	-	66.00	0.00	0.017	0.000	-	-	-	-	-
	4	3	-	-	-	-	-	-	-	-	-	-
	5	1	.21	81.75	8.97	0.009	0.003	.06	75.02	6.24	0.014	0.006
	5	2	-1.00	67.67	3.79	0.013	0.000	-	64.00	0.00	0.011	0.000
	5	3	.46	80.43	6.97	0.010	0.002	-.02	78.67	4.24	0.010	0.002
	6	1	.03	72.59	1.87	0.011	0.002	-.90	72.20	5.17	0.010	0.002
	6	2	-.60	73.89	6.86	0.011	0.003	-.19	82.23	4.33	0.010	0.003
	6	3	.50	83.67	5.86	0.009	0.001	-	71.00	0.00	0.009	0.000
LU	3	2	.25	70.57	1.40	0.012	0.003	-	86.00	0.00	0.010	0.000
	3	10	-	68.00	0.00	0.008	0.000	.80	85.25	2.22	0.024	0.005
	3	11	.14	72.67	4.59	0.011	0.002	.10	76.82	4.73	0.012	0.004
TI	2	1	-.21	82.90	6.47	0.012	0.003	1.00	75.33	11.02	0.008	0.002
	2	8	-	87.00	0.00	0.009	0.000	-	-	-	-	-
	3	1	-.22	79.92	7.25	0.012	0.004	.14	77.60	4.20	0.017	0.006
	3	8	.50	85.67	0.58	0.019	0.000	-	-	-	-	-
	9	1	-	-	-	-	-	-	72.00	0.00	0.010	0.000
	9	8	-.75	79.00	6.11	0.013	0.004	-1.00	78.00	12.73	0.012	0.006

* $p < 0.05$. ** $p < 0.01$. *** $p \ll 0.001$, corrected

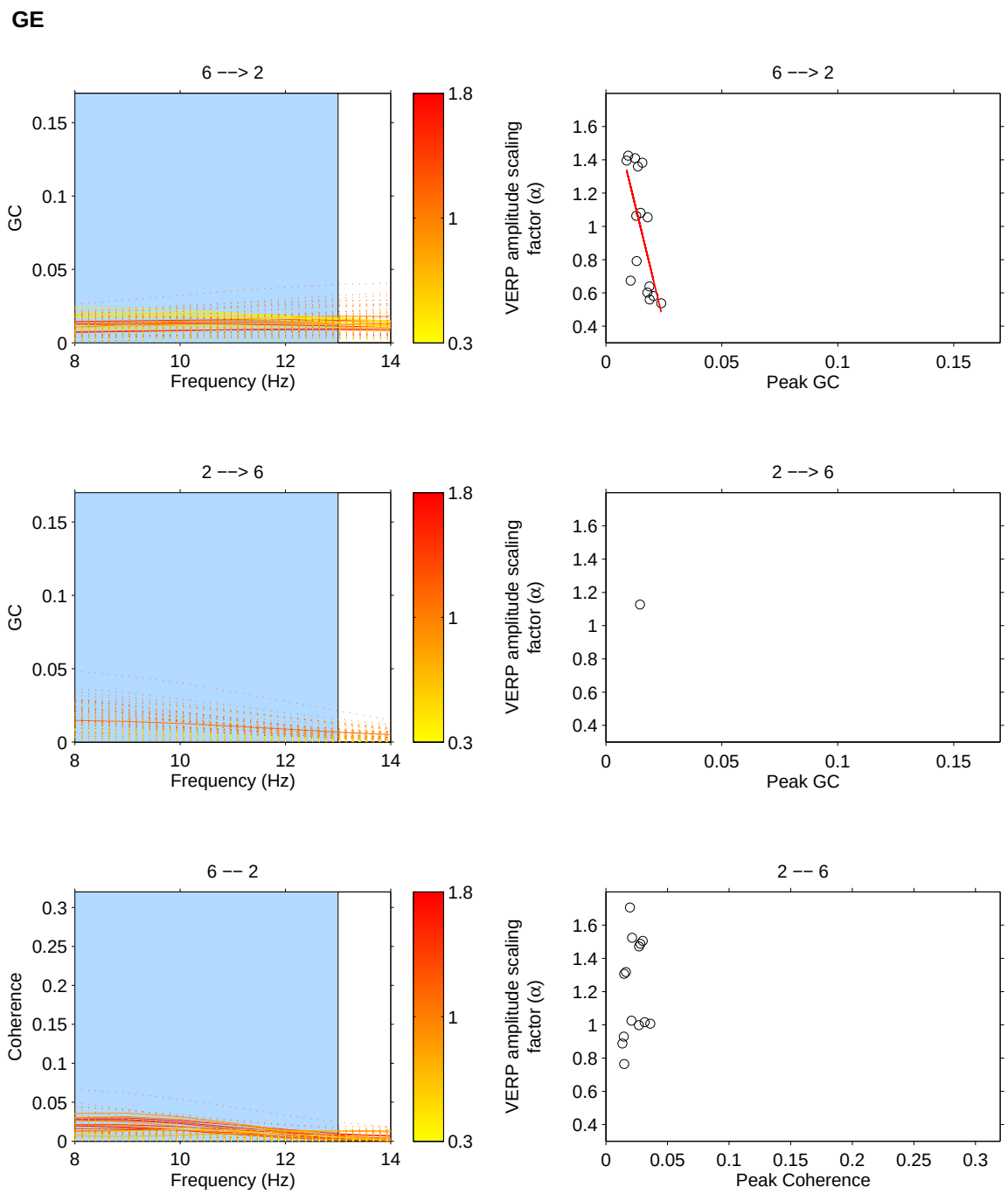

Figure 4.3: Subensemble spectra for top-down and bottom-up Granger causality and coherence (left panels) and the correlations between significant alpha-range Granger causality and coherence spectral peaks with subensemble mean striate VERP amplitude (right panels) for pair GE 6-2. Significant correlations are fit with a regression line. Spectra with significant peaks are drawn in solid lines. Spectra without significant peaks are drawn with dotted lines.

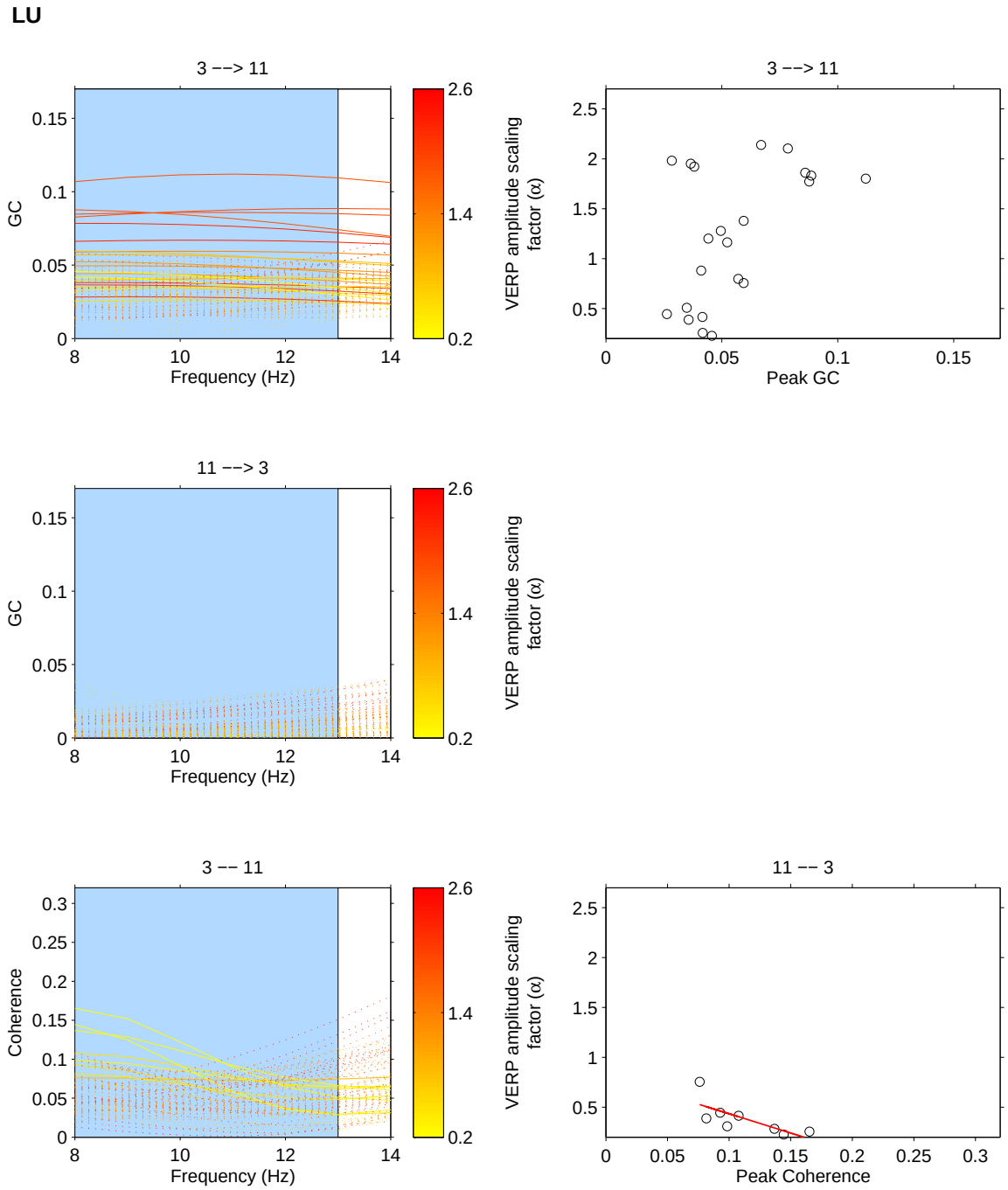

Figure 4.4: Subensemble spectra for top-down and bottom-up Granger causality and coherence (left panels) and the correlations between significant alpha-range Granger causality and coherence spectral peaks with subensemble mean striate VERP amplitude (right panels) for pair LU 3-11. Significant correlations are fit with a regression line. Spectra with significant peaks are drawn in solid lines. Spectra without significant peaks are drawn with dotted lines.

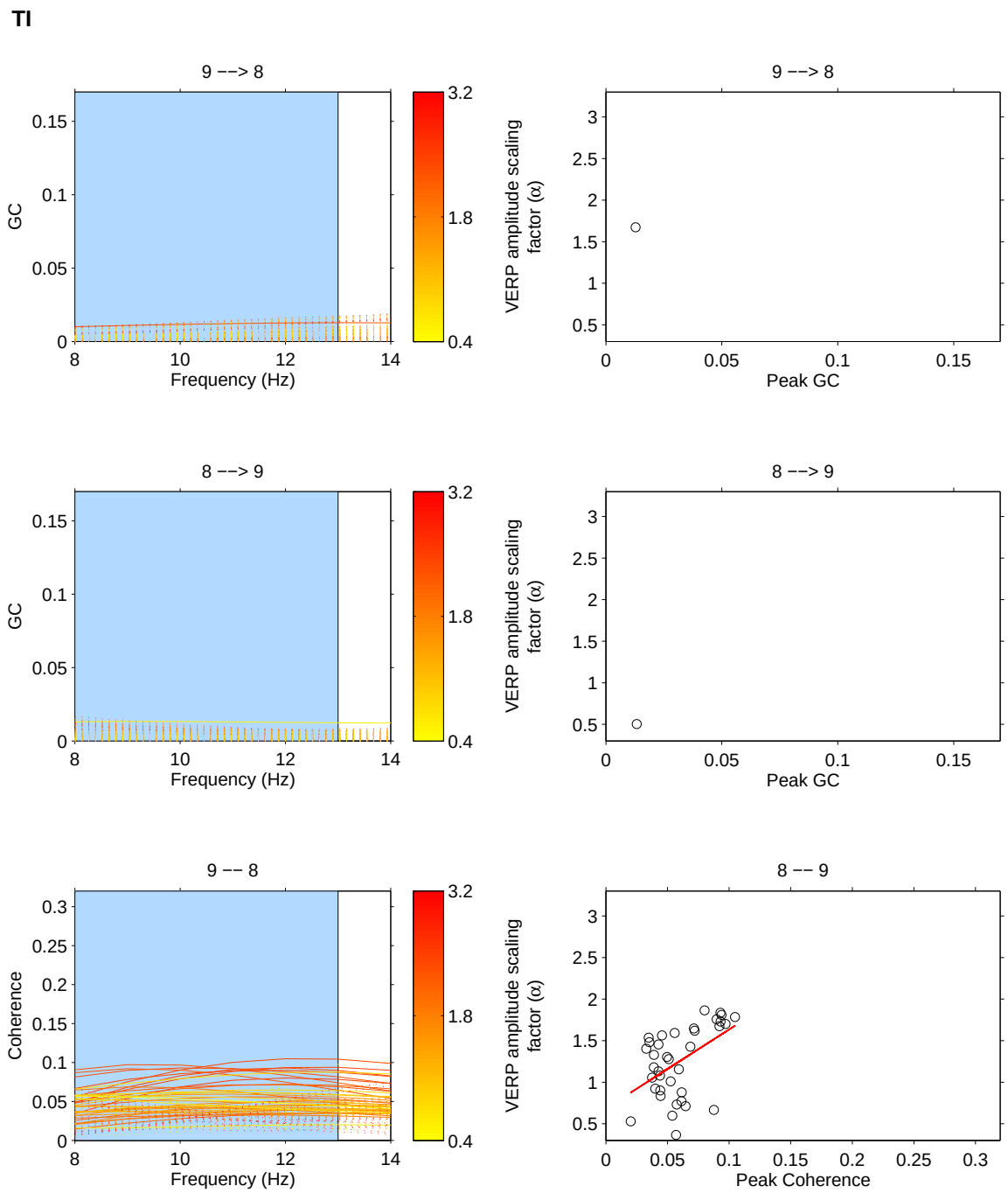

Figure 4.5: Subensemble spectra for top-down and bottom-up Granger causality and coherence (left panels) and the correlations between significant alpha-range Granger causality and coherence spectral peaks with subensemble mean striate VERP amplitude (right panels) for pair TI 9-8. Significant correlations are fit with a regression line. Spectra with significant peaks are drawn in solid lines. Spectra without significant peaks are drawn with dotted lines.

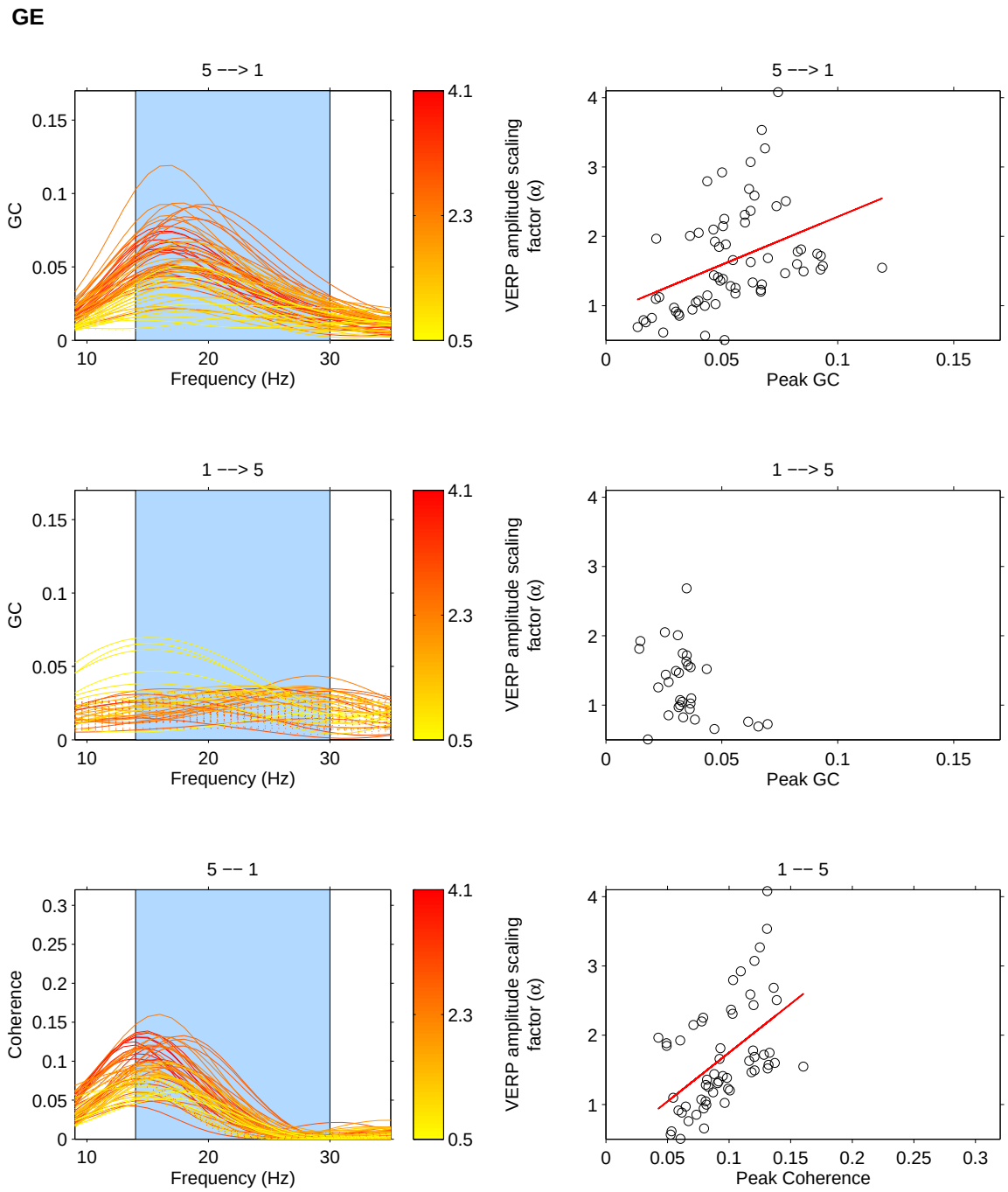

Figure 4.6: Subensemble spectra for top-down and bottom-up Granger causality and coherence (left panels) and the correlations between significant beta-range Granger causality and coherence spectral peaks with subensemble mean striate VERP amplitude (right panels) for pair GE 5-1. Significant correlations are fit with a regression line. Spectra with significant peaks are drawn in solid lines. Spectra without significant peaks are drawn with dotted lines.

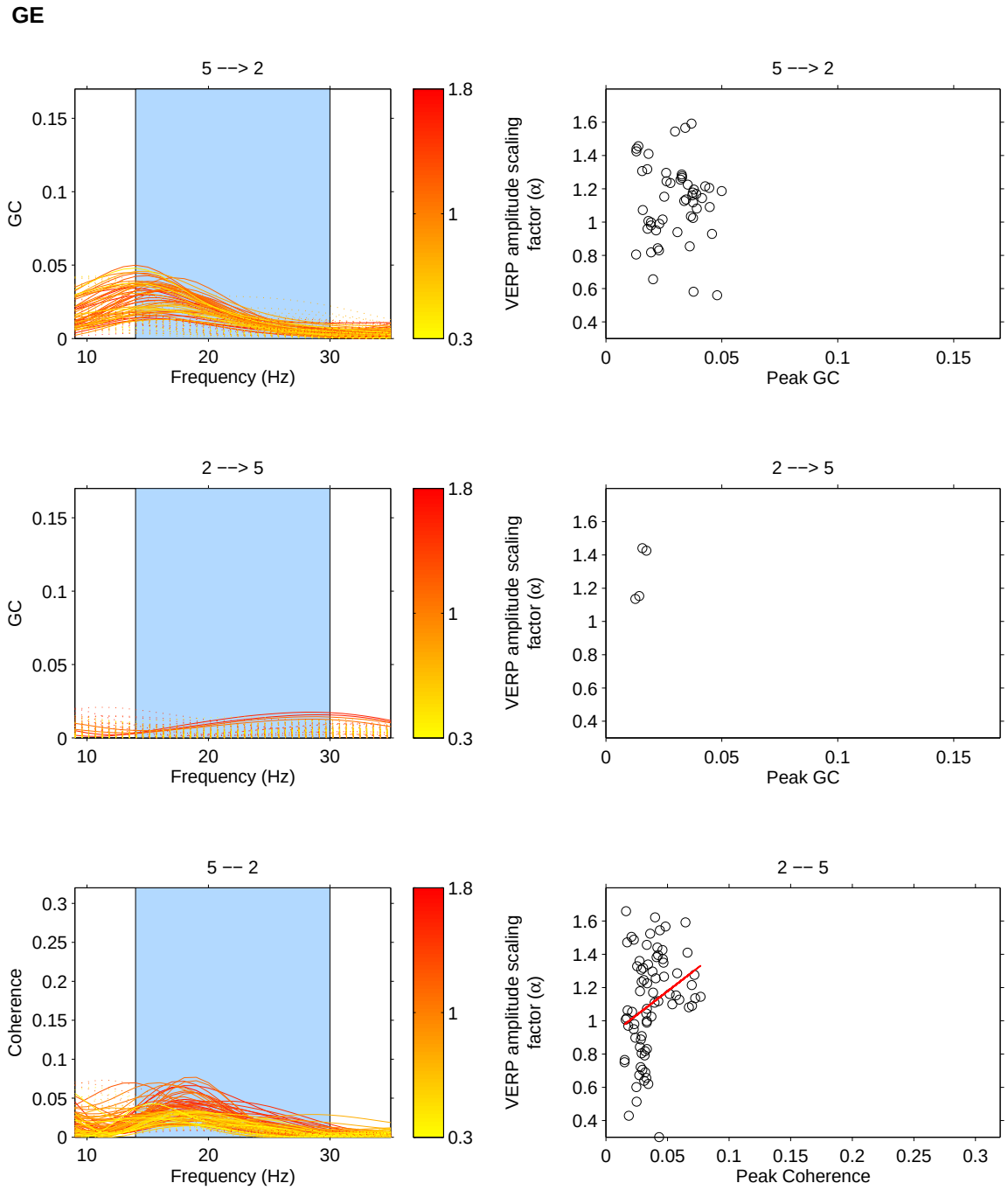

Figure 4.7: Subensemble spectra for top-down and bottom-up Granger causality and coherence (left panels) and the correlations between significant beta-range Granger causality and coherence spectral peaks with subensemble mean striate VERP amplitude (right panels) for pair GE 5-2. Significant correlations are fit with a regression line. Spectra with significant peaks are drawn in solid lines. Spectra without significant peaks are drawn with dotted lines.

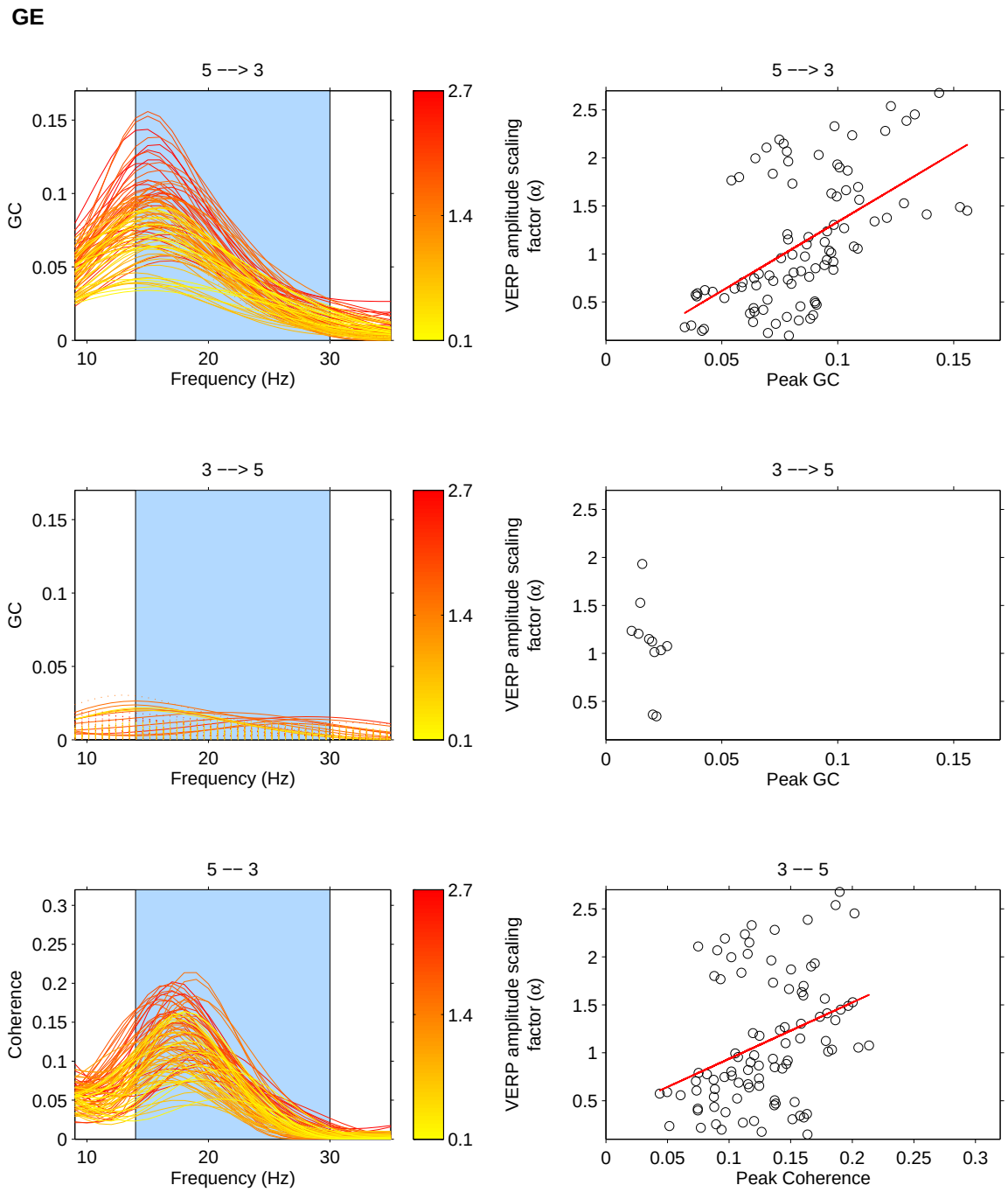

Figure 4.8: Subensemble spectra for top-down and bottom-up Granger causality and coherence (left panels) and the correlations between significant beta-range Granger causality and coherence spectral peaks with subensemble mean striate VERP amplitude (right panels) for pair GE 5-3. Significant correlations are fit with a regression line. Spectra with significant peaks are drawn in solid lines. Spectra without significant peaks are drawn with dotted lines.

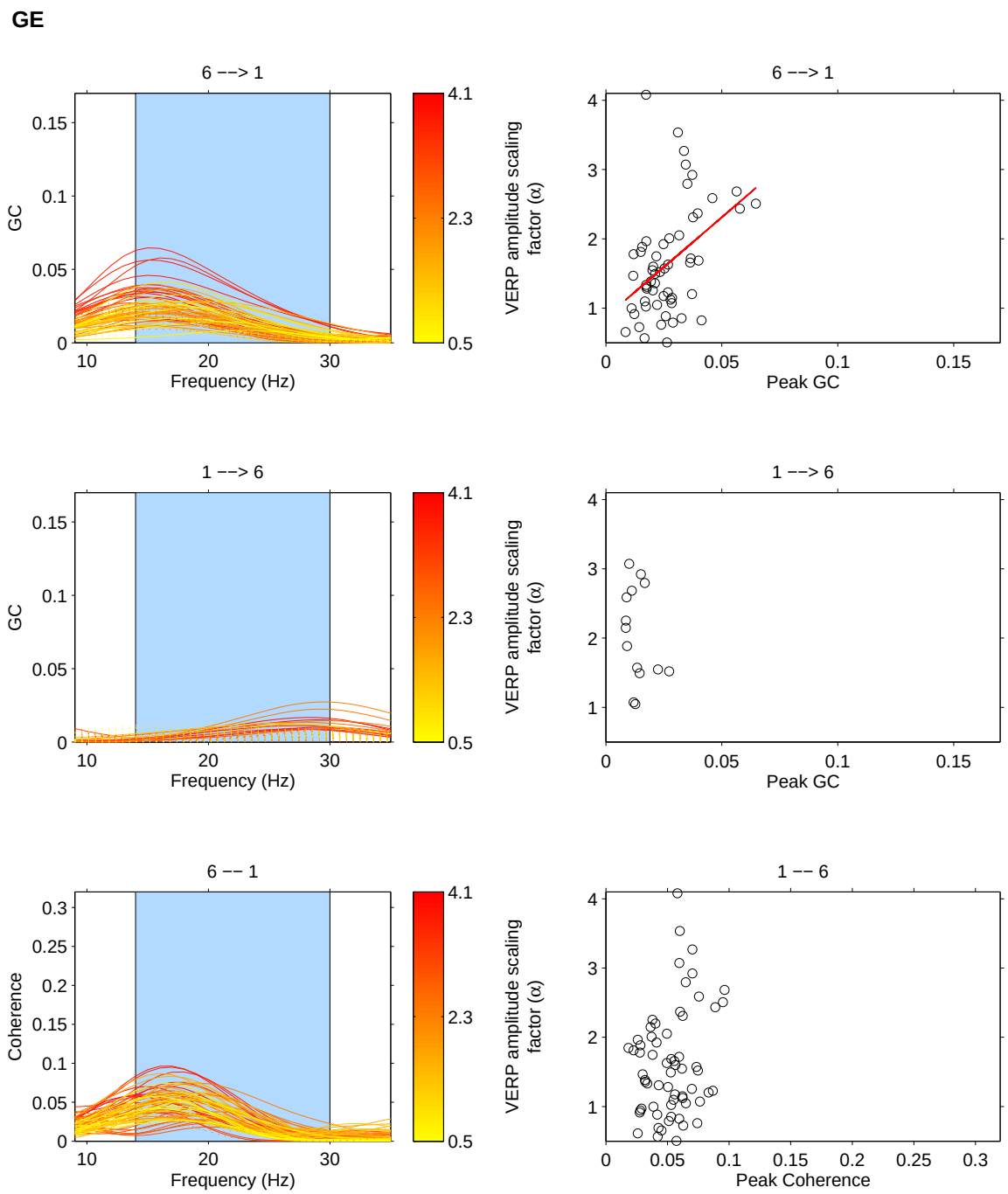

Figure 4.9: Subensemble spectra for top-down and bottom-up Granger causality and coherence (left panels) and the correlations between significant beta-range Granger causality and coherence spectral peaks with subensemble mean striate VERP amplitude (right panels) for pair GE 6-1. Significant correlations are fit with a regression line. Spectra with significant peaks are drawn in solid lines. Spectra without significant peaks are drawn with dotted lines.

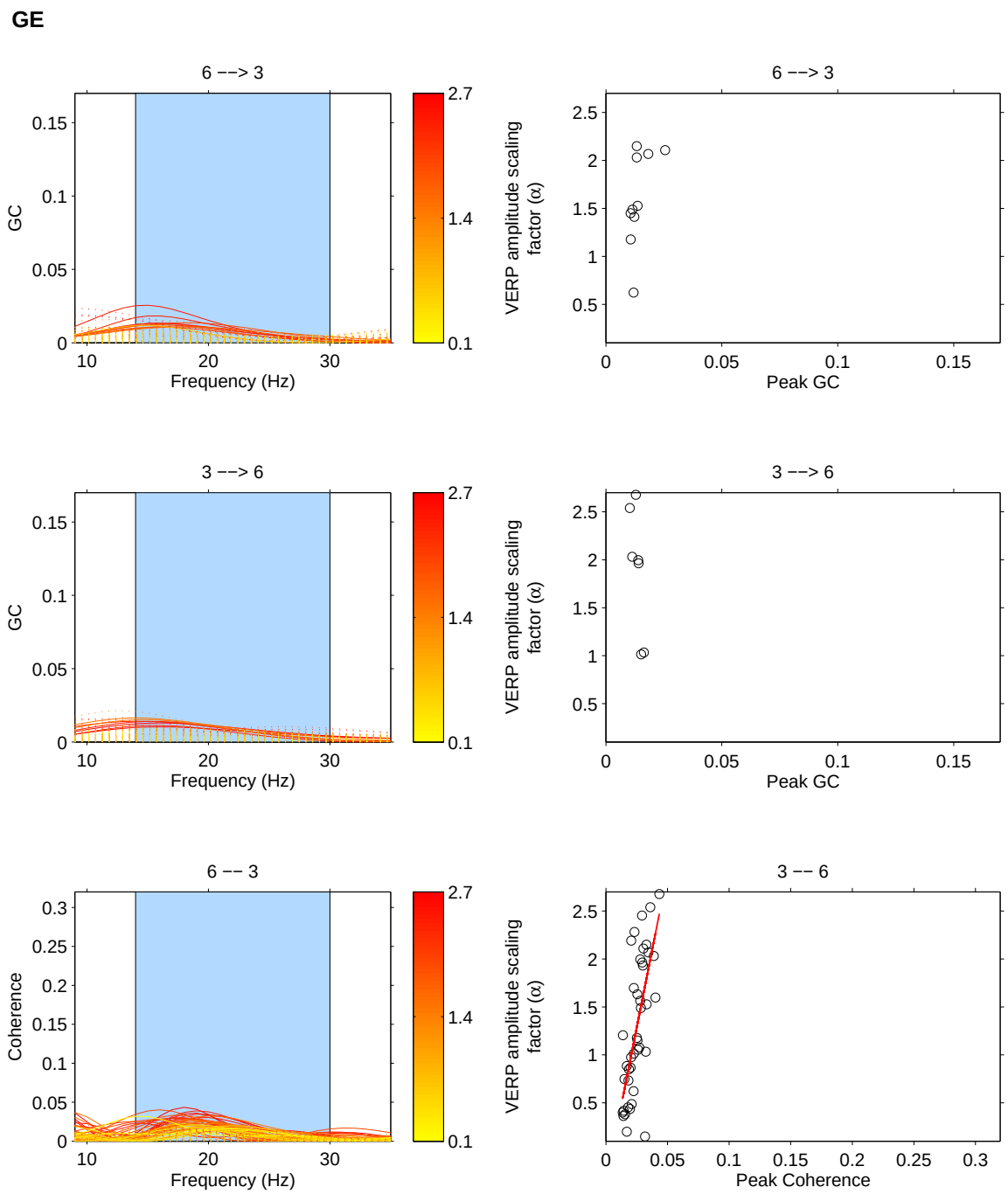

Figure 4.10: Subensemble spectra for top-down and bottom-up Granger causality and coherence (left panels) and the correlations between significant beta-range Granger causality and coherence spectral peaks with subensemble mean striate VERP amplitude (right panels) for pair GE 6-3. Significant correlations are fit with a regression line. Spectra with significant peaks are drawn in solid lines. Spectra without significant peaks are drawn with dotted lines.

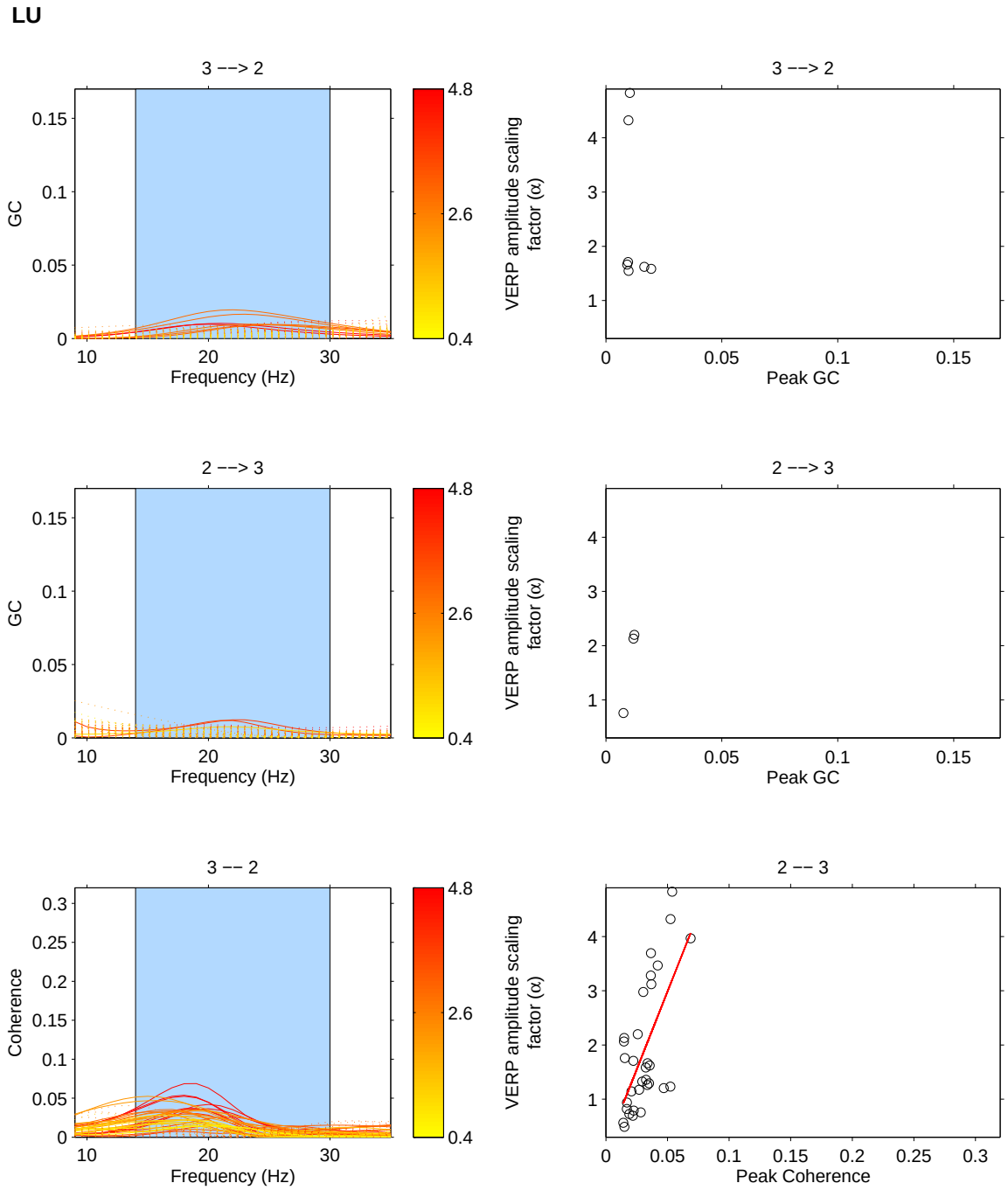

Figure 4.11: Subensemble spectra for top-down and bottom-up Granger causality and coherence (left panels) and the correlations between significant beta-range Granger causality and coherence spectral peaks with subensemble mean striate VERP amplitude (right panels) for pair LU 3-2. Significant correlations are fit with a regression line. Spectra with significant peaks are drawn in solid lines. Spectra without significant peaks are drawn with dotted lines.

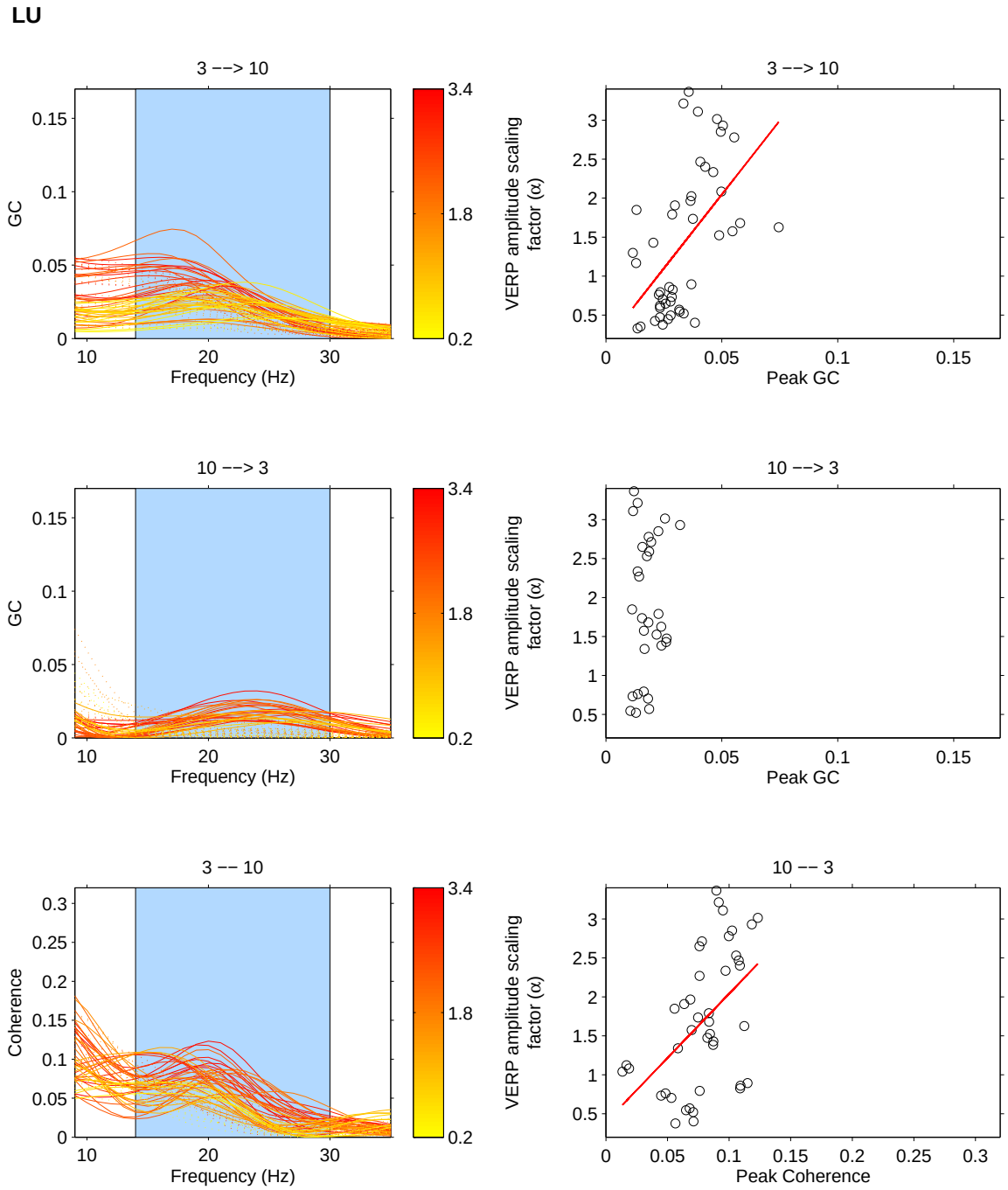

Figure 4.12: Subensemble spectra for top-down and bottom-up Granger causality and coherence (left panels) and the correlations between significant beta-range Granger causality and coherence spectral peaks with subensemble mean striate VERP amplitude (right panels) for pair LU 3-10. Significant correlations are fit with a regression line. Spectra with significant peaks are drawn in solid lines. Spectra without significant peaks are drawn with dotted lines.

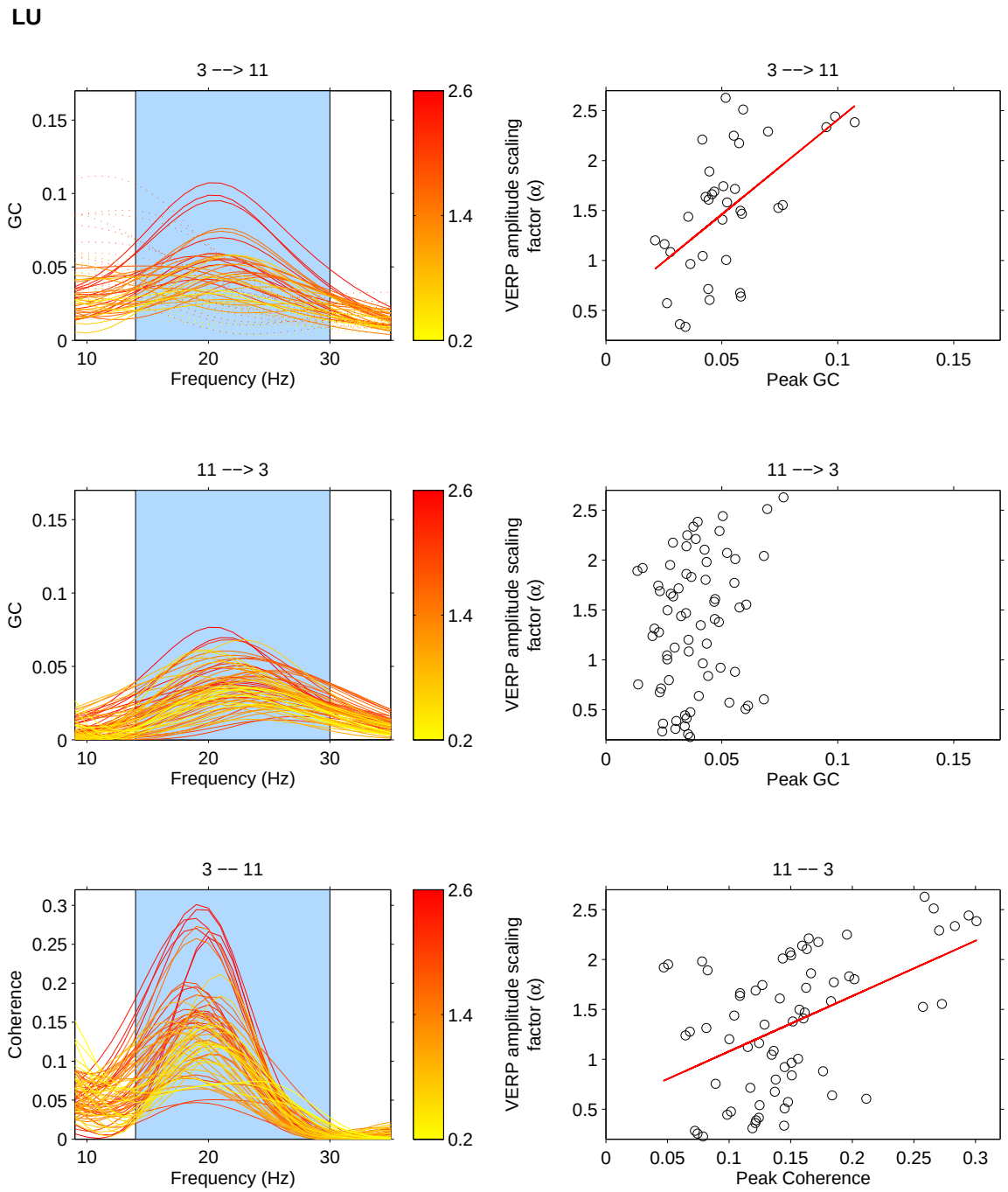

Figure 4.13: Subensemble spectra for top-down and bottom-up Granger causality and coherence (left panels) and the correlations between significant beta-range Granger causality and coherence spectral peaks with subensemble mean striate VERP amplitude (right panels) for pair LU 3-11. Significant correlations are fit with a regression line. Spectra with significant peaks are drawn in solid lines. Spectra without significant peaks are drawn with dotted lines.

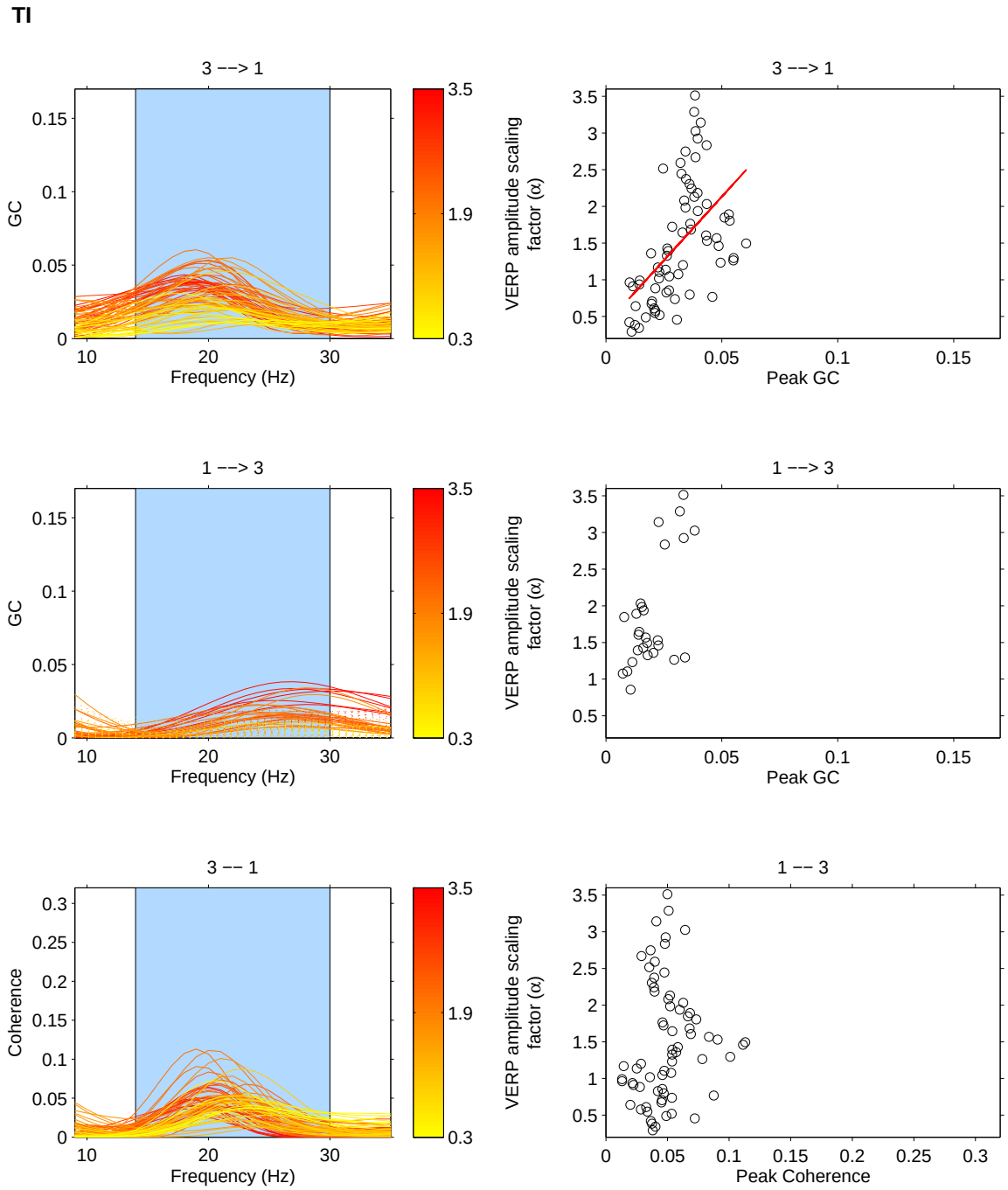

Figure 4.14: Subensemble spectra for top-down and bottom-up Granger causality and coherence (left panels) and the correlations between significant beta-range Granger causality and coherence spectral peaks with subensemble mean striate VERP amplitude (right panels) for pair TI 3-1. Significant correlations are fit with a regression line. Spectra with significant peaks are drawn in solid lines. Spectra without significant peaks are drawn with dotted lines.

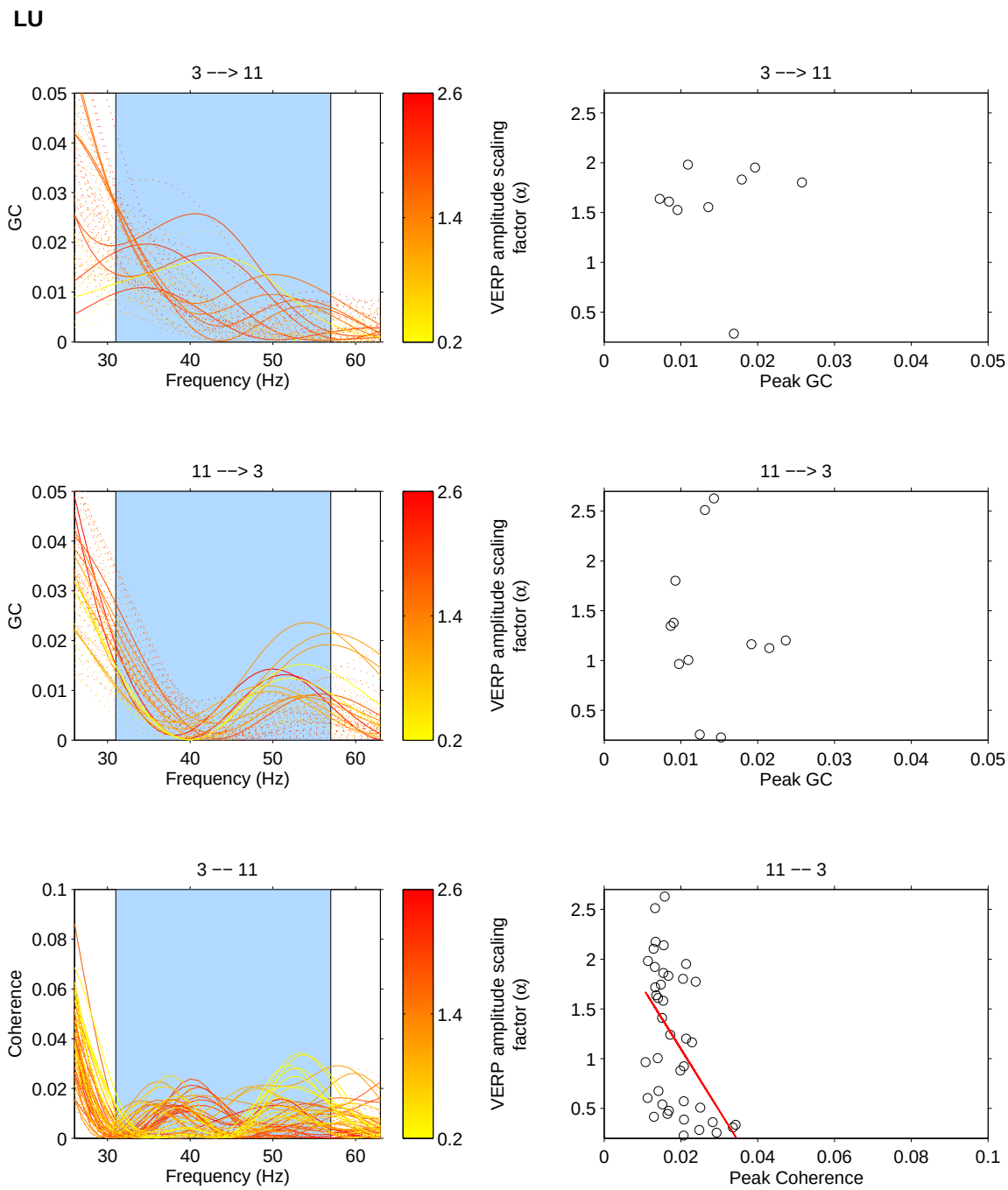

Figure 4.15: Subensemble spectra for top-down and bottom-up Granger causality and coherence (left panels) and the correlations between significant low gamma-range Granger causality and coherence spectral peaks with subensemble mean striate VERP amplitude (right panels) for pair LU 3-11. Significant correlations are fit with a regression line. Spectra with significant peaks are drawn in solid lines. Spectra without significant peaks are drawn with dotted lines.

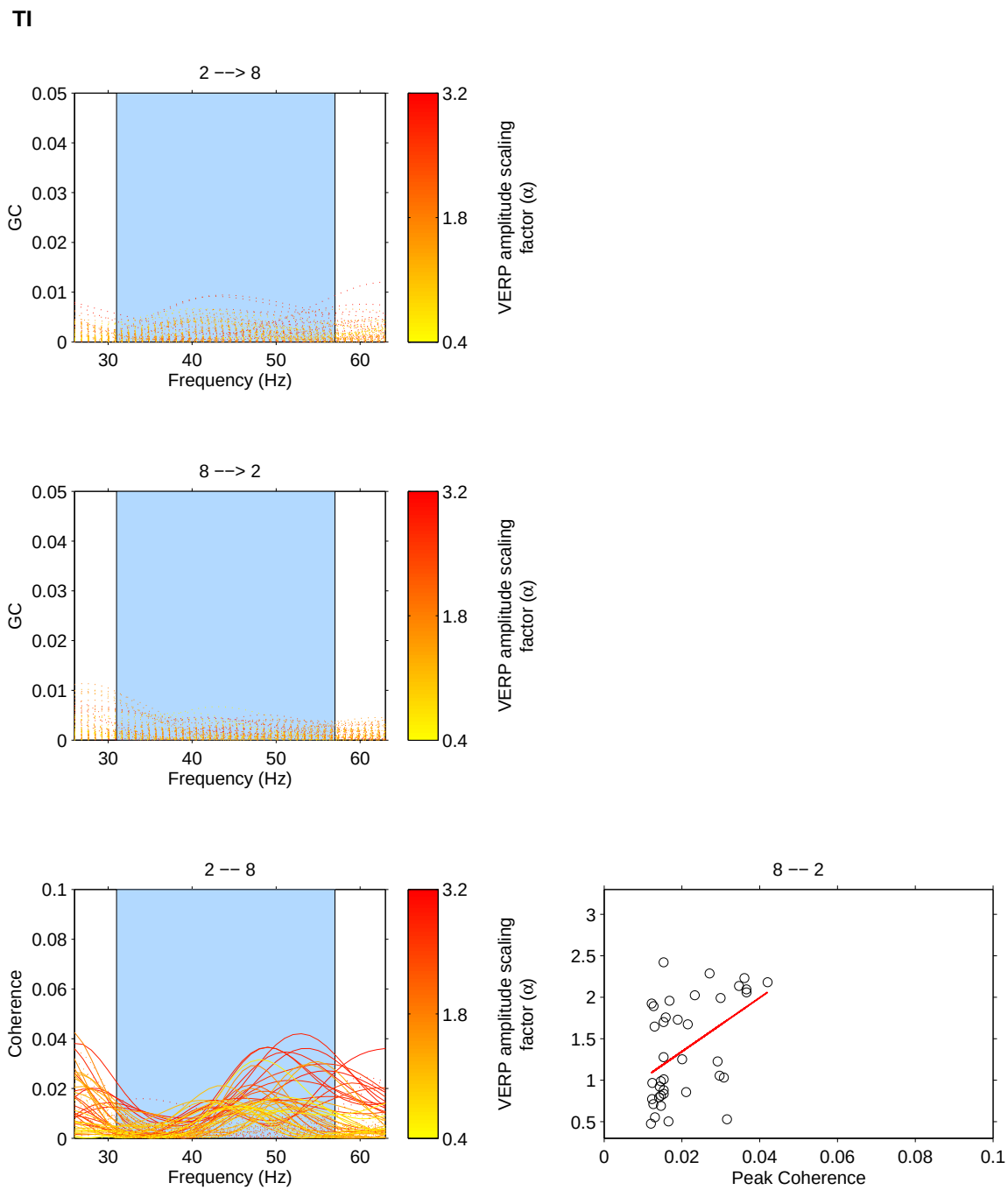

Figure 4.16: Subensemble spectra for top-down and bottom-up Granger causality and coherence (left panels) and the correlations between significant low gamma-range Granger causality and coherence spectral peaks with subensemble mean striate VERP amplitude (right panels) for pair TI 2-8. Significant correlations are fit with a regression line. Spectra with significant peaks are drawn in solid lines. Spectra without significant peaks are drawn with dotted lines.

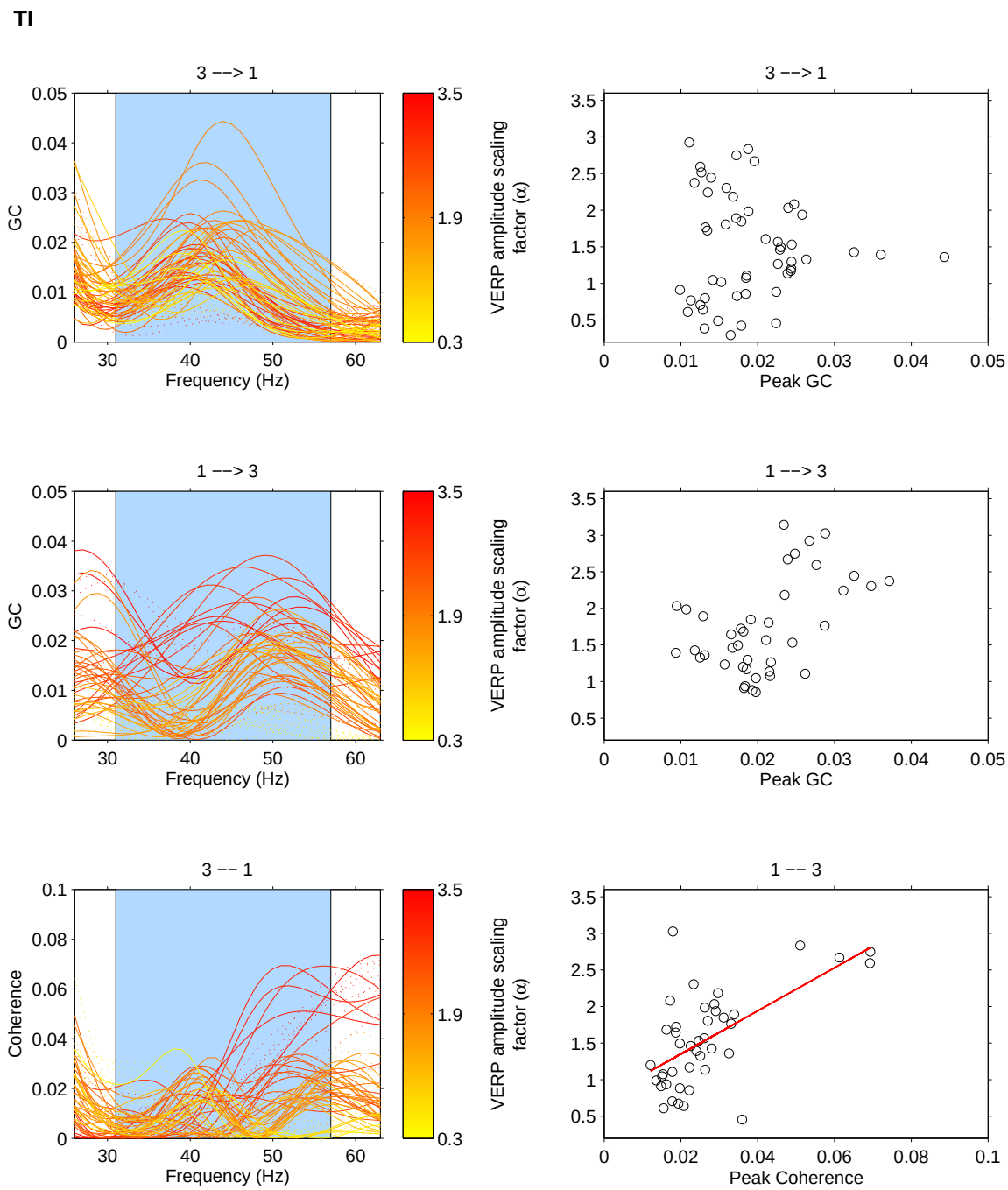

Figure 4.17: Subensemble spectra for top-down and bottom-up Granger causality and coherence (left panels) and the correlations between significant low gamma-range Granger causality and coherence spectral peaks with subensemble mean striate VERP amplitude (right panels) for pair TI 3-1. Significant correlations are fit with a regression line. Spectra with significant peaks are drawn in solid lines. Spectra without significant peaks are drawn with dotted lines.

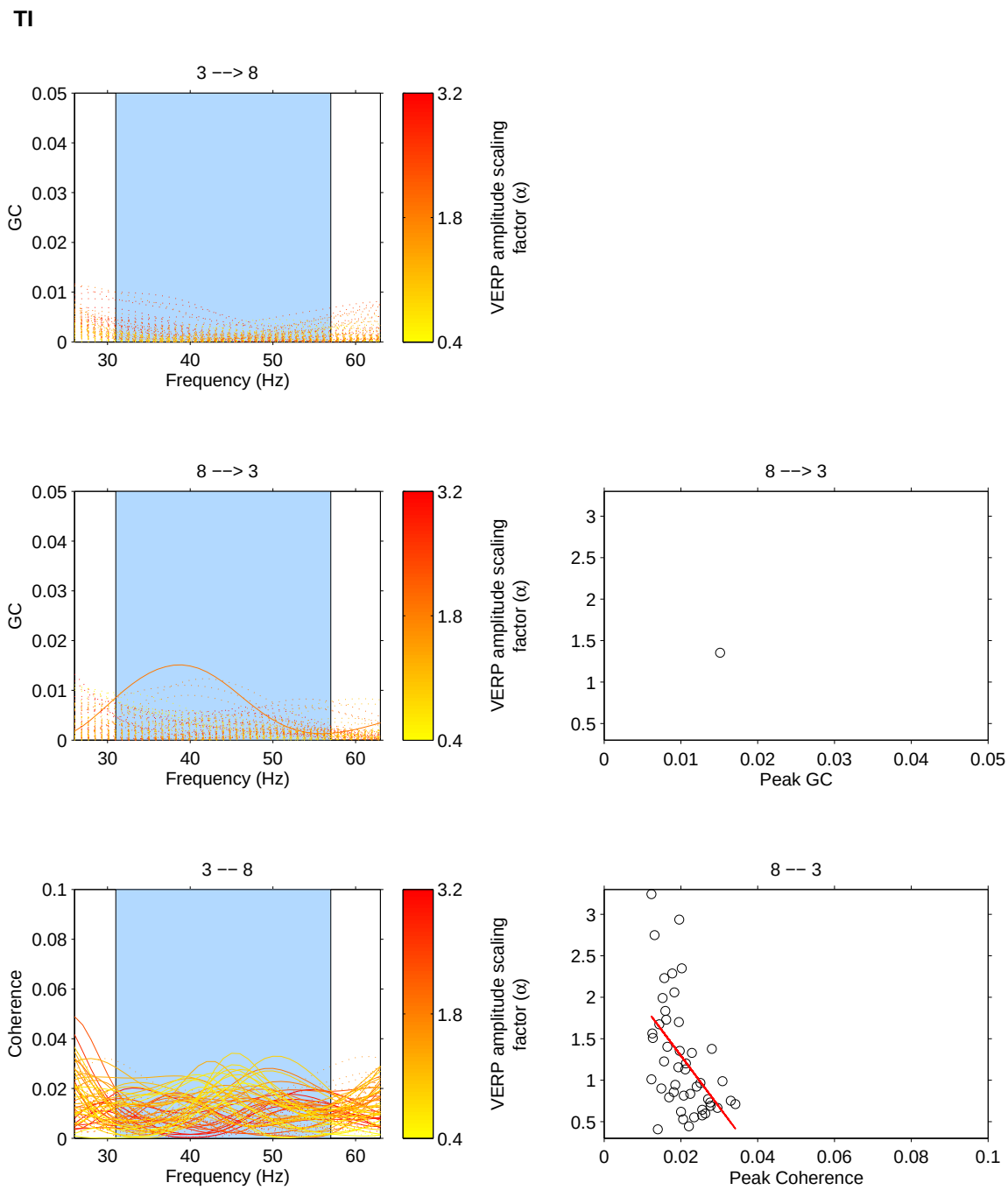

Figure 4.18: Subensemble spectra for top-down and bottom-up Granger causality and coherence (left panels) and the correlations between significant low gamma-range Granger causality and coherence spectral peaks with subensemble mean striate VERP amplitude (right panels) for pair TI 3-8. Significant correlations are fit with a regression line. Spectra with significant peaks are drawn in solid lines. Spectra without significant peaks are drawn with dotted lines.

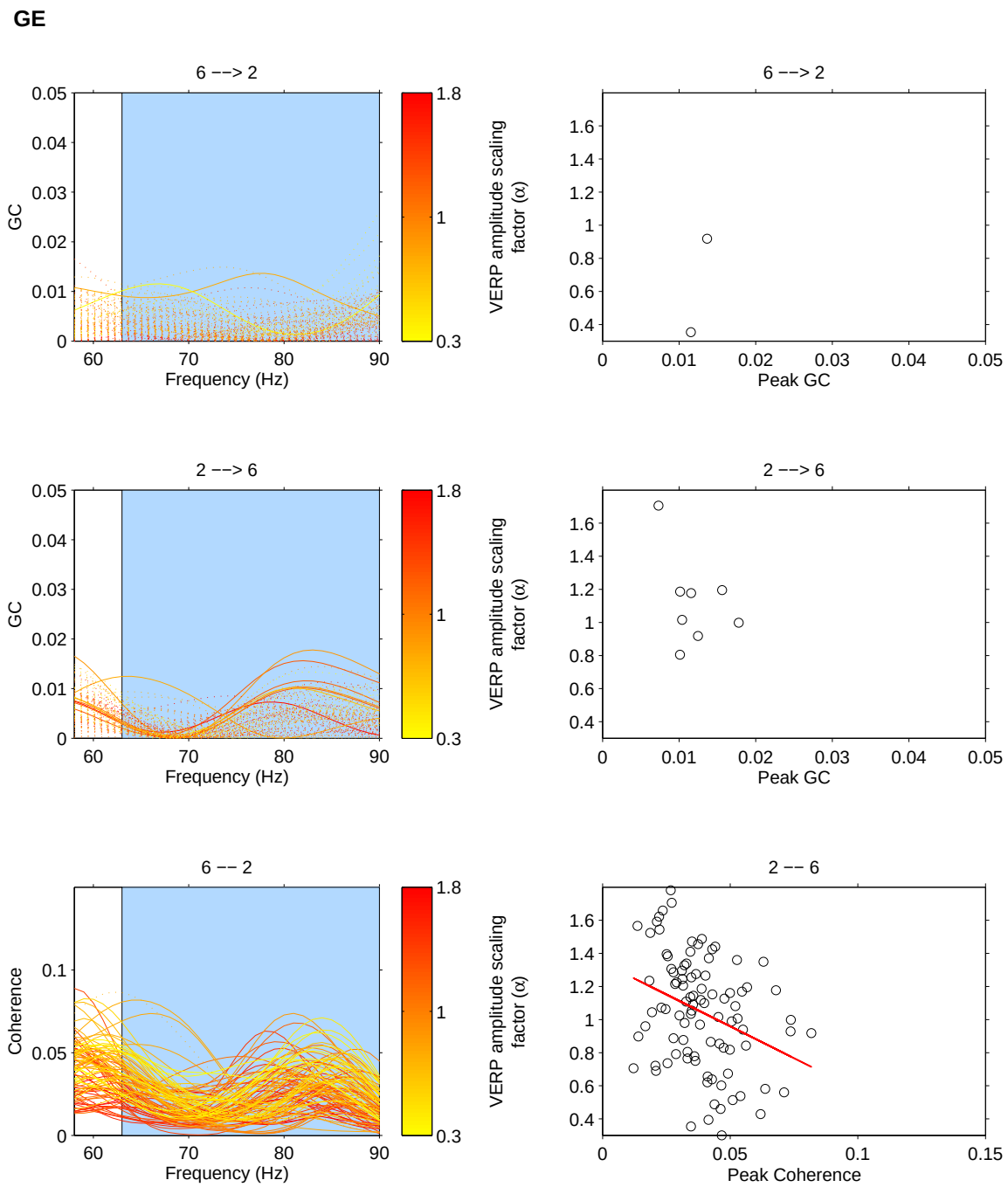

Figure 4.19: Subensemble spectra for top-down and bottom-up Granger causality and coherence (left panels) and the correlations between significant high gamma-range Granger causality and coherence spectral peaks with subensemble mean striate VERP amplitude (right panels) for pair GE 6-2. Significant correlations are fit with a regression line. Spectra with significant peaks are drawn in solid lines. Spectra without significant peaks are drawn with dotted lines.

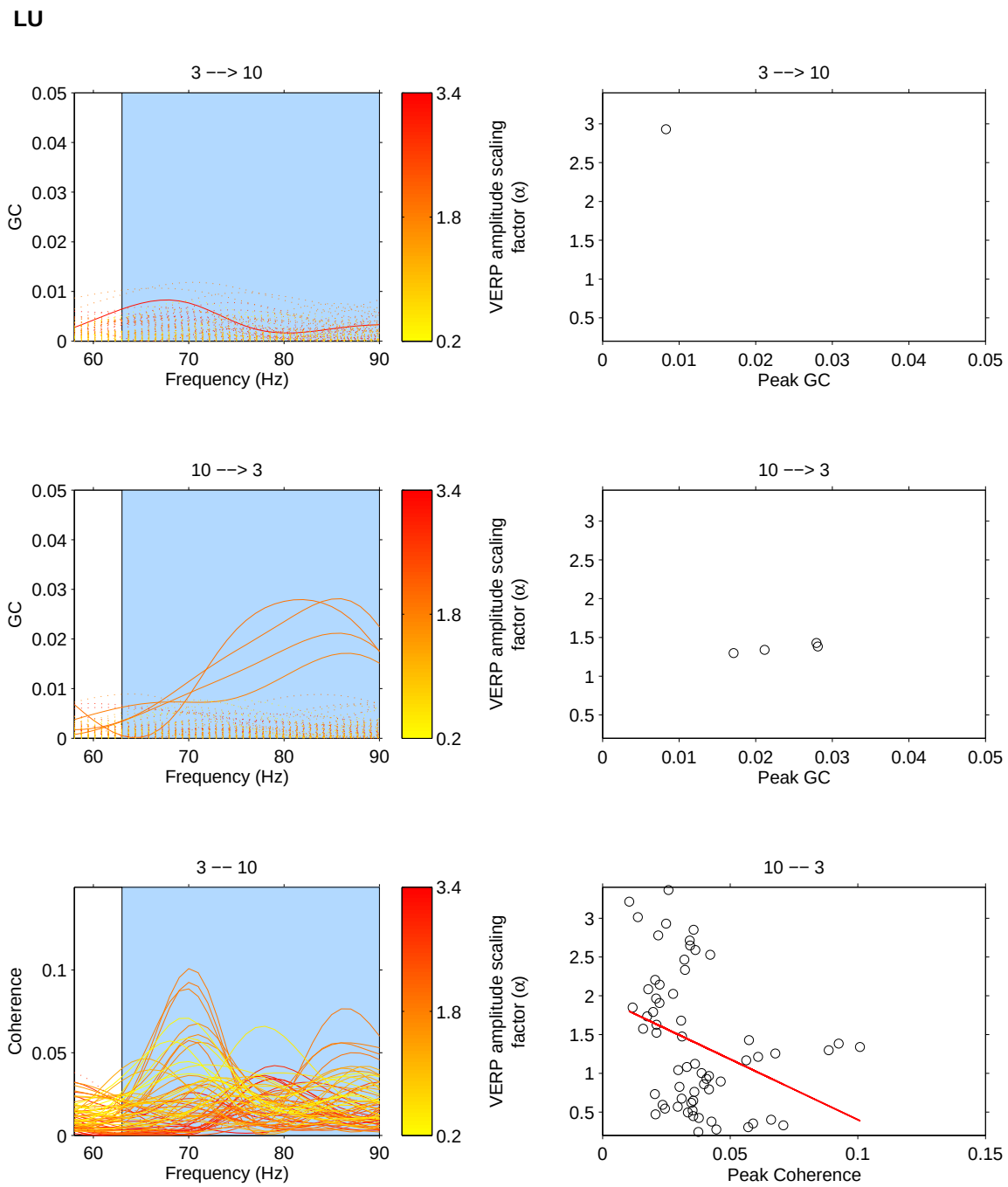

Figure 4.20: Subensemble spectra for top-down and bottom-up Granger causality and coherence (left panels) and the correlations between significant high gamma-range Granger causality and coherence spectral peaks with subensemble mean striate VERP amplitude (right panels) for pair LU 3-10. Significant correlations are fit with a regression line. Spectra with significant peaks are drawn in solid lines. Spectra without significant peaks are drawn with dotted lines.

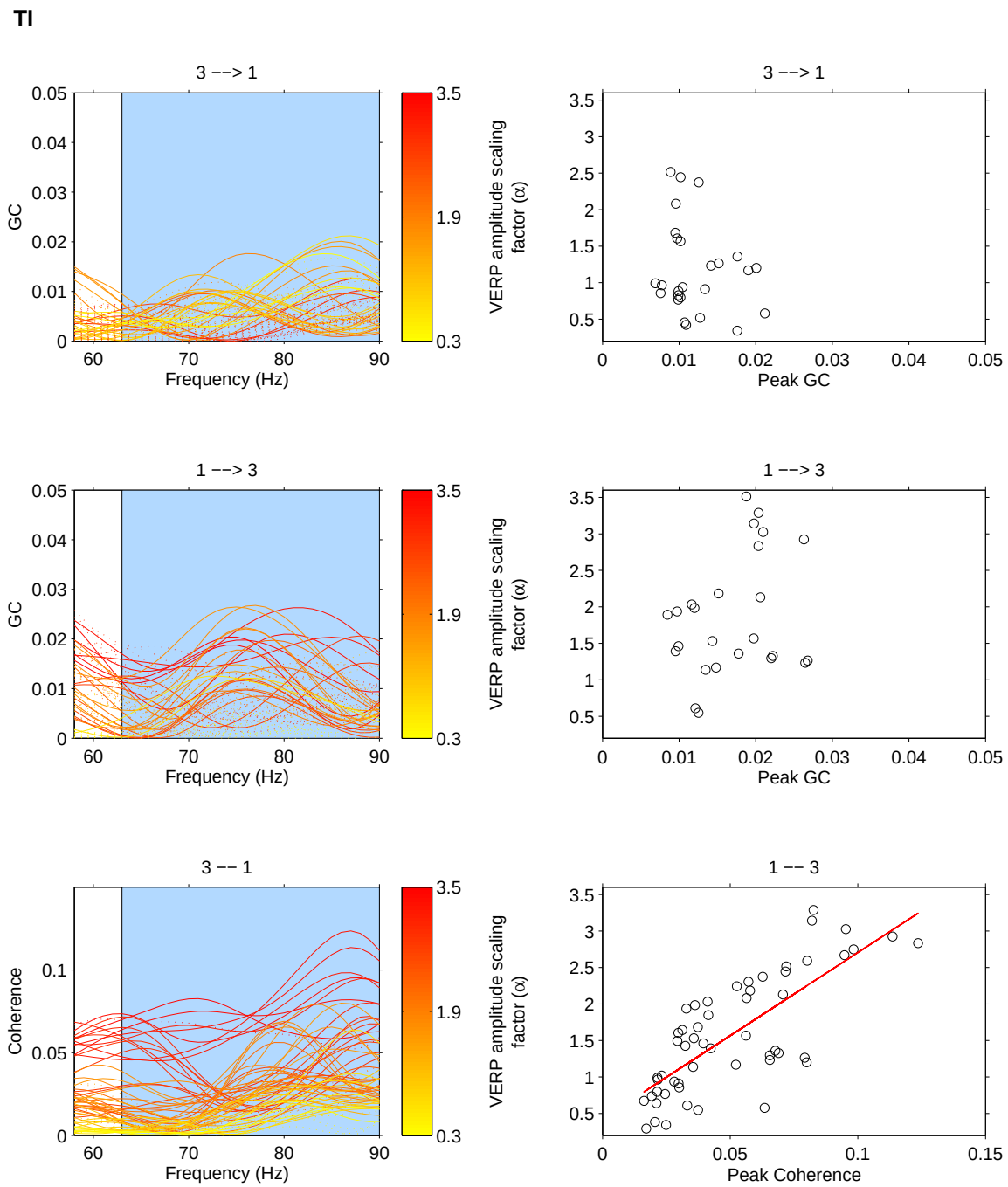

Figure 4.21: Subensemble spectra for top-down and bottom-up Granger causality and coherence (left panels) and the correlations between significant high gamma-range Granger causality and coherence spectral peaks with subensemble mean striate VERP amplitude (right panels) for pair TI 3-1. Significant correlations are fit with a regression line. Spectra with significant peaks are drawn in solid lines. Spectra without significant peaks are drawn with dotted lines.

Due to the prevalence of top-down interactions within the beta band, the following focuses specifically on the investigation of beta frequency interactions. Figure 4.22 shows histograms of the top-down beta band Granger causality values for each of the 18 extrastriate-striate pairs. The histograms are ordered by their maximum value. When organized in this way it is apparent that the top six pairs are significantly correlated with mean VERP amplitude, as denoted by the red shading on the x-z plane. These pairs show considerably larger top-down Granger causality values than the non-significant pairs, and a larger spread in the values. This may indicate that a threshold in the magnitude of the top-down influence must be crossed before top-down influences have an appreciable effect on the VERP amplitude.

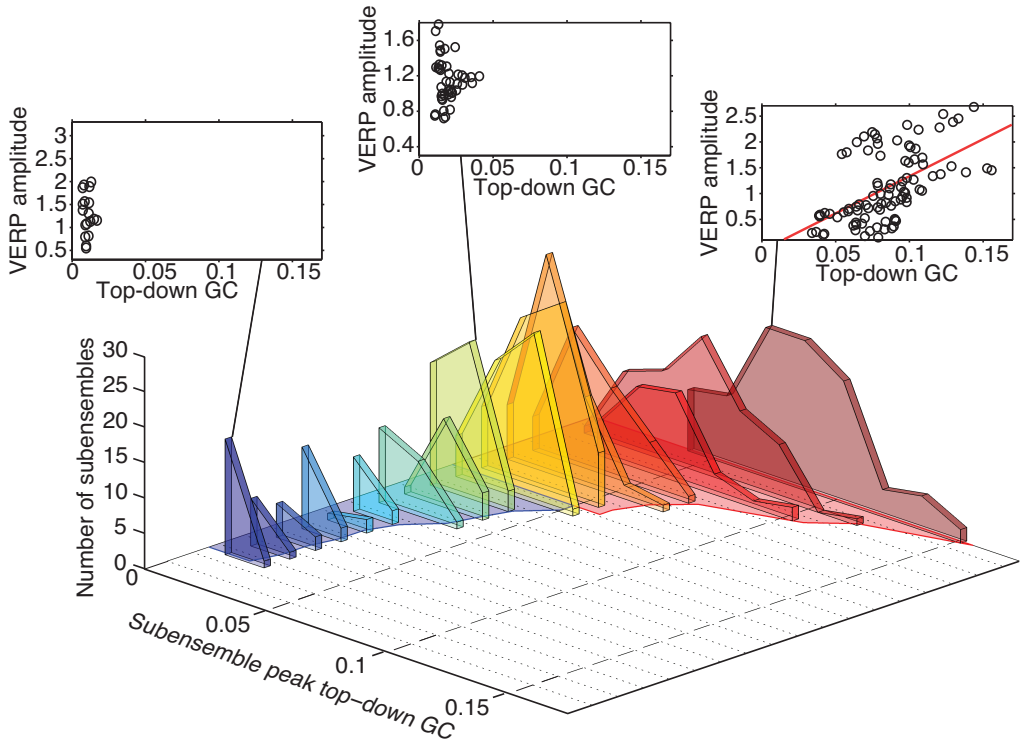

Figure 4.22: Histograms of beta range top-down subensemble Granger causality values ordered by their maximum Granger causality value for each extrastriate-striate pair. Red shading on the x-z plane indicates significant positive correlation between top-down Granger causality and the mean VERP amplitude while non-significant correlations are shaded in blue. The profile of the shaded regions is defined by the maximum value from each pair. The boxes show the correlation for the indicated pair. Correlations with regression lines are significant.

4.3.2 Relationship between subensemble Granger causality and coherence

To assess any possible relationship between the subensemble Granger causality estimates and the subensemble coherence estimates, Spearman correlation was computed between the subensemble top-down and bottom-up Granger causality values, for each pair, for each monkey, and the corresponding subensemble coherence value. At the level of single pairs, Figure 4.23 shows that the correlation is significant and very large for the top-

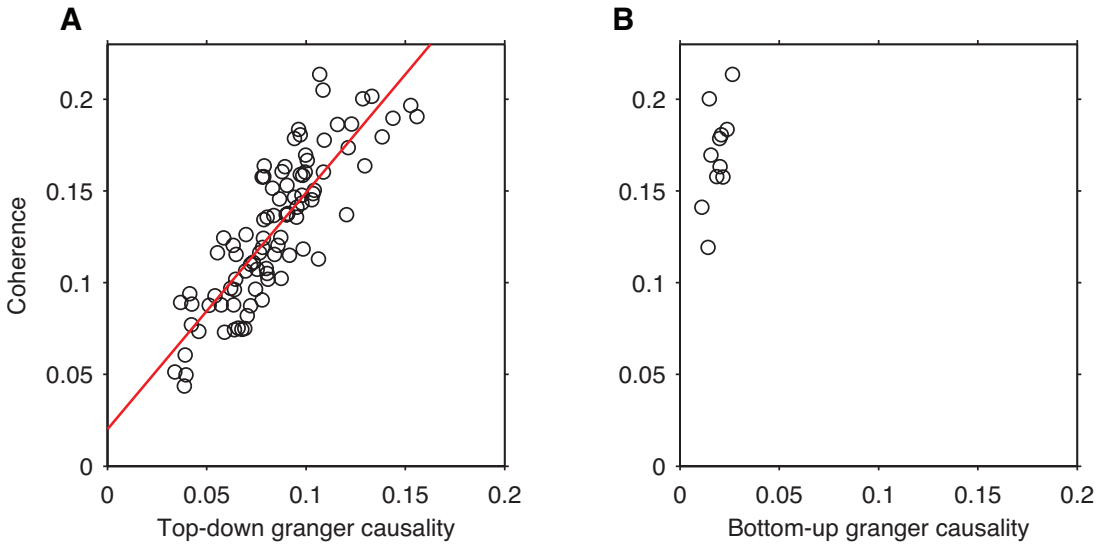

Figure 4.23: Correlation of top-down and bottom-up subensemble Granger causality with subensemble coherence for pair GE 5-3.

down direction, and is not significant in the bottom-up direction. Over all the six pairs where subensemble top-down Granger causality was significantly correlated with subsensemble mean VERP amplitude, all six had subsensemble top-down Granger causality significantly positively correlated with subsensemble coherence, whereas only one pair had bottom-up Granger causality significantly correlated with subsensemble coherence. Over all of the pairs, seven had subsensemble top-down Granger causality significantly positively correlated with subsensemble coherence, whereas only one pair had bottom-up Granger causality significantly correlated with subsensemble coherence. This pattern of results show that of the pairs with a significant correlation between subensemble top-down Granger causality and coherence, six of the seven also were pairs with significant positive correlations between subsensemble top-down Granger causality and subsensemble mean VERP amplitude.

Over all pairs, the mean subensemble Granger causality and the mean subensemble coherence, from each pair, show a very strong correlation for top-down Granger causality, and a much weaker correlation for bottom-up Granger causality, which lies on the thresh-

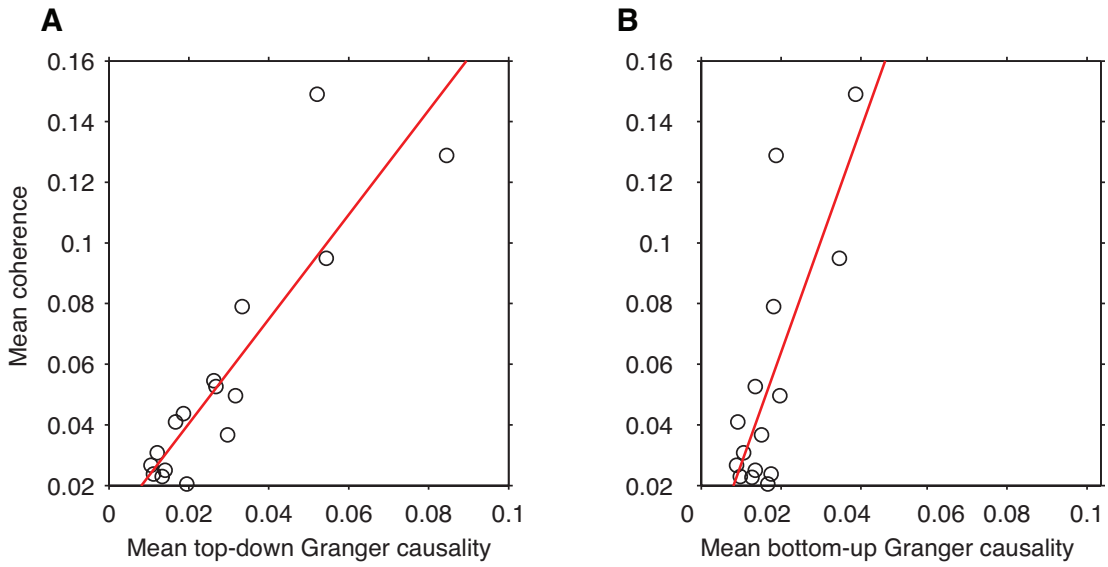

Figure 4.24: Correlation of mean peak coherence with mean peak top-down Granger Causality across site pairs was very significant ($\rho(14) = .82, p < 3.01e - 04$, corrected). B. Correlation of mean peak coherence with mean peak bottom-up Granger Causality is less significant ($\rho(13) = .60, p < .041$, corrected.

old of statistical significance, as shown in Figure 4.24. This indicates that in general top-down Granger causality is more strongly correlated with coherence, than bottom-up Granger causality.

4.3.3 Relationship between Granger causality and relative phase

To investigate a possible link between the relative phase shared by coherent oscillations and Granger causal influences the circular variance of the relative phase of each subensemble was determined for each striate-extrastriate pair by taking the circular variance of the relative phase values at the corresponding frequency of the significant peak coherence for that subensemble. Circular variance is a measure between 0 and 1, where zero indicates a tight clustering of values around the circular mean. The circular variance of the relative phase was correlated, via a Spearman rank correlation, with the mean of the significant peak top-down (Figure 4.25 A), and bottom-up (Figure 4.25 B) Granger

causality values of each subensemble for each striate-extrastriate pair. Figure 4.25 A reveals a significant negative correlation between the relative phase variance and the mean top-down Granger causality value for each pair. The correlation is not significant in the bottom-up direction. This result is in agreement with the coherence results, since a low relative phase variance is analogous to a high coherence value.

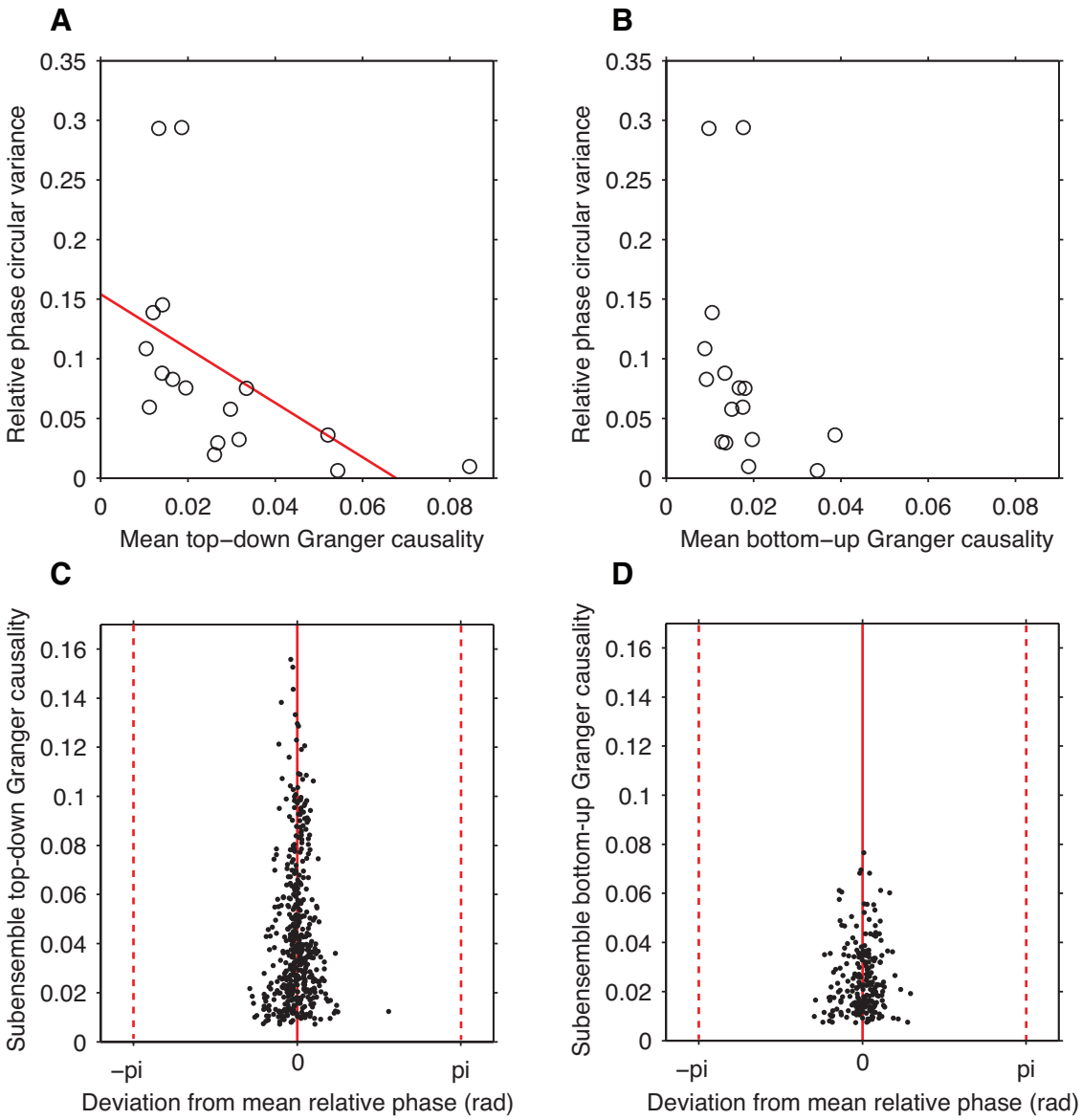

Figure 4.25: A. Top-down mean peak Granger causality is significantly correlated with relative phase variance ($\rho(15) = -.74, p < 2.26e-03$, corrected) across site pairs, but (B) bottom-up mean peak GC is not ($\rho(14) = -.559, p < .053$, corrected). C. Top-down Granger causality vs relative phase across all subensembles of all site pairs (with mean relative phase removed). A progressive decrease in relative phase variation is seen with increasing top-down Granger causality. D. Bottom-up Granger causality vs relative phase across subensembles. Higher values of top-down Granger causality are not observed.

To determine the connection between subensemble coherence and Granger causality with relative phase, the relative phase values of each subensemble, for each striate-

extrastriate pair, were obtained at the frequency of each significant subensemble coherence peak. For each striate-extrastriate pair, the circular mean of the relative phase values was calculated and then subtracted from each relative phase value. This functioned to center the relative phase values from each striate-extrastriate pair to a common circular mean value of zero. Scatter plots are shown in Figure 4.25 C and D of the relative phase values versus top-down Granger causality and bottom-up Granger causality. Inspection of Figure 4.25 A reveals that, as indicated by Figure 4.25 A, relative phase values cluster more tightly around the mean value for a given pair as the top-down Granger causality value increases. A similar phenomenon is observed for the bottom-up direction, shown in Figure 4.25 D, but the values do not cluster as tightly around zero. These results indicate that higher Granger causal influences may function to induce more consistent phase coupling between visual areas, which in turn may increase the efficacy of their interareal communication.

4.3.4 Relative phase relationships between pairs

Figure 4.26 displays the relative phase values in A for all pairs, B for all pairs with a significant correlation between top-down subensemble Granger causality and mean subensemble VERP amplitude, and C for all pairs that did not show this correlation. It is evident from these plots that the circular mean is near $\pi/4$ for A, C, and E, and that the pairs that exhibited a significant correlation between top-down subensemble Granger causality and mean subensemble VERP amplitude (Figure 4.26 B) are most closely clustered around this value, whereas the non-significant pairs have a significantly larger variance (Mardia-Watson-Wheeler test, $W = 70.33, p << .001$).

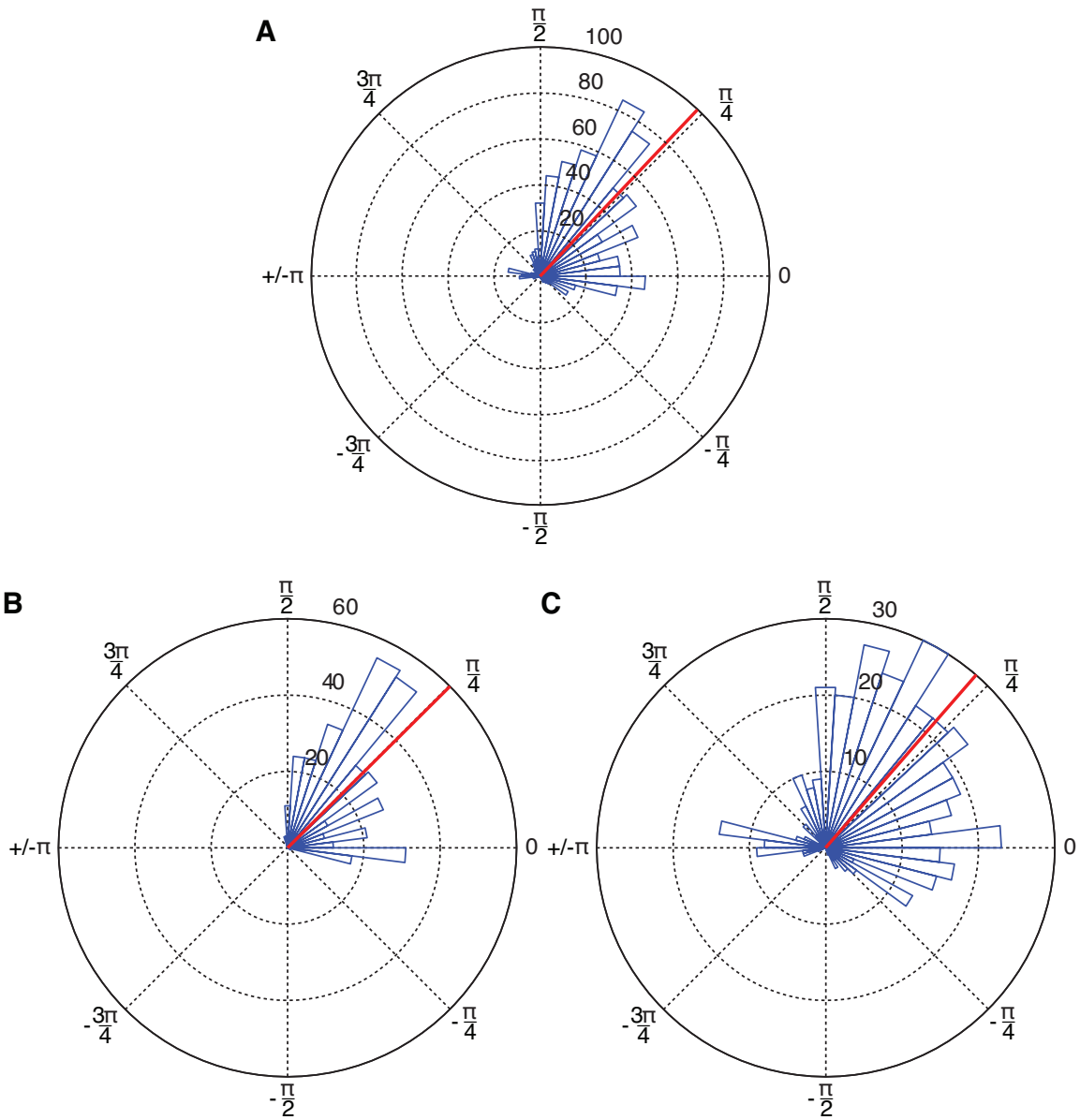

Figure 4.26: Rose plots of subensemble relative phase values. (A) All pairs. (B) Pairs with significant correlation between top-down beta Granger causality and subensemble mean VERP amplitude. (C) Pairs without significant correlation between top-down beta Granger causality and subensemble mean VERP amplitude. The red line marks the circular mean. The circular means of the significantly correlated pairs and non-significant pairs were not significantly different (Watson-Williams test, $p = .194$), yet the variance of non-signficant pairs was significantly larger than that of the significant pairs (Mardia-Watson-Wheeler test, $W = 70.33, p << .001$).

Figure 4.27 displays the mean relative phase values for all pairs converted to millisec-

onds. Blue circles denote pairs that were not significantly correlated between top-down subensemble Granger causality and mean subensemble VERP amplitude, with the red circles denoting significantly correlated pairs. Overall, the extrastriate sites lead the striate sites by 7.2 milliseconds. This delay is on the order of magnitude that one would expect for transmission delays between these regions of the visual system (Nowak and Bullier, 1997). The significantly correlated pairs had a significantly lower time lag of 6.6 milliseconds compared to the non-significant pairs with a lag of 7.7 milliseconds ($t(839) = -2.56, p < .05$) The significant pairs also have lower variance of the time lag than the non-signficant pairs (Levene's test, $p << .001$). This may indicate that the lag between these pairs is more optimally tuned for efficient interareal communication (Fries, 2005; Bressler, 2004).

4.3.5 Assessment of single-trial VERP estimates within and across sessions

No significant correlations were found between the session epoch and the mean VERP amplitude, as depicted in Figure 4.28. This indicates that the size of the VERP amplitude estimates did not change systematically during the sessions. Visual inspection of Figure 4.28 reveals that the mean and variance of the VERP amplitude estimates were approximately stationary. The means of the VERP amplitude estimates were stable across each session, for each of the striate recording sites. The variances, depicted by the blue shading, of the VERP amplitude estimates were also quite stable across the session epochs, which demonstrates that as each session proceeded the distribution of VERP amplitude estimates did not change appreciably. Thus, systematic changes in the VERP amplitude estimates are unlikely to be due to intra-session related factors such as fatigue.

Figure 4.29 displays the mean and variance of the VERP amplitude estimates for each striate recording site. There were no significant correlations between the temporal order

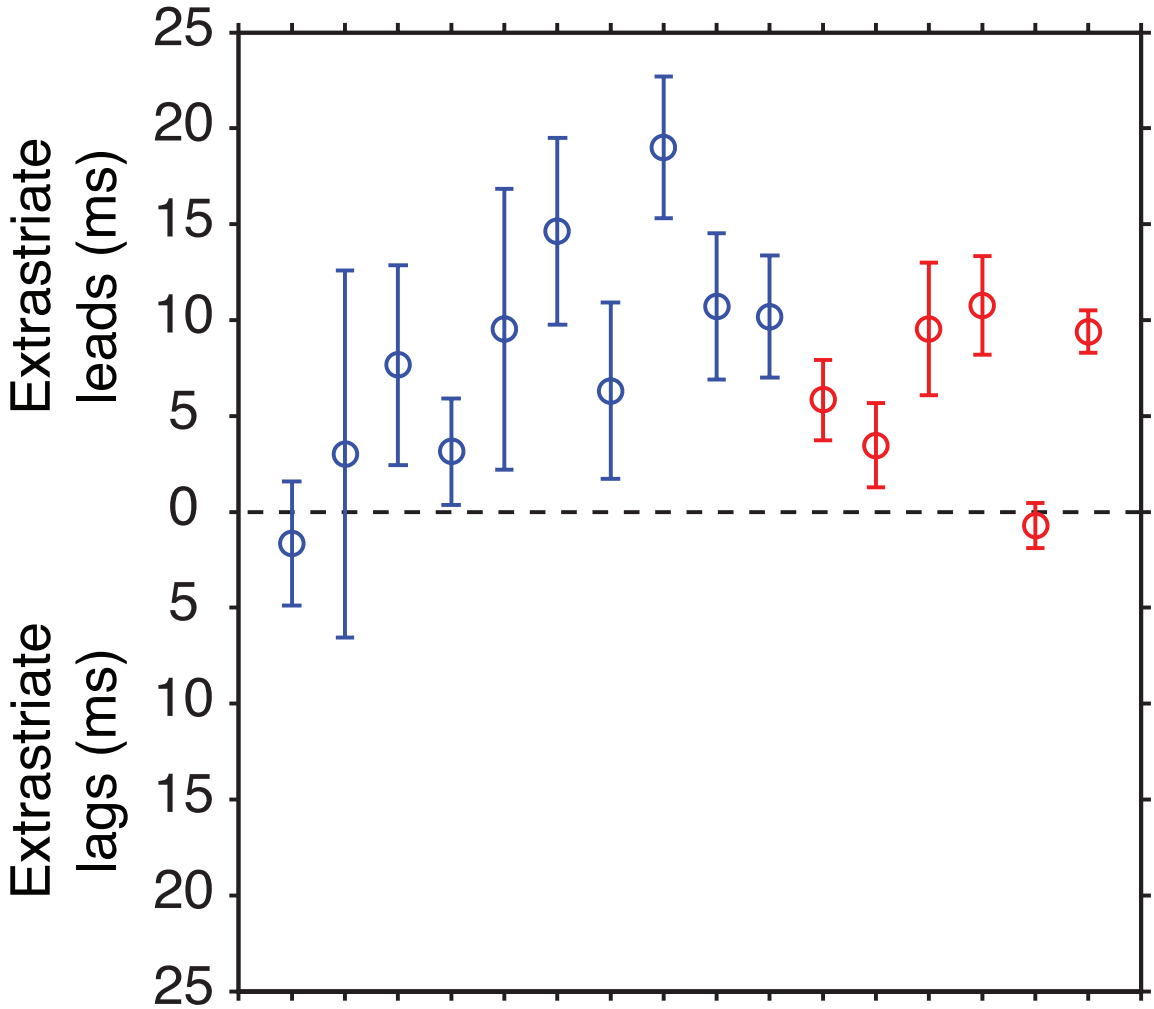

Figure 4.27: When the relative phase values are converted to time lags, extrastriate sites lead by 7.2 ms on average. Red circles depict pairs with significant top-down beta Granger causality versus mean VERP amplitude correlations, while those with blue circles are not significant.

of the recording sessions and the mean VERP amplitude estimate. This indicates that no systematic changes in the mean VERP amplitude estimate occurred over the recording period.

Though there were no significant correlations between the time of the recording session and the mean VERP, many of the striate recording sites show variation in the mean and variance of the VERP amplitude scaling factors over the course of the recording period. This is most evident in Figure 4.29 A, C and G). These channels show large variation between certain sessions, which indicates that certain recording days gave rise to larger VERP amplitude estimates. Interestingly, these fluctuations do not occur for all the recording sites of a given monkey, as is evident from Figure 4.29 A, B, and C, from monkey GE, and G and H from monkey TI. Thus it is difficult to attribute these differences to arousal, since this effect would likely act in a global fashion upon V1, uniformly increasing or decreasing the excitability of cortical tissue. Additionally, the VERPs from striate channels 1 and 3 (Figure 4.29 A, and C) were found to be modulated by top-down beta band influences, whereas channel 2 was not. In TI, channel 1 VERPs (Figure 4.29 G) were also modulated by top-down beta band influences, while those from channel 8 (Figure 4.29 H) were not. The profiles of the mean and variance for the non-modulated channels are quite stationary (Figure 4.29, B and H), whereas large variation is present in the modulated channels. This suggests that the variation may be due to fluctuations in the top-down modulatory influences that occur between the recording sessions. If these fluctuations are due to changes in motivational factors, it would appear that these factors have an impact on mechanisms that modulate the degree of interareal coupling and directional influence.

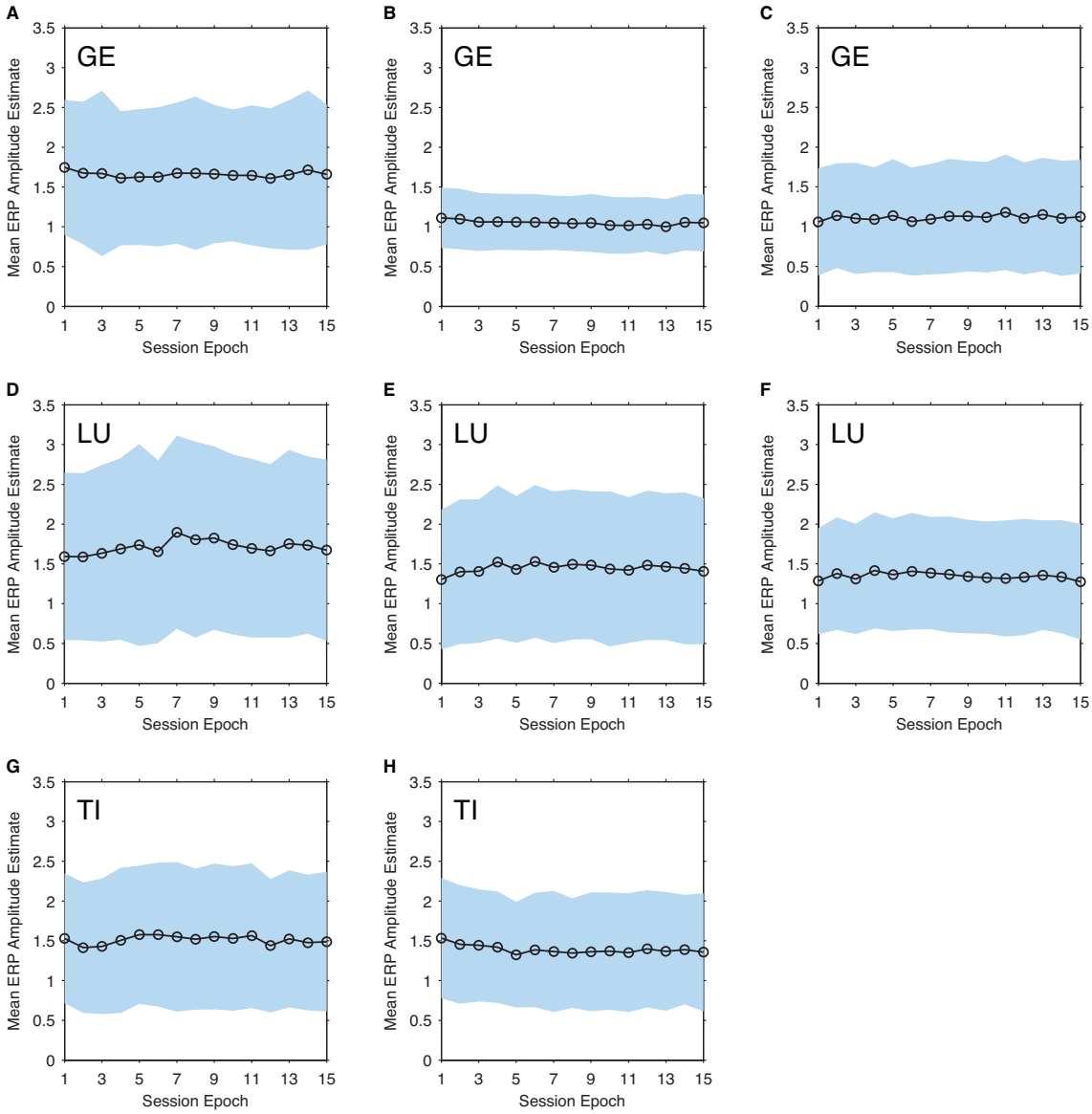

Figure 4.28: Correlation of mean VERP amplitude scaling estimate and session epoch displaying the mean VERP amplitude scaling estimate for 15 bins equally spaced across the temporally ordered ensemble of trials from each session. None of the correlations were significant. (A) GE channel 1, ($\rho(13) = -.18, p < 0.53$, uncorrected); (B) GE channel 2, ($\rho(13) = -0.19, p < 0.51$, uncorrected); (C) GE channel 3, ($\rho(13) = 0.22, p < 0.44$, uncorrected); (D) LU channel 2, ($\rho(13) = 030, p < 0.29$, uncorrected); (E) LU channel 10, ($\rho(13) = -0.02, p < 0.94$, uncorrected); (F) LU channel 11, ($\rho(13) = -0.10, p < 0.73$, uncorrected); (G) TI channel 1, ($\rho = -0.06, p < 0.85$, uncorrected); (G) TI channel 8, ($\rho(13) = -0.37, p < 0.17$, uncorrected). Blue shaded regions indicate +/- one standard deviation from the mean.

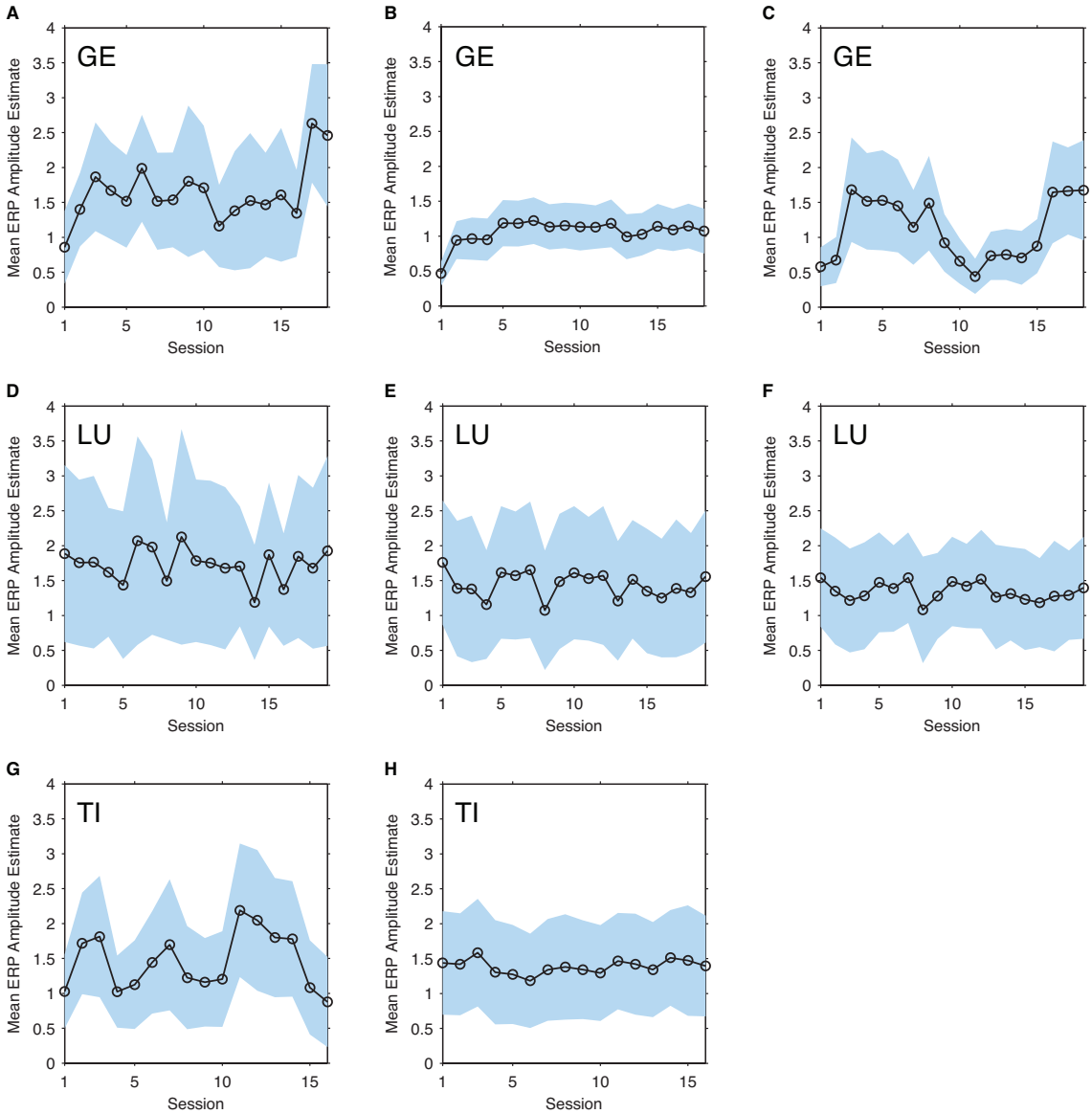

Figure 4.29: Correlation of mean VERP amplitude scaling estimate and recording session displaying the mean VERP amplitude scaling estimate for each of the sessions ordered by the recording sequence. None of the correlations were significant. (A) GE channel 1, ($\rho(16) = 0.20, p < 0.42$, uncorrected); (B) GE channel 2, ($\rho(16) = 0.24, p < 0.34$, uncorrected); (C) GE channel 3, ($\rho(16) = 0.18, p < 0.48$, uncorrected); (D) LU channel 2, ($\rho(17) = -0.11, p < 0.64$, uncorrected); (E) LU channel 10, ($\rho(17) = -0.25, p < 0.31$, uncorrected); (F) LU channel 11, ($\rho(17) = -0.26, p < 0.28$, uncorrected); (G) TI channel 1, ($\rho(16) = 0.08, p < 0.79$, uncorrected); (G) TI channel 8, ($\rho(16) = 0.20, p < 0.45$, uncorrected). Blue shaded regions indicate +/- one standard deviation from the mean.

4.4 Discussion

The results from the correlation analysis between subsensemble peak coherence and mean VERP amplitude revealed a mixed pattern of positive and negative correlation for the alpha, low gamma and high gamma ranges, with two, four, and three significant correlations, respectively. The mixed results indicate that within these bands pre-stimulus extrastriate-striate coherence may increase or decrease the magnitude of the subsequent VERP depending on the pair considered. Results from the beta band are far less ambiguous with seven pairs exhibiting a significant positive correlation. This indicates that in these seven pairs pre-stimulus beta band coherence is associated with increased amplitude of the subsequent VERP. The beta band coherence peaks are also of a considerably larger magnitude than those in the alpha, low gamma and high gamma ranges. Thus, overall, the beta band appears to be supporting a mechanism of VERP amplification that occurs due to increased coherence between extrastriate and striate cortex. This effect does not appear in all of the pairs, which demonstrates spatial specificity. This specificity may be related to retinotopy, since one striate site in each of the monkeys does not show modulation, which indicates that the part of visual space that maps to these regions is not targeted for modulation.

The correlations between subsensemble Granger causality and mean VERP amplitude support the role of beta band interdependence in VERP amplitude modulation. Aside from a singular negative correlation between top-down alpha band Granger causality and VERP amplitude, the beta band is the only frequency range to show correlations between directional influences and VERP amplitude. Like the coherence results, all of the beta band correlations are positive. These correlations are also exclusively in the top-down direction. So as does coherence, the magnitude of top-down pre-stimulus Granger causal influences predict the level of amplification of the subsequent VERP. The alpha band

negative correlation may be interpreted as inhibiting activity in the targeted area, which is consistent with findings of (Ergenoglu et al., 2004), but as a singular case the current analysis cannot determine if this is a general mechanism.

The presence of the pre-stimulus coherent oscillations and top-down Granger causal influences may be attributable to a gain control mechanism (Hillyard and Anllo-Vento, 1998; Hillyard et al., 1998). This mechanism may function in a fashion where top-down influences, carried by coherent oscillations, alter the response properties of target neuronal populations. Indeed it has been proposed that the frequency content of ongoing cortical activity may be a distinct determinant of the excitability of cortical tissue (Ploner et al., 2006). This increased excitability is then expressed as enhanced VERP amplitude during stimulus processing. Figure 4.22 supports this idea, demonstrating that pre-stimulus top-down influences show a threshold at which top-down Granger causal influences become effective in modulating the VERP. Pairs that exhibit a significant correlation have larger values overall, and a greater spread of values. This may indicate that there is a threshold which must be exceeded before the striate region is sufficiently impacted by extrastriate activity. The top-down input may then entrain or overcome the intrinsic dynamics of the striate region. In this way the intrinsic dynamics of the striate region may govern the VERP amplitude when top-down influence is small, which is evident from the variability of the VERP amplitude even at very low levels of top-down influence, yet as top-down influence increases the striate region's dynamics may be altered yielding a larger VERP.

Coherence and top-down Granger causal influences were highly correlated in all six pairs that exhibited a significant correlation between top-down Granger causality and VERP amplitude. One pair also showed a significant correlation between bottom-up Granger causality and VERP amplitude. Overall, the mean top-down Granger causality form each pair was strongly correlated with mean coherence, whereas bottom-up Granger causality was significantly correlated, but on the borderline of significance. This result

indicates that top-down Granger causality and coherence are intimately related during the pre-stimulus period, whereas bottom-up influences are not to the same degree. The relative phase results shown in 4.25 echo this result since the relative phase circular variance is negatively correlated with mean top-down Granger causal influences, but bottom-up influences are not. This suggests that top-down down influences may be adjusting relative phase relations so that the relative phase between pairs is more tightly clustered around a mean value. 4.26 supports this conclusion as the pairs with significant correlations between top-down Granger causality and mean VERP amplitude are significantly more tightly clustered around 45 degrees than the non-significantly correlated pairs. 4.27 shows a similar result, where significantly correlated pairs are more tightly clustered around roughly 6.6 milliseconds, whereas the not significantly correlated pairs (in blue) show a significantly larger variance around 7.7 milliseconds. The 7.2 millisecond lead by extrastriate sites is also of importance, since this value is in the range expected for transmission delays in this part of the visual system (Nowak and Bullier, 1997). This indicates that the relative phase values may be specifically adjusted so that action potentials originating at the peak of one site arrive at the peak of the oscillation at the other site enhancing interareal communication (Fries, 2005).

One important aspect of the results that needs to be addressed is that not all significant top-down VERP modulations are accompanied by significantly correlated coherence with the mean VERP. This can be explained by the fact that mathematically coherence is related to Granger causality. The total interdependence can be decomposed into three terms: two unidirectional influences, and an instantaneous term (Ding et al., 2006),

$$f_{X,Y}(\omega) = f_{X\rightarrow Y}(\omega) + f_{Y\rightarrow X}(\omega) + f_{X\cdot Y}(\omega). \tag{4.3}$$

This is related to the coherence by the following relation:

$$f_{X,Y}(\omega) = -\ln(1 - C(\omega)). \tag{4.4}$$

Thus if only the top-down Granger causal influences are correlated with VERP amplitude, then pairs where the coherence is also largely influenced by the instantaneous and bottom-up components of the total interdependence may not show a correlation between coherence and VERP amplitude, since the top-down correlated component may be washed out by the other two components. A situation like this may be occurring for GE pair 6-1 Figure 4.9 and TI pair 3-1 4.14.

A related situation is where a pair shows a significant coherence correlation without a significant correlation between top-down Granger causality with mean VERP amplitude. This could occur if both the extrastriate and striate components of the pair are mutually influenced by a third unmeasured region. This would lead to a large correlated instantaneous causality term, without correlation in either of the unidirectional terms. Preliminary analysis of this possibility has been performed and the results indicate that this is indeed the case.

Overall, the current analyses suggest a prominent role for interareal beta frequency interactions in modulating VERP amplitude. It appears that these modulatory effects are due to top-down influences that are carried by coherent oscillations between extrastriate regions and targeted regions of striate visual cortex.

CHAPTER 5

TOP-DOWN MODULATION AND ONSET ASYNCHRONY

5.1 Introduction

Based on the finding of the previous study (Chapter 4) that top-down beta Granger causality modulates the VERP amplitude in a six of 18 extrastriate-striate pairs across the three monkeys, it is of great interest as to what factors my control the single-trial variation of the VERP. As discussed in section 4.3.5, there is large variation between the mean VERP estimates across sessions for certain striate recording sites. This might suggest that these differences could be due to session differences that impact the size of the top-down influences, but since they were not controlled for in the experiment, such factors cannot be determined. Thus it becomes important to determine what single-trial aspects of the task may have contributed to the single-trial modulation of the top-down influences. A pertinent task parameter is the stimulus onset asynchrony. This refers to the randomized delay of 200 - 1215 milliseconds that is initiated by the monkey's lever press, which initiates the trial. Since the probability density function for the onset of the stimulus is uniform, this gives rise to an increasing hazard function (Weisstein, 2009),

$$h(x) = \frac{P(x)}{1 - D(x)}, \tag{5.1}$$

where $P(x)$ is the probability density function, and $D(x)$ is the cumulative distribution function.

The increasing hazard function dictates that the longer the monkey waits for the stimulus to occur, the more likely the stimulus is to occur due to the finite probability that in all trials the stimulus appears by at least 1250 milliseconds. This fact raises the possibility that the monkey's level of anticipation may vary with the onset time of the stimulus, which is the specific interval between the lever press and the delivery of the visual stimulus, and thus the strength of the top-down modulation may also vary with the onset time. One intriguing possibility is that the strength of the beta top-down modulatory influence is tracking the conditional probability of the occurrence of the stimulus, aiding the prediction of its onset (Fries, 2009, personal communication). Riehle et al. (1997) systematically varied the conditional probability of the cue to touch a visual target while recording from two to seven neurons simultaneously in the motor cortex. The cue could appear at four distinct times (600, 900, 1200, or 1500 milliseconds post cue) during the trial, each with a conditional probability of 0.25, 0.33, 0.50 and 1. They found decreasing response times with increasing onset time of the stimulus and that periods of significant spike synchrony were clustered around the four times when the stimulus was expected. Thus their findings suggest that the spike synchrony increases during the periods when the occurrence of the stimulus is most probable, readying the motor system for the behavioral response. A similar result was obtained by Schoffelen et al. (2005) while measuring cortical-spinal coherence. Using a paradigm where a change in a visual cue signaled a wrist movement they varied the hazard function which governed the change in the visual cue by linearly increasing and decreasing the conditional probability of the stimulus change in two conditions. They found that cortico-spinal coherence in the gamma fre-

quency range was positively correlated with the hazard function, and that response times decreased with increasing probability of the stimulus change. Interestingly, they found during the condition with increasing conditional probability of the stimulus change that beta power and low beta (below 20 Hz) coherence measured between MEG sensors over the motor cortex were negatively correlated with the hazard function, such that beta frequency coherence decreased the longer the subject waited for the stimulus change, and hence as the stimulus change became more probable.

The current analysis attempts to test the prediction that pre-stimulus beta range coherence and Granger causality systematically vary with onset time, and hence, demonstrate a relationship with the increasing hazard function used in this experiment.

5.2 Methods

5.2.1 Recording

The recording methodology used for this experiment was the same as described in section 3.2.1.

5.2.2 Task

The task used for this experiment was the same as described in section 3.2.2.

5.2.3 Data preprocessing

Data was preprocessed as described in section 3.2.4.

5.2.4 Trial subensembles

Like the process described in section 4.2.5. single-trial onset times were obtained for each of the trials, for each session of each monkey. For each monkey these onset times were sorted by size and then binned into 400 trial subensembles with a 75% overlap.

5.2.5 Correlation of pre-stimulus coherence and Granger causality with mean subsensemble onset time

For each subensemble of trials, we computed peak coherence and Granger causality for each striate-extrastriate pair over the beta frequency range as the local spectral maximum, employing the same AR preprocessing stages and parameters described in section 3.2.5. These peaks were thresholded for significance using the same randomization distribution and multiple comparisons correction as described in section 3.2.6. A Spearman rank cor-

relation coefficient was then computed between the magnitude of the significant peaks in the Granger causality and coherence spectra, and the mean onset time of the corresponding subensembles. The correlation was computed separately for Granger causality in both the top-down and bottom-up directions. The correlation p-values were corrected for multiple comparisons using Dunn's method.

5.3 Results

5.3.1 Response time

The correlation between onset time and response time for the Go trials was calculated, revealing significant negative correlation for each monkey (Figure 5.1). The negative correlation indicates that longer onset times resulted in faster response times.

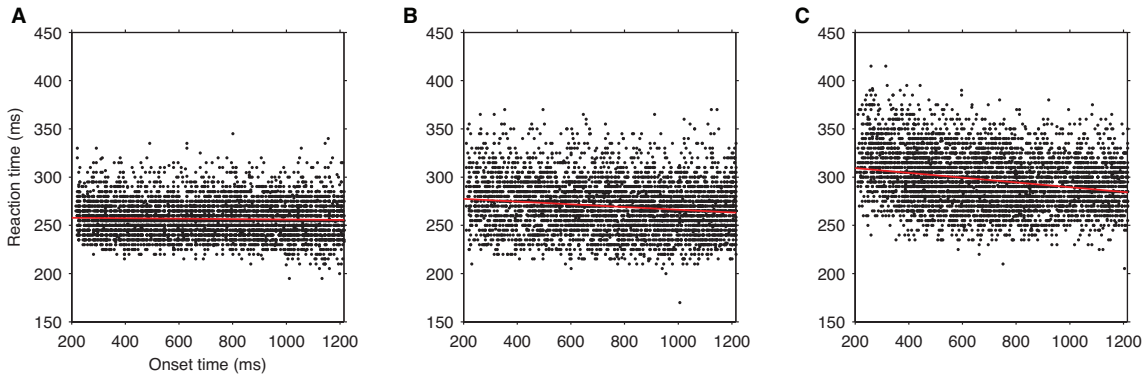

Figure 5.1: Correlation of onset time versus response time for the Go trials from each monkey. Monkey GE (A) was significant ($\rho(5223) = -.036, p < 0.0296$, corrected), LU (B) was also significant ($\rho(4406) = -.147, p << 0.001$, corrected), as was TI (C) ($\rho(4774) = -.240, p << 0.001$, corrected).

5.3.2 Correlation analysis

For each site pair, 400 trial subensembles were created that were ordered by the single-trial stimulus onset time. A Spearman rank correlation was then computed between the pre-stimulus beta significant peak coherence and the subsensemble mean onset time. This process was repeated with top-down Granger causality, and bottom-up Granger causality spectra. The correlation results for coherence and mean onset time are tabulated in Table 5.1, while those for Granger causality are found in Table 5.2. Figures 5.2 through 5.12 show spectral and correlation results for pairs with subsensemble beta band coherence or Granger causality values that are correlated with the mean onset times.

Correlation analysis of subsensemble coherence and mean onset time

Over all of the 18 pairs across the three monkeys, eight pairs showed a significant negative correlation between beta band subsensemble coherence and the subsensemble mean onset time, while one pair showed a positive correlation. Five of the negative correlations were found in GE (pairs 5-1 Figure 5.2, 5-2 Figure 5.3, 5-3 Figure 5.4, 6-1 Figure 5.5, and 6-3 Figure 5.7). Monkey LU showed two negative correlations between beta band subsensemble coherence and the subsensemble mean onset time in pairs 3-10 (Figure 5.8) and 3-11 (Figure 5.9). Monkey TI exhibited one positive correlation between beta band subsensemble coherence and the subsensemble mean onset time in pair 3-1 (Figure 5.11) and one negative correlation for pair 9-8 (Figure 5.12).

Correlation analysis of subsensemble Granger causality and mean onset time

Of the 18 pairs, beta band subsensemble Granger causality and the subsensemble mean onset time were significantly negatively correlated for six pairs in the top-down direction, and negatively correlated for one pair in the bottom-up direction. Two of the 18 pairs were significantly positively correlated in the top-down direction, which indicates that unlike the other pairs, beta band top-down influence increased with later onset times. GE had three negative correlations between top-down beta band subsensemble Granger causality and the subsensemble mean onset time in pairs 5-1 (Figure 5.2), 5-3 (Figure 5.4), and 6-1(Figure 5.5), and a positive correlation for pair 6-2 (Figure 5.6). The three negatively correlated pairs also showed significant coherence correlations, as reported in the previous section. Most importantly, these three pairs were the only pairs in GE to show a significant positive correlation between subensemble top-down beta range Granger causality and subensemble mean VERP amplitude. Thus in monkey GE, negative correlation of top-down subensemble Granger causality with the subsensemble mean onset time is only present in pairs where the VERP is significantly modulated by the top-down

influence. Monkey LU shows the same pattern, with pairs 3-10 (Figure 5.8) and 3-11 (Figure 5.9) exhibiting both significant negative correlations between top-down subensemble Granger causality and subsensemble mean onset time and significant positive correlations between top-down subensemble Granger causality and subsensemble mean VERP amplitude. These two pairs also showed significant negative correlations between subensemble coherence and subsensemble mean onset time. LU possessed the only case of a bottom-up Granger causality correlation, also in the negative direction, with mean onset time (pair 3-11 Figure 5.9). This pair also showed a negative top-down correlation, and a negative coherence correlation. Monkey TI presented a paradoxical result with a positive correlation between top-down Granger causality and onset time in pair 3-1 (Figure 5.11), which coincided with the positive top-down correlation between top-down Granger causality and the mean VERP amplitude. Coherence and onset time were also positively correlated for this pair. TI also had a significant negative correlation between top-down Granger causality and mean onset time in pair 2-1 (Figure 5.10).

Overall, all of the six pairs that showed a significant positive correlation between top-down Granger causality and mean VERP amplitude, also showed a significant negative correlation between coherence with mean onset time and top-down Granger causality with mean onset time, with the exception of TI, where the latter two correlations were positive.

Table 5.1: Correlation results of subsensemble peak coherence versus subensemble mean onset time.

Monkey	Pair		ρ	Coherence f (Hz)		Coherence	
	E	S		*M*	*SD*	*M*	*SD*
GE	4	1	-.01	27.25	2.16	0.037	0.012
	4	2	.00	23.48	4.93	0.023	0.007
	4	3	.55	20.50	1.85	0.047	0.022
	5	1	-.63***	15.45	1.12	0.085	0.044
	5	2	-.48***	18.23	1.74	0.035	0.022
	5	3	-.60***	18.37	1.56	0.128	0.046
	6	1	-.60***	17.34	1.67	0.054	0.030
	6	2	.01	19.39	2.74	0.020	0.007
	6	3	-.51***	19.15	2.47	0.023	0.010
LU	3	2	-.34	20.71	3.80	0.024	0.011
	3	10	-.64***	19.49	4.02	0.086	0.038
	3	11	-.83***	18.90	2.25	0.127	0.057
TI	2	1	-.16	23.31	3.84	0.024	0.009
	2	8	.00	23.44	3.58	0.022	0.006
	3	1	.36**	21.31	2.75	0.054	0.021
	3	8	.02	22.38	3.23	0.027	0.009
	9	1	.15	21.70	5.31	0.018	0.004
	9	8	-.69***	19.15	5.01	0.058	0.024

* $p < 0.05$. ** $p < 0.01$. *** $p << 0.001$, corrected

Table 5.2: Correlation results of subsensemble peak Granger causality versus subensemble mean onset time.

Monkey	Pair		Top-down					Bottom-up				
				GC f (Hz)		GC			GC f (Hz)		GC	
	E	S	ρ	*M*	*SD*	*M*	*SD*	ρ	*M*	*SD*	*M*	*SD*
GE	4	1	.02	27.62	3.77	0.023	27.62	-	-	-	-	-
	4	2	.20	21.25	1.26	0.013	21.25	-	-	-	-	-
	4	3	.36	21.09	2.77	0.023	21.09	1.00	14.50	0.71	0.017	0.000
	5	1	-.67***	18.39	1.71	0.05	18.39	-.64	23.36	5.94	0.028	0.009
	5	2	.08	15.96	1.24	0.019	15.96	-1.00	21.67	7.23	0.014	0.003
	5	3	-.42***	16.09	1.14	0.077	16.09	-.31	20.83	5.02	0.019	0.008
	6	1	-.51***	16.62	1.93	0.028	16.62	.09	28.00	0.88	0.01	0.00
	6	2	.46**	17.45	3.45	0.018	17.45	-.20	29.46	0.66	0.013	0.005
	6	3	-.37	16.83	2.14	0.012	16.83	.30	16.60	0.55	0.015	0.005
LU	3	2	-.24	24.38	2.55	0.01	24.38	-.43	22.57	1.90	0.009	0.002
	3	10	-.72***	18.70	1.55	0.038	18.70	-.15	19.83	2.62	0.018	0.005
	3	11	-.41*	21.90	3.60	0.038	21.90	-.81***	21.59	2.76	0.04	0.02
TI	2	1	-.66***	17.91	3.86	0.016	17.91	-.42	16.94	1.43	0.017	0.005
	2	8	-1.00	15.75	2.36	0.015	15.75	-	-	-	-	-
	3	1	.58***	20.58	3.01	0.035	20.58	.04	26.22	2.35	0.013	0.004
	3	8	-.14	21.38	2.61	0.013	21.38	.60	29.50	0.58	0.008	0.001
	9	1	-	18.00	0.00	0.012	18.00	.50	22.33	0.58	0.009	0.001
	9	8	.14	18.07	2.03	0.023	18.07	-.36	20.73	4.67	0.013	0.003

* $p < 0.05$. ** $p < 0.01$. *** $p << 0.001$, corrected

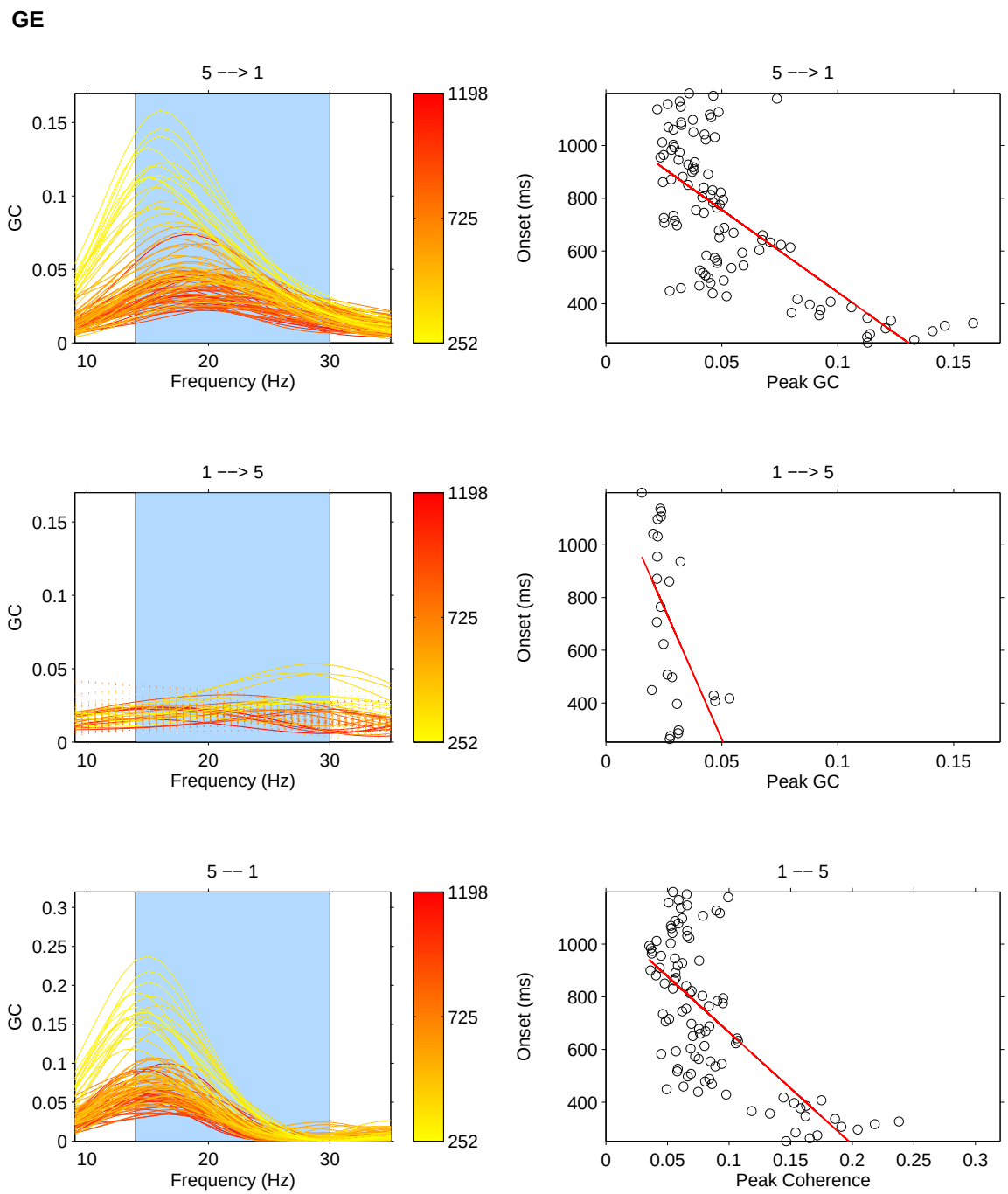

Figure 5.2: Subensemble spectra for top-down and bottom-up Granger causality and coherence (left panels) and the correlations between significant beta range Granger causality and coherence spectral peaks, and subensemble mean onset time (right panels) for pair GE 5-1. Significant correlations are fit with a regression line. Spectra with significant peaks are drawn in solid lines, with spectra without significant peaks drawn with dotted lines.

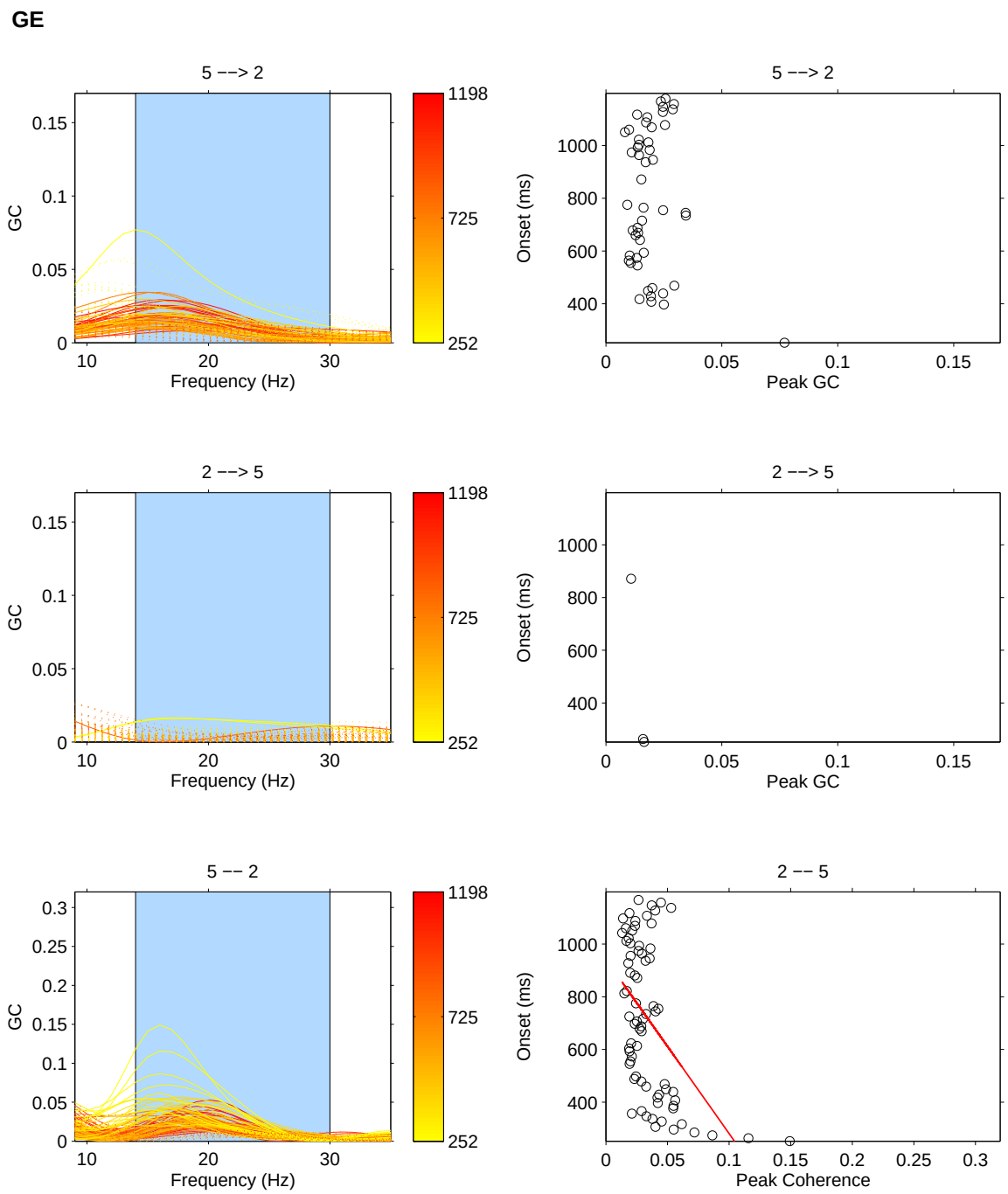

Figure 5.3: Subensemble spectra for top-down and bottom-up Granger causality and coherence (left panels) and the correlations between significant beta range Granger causality and coherence spectral peaks, and subensemble mean onset time (right panels) for pair GE 5-2. Significant correlations are fit with a regression line. Spectra with significant peaks are drawn in solid lines, with spectra without significant peaks drawn with dotted lines.

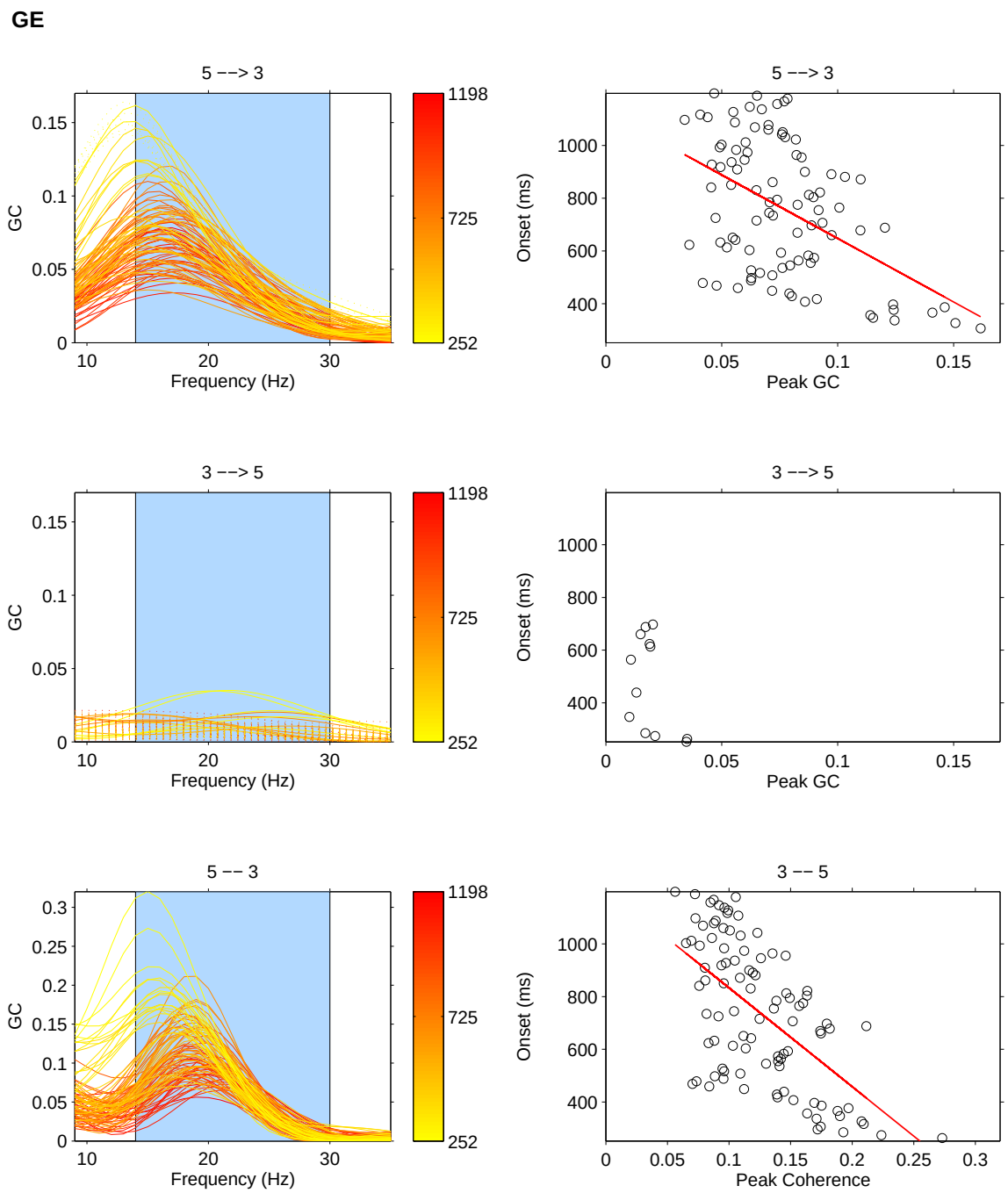

Figure 5.4: Subensemble spectra for top-down and bottom-up Granger causality and coherence (left panels) and the correlations between significant beta range Granger causality and coherence spectral peaks, and subensemble mean onset time (right panels) for pair GE 5-3. Significant correlations are fit with a regression line. Spectra with significant peaks are drawn in solid lines, with spectra without significant peaks drawn with dotted lines.

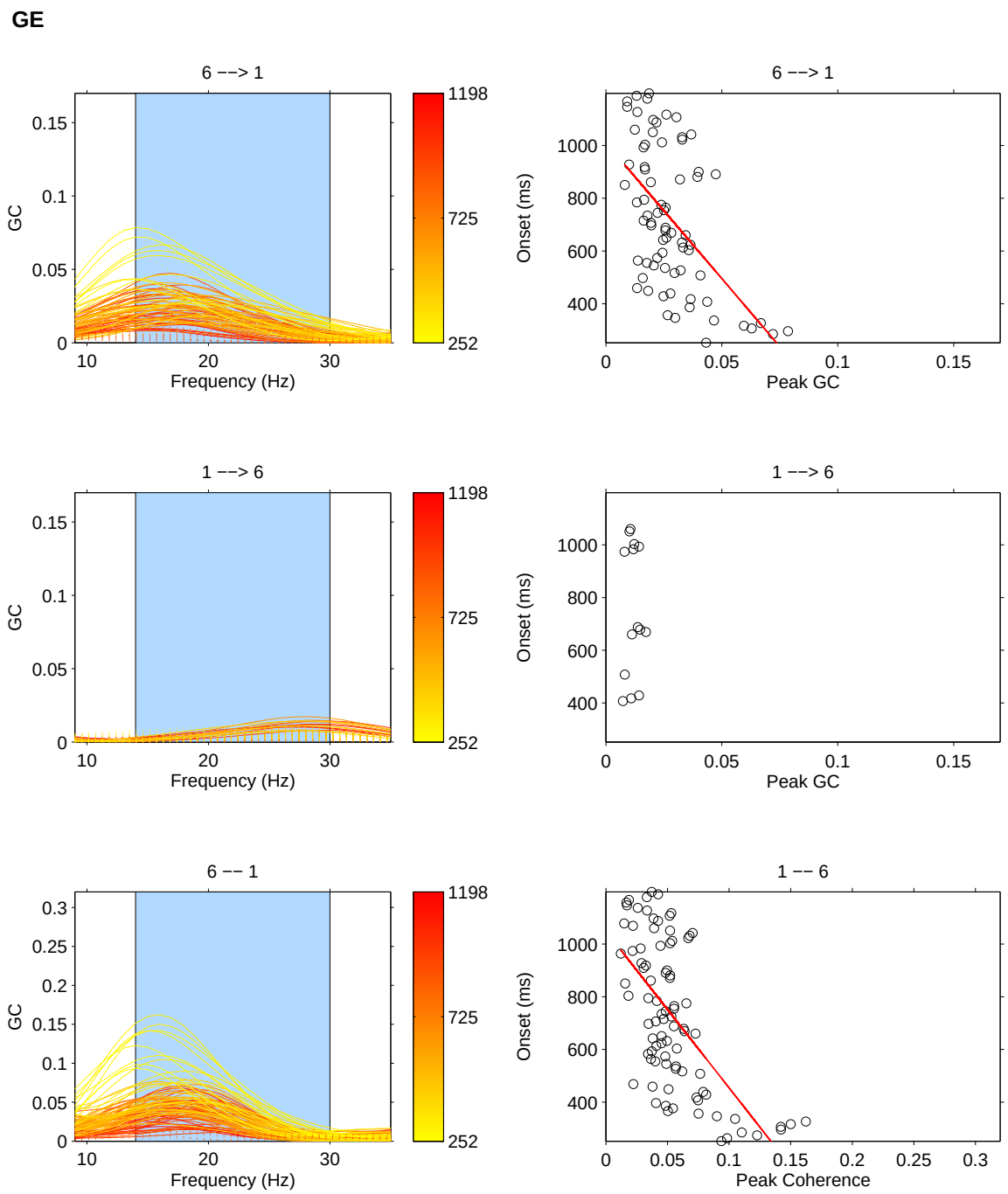

Figure 5.5: Subensemble spectra for top-down and bottom-up Granger causality and coherence (left panels) and the correlations between significant beta range Granger causality and coherence spectral peaks, and subensemble mean onset time (right panels) for pair GE 6-1. Significant correlations are fit with a regression line. Spectra with significant peaks are drawn in solid lines, with spectra without significant peaks drawn with dotted lines.

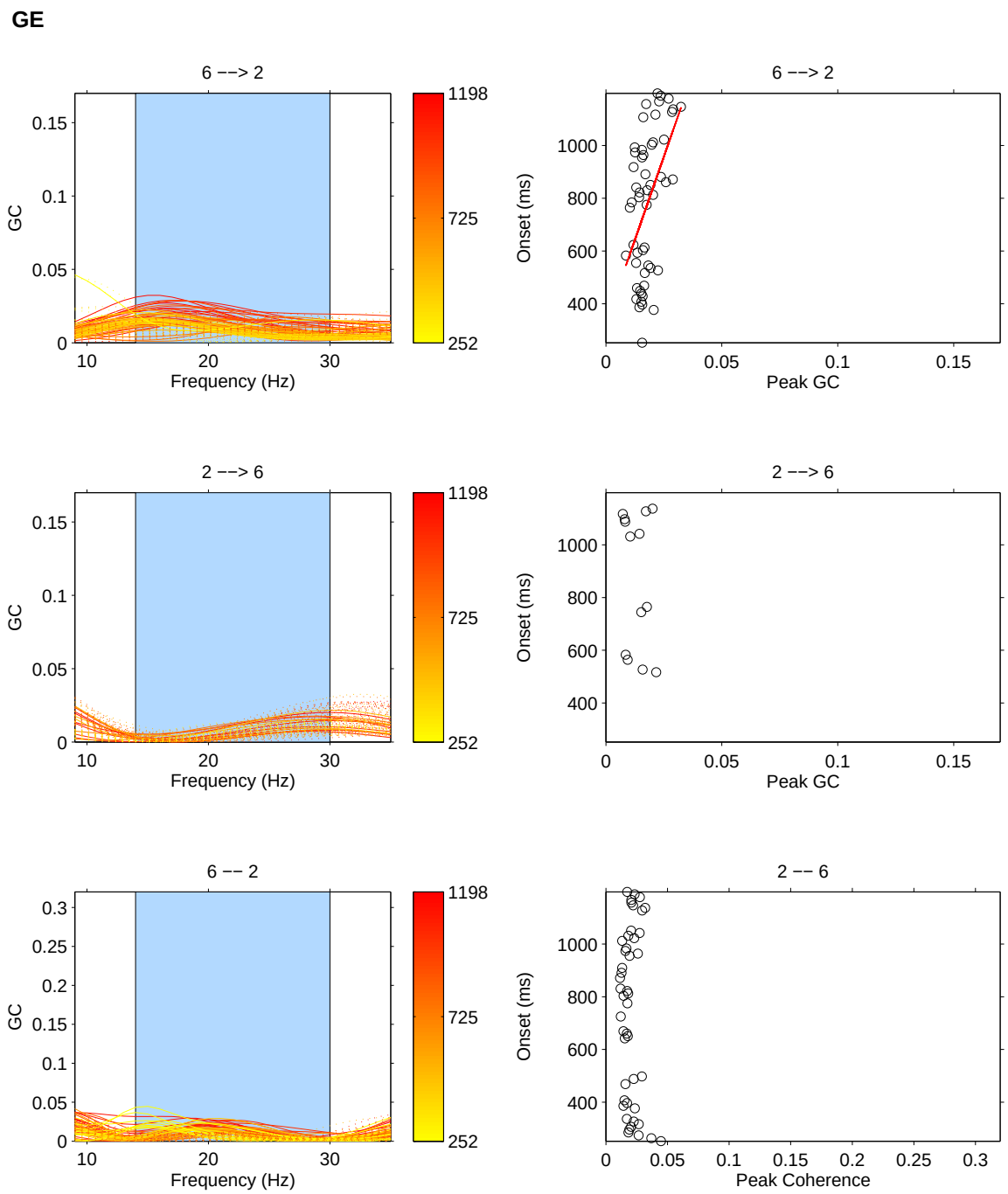

Figure 5.6: Subensemble spectra for top-down and bottom-up Granger causality and coherence (left panels) and the correlations between significant beta range Granger causality and coherence spectral peaks, and subensemble mean onset time (right panels) for pair GE 6-2. Significant correlations are fit with a regression line. Spectra with significant peaks are drawn in solid lines, with spectra without significant peaks drawn with dotted lines.

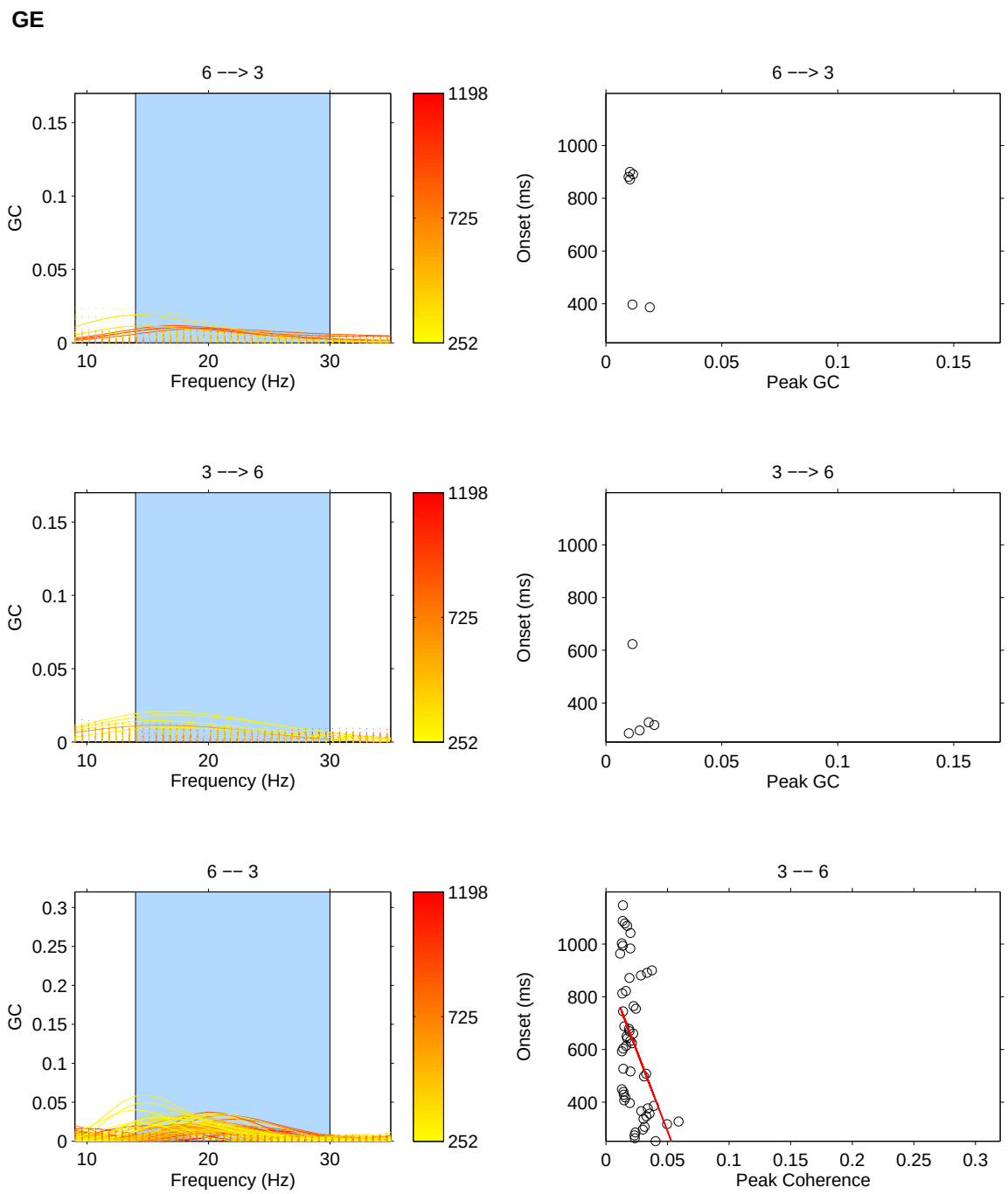

Figure 5.7: Subensemble spectra for top-down and bottom-up Granger causality and coherence (left panels) and the correlations between significant beta range Granger causality and coherence spectral peaks, and subensemble mean onset time (right panels) for pair GE 6-3. Significant correlations are fit with a regression line. Spectra with significant peaks are drawn in solid lines, with spectra without significant peaks drawn with dotted lines.

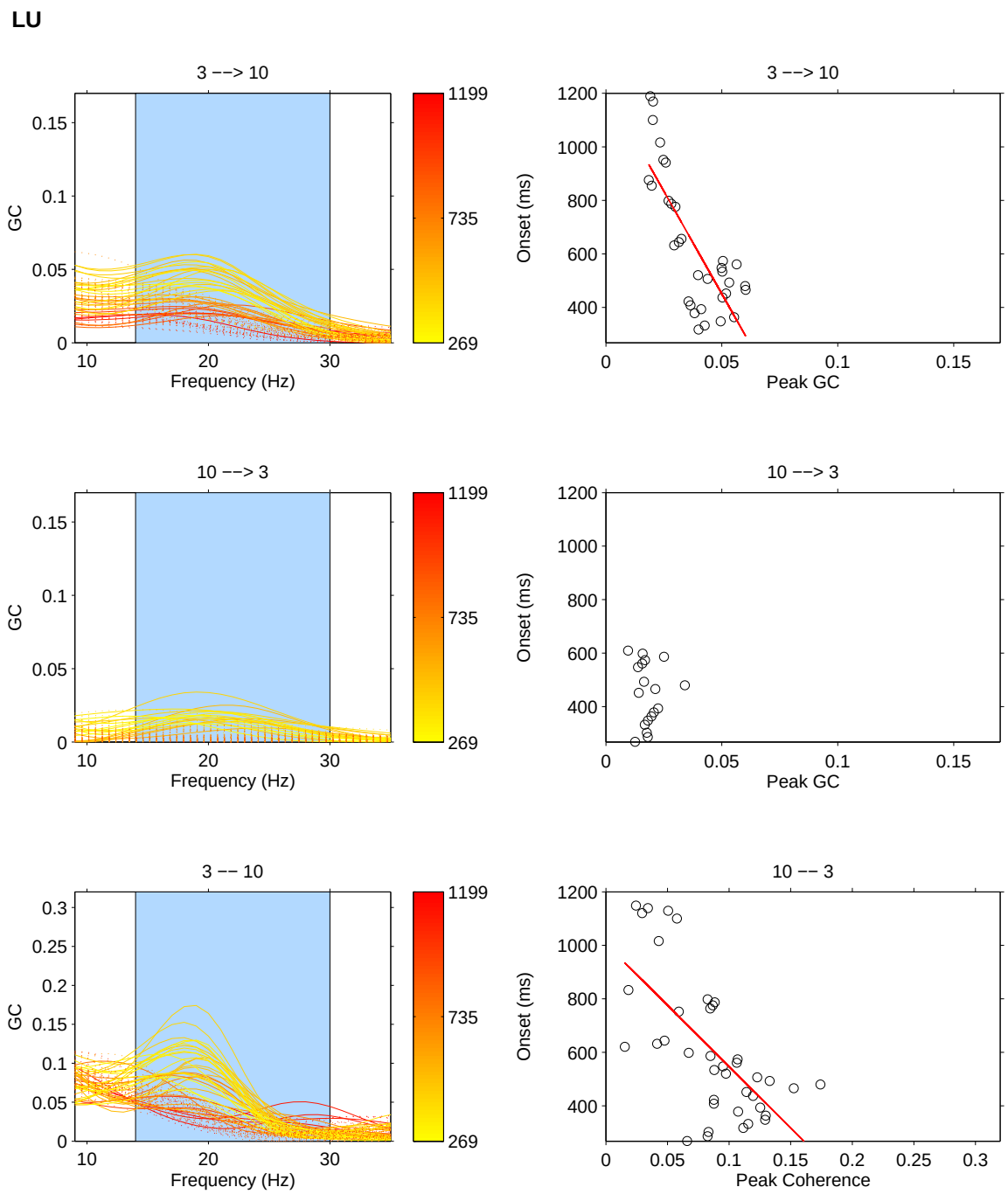

Figure 5.8: Subensemble spectra for top-down and bottom-up Granger causality and coherence (left panels) and the correlations between significant beta range Granger causality and coherence spectral peaks, and subensemble mean onset time (right panels) for pair LU 3-10. Significant correlations are fit with a regression line. Spectra with significant peaks are drawn in solid lines, with spectra without significant peaks drawn with dotted lines.

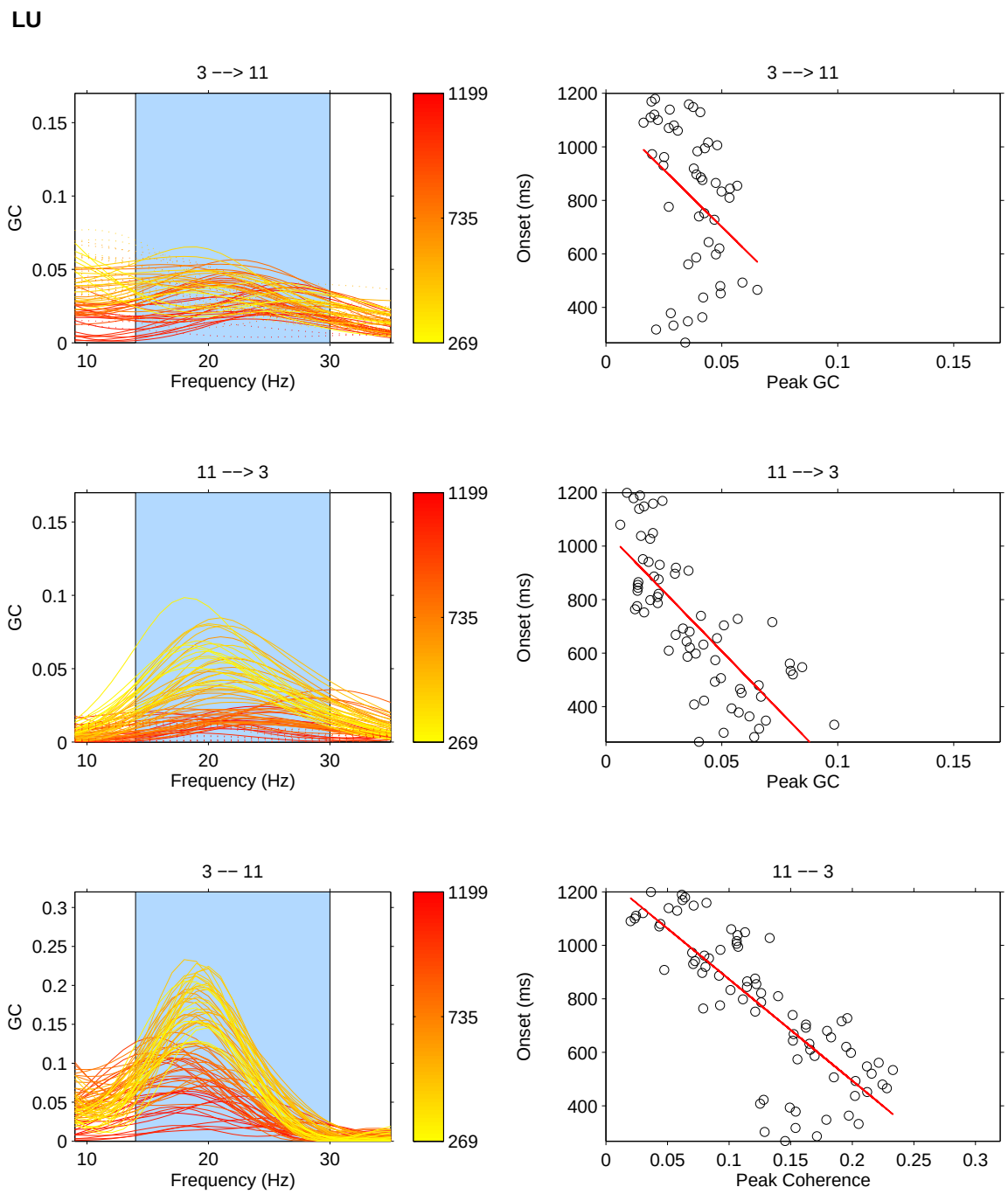

Figure 5.9: Subensemble spectra for top-down and bottom-up Granger causality and coherence (left panels) and the correlations between significant beta range Granger causality and coherence spectral peaks, and subensemble mean onset time (right panels) for pair LU 3-11. Significant correlations are fit with a regression line. Spectra with significant peaks are drawn in solid lines, with spectra without significant peaks drawn with dotted lines.

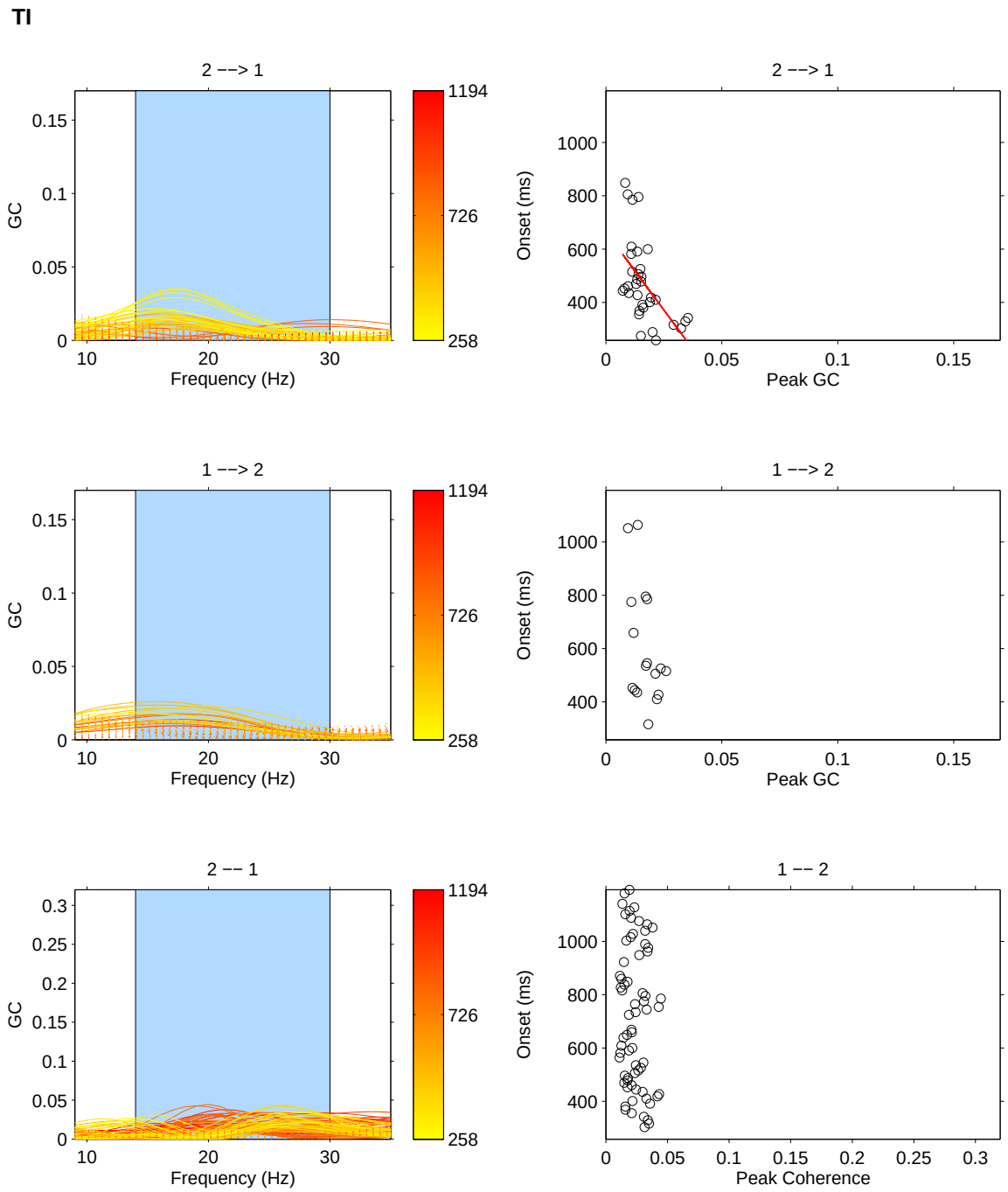

Figure 5.10: Subensemble spectra for top-down and bottom-up Granger causality and coherence (left panels) and the correlations between significant beta range Granger causality and coherence spectral peaks, and subensemble mean onset time (right panels) for pair TI 2-1. Significant correlations are fit with a regression line. Spectra with significant peaks are drawn in solid lines, with spectra without significant peaks drawn with dotted lines.

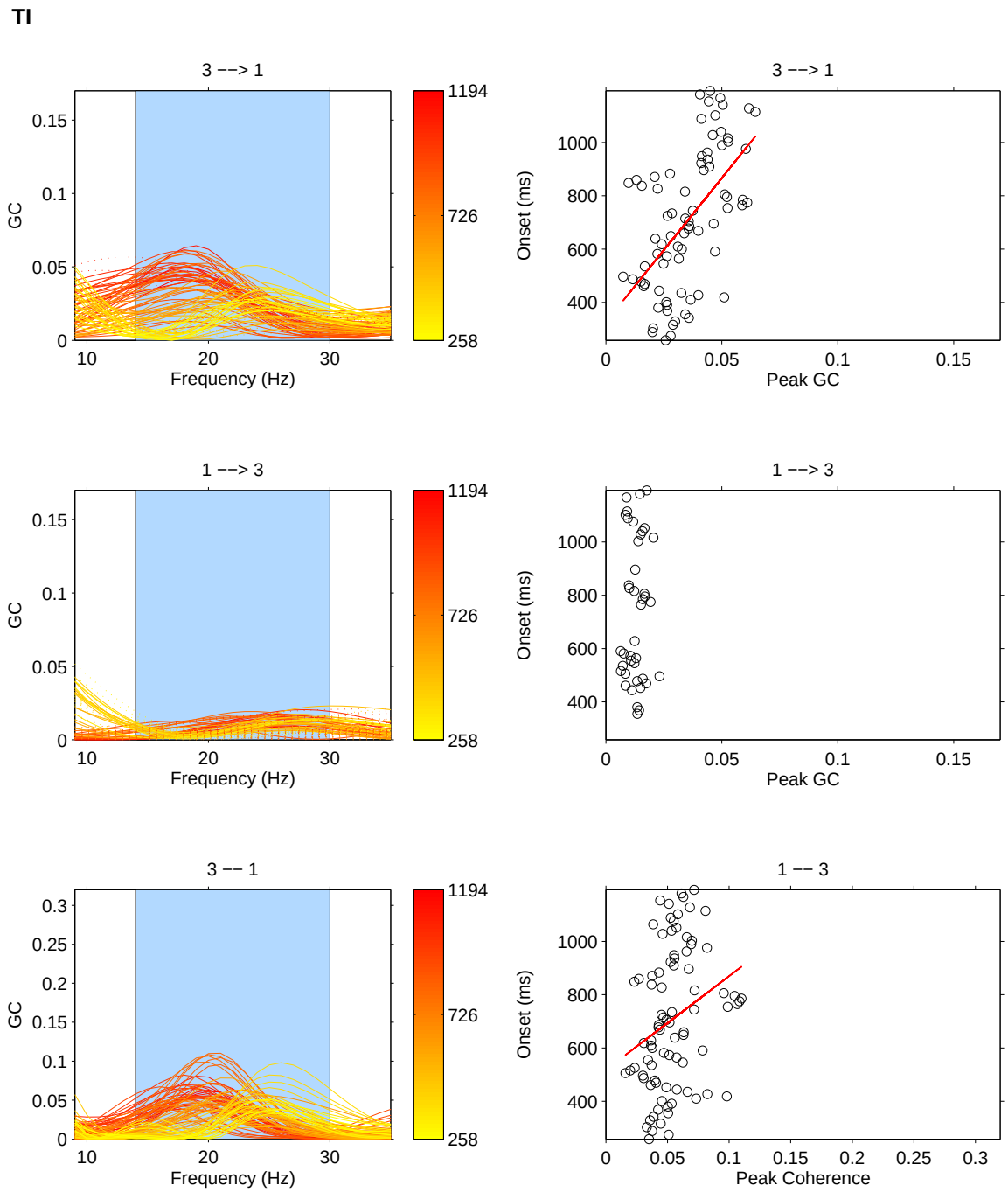

Figure 5.11: Subensemble spectra for top-down and bottom-up Granger causality and coherence (left panels) and the correlations between significant beta range Granger causality and coherence spectral peaks, and subensemble mean onset time (right panels) for pair TI 3-1. Significant correlations are fit with a regression line. Spectra with significant peaks are drawn in solid lines, with spectra without significant peaks drawn with dotted lines.

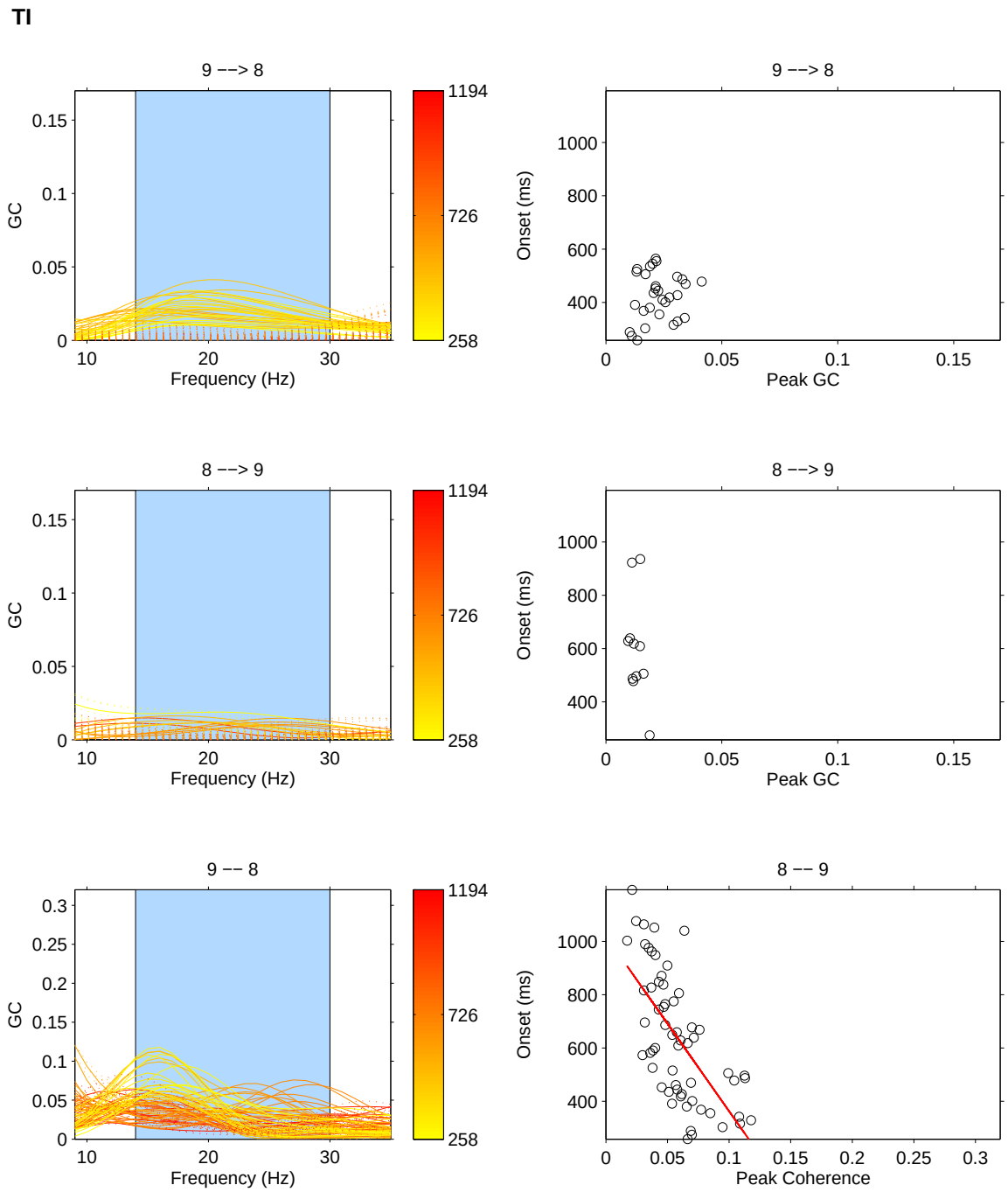

Figure 5.12: Subensemble spectra for top-down and bottom-up Granger causality and coherence (left panels) and the correlations between significant beta range Granger causality and coherence spectral peaks, and subensemble mean onset time (right panels) for pair TI 3-1. Significant correlations are fit with a regression line. Spectra with significant peaks are drawn in solid lines, with spectra without significant peaks drawn with dotted lines.

5.4 Discussion

The response time results displayed in Figure 5.1 decrease with increasing onset time, and thus are in agreement with the findings of Riehle et al. (1997) and Schoffelen et al. (2005). This result is well explained by the interpretation that as the onset of the stimulus becomes more predictable, as it does the longer the onset interval, that the perceptual-motor system may become more primed to respond. In the study by Schoffelen et al. (2005) this effect occurred in relation to increases in gamma band, and a decrease in low beta band synchronization and coherence in the motor system. The current analysis was restricted to the visual system where beta band coherence also decreased with faster response times. This is suggestive that a similar mechanism may underlie events in the visual system that lead to enhanced response times that is shared with the motor system, yet since both tasks involved a visual and motor component, it cannot be determined if the decrease in response time is due solely to mechanisms in the motor system, or if mechanisms in the visual system also contribute. The parallel beta coherence-response time result shared by both studies in the two different systems is an encouraging commonality that is suggestive of a common mechanism.

As reported by (Schoffelen et al., 2005) in the motor system, low-frequency beta coherence decreased as the hazard function increased. This indicates that as the stimulus onset becomes more predictable, beta coherence decreases. In the current results, all pairs with significant correlations between beta coherence and onset time, or top-down Granger causality and onset time are below 21 Hz, and thus lie in the low beta range, and in eight of the nine significant coherence versus onset time correlations beta coherence decreased with increasing onset time. Thus as found by Schoffelen et al. (2005), low beta coherence appears to track the cumulative probability of stimulus onset in the visual system in a similar way to that found in the motor system. The current findings extend these results

by demonstrating that six of the eight significant correlations between top-down Granger causality and mean onset time were negative, which indicates that like coherence, the top-down causal influences from extrastriate to striate regions also scale with the level of predictability of the the stimulus onset. This phenomenon appears to be connected with the modulation of VERP amplitude by top-down influences, as found in the previous study. All six pairs that were found to have significant top-down modulation of VERP amplitude, also have the magnitude of this top-down modulation, and the corresponding coherence peaks, correlated with the onset time. In five of the cases the correlation is negative, in agreement with the results of Schoffelen et al. (2005), but one case (TI pair 3-1 Figure 5.11) the correlation is positive. In the case of the negative correlations, low beta top-down influences and coherence may mediate hierarchical bayesian inference (Lee et al., 2003). In such a scheme top-down processes may convey information regarding expected stimulus properties, which may occur prior to stimulus onset. In the current study it is possible that descending information regarding the probability of stimulus onset is carried by top-down beta range influences, and that these influences scale inversely with stimulus onset probability. The positive correlation between onset time and beta band coherence and Granger causality found in monkey TI does not conform to this framework, but may be the result of under-sampling. It is thought that perceptual processing may involve mesoscopic spatial patterns of amplitude modulation: wave packets, that correlate with the context and value of the sensory stimulus (Freeman, 2003). Thus in the context of the current experiment, the extrastriate-striate wave packet would be predicted to have both peaks and troughs of electrical activity spanning the area. It is thus likely that sparse sampling of the area may result in conflicting results. With the advancement of recording technology it is becoming increasingly possible to sample cortical activity more densely, which may reveal these detailed patterns of activity in visual cortex.

In conclusion, these results point to an important relationship between the onset time,

interareal coherence, top-down Granger causal influences and the amplitude of the subsequent VERP. It is an attractive hypothesis that the strength of pre-stimulus top-down influences, carried by coherent interactions between extrastriate and striate cortex, may track the likelihood of the stimulus occurring at any given time across a trial. Via these interactions enhanced communication may be fostered between the regions, which may sensitize striate cortex causing an evoked response of increased magnitude that is dependent on these pre-stimulus dynamic interactions within the anticipatory visual network.

CHAPTER 6

SUMMARY AND CONCLUSIONS

The overall goal of the present work was to study interdependent interactions between visual components of a neurocognitive network during the anticipation of a visual stimulus. This neurocognitive network was hypothesized to convey knowledge from higher level transmodal cortical regions to unimodal visual sensory areas. This activity was hypothesized to be transmitted via top-down influences carried by coherent oscillations.

Analysis one (chapter 3) demonstrated that during the anticipatory period of the visual discrimination task, coherent and Granger causal interactions occurred between extrastriate and striate visual regions at a number of frequencies in the three monkeys. This activity appeared to be the most robust in the beta frequency range. The predominance of beta frequency activity is consistent with the proposed role of beta frequency oscillations as effective mediators of long-range cortical-cortical interactions (see section 2.2.1). The functional importance of this anticipatory activity was probed in the second analysis (chapter 4), where a relationship was found between anticipatory coherent and Granger causal activity and VERP amplitude. Correlation between coherence and VERP amplitude was found in all frequency bands (alpha, beta, low gamma and high gamma), but this relationship was only found to be consistently positive in the beta band. Correlation between Granger causal influences and the VERP amplitude were only found in the alpha and beta bands, and these correlations were only in the top-down direction. The

alpha band correlation was only present in one monkey, yet the beta band correlations were present in six cases across the three animals. These results indicate that beta frequency oscillations carry top-down Granger causal influences from extrastriate cortex to striate cortex, which modulate the activity of striate cortex resulting in a larger potential evoked by the visual stimulus. Extrastriate-striate pairs that exhibited this behavior also showed a tighter clustering of relative phase values and a correlation between top-down Granger causality and coherence. This suggests that Granger causality and coherence are measuring a mechanism that is highly dependent on relative phase, and that top-down influences may be of particular importance in maintaining a precise phase relationship. Alternatively, the larger levels of coherence may be increasing the efficiency of communication between the areas so that top-down influences are transmitted more effectively to striate cortex. What both these putative mechanisms have in common is that top-down influences modulate parts of striate cortex such that the targeted area is more responsive to visual stimulation. These influences may be the substrate of neural context, aligning the activity of primary sensory cortex within the greater context of the task. In this way influence flows throughout the neurocognitive network, and in the regions analyzed, during the anticipatory phase of the task, these influences allow prior knowledge to influence the response properties of primary visual cortex to expected events. Via this mechanism, higher-level cortical areas may be functionally coupled to lower level regions, imposing constraint upon the lower-level regions in a manner consistent with Jackson's notion of a functional hierarchy (see section 2.1.1).

Analysis three (chapter 5) investigated the effect of stimulus onset asynchrony upon the strength of coherent and Granger causal interactions. This analysis revealed a strong relationship between beta frequency coherence and top-down Granger causal interactions and the stimulus onset asynchrony. In five of the six pairs which showed a significant correlation between top-down Granger causality and the VERP amplitude the correlation

between top-down Granger causality and coherence with onset time was negative. This relationship raises the possibility that the beta frequency modulation may be an index of the conditional probability of the occurrence of the stimulus. The current results certainly suggest that further investigation should be conducted to determine if this is indeed the function of the oscillatory modulation.

In summary, it appears from the current work that the *prepared mind* that Pasteur speaks of is one that contains an elaborate system of interacting cortical systems, where prior knowledge may be deployed via these interactions to guide the mind to states of anticipation and prediction. In this way the mind is not passively *affected* by events in the world, but instead it is part of a dynamic interaction between knowledge rich brain states, the body and environmental events. The environment does not strictly *affect* the organism; the organism purposively processes the environment. The effect that an environmental event may have on the organism is thus highly dependent upon the current state of its mind, and the neurocognitive network dynamics that govern it. This deployment of knowledge is extant in the very neuronal fabric that comprises the brain and appears to be what allows organisms to make sense of an unpredictable changing world, and ultimately to construct its meaning.

APPENDIX A

NON-SIGNIFICANT SUBSENSEMBLE COHERENCE AND GRANGER CAUSALITY VERSUS MEAN SUBSENSEMBLE VERP AMPLITUDE CORRELATION RESULTS

Figures A.1 through A.15 show pairs in the alpha band with subsensemble coherence and Granger causality values that are not correlated with the mean VERP amplitude.

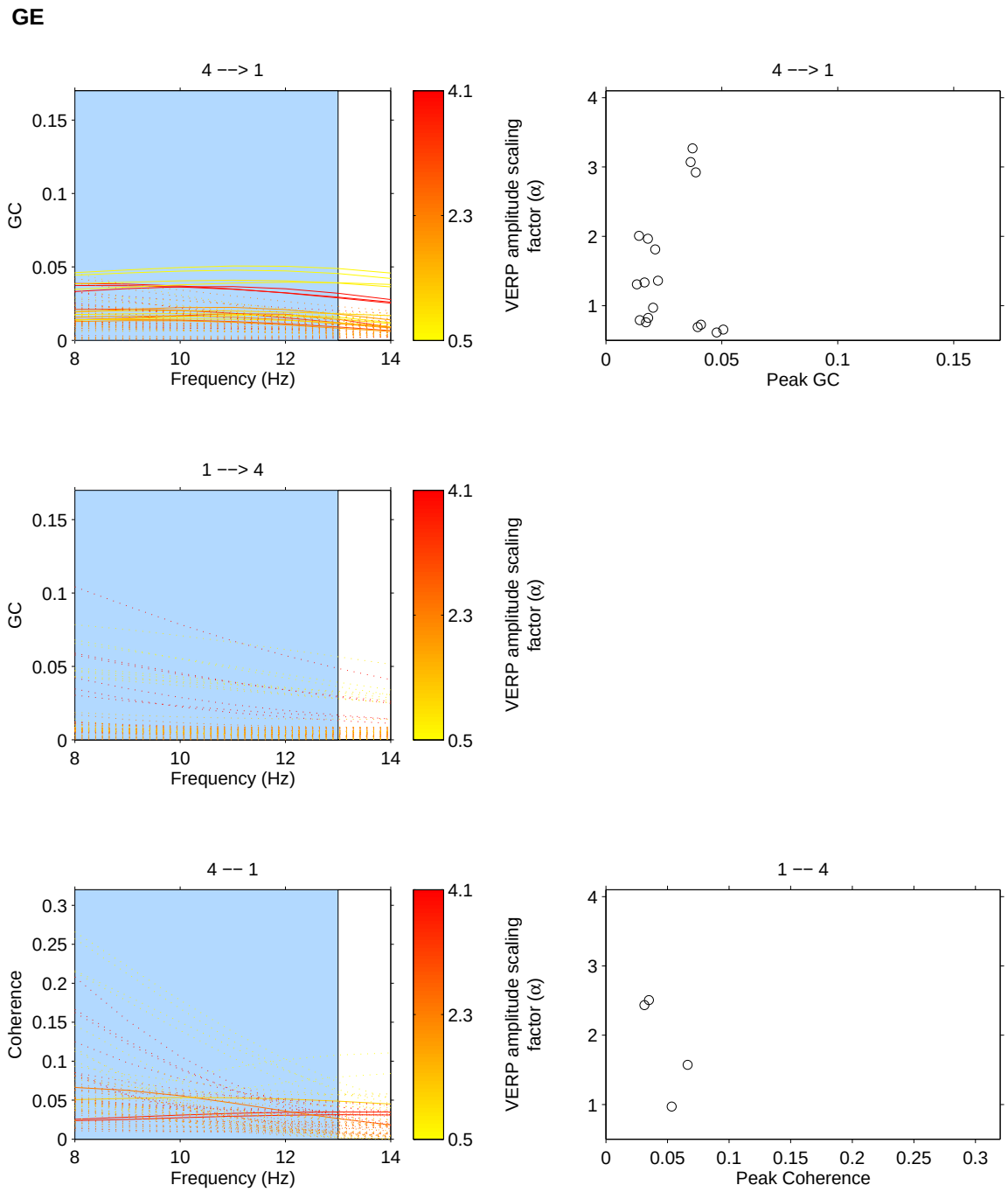

Figure A.1: Subensemble spectra for top-down and bottom-up Granger causality and coherence (left panels) and the correlations between significant alpha-range Granger causality and coherence spectral peaks with subensemble mean striate VERP amplitude (right panels) for pair GE 4-1. Significant correlations are fit with a regression line. Spectra with significant peaks are drawn in solid lines. Spectra without significant peaks are drawn with dotted lines.

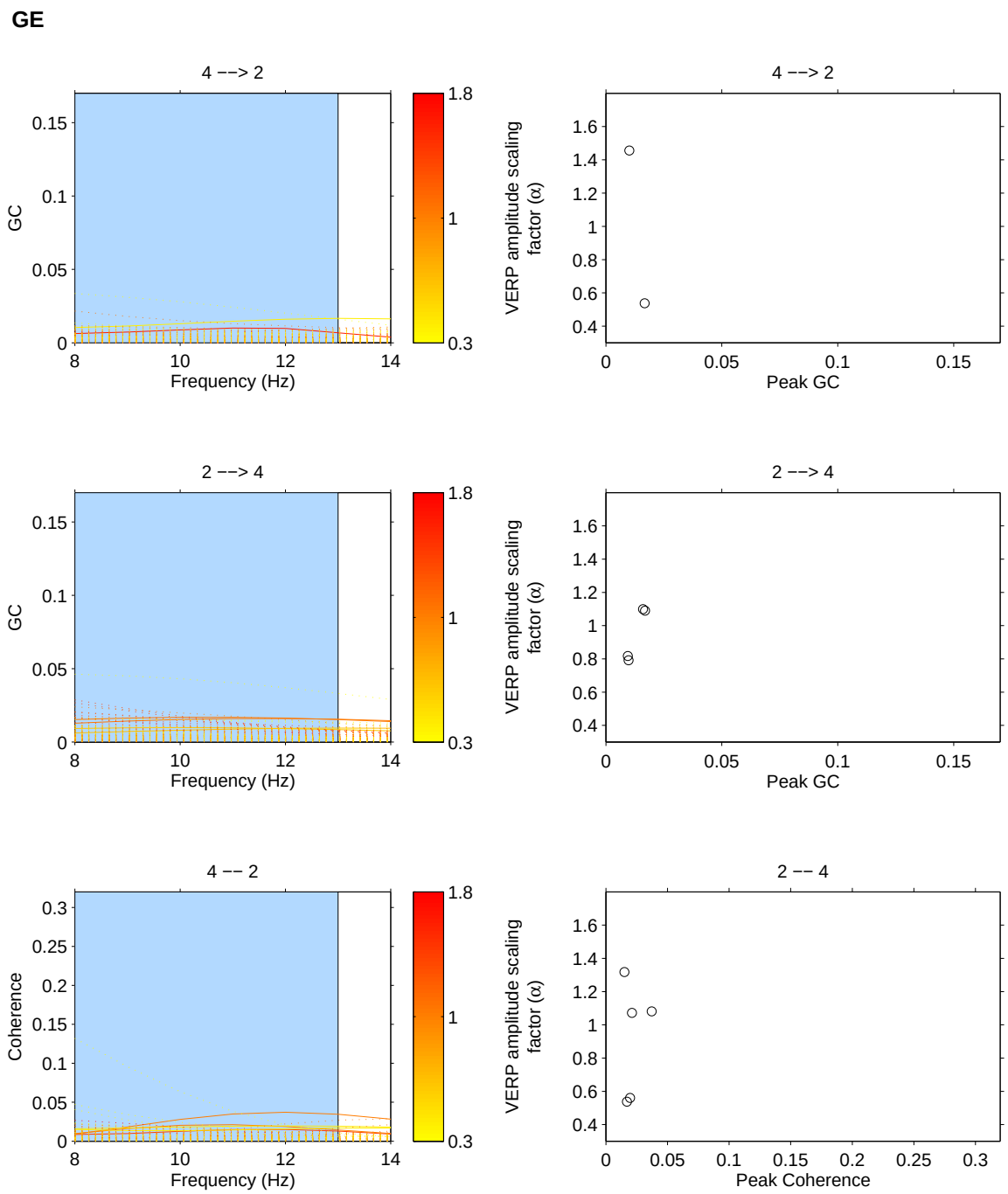

Figure A.2: Subensemble spectra for top-down and bottom-up Granger causality and coherence (left panels) and the correlations between significant alpha-range Granger causality and coherence spectral peaks with subensemble mean striate VERP amplitude (right panels) for pair GE 4-2. Significant correlations are fit with a regression line. Spectra with significant peaks are drawn in solid lines. Spectra without significant peaks are drawn with dotted lines.

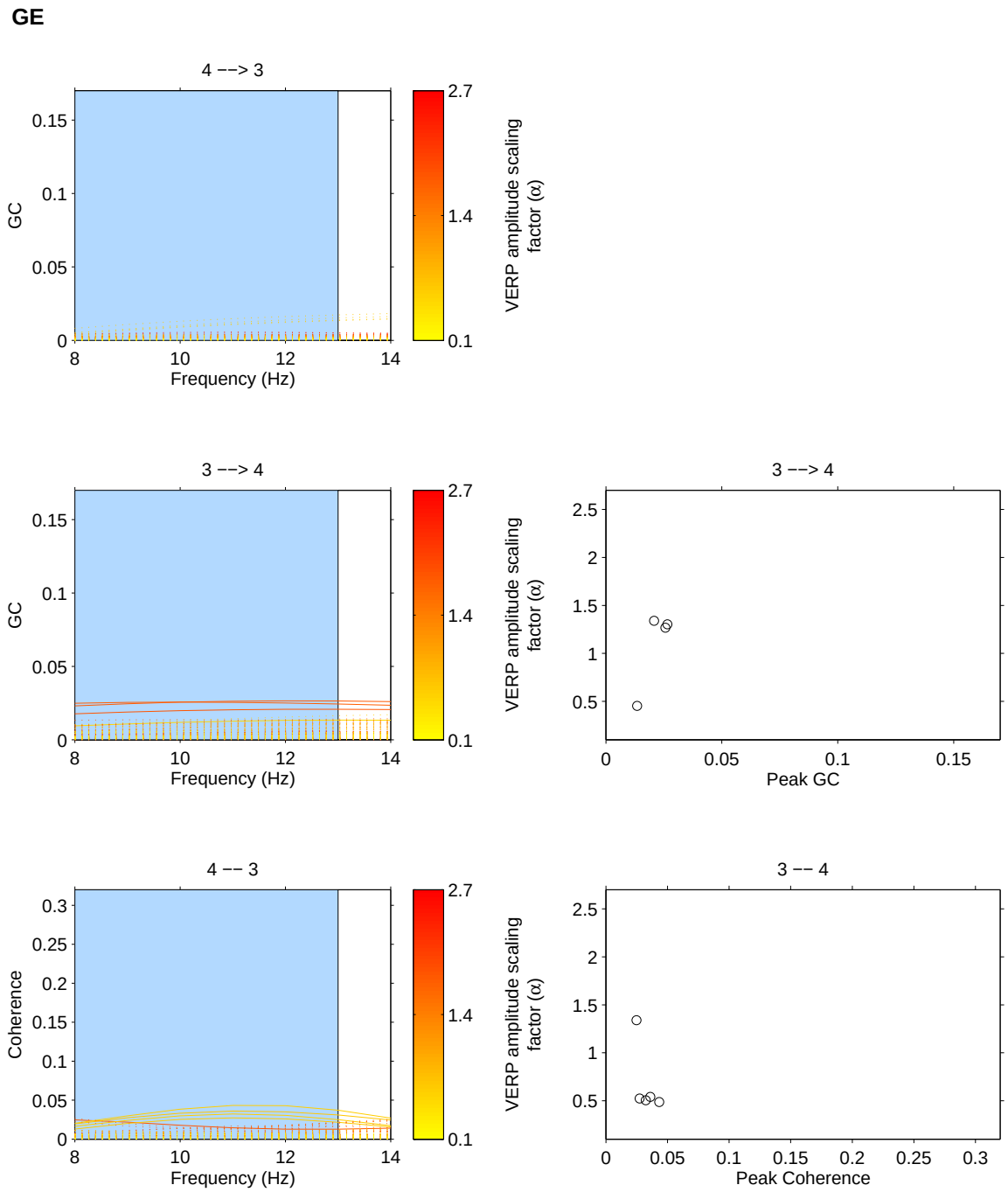

Figure A.3: Subensemble spectra for top-down and bottom-up Granger causality and coherence (left panels) and the correlations between significant alpha-range Granger causality and coherence spectral peaks with subensemble mean striate VERP amplitude (right panels) for pair GE 4-3. Significant correlations are fit with a regression line. Spectra with significant peaks are drawn in solid lines. Spectra without significant peaks are drawn with dotted lines.

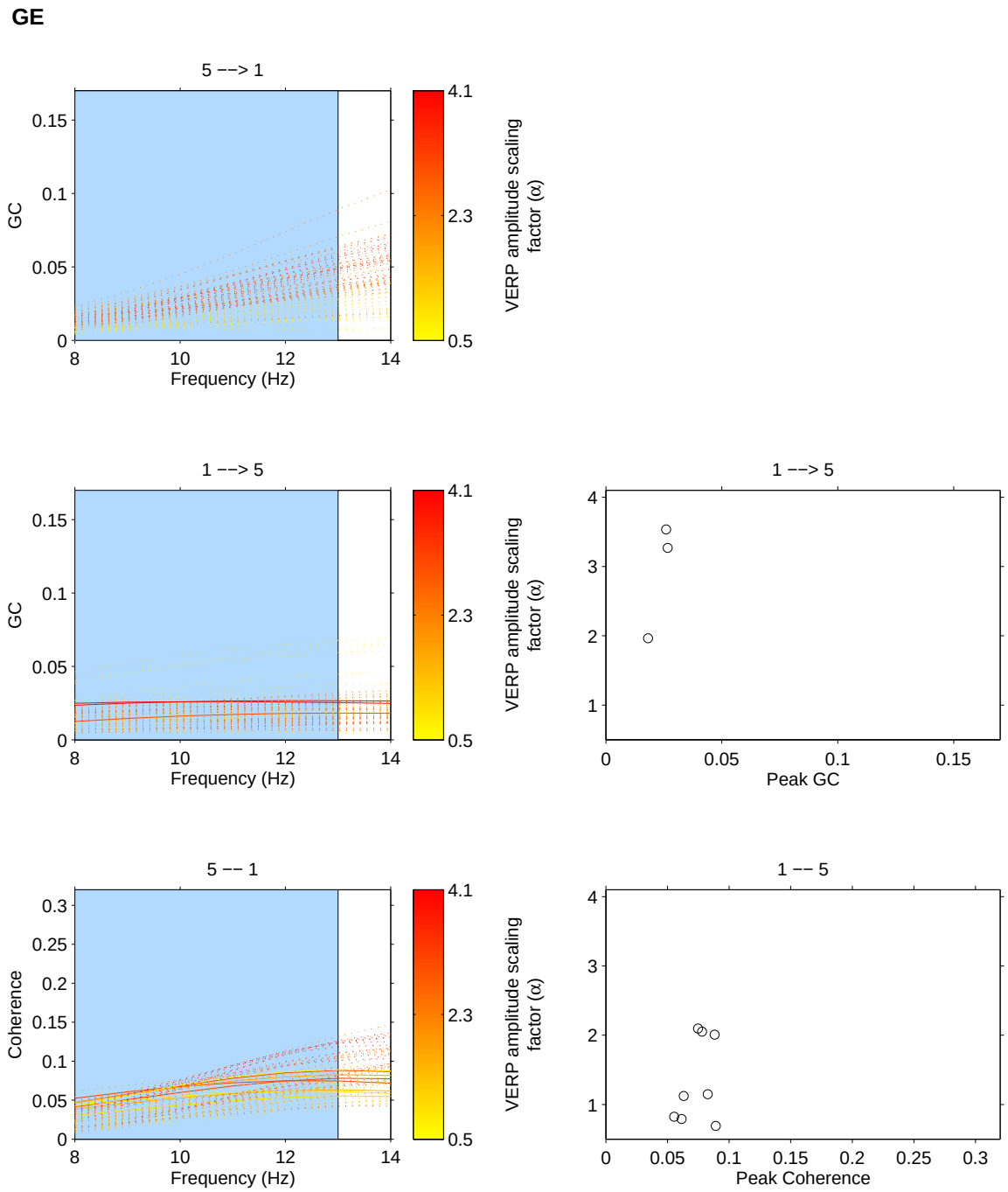

Figure A.4: Subensemble spectra for top-down and bottom-up Granger causality and coherence (left panels) and the correlations between significant alpha-range Granger causality and coherence spectral peaks with subensemble mean striate VERP amplitude (right panels) for pair GE 5-1. Significant correlations are fit with a regression line. Spectra with significant peaks are drawn in solid lines. Spectra without significant peaks are drawn with dotted lines.

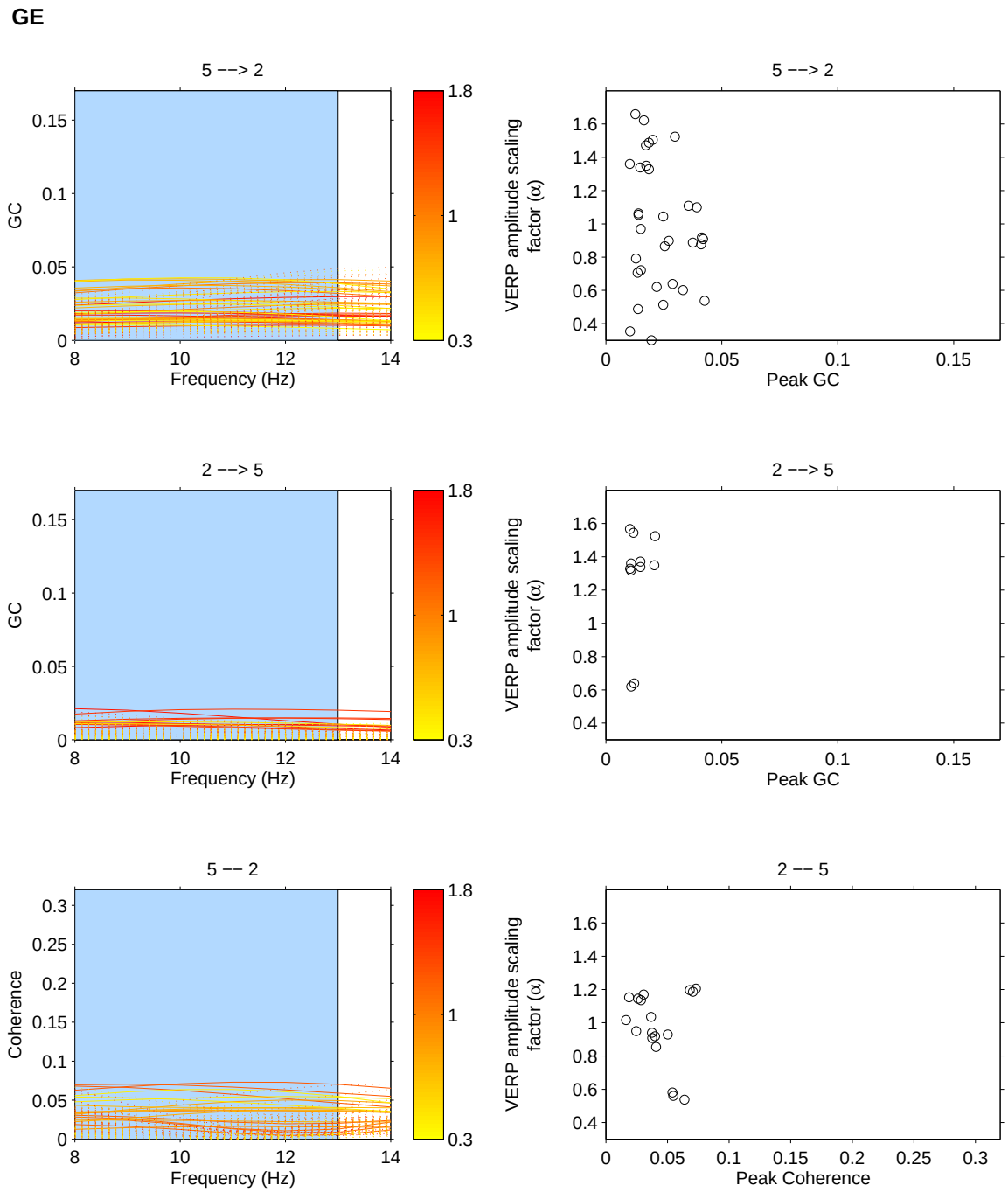

Figure A.5: Subensemble spectra for top-down and bottom-up Granger causality and coherence (left panels) and the correlations between significant alpha-range Granger causality and coherence spectral peaks with subensemble mean striate VERP amplitude (right panels) for pair GE 5-2. Significant correlations are fit with a regression line. Spectra with significant peaks are drawn in solid lines. Spectra without significant peaks are drawn with dotted lines.

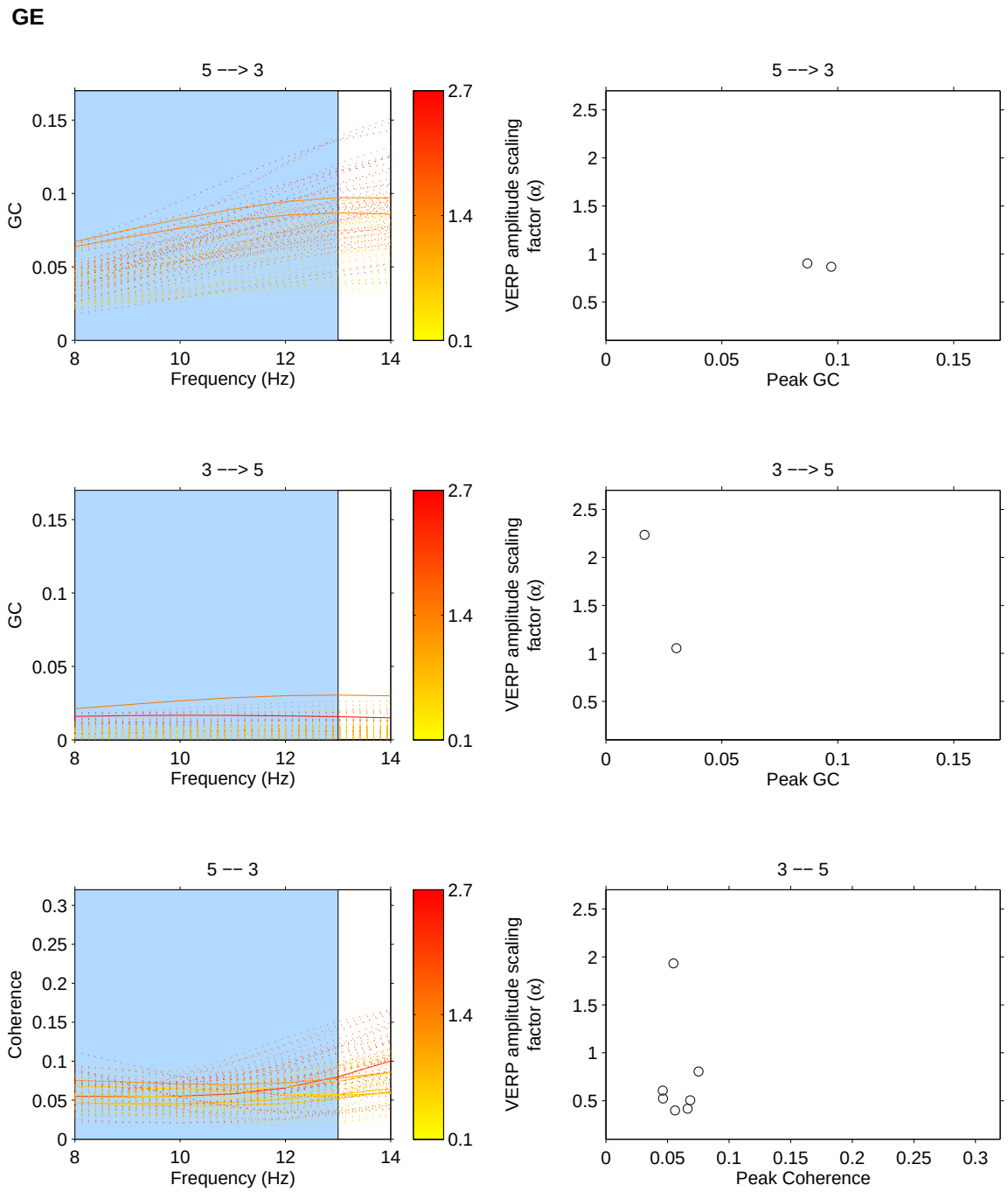

Figure A.6: Subensemble spectra for top-down and bottom-up Granger causality and coherence (left panels) and the correlations between significant alpha-range Granger causality and coherence spectral peaks with subensemble mean striate VERP amplitude (right panels) for pair GE 5-3. Significant correlations are fit with a regression line. Spectra with significant peaks are drawn in solid lines. Spectra without significant peaks are drawn with dotted lines.

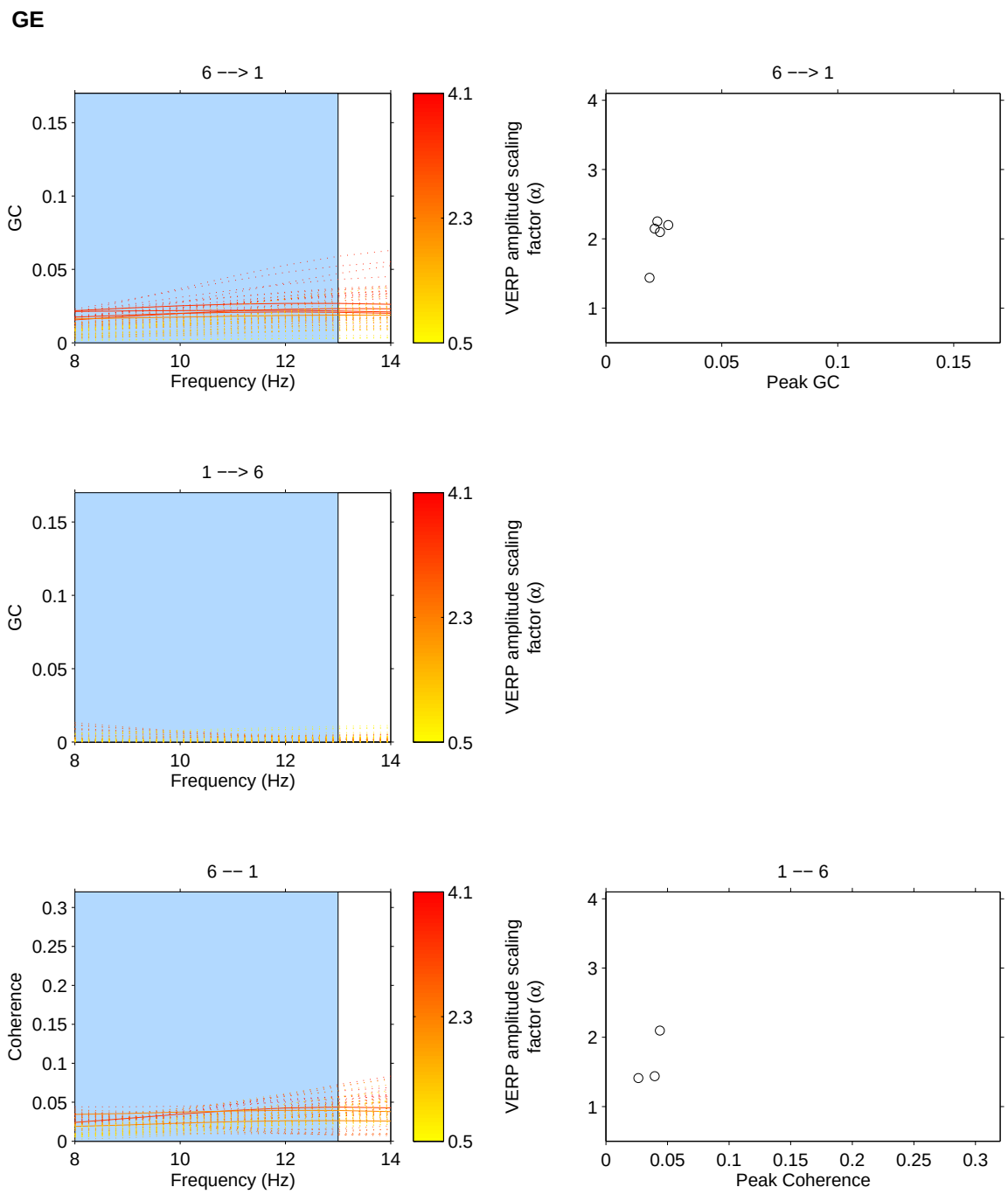

Figure A.7: Subensemble spectra for top-down and bottom-up Granger causality and coherence (left panels) and the correlations between significant alpha-range Granger causality and coherence spectral peaks with subensemble mean striate VERP amplitude (right panels) for pair GE 6-1. Significant correlations are fit with a regression line. Spectra with significant peaks are drawn in solid lines. Spectra without significant peaks are drawn with dotted lines.

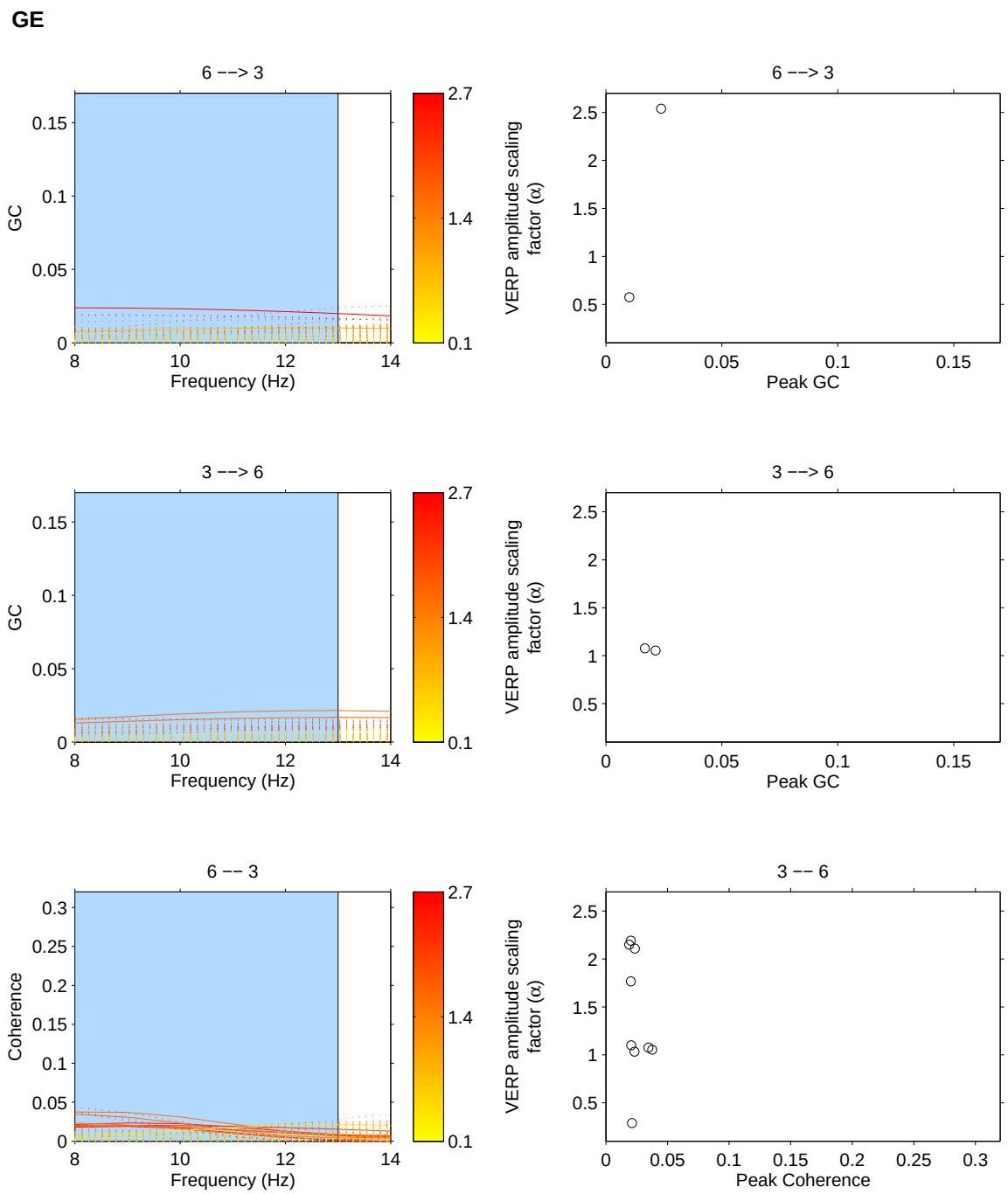

Figure A.8: Subensemble spectra for top-down and bottom-up Granger causality and coherence (left panels) and the correlations between significant alpha-range Granger causality and coherence spectral peaks with subensemble mean striate VERP amplitude (right panels) for pair GE 6-3. Significant correlations are fit with a regression line. Spectra with significant peaks are drawn in solid lines. Spectra without significant peaks are drawn with dotted lines.

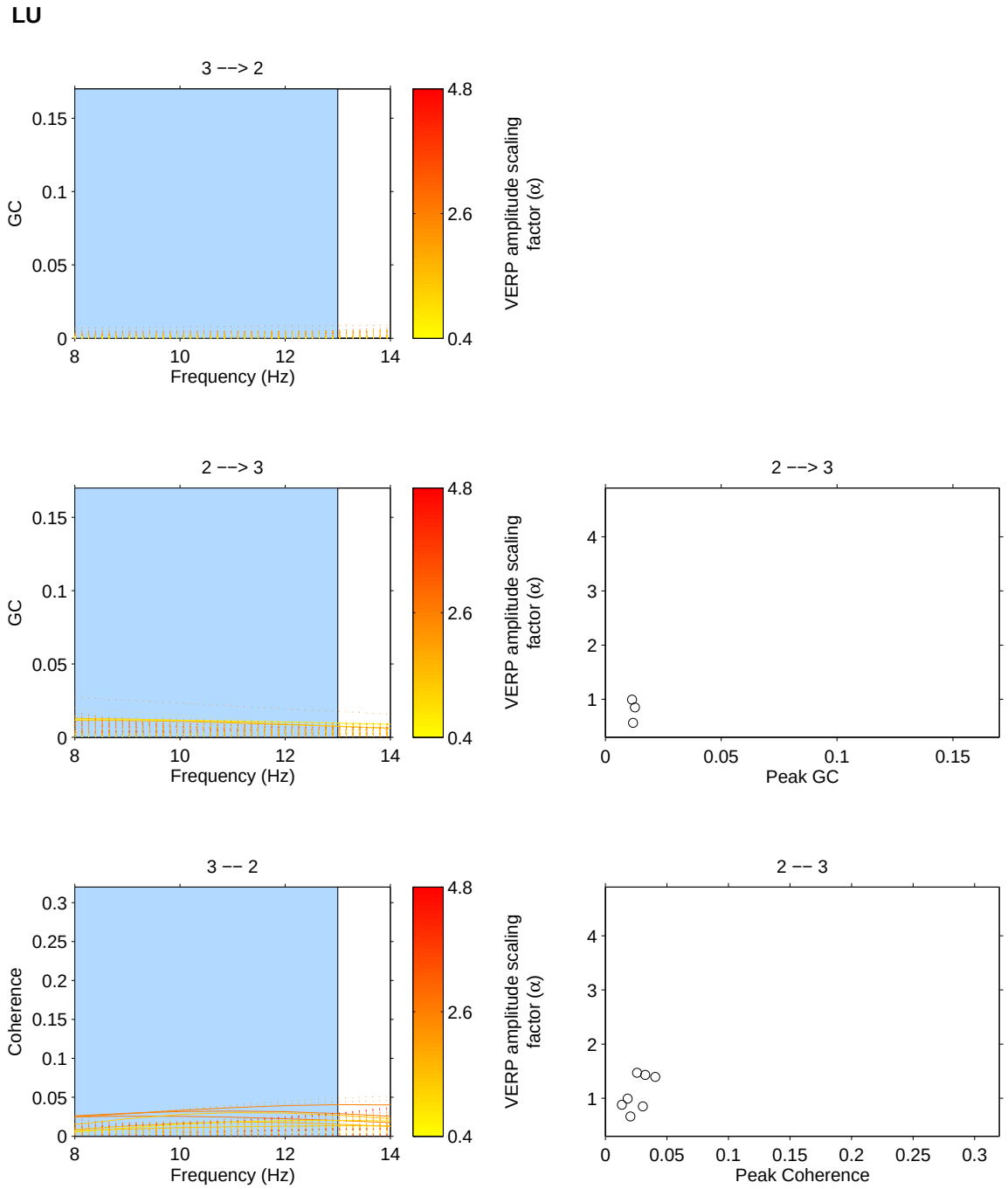

Figure A.9: Subensemble spectra for top-down and bottom-up Granger causality and coherence (left panels) and the correlations between significant alpha-range Granger causality and coherence spectral peaks with subensemble mean striate VERP amplitude (right panels) for pair LU 3-2. Significant correlations are fit with a regression line. Spectra with significant peaks are drawn in solid lines. Spectra without significant peaks are drawn with dotted lines.

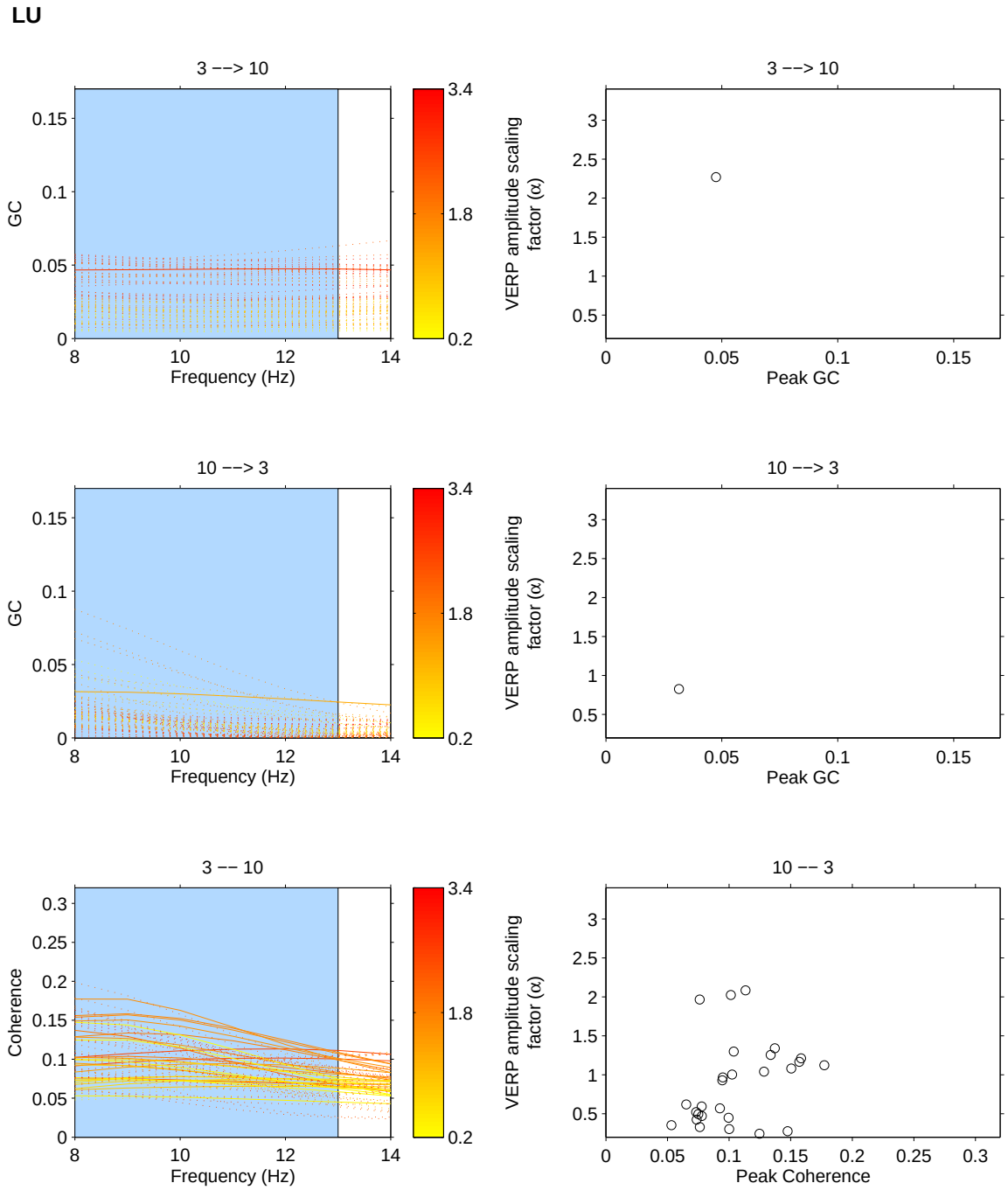

Figure A.10: Subensemble spectra for top-down and bottom-up Granger causality and coherence (left panels) and the correlations between significant alpha-range Granger causality and coherence spectral peaks with subensemble mean striate VERP amplitude (right panels) for pair LU 3-10. Significant correlations are fit with a regression line. Spectra with significant peaks are drawn in solid lines. Spectra without significant peaks are drawn with dotted lines.

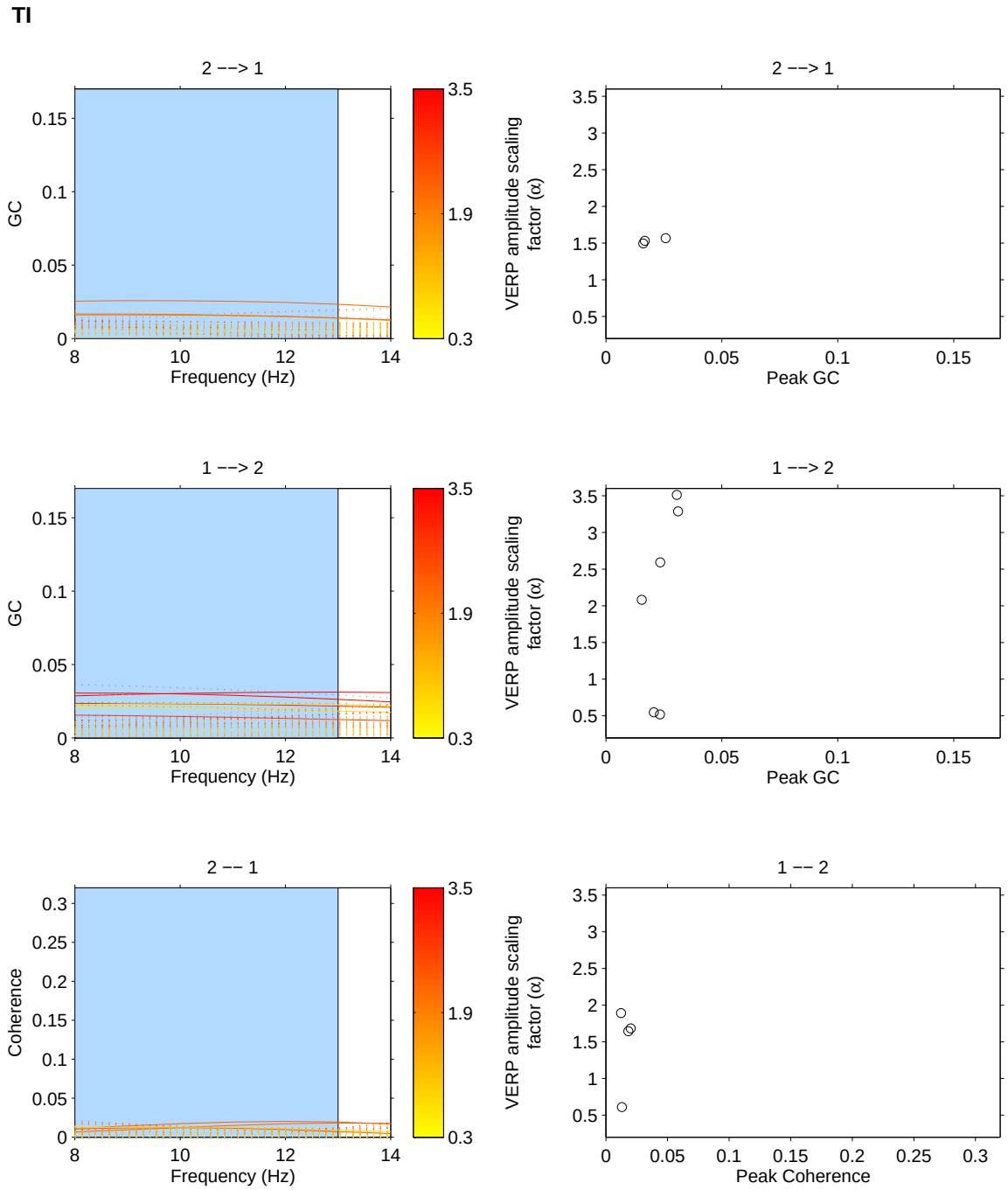

Figure A.11: Subensemble spectra for top-down and bottom-up Granger causality and coherence (left panels) and the correlations between significant alpha-range Granger causality and coherence spectral peaks with subensemble mean striate VERP amplitude (right panels) for pair TI 2-1. Significant correlations are fit with a regression line. Spectra with significant peaks are drawn in solid lines. Spectra without significant peaks are drawn with dotted lines.

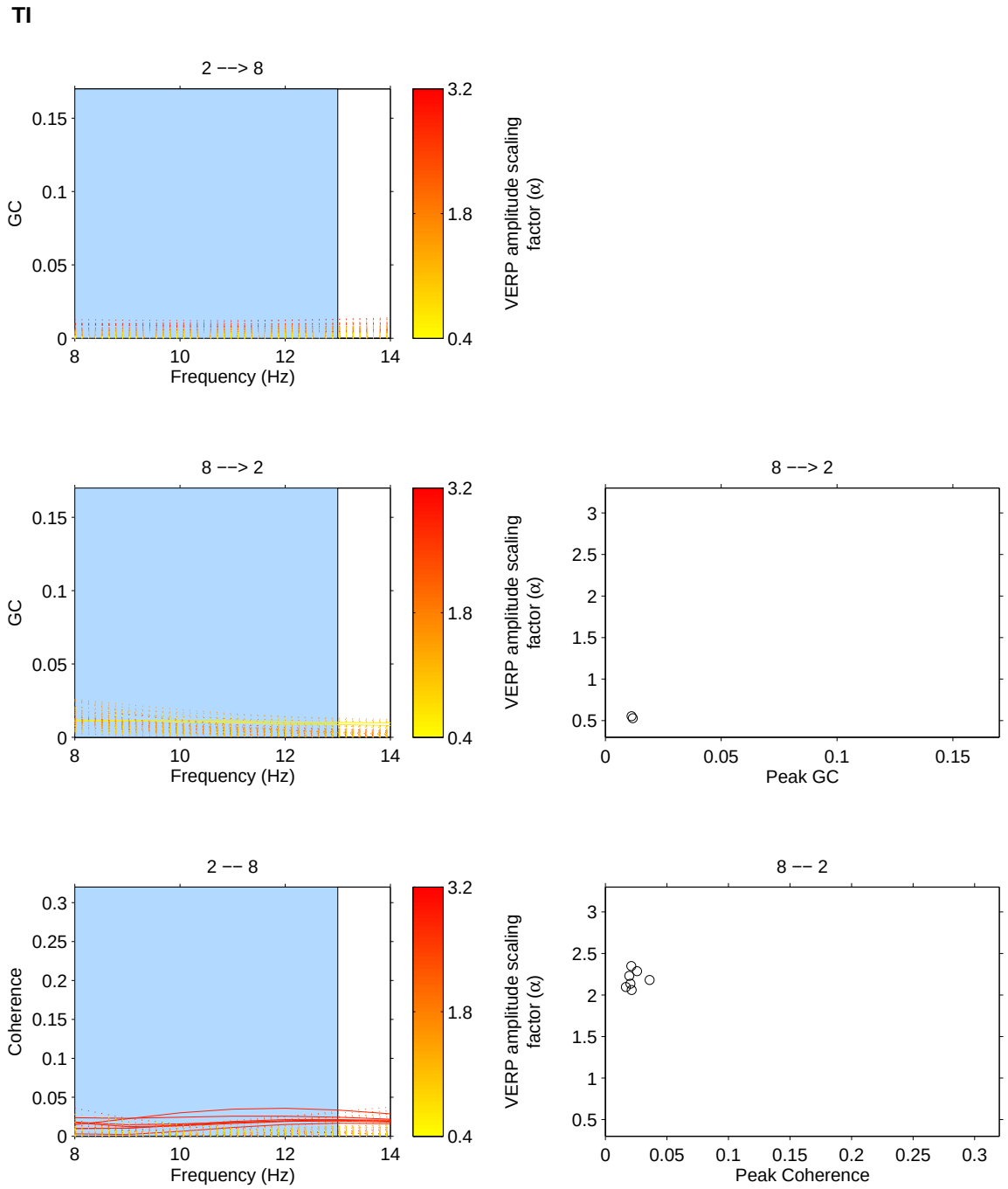

Figure A.12: Subensemble spectra for top-down and bottom-up Granger causality and coherence (left panels) and the correlations between significant alpha-range Granger causality and coherence spectral peaks with subensemble mean striate VERP amplitude (right panels) for pair TI 2-8. Significant correlations are fit with a regression line. Spectra with significant peaks are drawn in solid lines. Spectra without significant peaks are drawn with dotted lines.

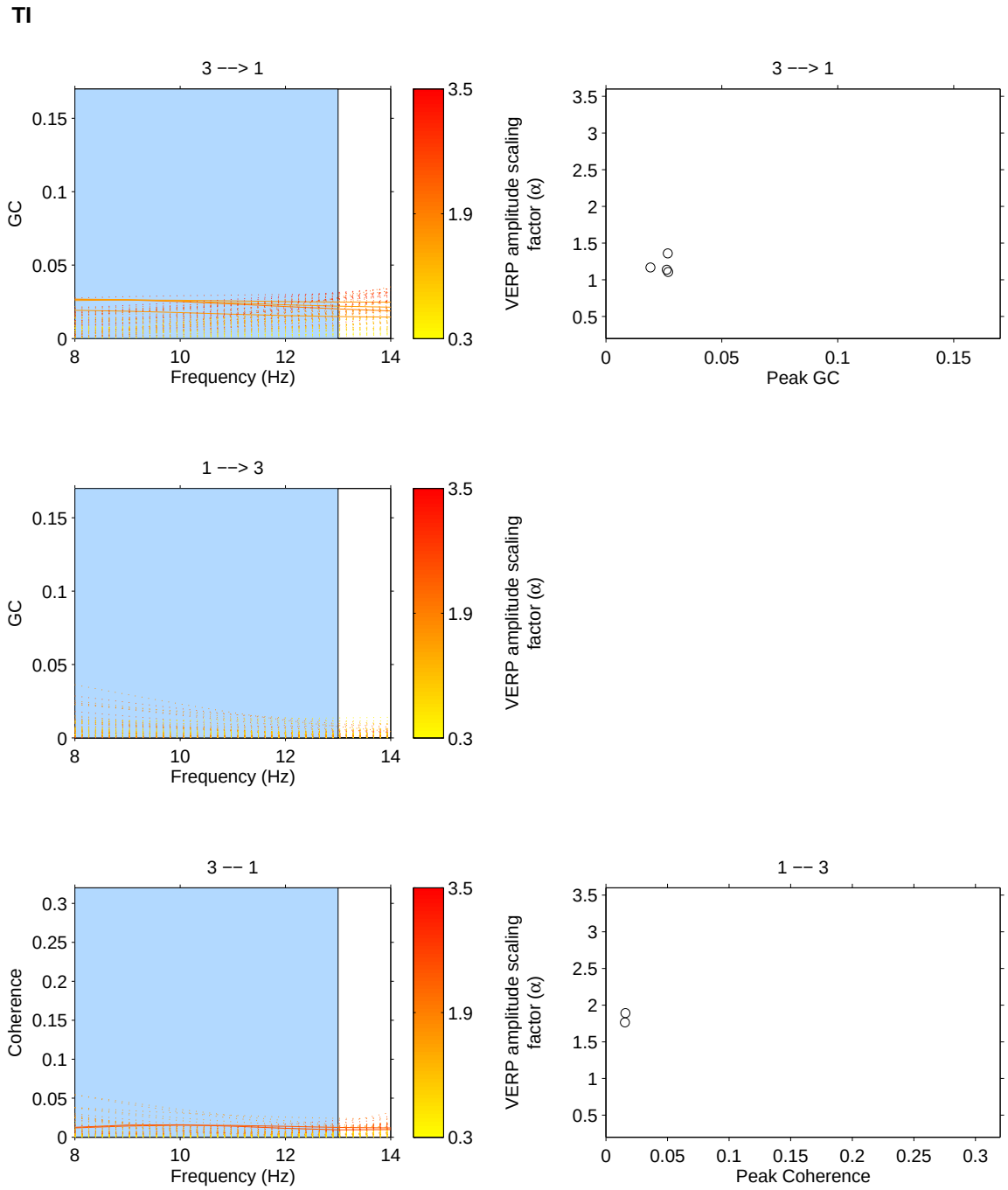

Figure A.13: Subensemble spectra for top-down and bottom-up Granger causality and coherence (left panels) and the correlations between significant alpha-range Granger causality and coherence spectral peaks with subensemble mean striate VERP amplitude (right panels) for pair TI 3-1. Significant correlations are fit with a regression line. Spectra with significant peaks are drawn in solid lines. Spectra without significant peaks are drawn with dotted lines.

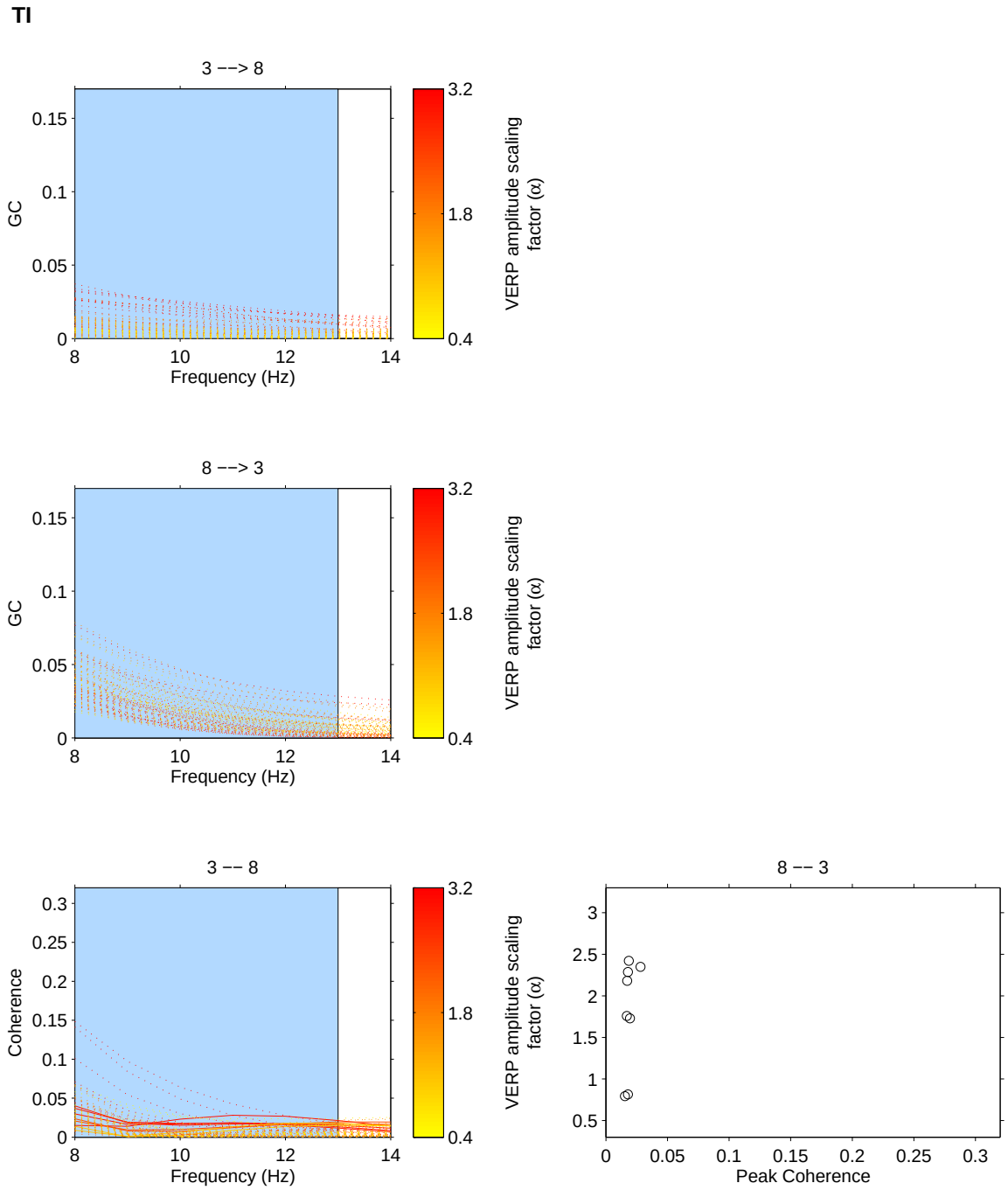

Figure A.14: Subensemble spectra for top-down and bottom-up Granger causality and coherence (left panels) and the correlations between significant alpha-range Granger causality and coherence spectral peaks with subensemble mean striate VERP amplitude (right panels) for pair TI 3-8. Significant correlations are fit with a regression line. Spectra with significant peaks are drawn in solid lines. Spectra without significant peaks are drawn with dotted lines.

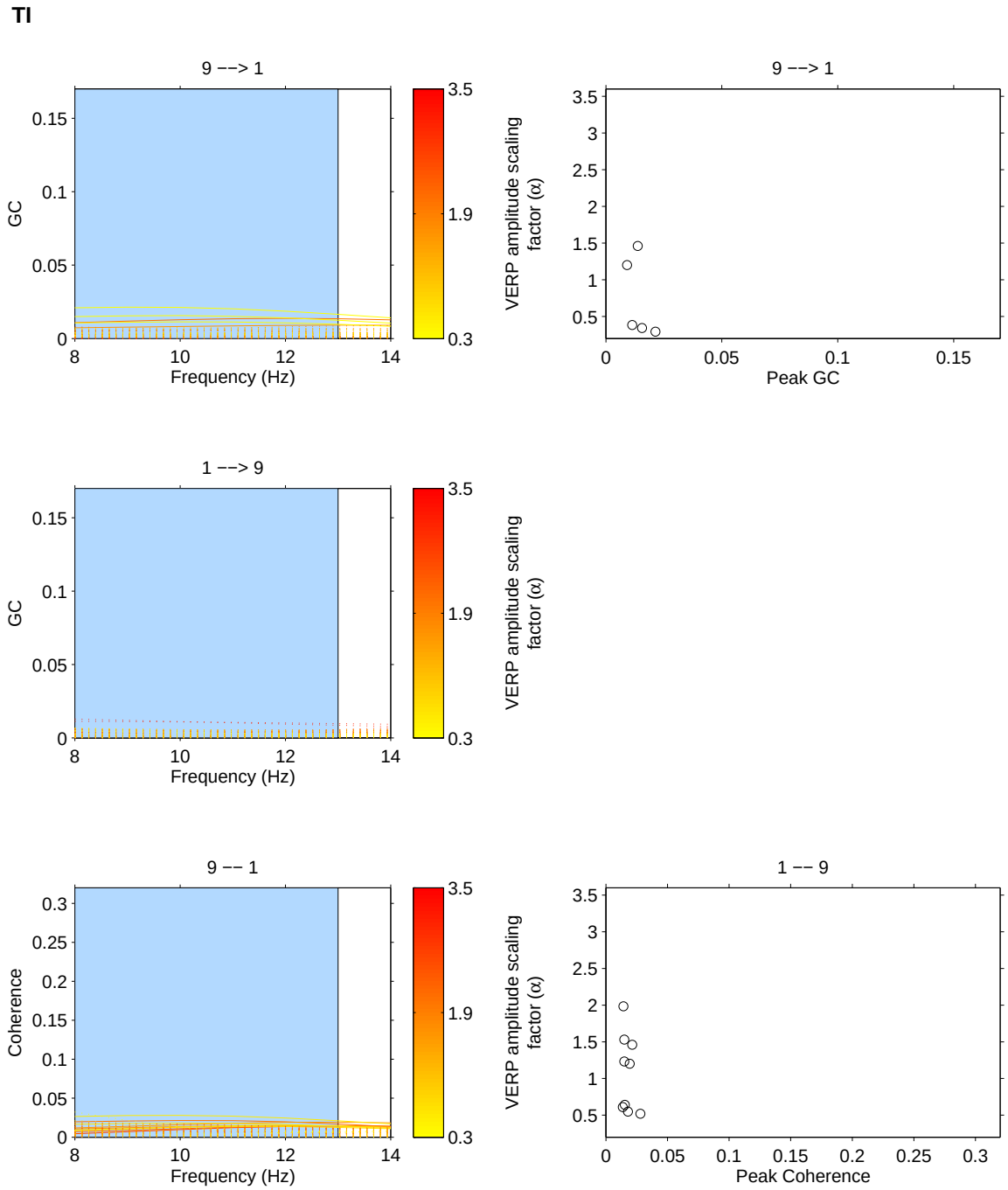

Figure A.15: Subensemble spectra for top-down and bottom-up Granger causality and coherence (left panels) and the correlations between significant alpha-range Granger causality and coherence spectral peaks with subensemble mean striate VERP amplitude (right panels) for pair TI 9-1. Significant correlations are fit with a regression line. Spectra with significant peaks are drawn in solid lines. Spectra without significant peaks are drawn with dotted lines.

Figures A.1 through A.24 show pairs in the beta band with subsensemble coherence and Granger causality values that are not correlated with the mean VERP amplitude.

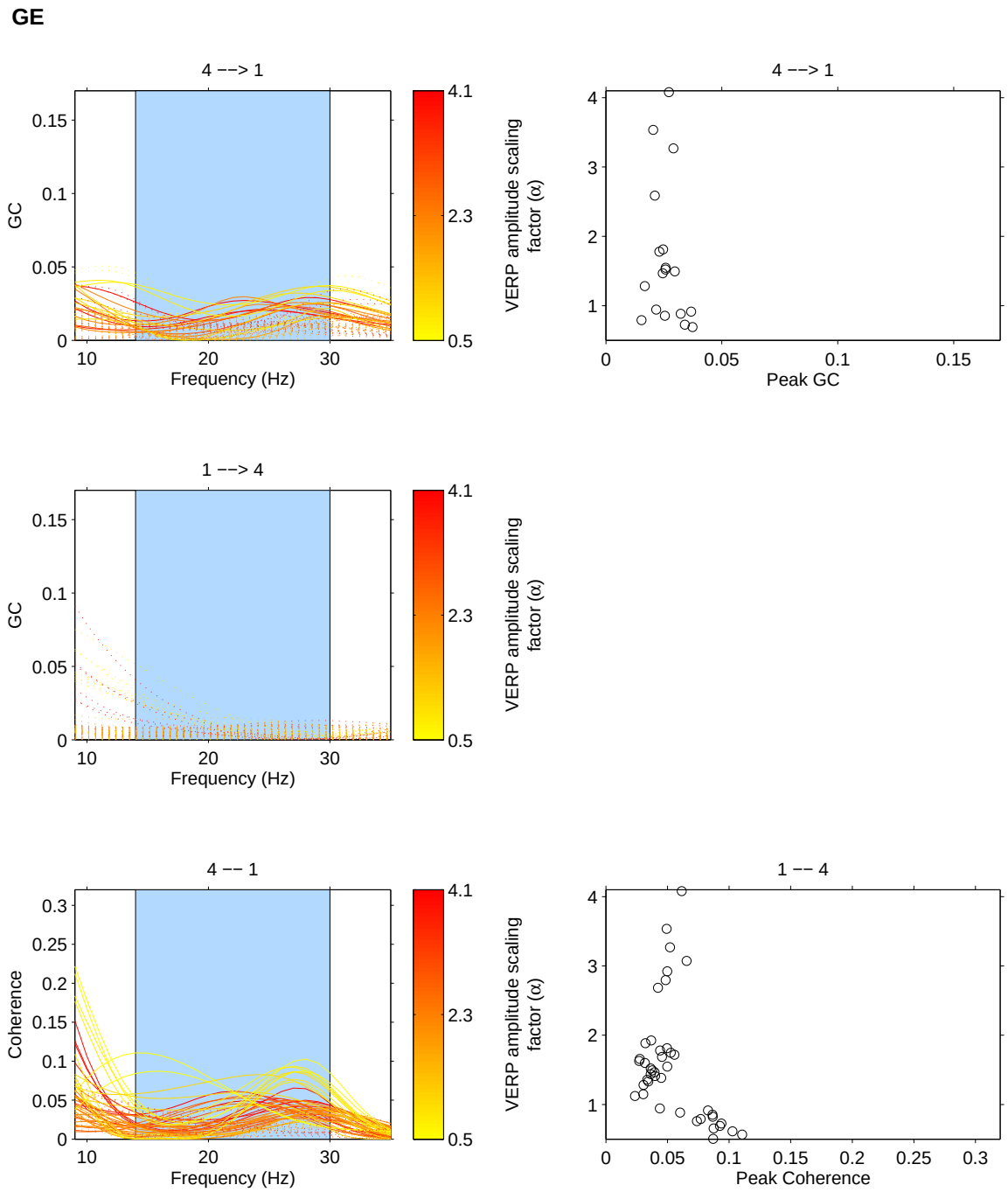

Figure A.16: Subensemble spectra for top-down and bottom-up Granger causality and coherence (left panels) and the correlations between significant beta-range Granger causality and coherence spectral peaks with subensemble mean striate VERP amplitude (right panels) for pair GE 4-1. Significant correlations are fit with a regression line. Spectra with significant peaks are drawn in solid lines. Spectra without significant peaks are drawn with dotted lines.

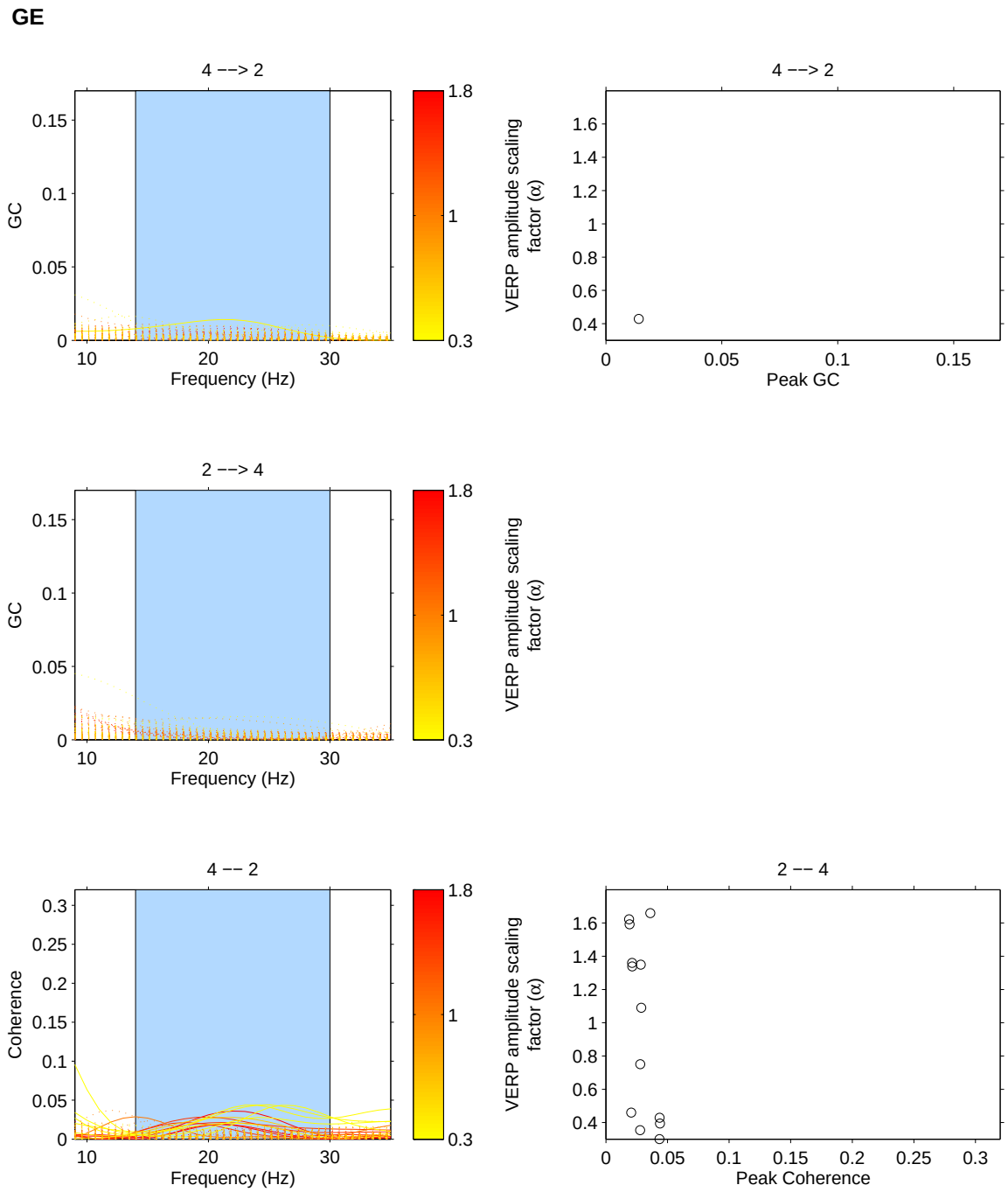

Figure A.17: Subensemble spectra for top-down and bottom-up Granger causality and coherence (left panels) and the correlations between significant beta-range Granger causality and coherence spectral peaks with subensemble mean striate VERP amplitude (right panels) for pair GE 4-2. Significant correlations are fit with a regression line. Spectra with significant peaks are drawn in solid lines. Spectra without significant peaks are drawn with dotted lines.

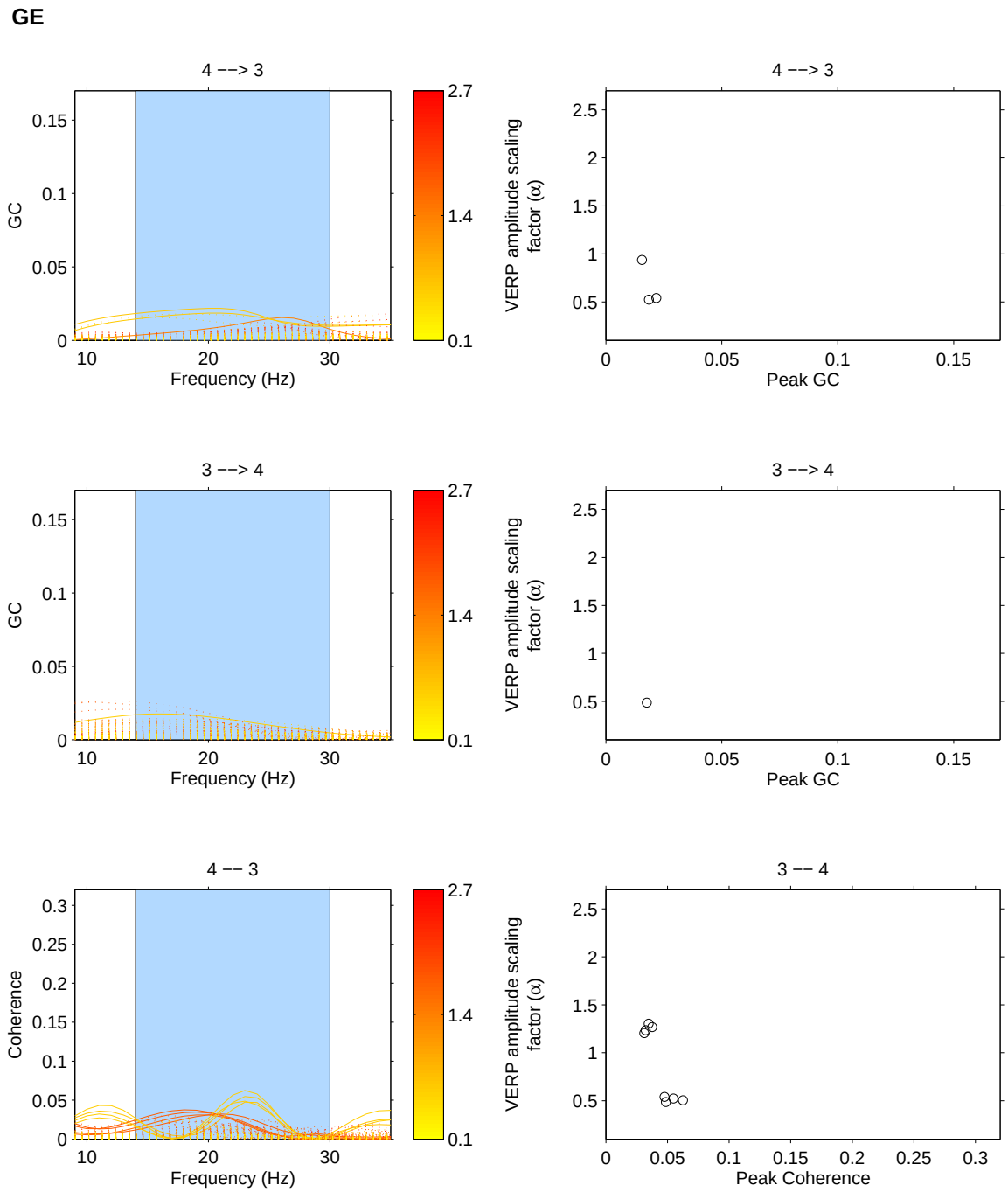

Figure A.18: Subensemble spectra for top-down and bottom-up Granger causality and coherence (left panels) and the correlations between significant beta-range Granger causality and coherence spectral peaks with subensemble mean striate VERP amplitude (right panels) for pair GE 4-3. Significant correlations are fit with a regression line. Spectra with significant peaks are drawn in solid lines. Spectra without significant peaks are drawn with dotted lines.

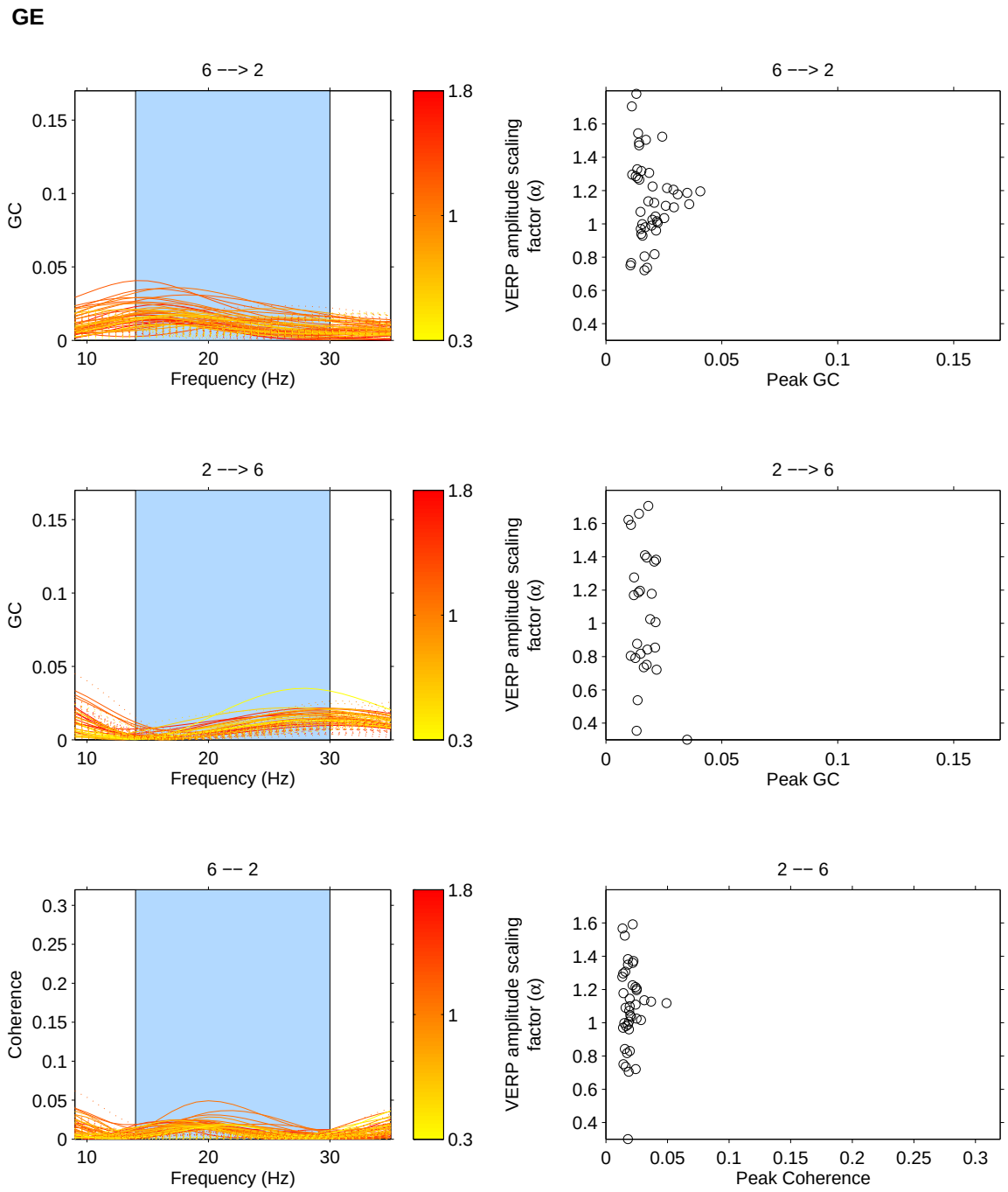

Figure A.19: Subensemble spectra for top-down and bottom-up Granger causality and coherence (left panels) and the correlations between significant beta-range Granger causality and coherence spectral peaks with subensemble mean striate VERP amplitude (right panels) for pair GE 6-2. Significant correlations are fit with a regression line. Spectra with significant peaks are drawn in solid lines. Spectra without significant peaks are drawn with dotted lines.

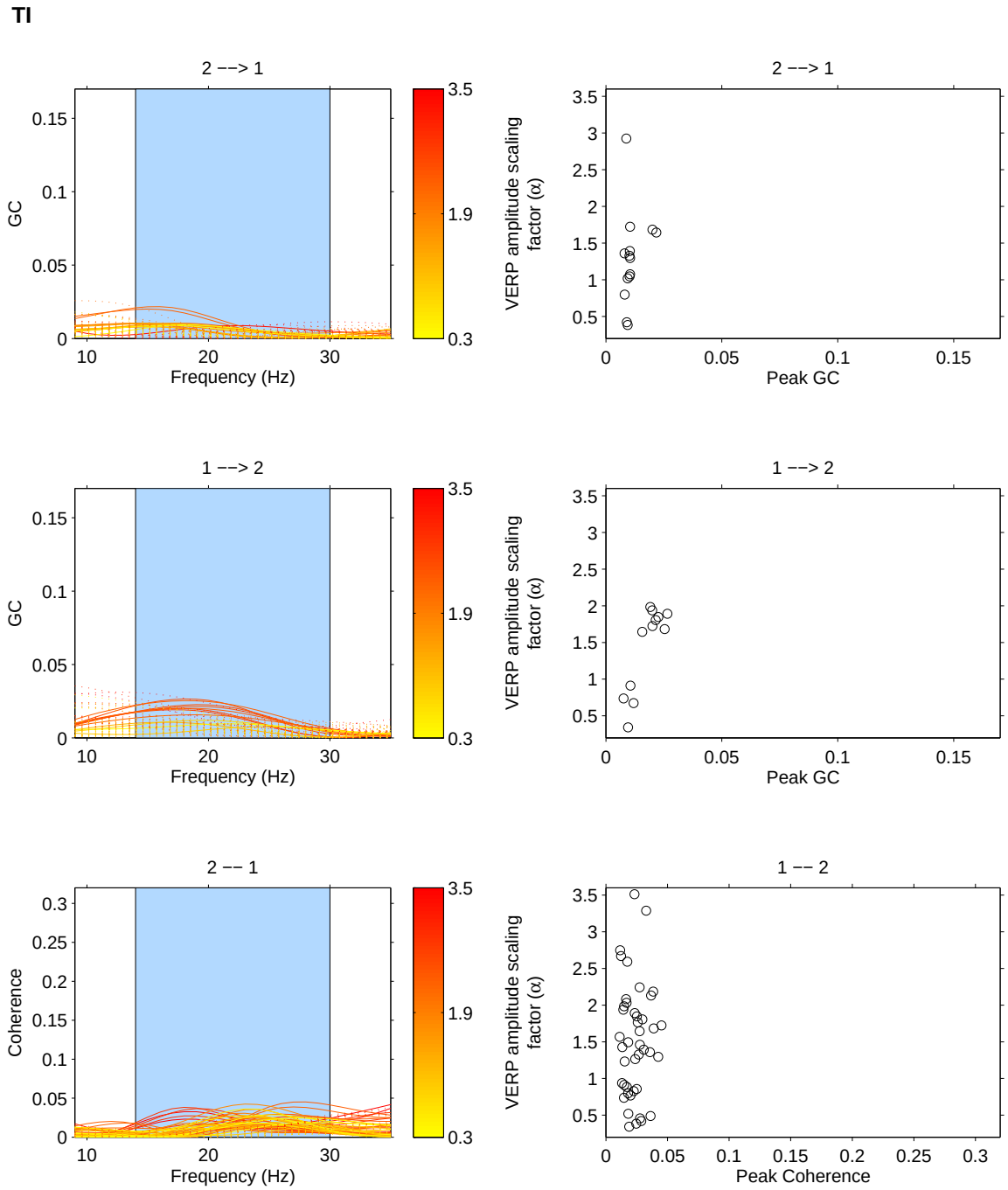

Figure A.20: Subensemble spectra for top-down and bottom-up Granger causality and coherence (left panels) and the correlations between significant beta-range Granger causality and coherence spectral peaks with subensemble mean striate VERP amplitude (right panels) for pair TI 2-1. Significant correlations are fit with a regression line. Spectra with significant peaks are drawn in solid lines. Spectra without significant peaks are drawn with dotted lines.

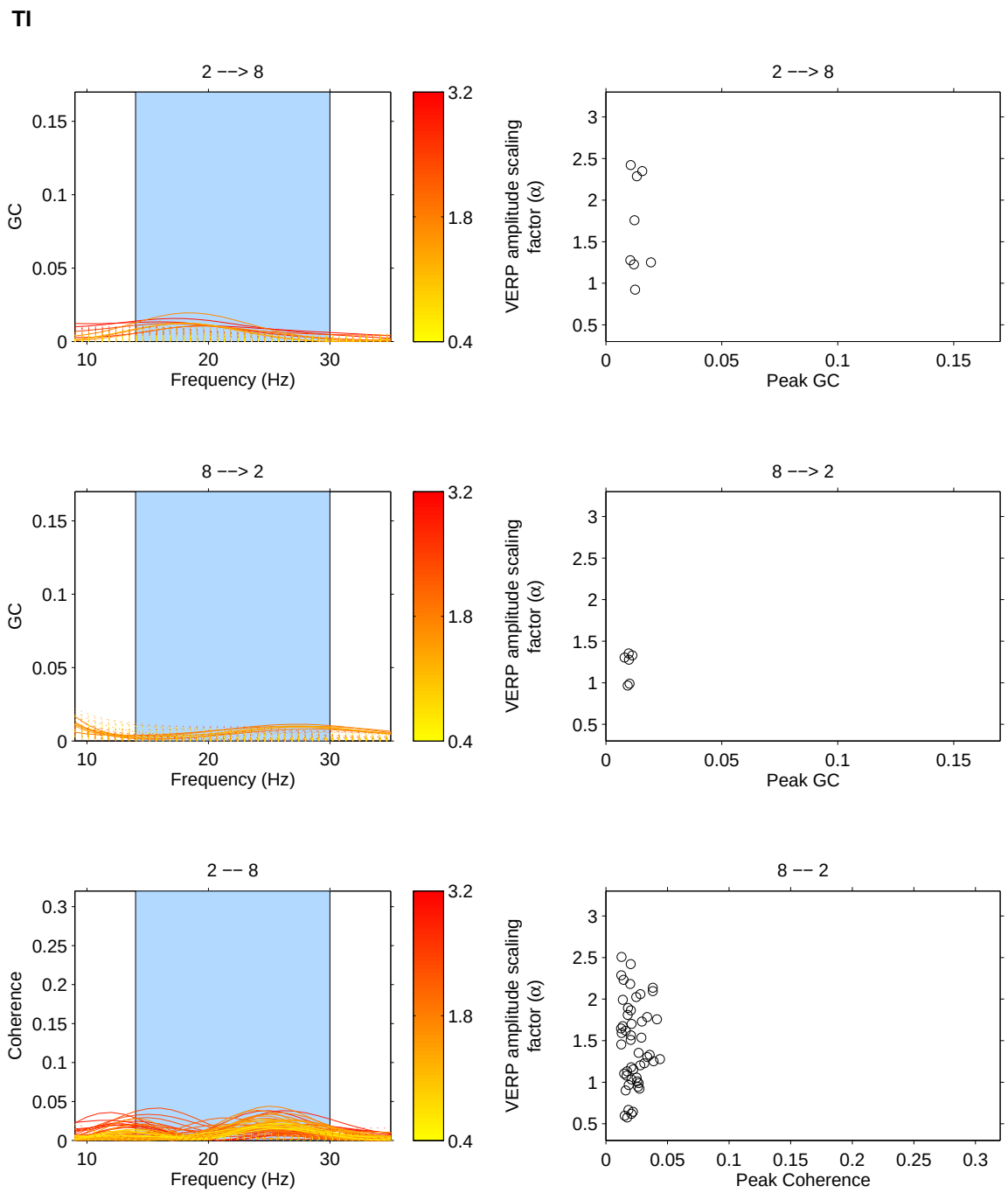

Figure A.21: Subensemble spectra for top-down and bottom-up Granger causality and coherence (left panels) and the correlations between significant beta-range Granger causality and coherence spectral peaks with subensemble mean striate VERP amplitude (right panels) for pair TI 2-8. Significant correlations are fit with a regression line. Spectra with significant peaks are drawn in solid lines. Spectra without significant peaks are drawn with dotted lines.

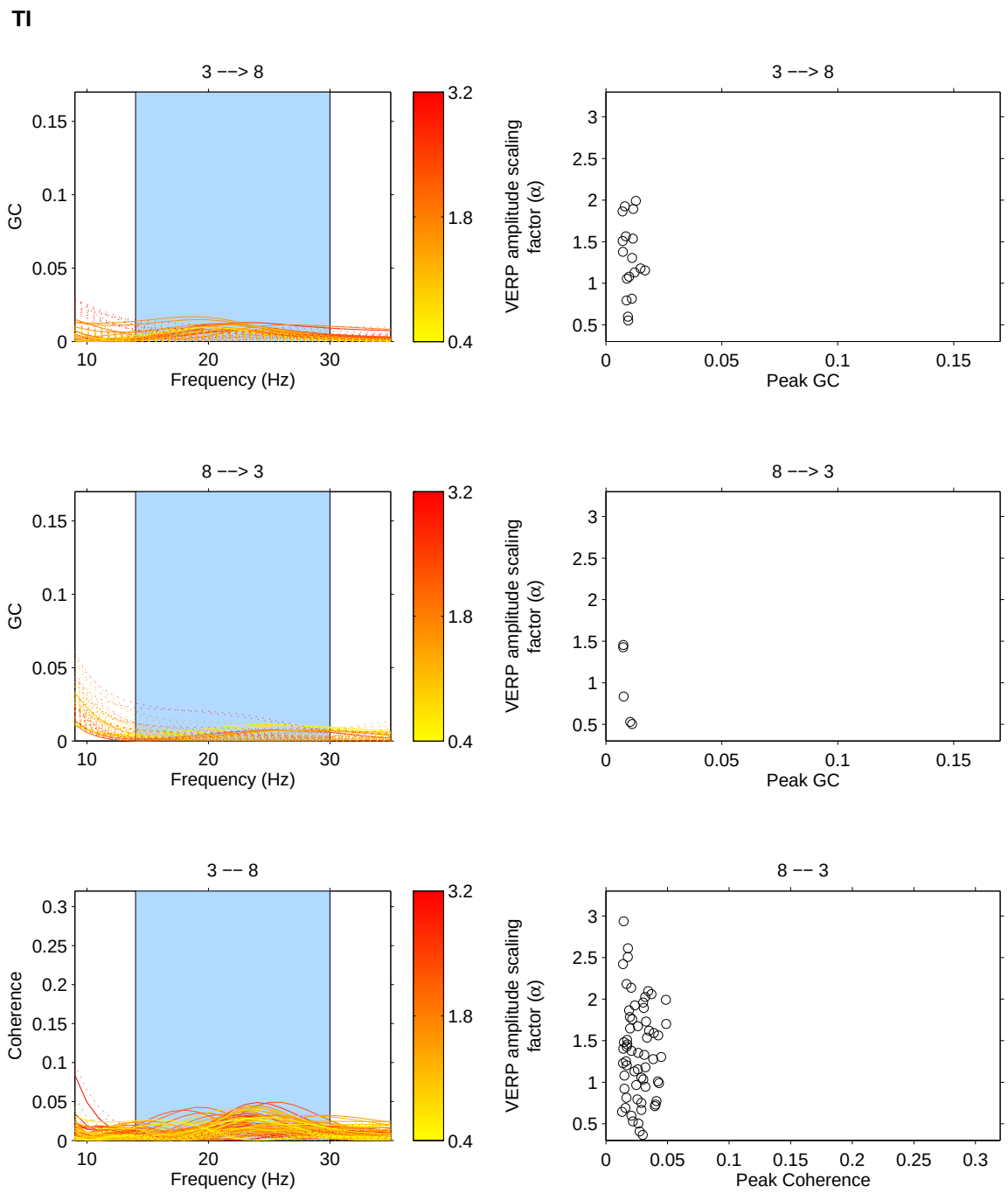

Figure A.22: Subensemble spectra for top-down and bottom-up Granger causality and coherence (left panels) and the correlations between significant beta-range Granger causality and coherence spectral peaks with subensemble mean striate VERP amplitude (right panels) for pair TI 3-8. Significant correlations are fit with a regression line. Spectra with significant peaks are drawn in solid lines. Spectra without significant peaks are drawn with dotted lines.

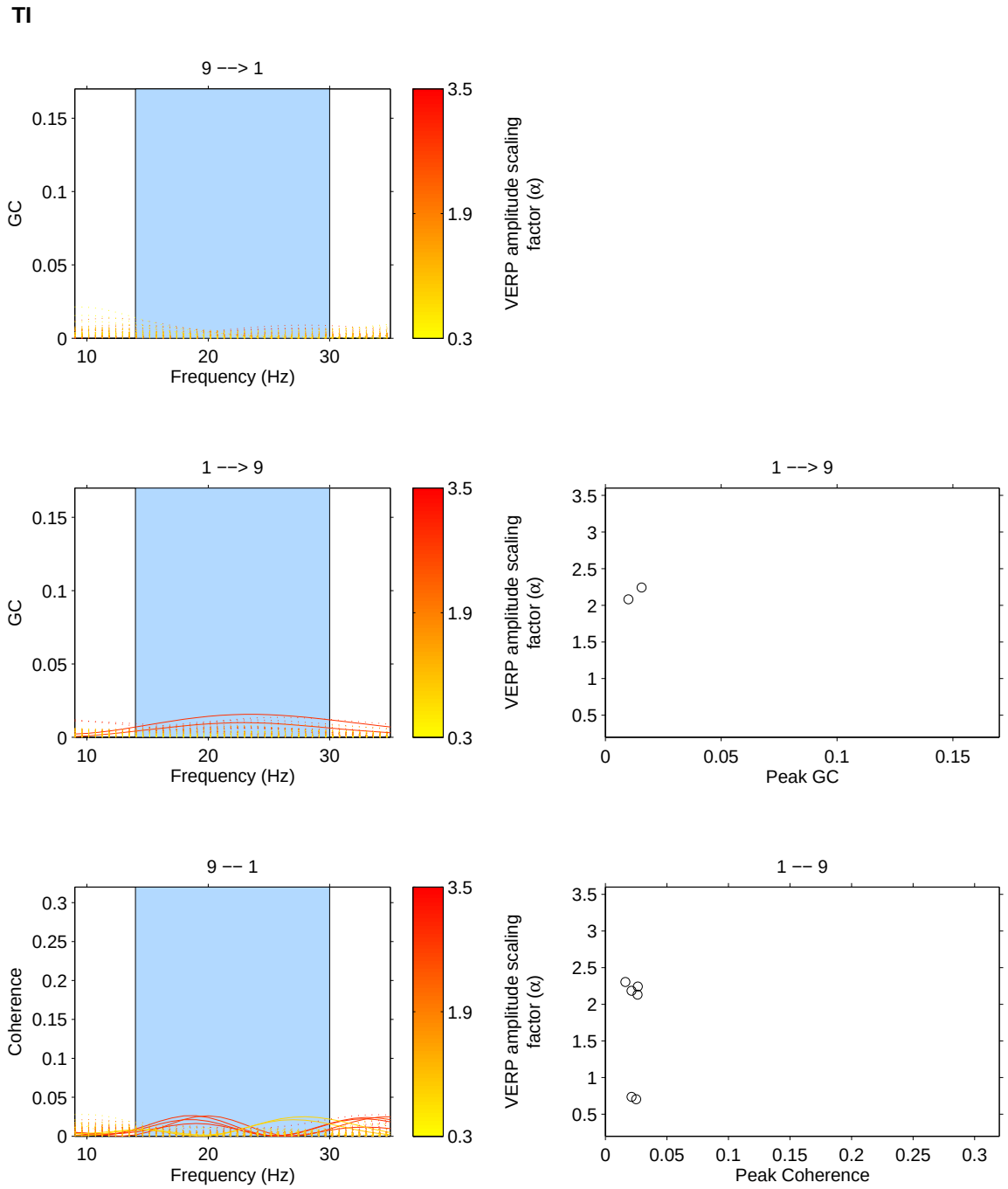

Figure A.23: Subensemble spectra for top-down and bottom-up Granger causality and coherence (left panels) and the correlations between significant beta-range Granger causality and coherence spectral peaks with subensemble mean striate VERP amplitude (right panels) for pair TI 9-1. Significant correlations are fit with a regression line. Spectra with significant peaks are drawn in solid lines. Spectra without significant peaks are drawn with dotted lines.

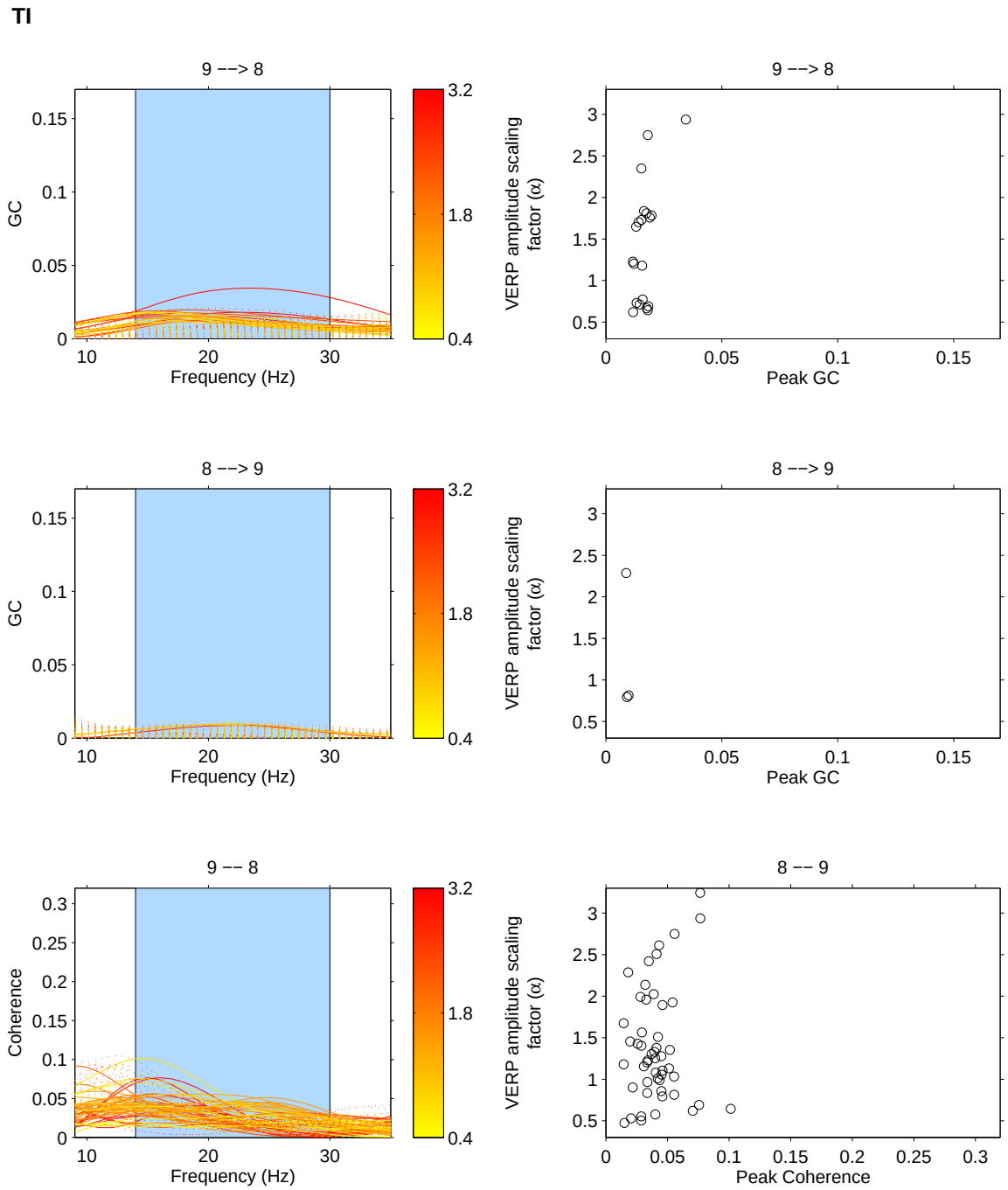

Figure A.24: Subensemble spectra for top-down and bottom-up Granger causality and coherence (left panels) and the correlations between significant beta-range Granger causality and coherence spectral peaks with subensemble mean striate VERP amplitude (right panels) for pair TI 9-8. Significant correlations are fit with a regression line. Spectra with significant peaks are drawn in solid lines. Spectra without significant peaks are drawn with dotted lines.

Figures A.25 through A.38 show pairs in the low gamma band with subsensemble coherence and Granger causality values that are not correlated with the mean VERP amplitude.

GE

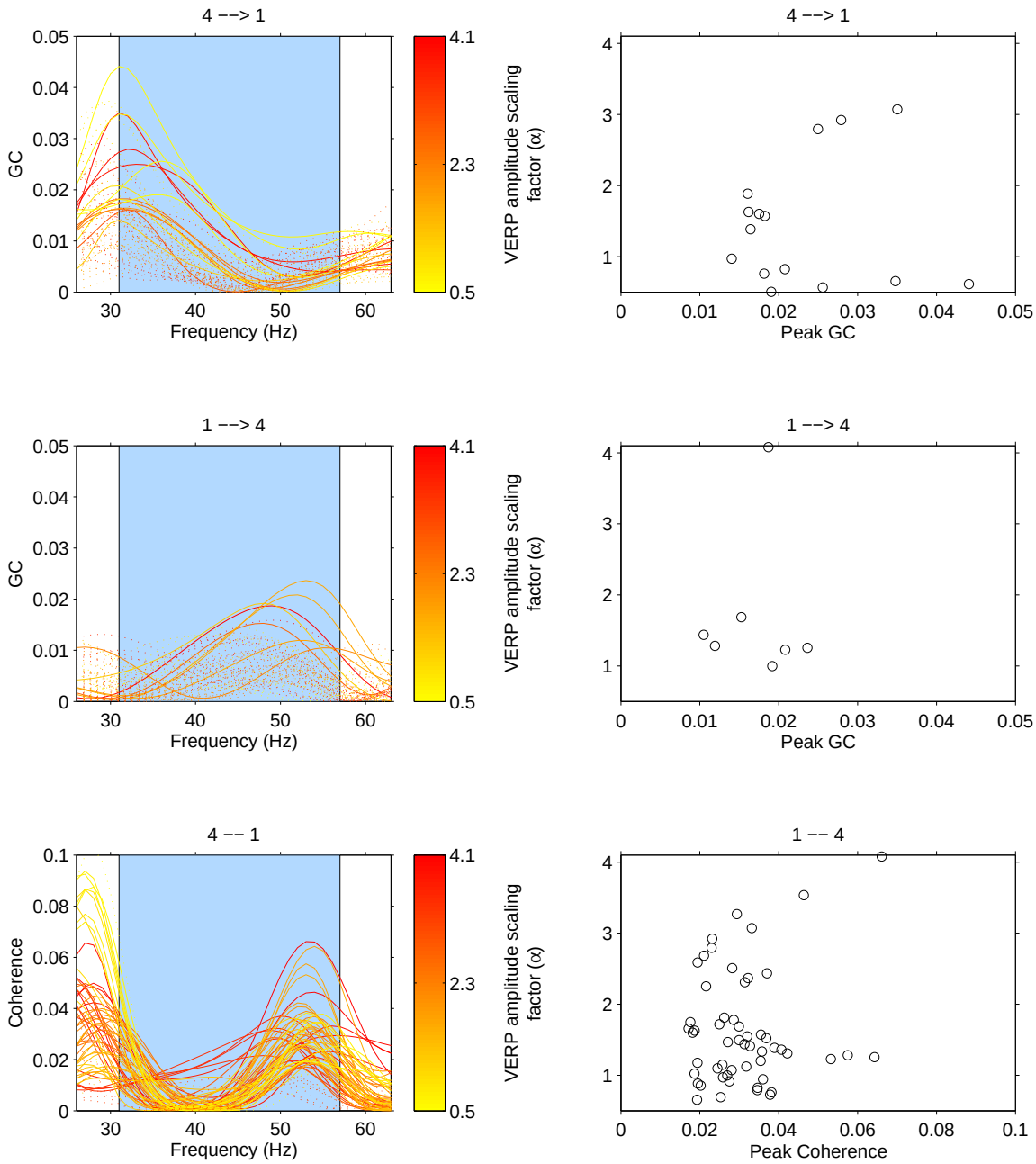

Figure A.25: Subensemble spectra for top-down and bottom-up Granger causality and coherence (left panels) and the correlations between significant low gamma-range Granger causality and coherence spectral peaks with subensemble mean striate VERP amplitude (right panels) for pair GE 4-1. Significant correlations are fit with a regression line. Spectra with significant peaks are drawn in solid lines. Spectra without significant peaks are drawn with dotted lines.

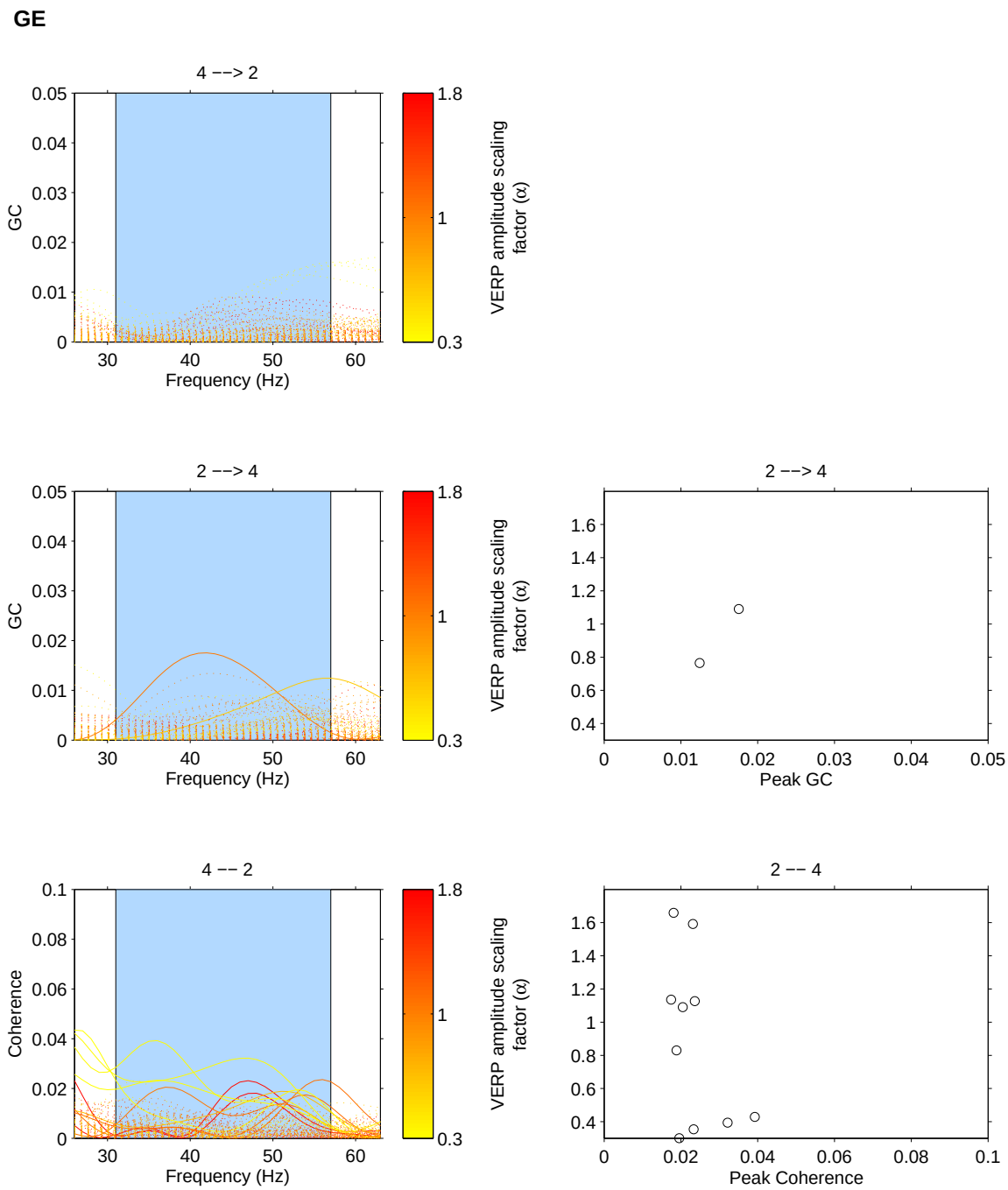

Figure A.26: Subensemble spectra for top-down and bottom-up Granger causality and coherence (left panels) and the correlations between significant low gamma-range Granger causality and coherence spectral peaks with subensemble mean striate VERP amplitude (right panels) for pair GE 4-2. Significant correlations are fit with a regression line. Spectra with significant peaks are drawn in solid lines. Spectra without significant peaks are drawn with dotted lines.

GE

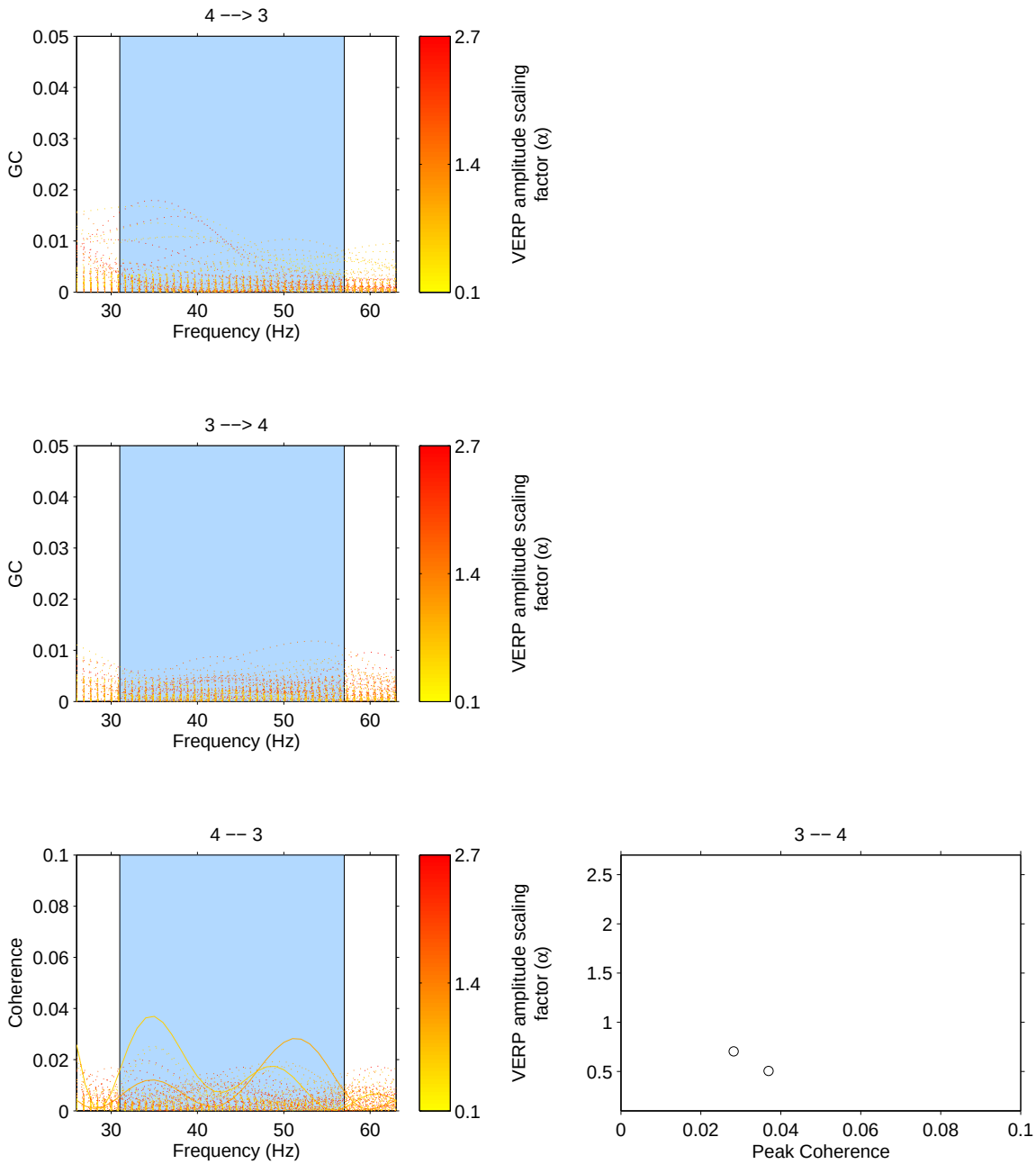

Figure A.27: Subensemble spectra for top-down and bottom-up Granger causality and coherence (left panels) and the correlations between significant low gamma-range Granger causality and coherence spectral peaks with subensemble mean striate VERP amplitude (right panels) for pair GE 4-3. Significant correlations are fit with a regression line. Spectra with significant peaks are drawn in solid lines. Spectra without significant peaks are drawn with dotted lines.

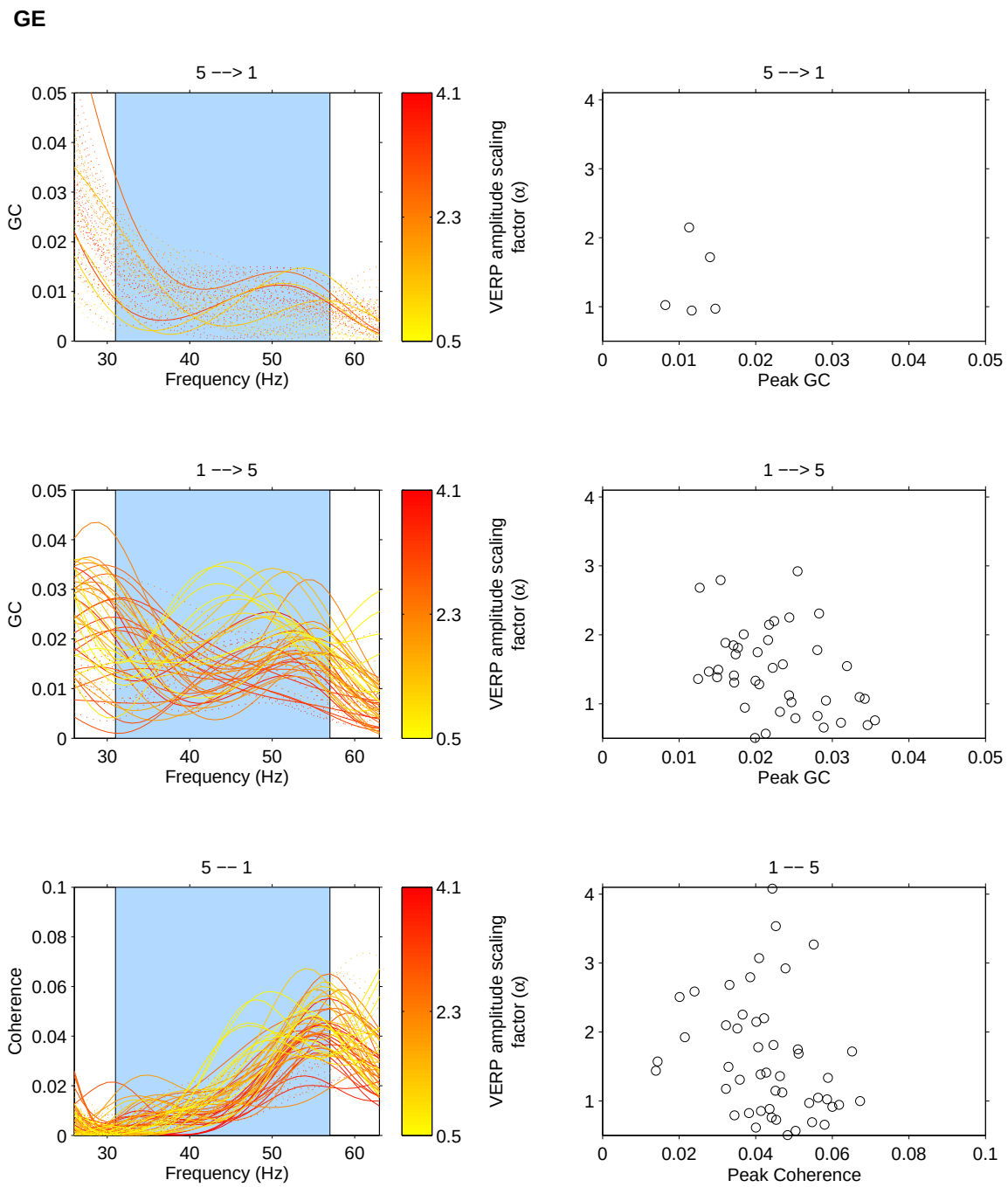

Figure A.28: Subensemble spectra for top-down and bottom-up Granger causality and coherence (left panels) and the correlations between significant low gamma-range Granger causality and coherence spectral peaks with subensemble mean striate VERP amplitude (right panels) for pair GE 5-1. Significant correlations are fit with a regression line. Spectra with significant peaks are drawn in solid lines. Spectra without significant peaks are drawn with dotted lines.

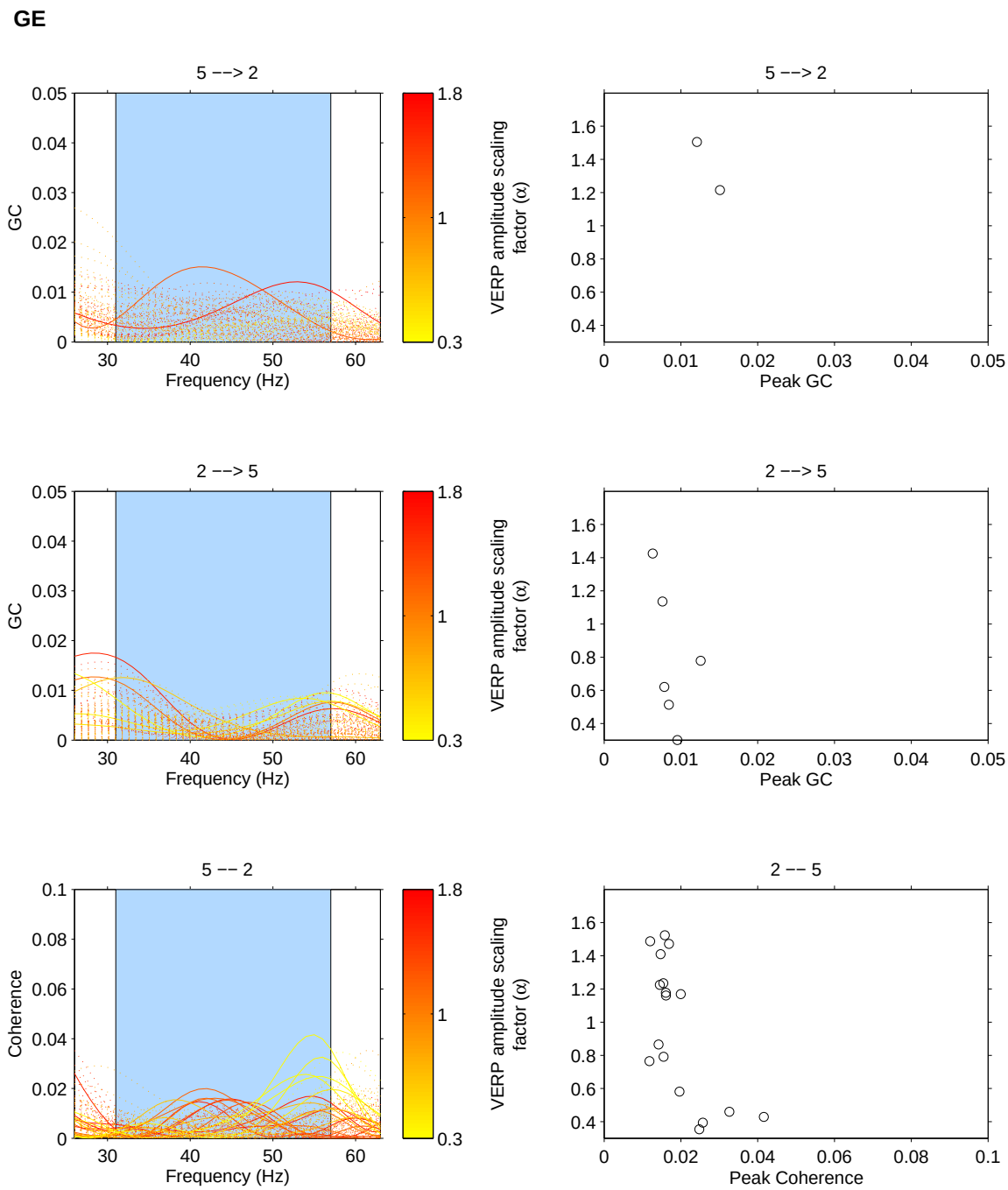

Figure A.29: Subensemble spectra for top-down and bottom-up Granger causality and coherence (left panels) and the correlations between significant low gamma-range Granger causality and coherence spectral peaks with subensemble mean striate VERP amplitude (right panels) for pair GE 5-2. Significant correlations are fit with a regression line. Spectra with significant peaks are drawn in solid lines. Spectra without significant peaks are drawn with dotted lines.

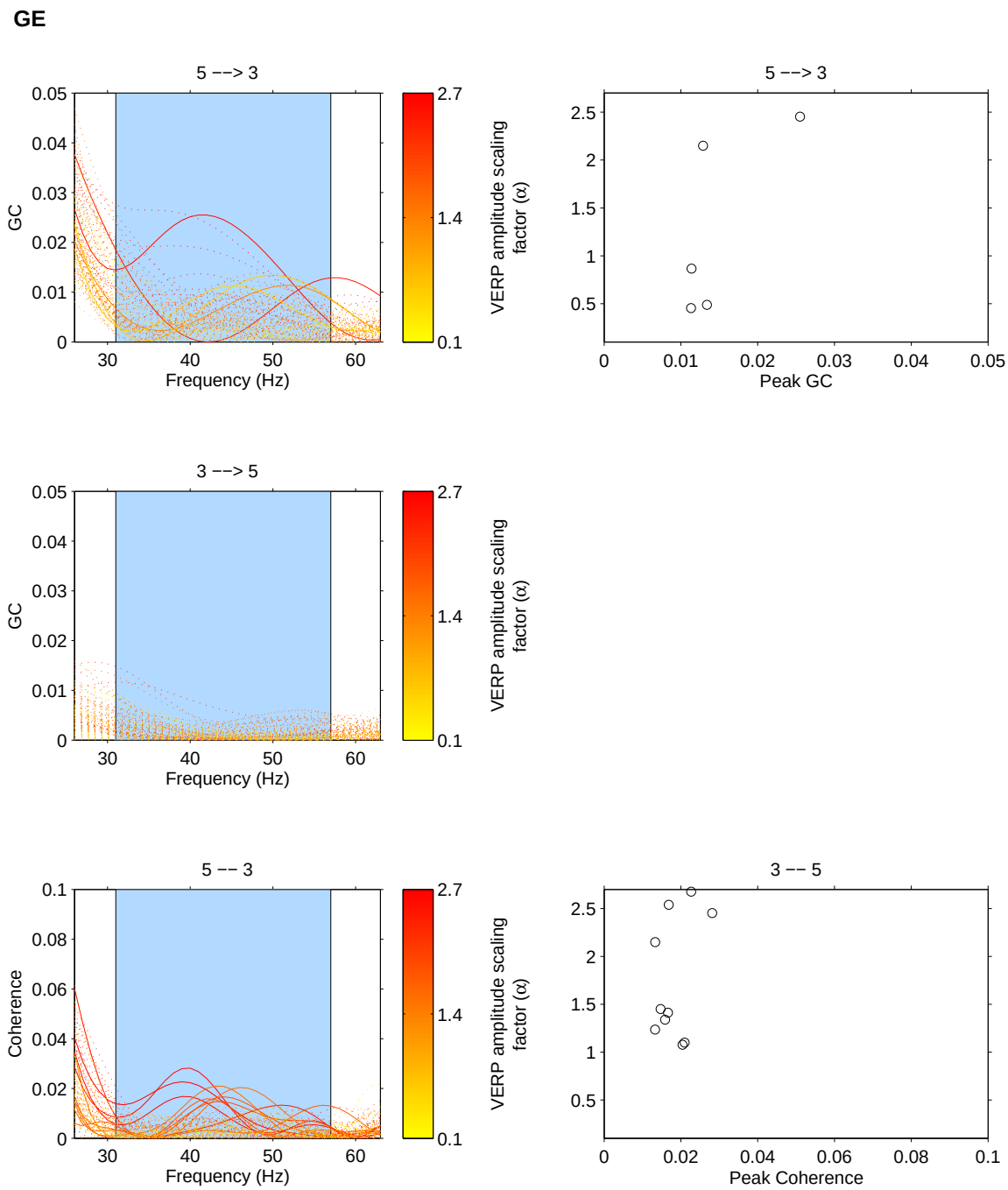

Figure A.30: Subensemble spectra for top-down and bottom-up Granger causality and coherence (left panels) and the correlations between significant low gamma-range Granger causality and coherence spectral peaks with subensemble mean striate VERP amplitude (right panels) for pair GE 5-3. Significant correlations are fit with a regression line. Spectra with significant peaks are drawn in solid lines. Spectra without significant peaks are drawn with dotted lines.

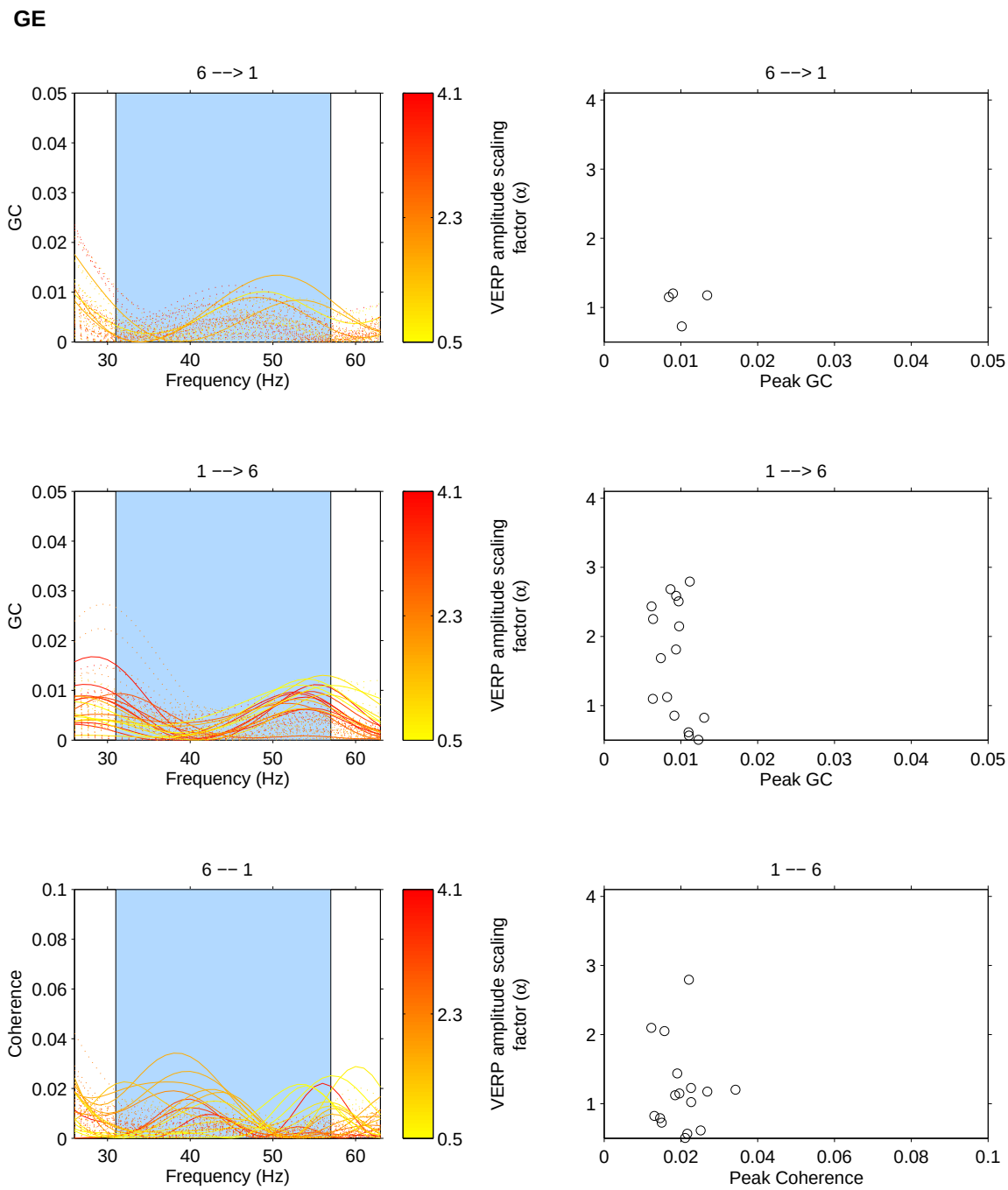

Figure A.31: Subensemble spectra for top-down and bottom-up Granger causality and coherence (left panels) and the correlations between significant low gamma-range Granger causality and coherence spectral peaks with subensemble mean striate VERP amplitude (right panels) for pair GE 6-1. Significant correlations are fit with a regression line. Spectra with significant peaks are drawn in solid lines. Spectra without significant peaks are drawn with dotted lines.

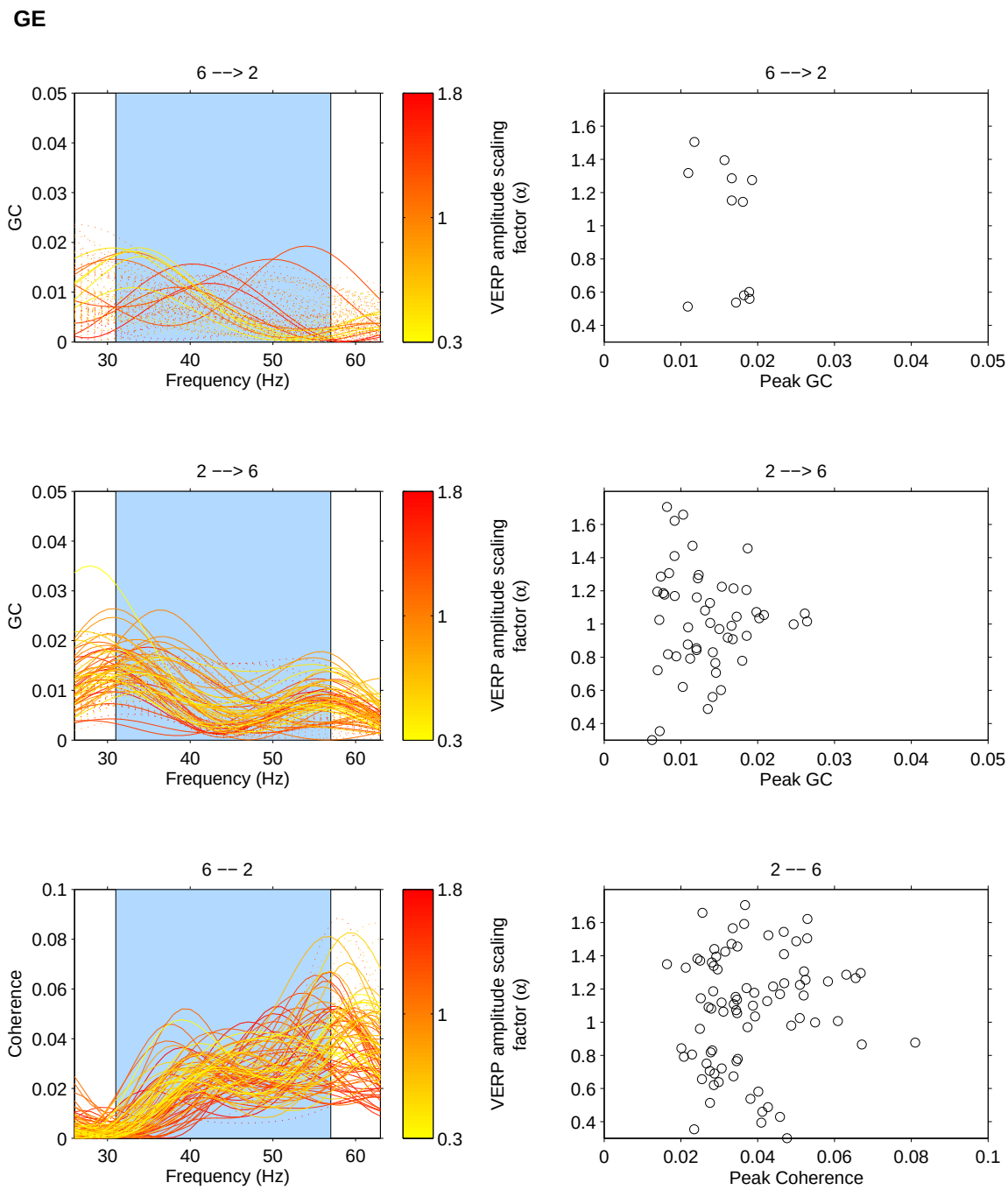

Figure A.32: Subensemble spectra for top-down and bottom-up Granger causality and coherence (left panels) and the correlations between significant low gamma-range Granger causality and coherence spectral peaks with subensemble mean striate VERP amplitude (right panels) for pair GE 6-2. Significant correlations are fit with a regression line. Spectra with significant peaks are drawn in solid lines. Spectra without significant peaks are drawn with dotted lines.

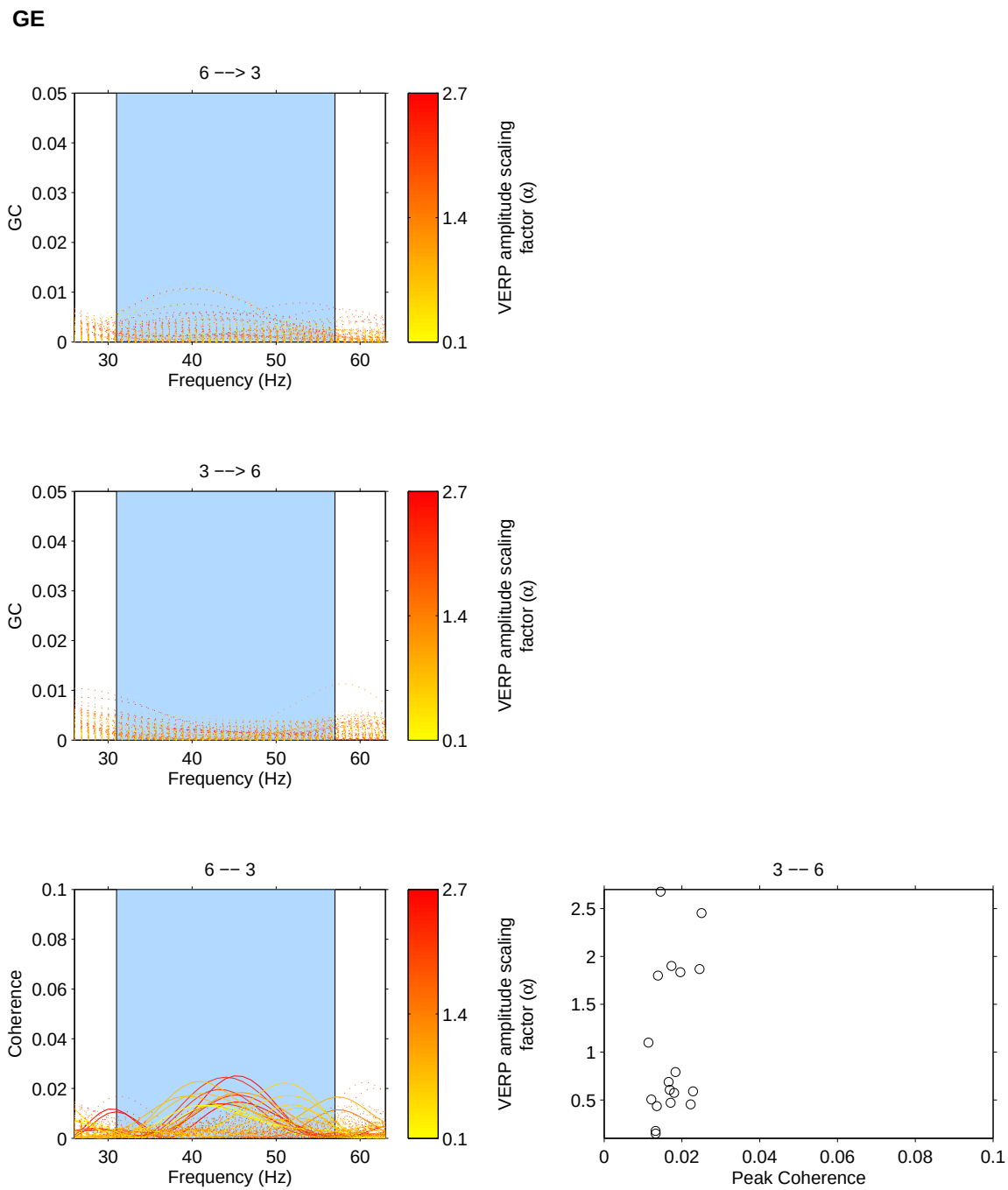

Figure A.33: Subensemble spectra for top-down and bottom-up Granger causality and coherence (left panels) and the correlations between significant low gamma-range Granger causality and coherence spectral peaks with subensemble mean striate VERP amplitude (right panels) for pair GE 6-3. Significant correlations are fit with a regression line. Spectra with significant peaks are drawn in solid lines. Spectra without significant peaks are drawn with dotted lines.

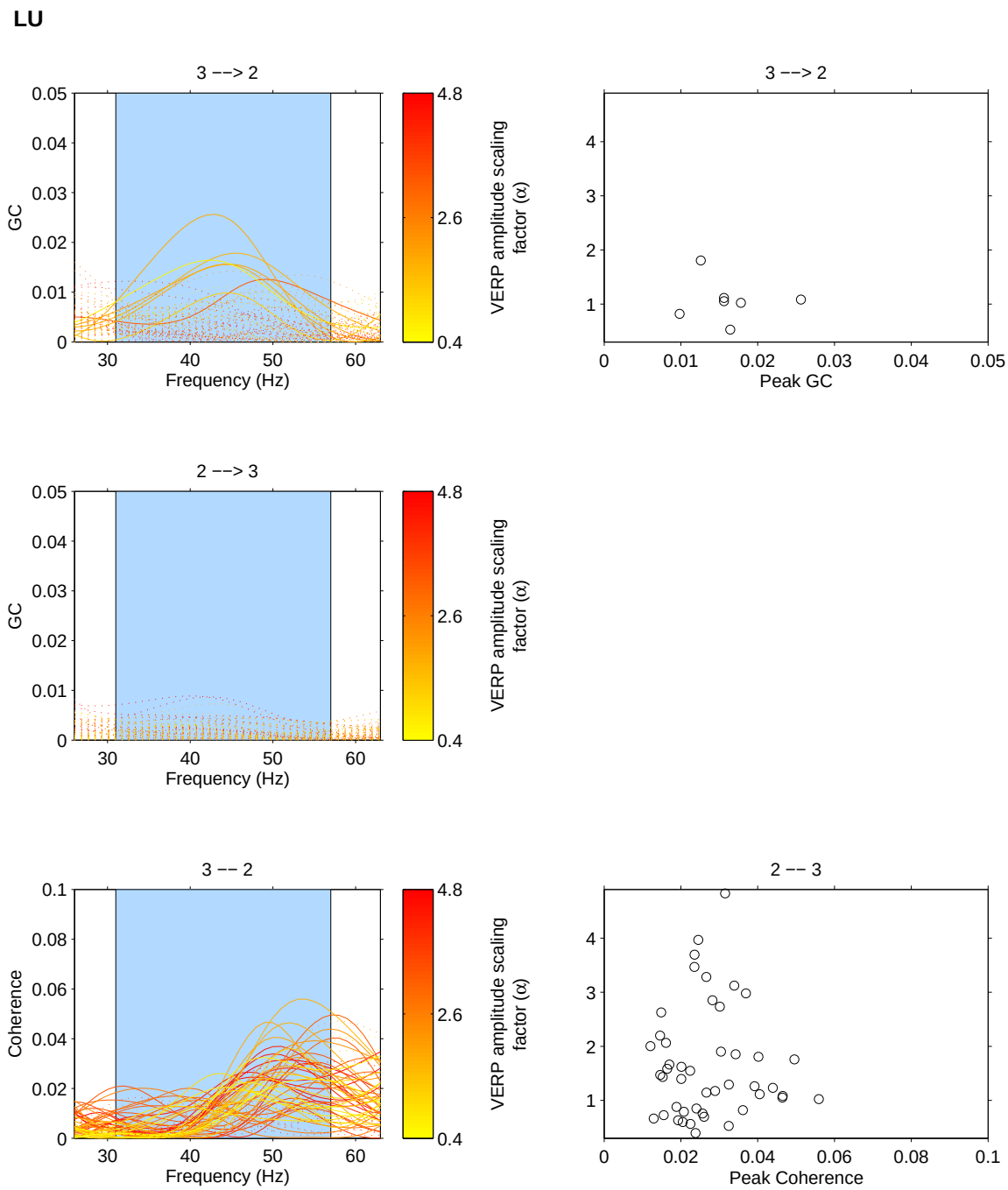

Figure A.34: Subensemble spectra for top-down and bottom-up Granger causality and coherence (left panels) and the correlations between significant low gamma-range Granger causality and coherence spectral peaks with subensemble mean striate VERP amplitude (right panels) for pair LU 3-2. Significant correlations are fit with a regression line. Spectra with significant peaks are drawn in solid lines. Spectra without significant peaks are drawn with dotted lines.

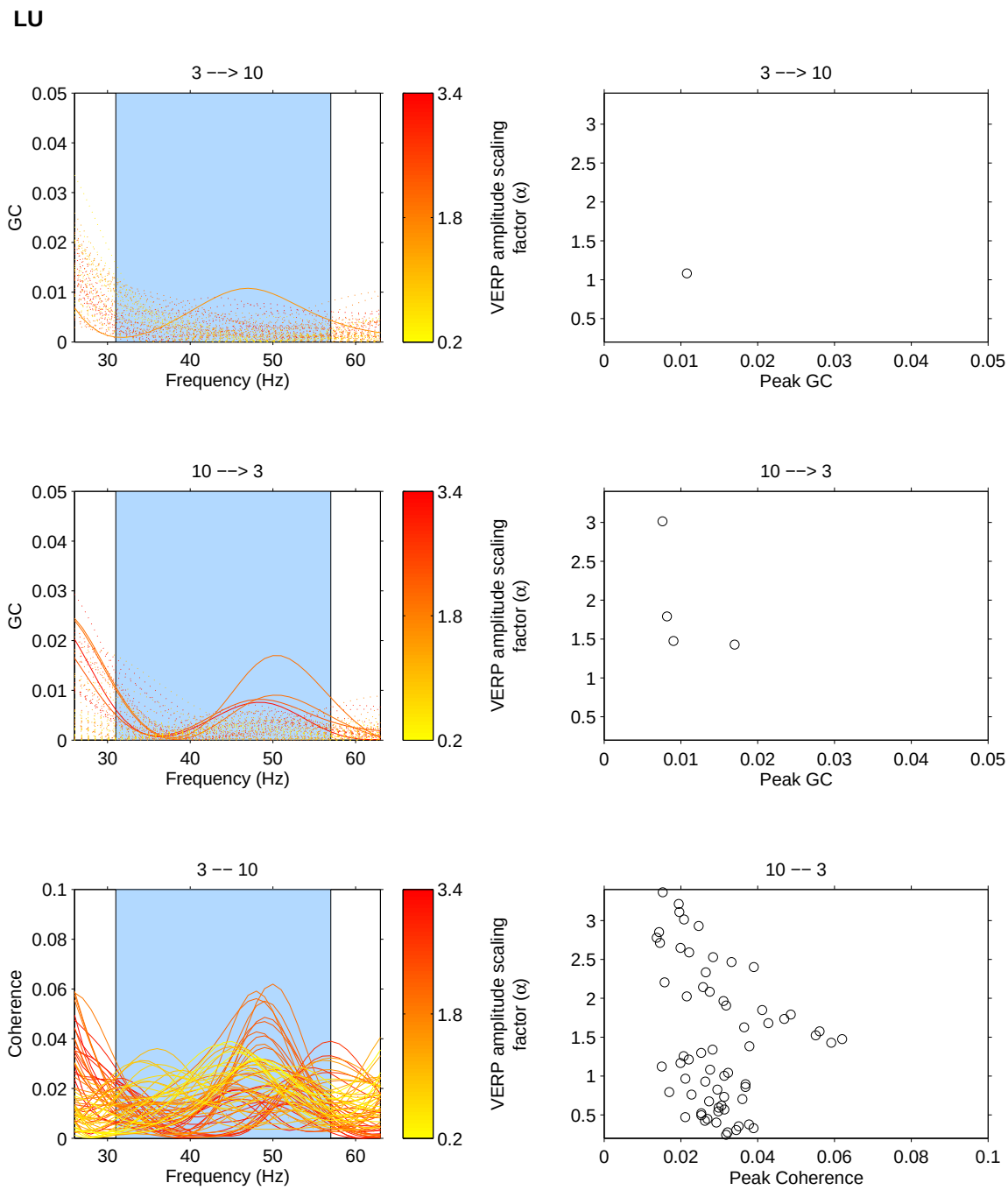

Figure A.35: Subensemble spectra for top-down and bottom-up Granger causality and coherence (left panels) and the correlations between significant low gamma-range Granger causality and coherence spectral peaks with subensemble mean striate VERP amplitude (right panels) for pair LU 3-10. Significant correlations are fit with a regression line. Spectra with significant peaks are drawn in solid lines. Spectra without significant peaks are drawn with dotted lines.

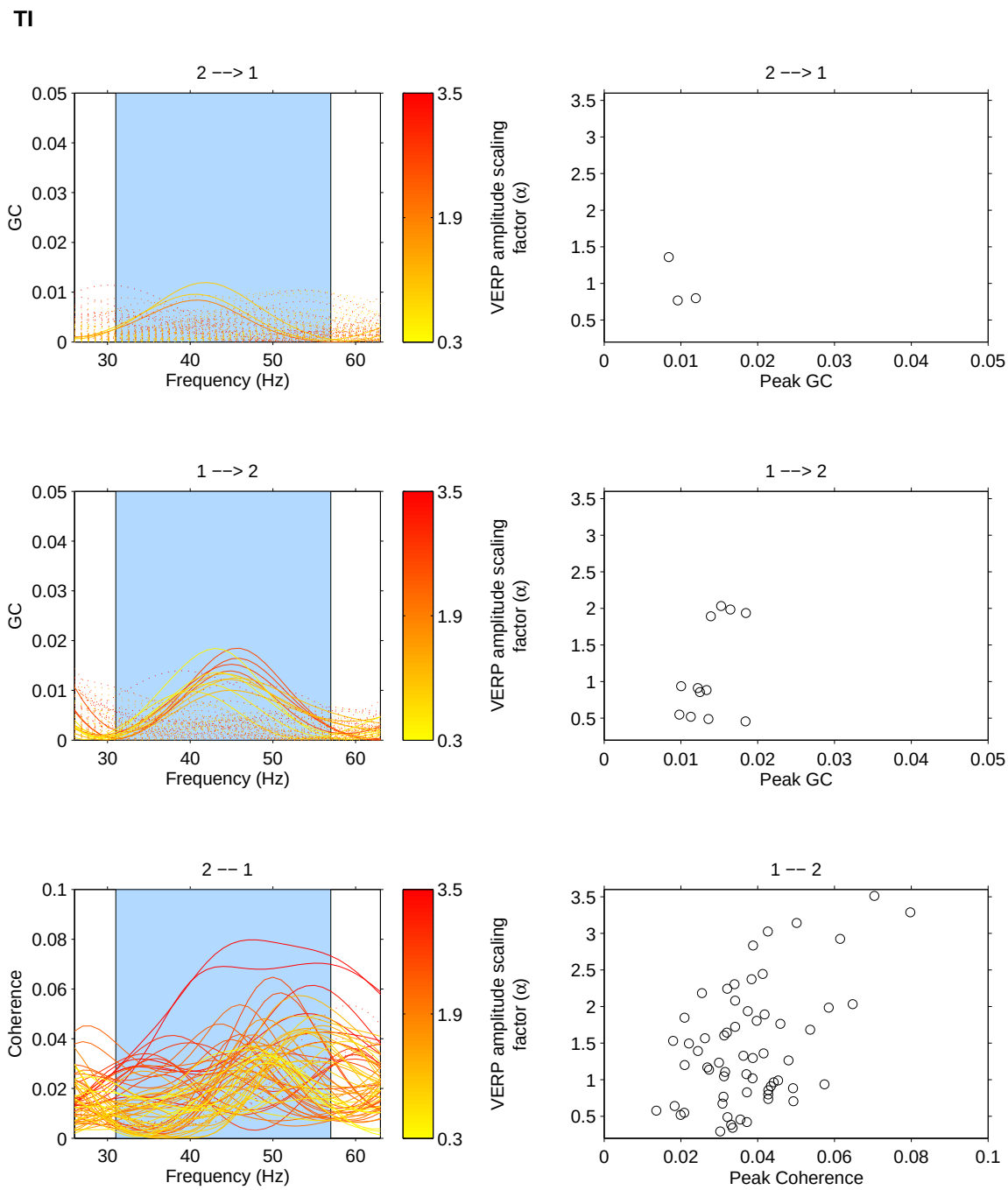

Figure A.36: Subensemble spectra for top-down and bottom-up Granger causality and coherence (left panels) and the correlations between significant low gamma-range Granger causality and coherence spectral peaks with subensemble mean striate VERP amplitude (right panels) for pair TI 2-1. Significant correlations are fit with a regression line. Spectra with significant peaks are drawn in solid lines. Spectra without significant peaks are drawn with dotted lines.

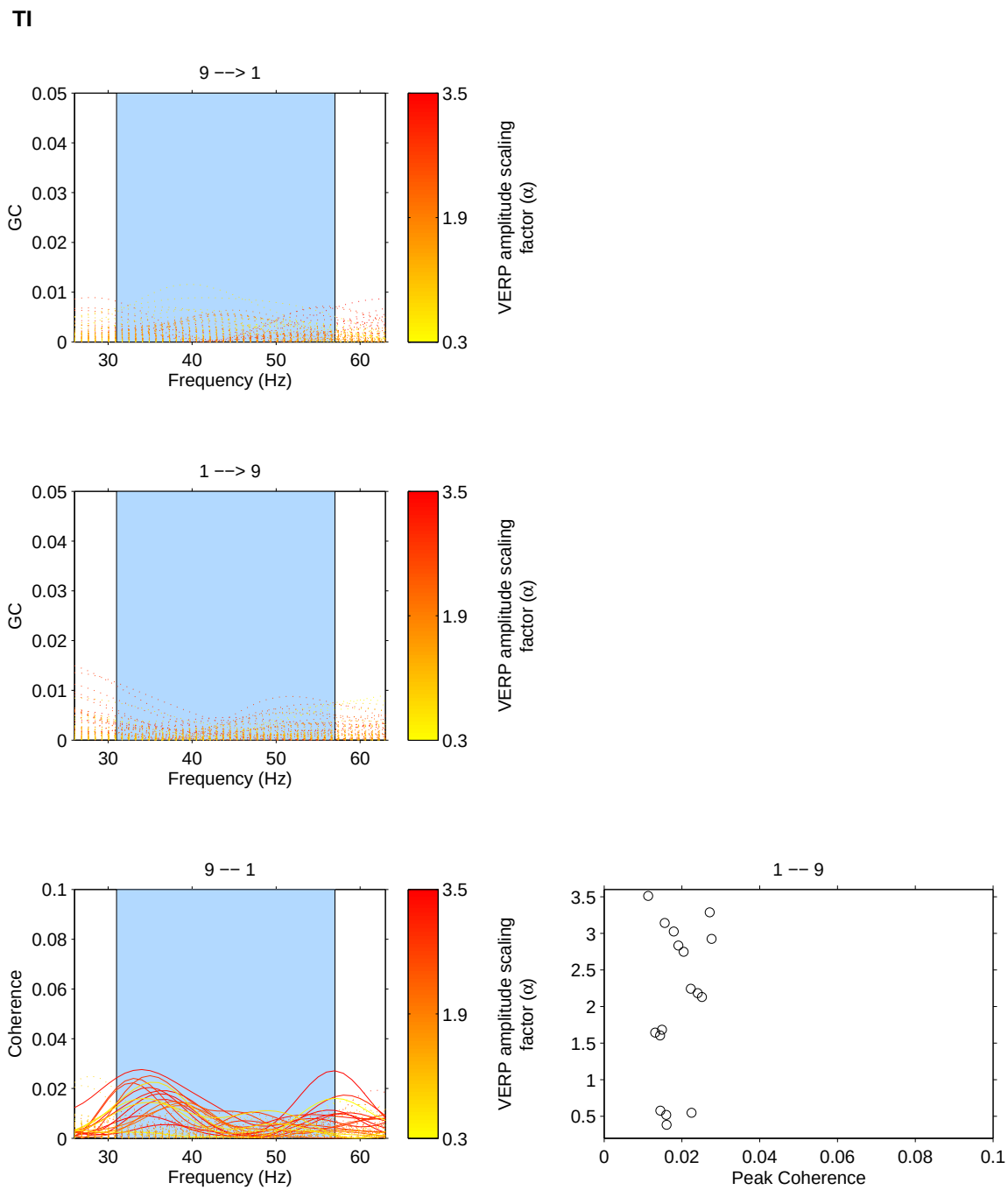

Figure A.37: Subensemble spectra for top-down and bottom-up Granger causality and coherence (left panels) and the correlations between significant low gamma-range Granger causality and coherence spectral peaks with subensemble mean striate VERP amplitude (right panels) for pair TI 9-1. Significant correlations are fit with a regression line. Spectra with significant peaks are drawn in solid lines. Spectra without significant peaks are drawn with dotted lines.

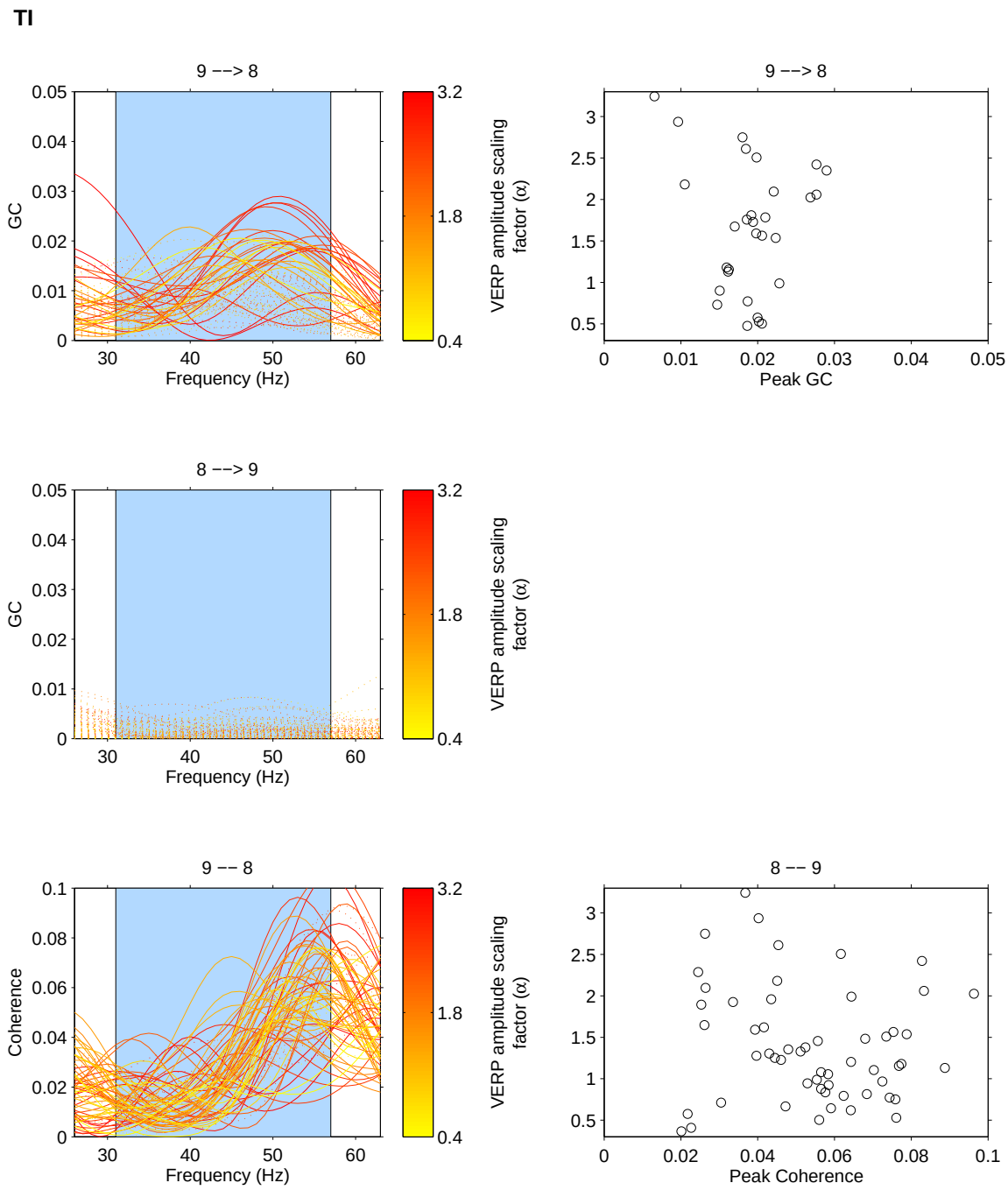

Figure A.38: Subensemble spectra for top-down and bottom-up Granger causality and coherence (left panels) and the correlations between significant low gamma-range Granger causality and coherence spectral peaks with subensemble mean striate VERP amplitude (right panels) for pair TI 9-8. Significant correlations are fit with a regression line. Spectra with significant peaks are drawn in solid lines. Spectra without significant peaks are drawn with dotted lines.

Figures A.25 through A.53 show pairs in the high gamma band with subsensemble coherence and Granger causality values that are not correlated with the mean VERP amplitude.

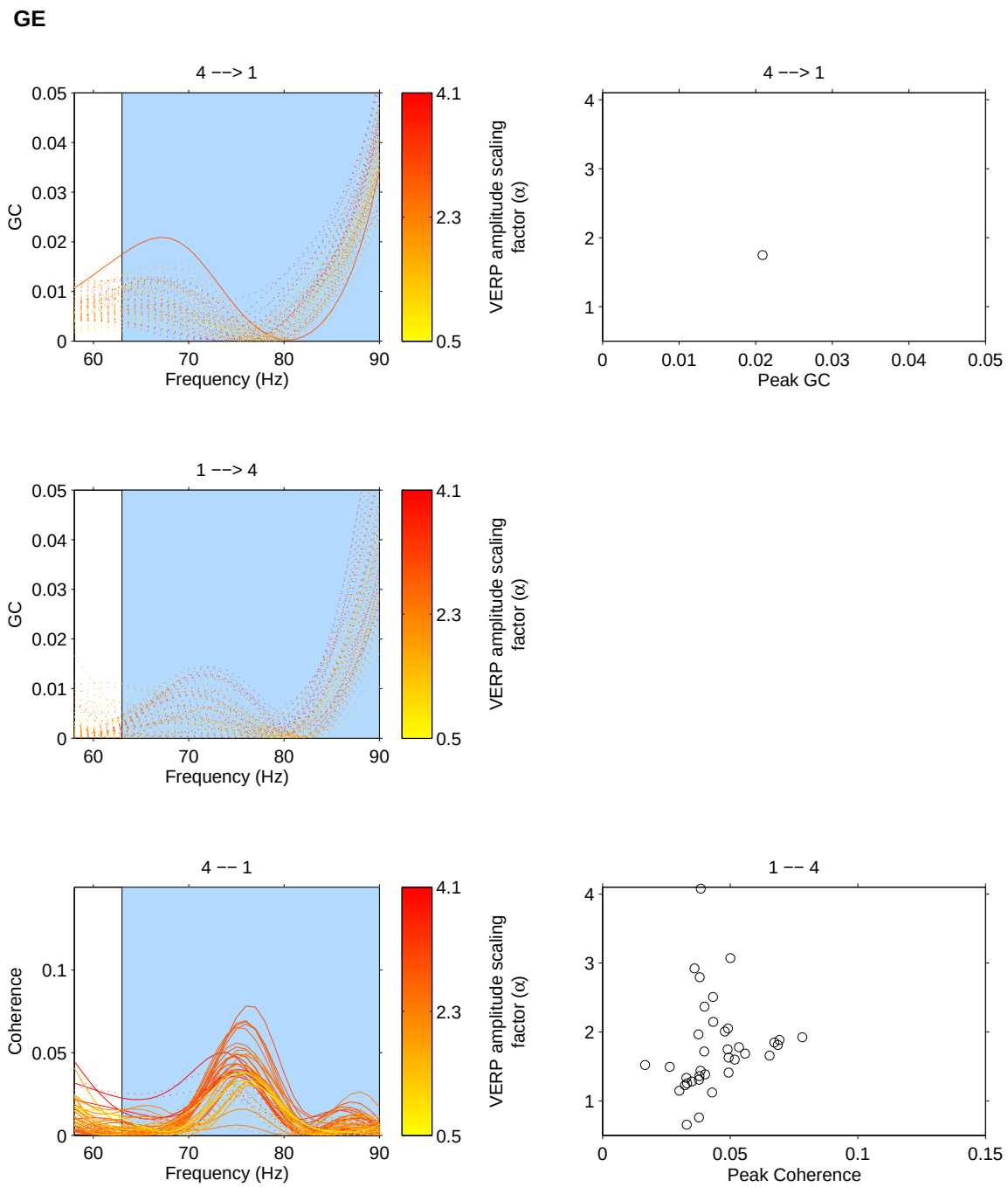

Figure A.39: Subensemble spectra for top-down and bottom-up Granger causality and coherence (left panels) and the correlations between significant high gamma-range Granger causality and coherence spectral peaks with subensemble mean striate VERP amplitude (right panels) for pair GE 4-1. Significant correlations are fit with a regression line. Spectra with significant peaks are drawn in solid lines. Spectra without significant peaks are drawn with dotted lines.

GE

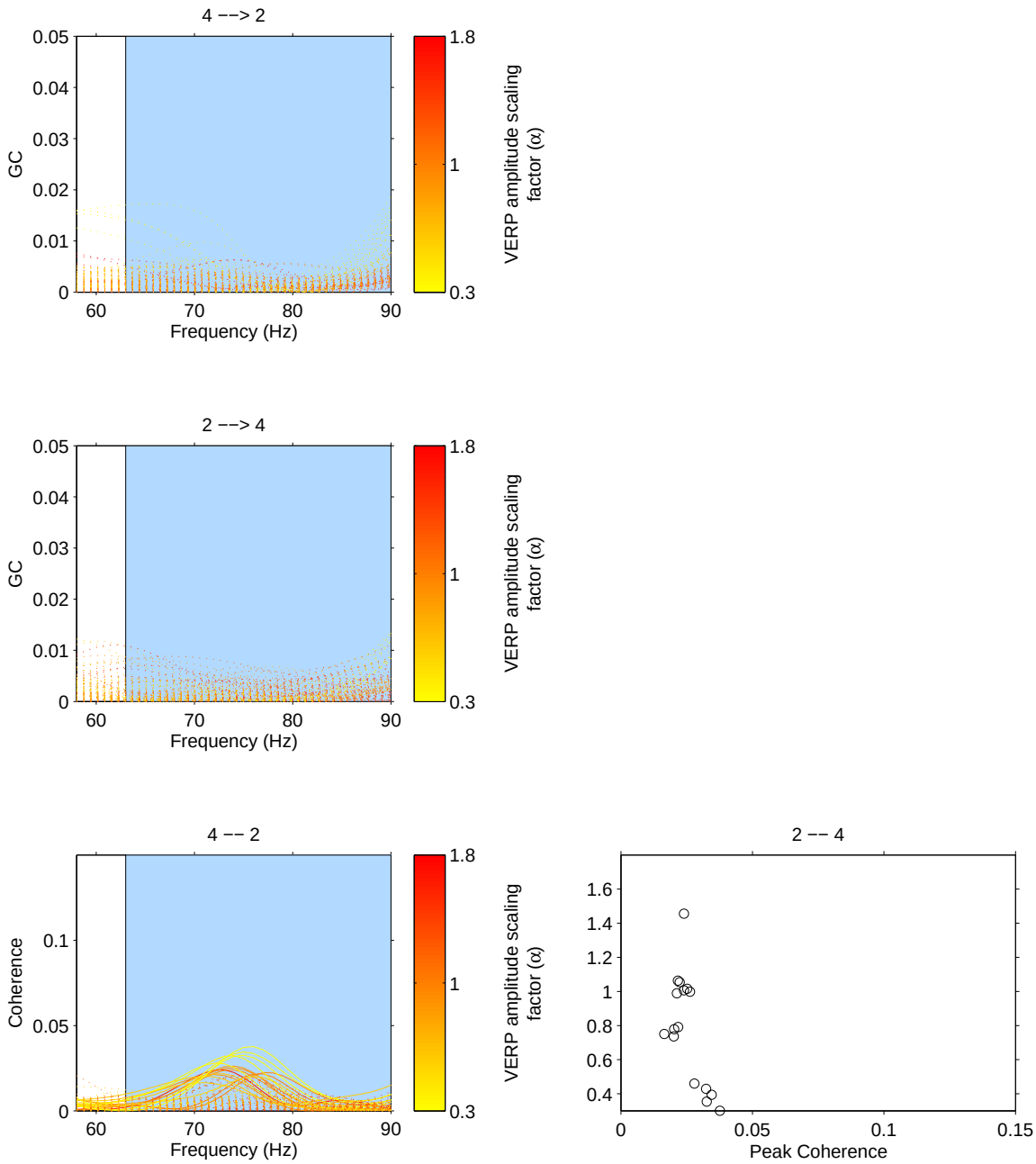

Figure A.40: Subensemble spectra for top-down and bottom-up Granger causality and coherence (left panels) and the correlations between significant high gamma-range Granger causality and coherence spectral peaks with subensemble mean striate VERP amplitude (right panels) for pair GE 4-2. Significant correlations are fit with a regression line. Spectra with significant peaks are drawn in solid lines. Spectra without significant peaks are drawn with dotted lines.

GE

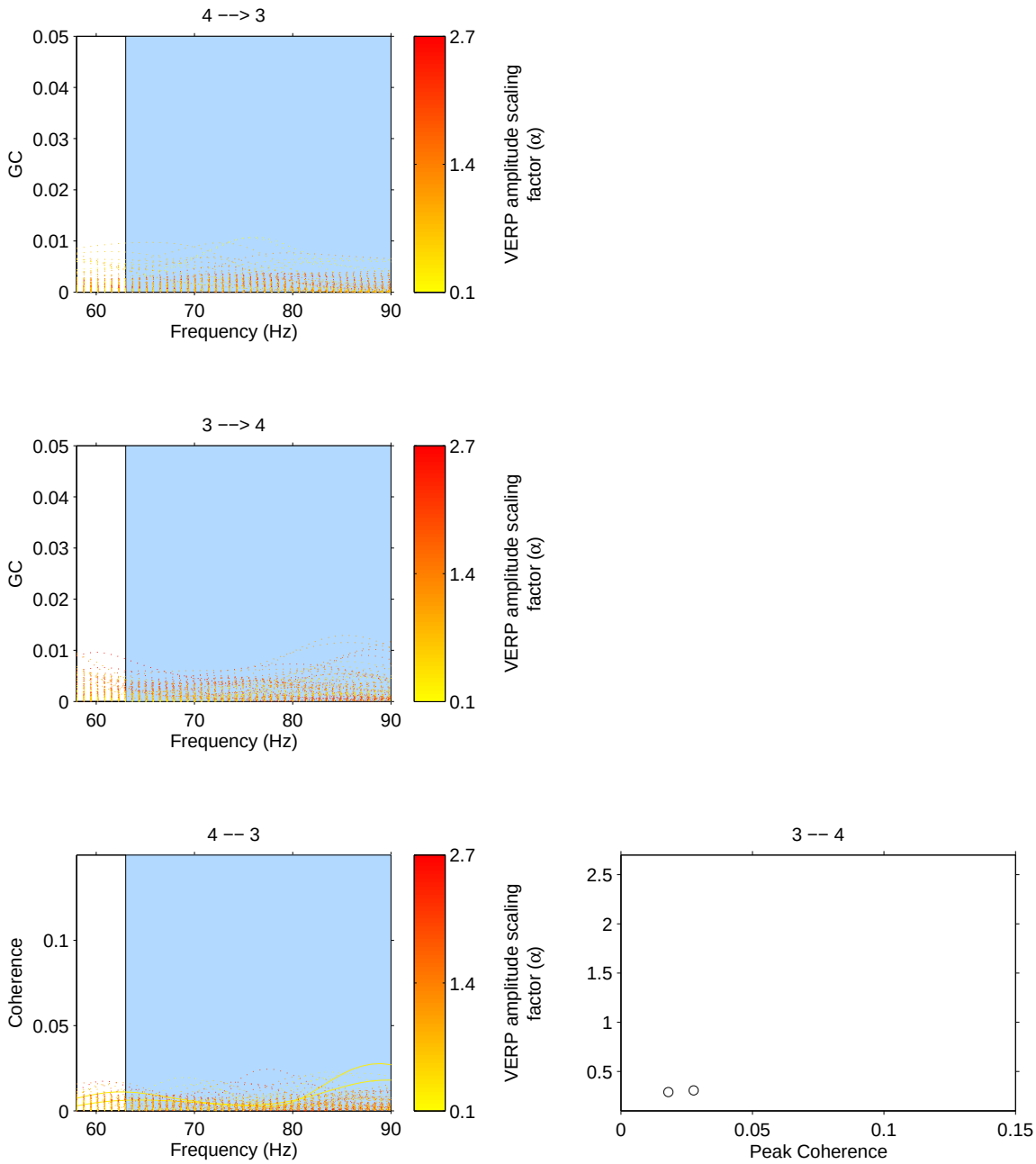

Figure A.41: Subensemble spectra for top-down and bottom-up Granger causality and coherence (left panels) and the correlations between significant high gamma-range Granger causality and coherence spectral peaks with subensemble mean striate VERP amplitude (right panels) for pair GE 4-3. Significant correlations are fit with a regression line. Spectra with significant peaks are drawn in solid lines. Spectra without significant peaks are drawn with dotted lines.

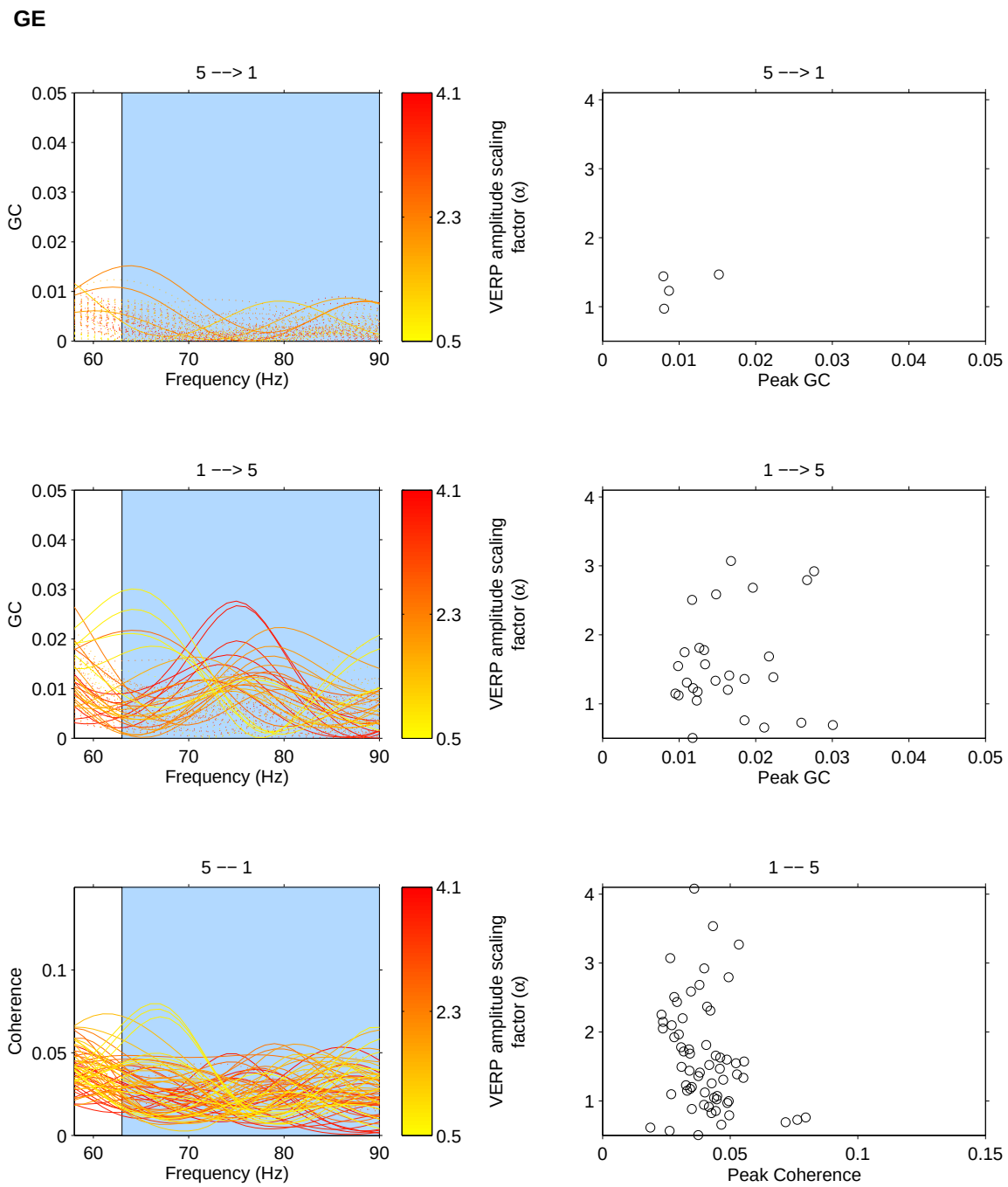

Figure A.42: Subensemble spectra for top-down and bottom-up Granger causality and coherence (left panels) and the correlations between significant high gamma-range Granger causality and coherence spectral peaks with subensemble mean striate VERP amplitude (right panels) for pair GE 5-1. Significant correlations are fit with a regression line. Spectra with significant peaks are drawn in solid lines. Spectra without significant peaks are drawn with dotted lines.

GE

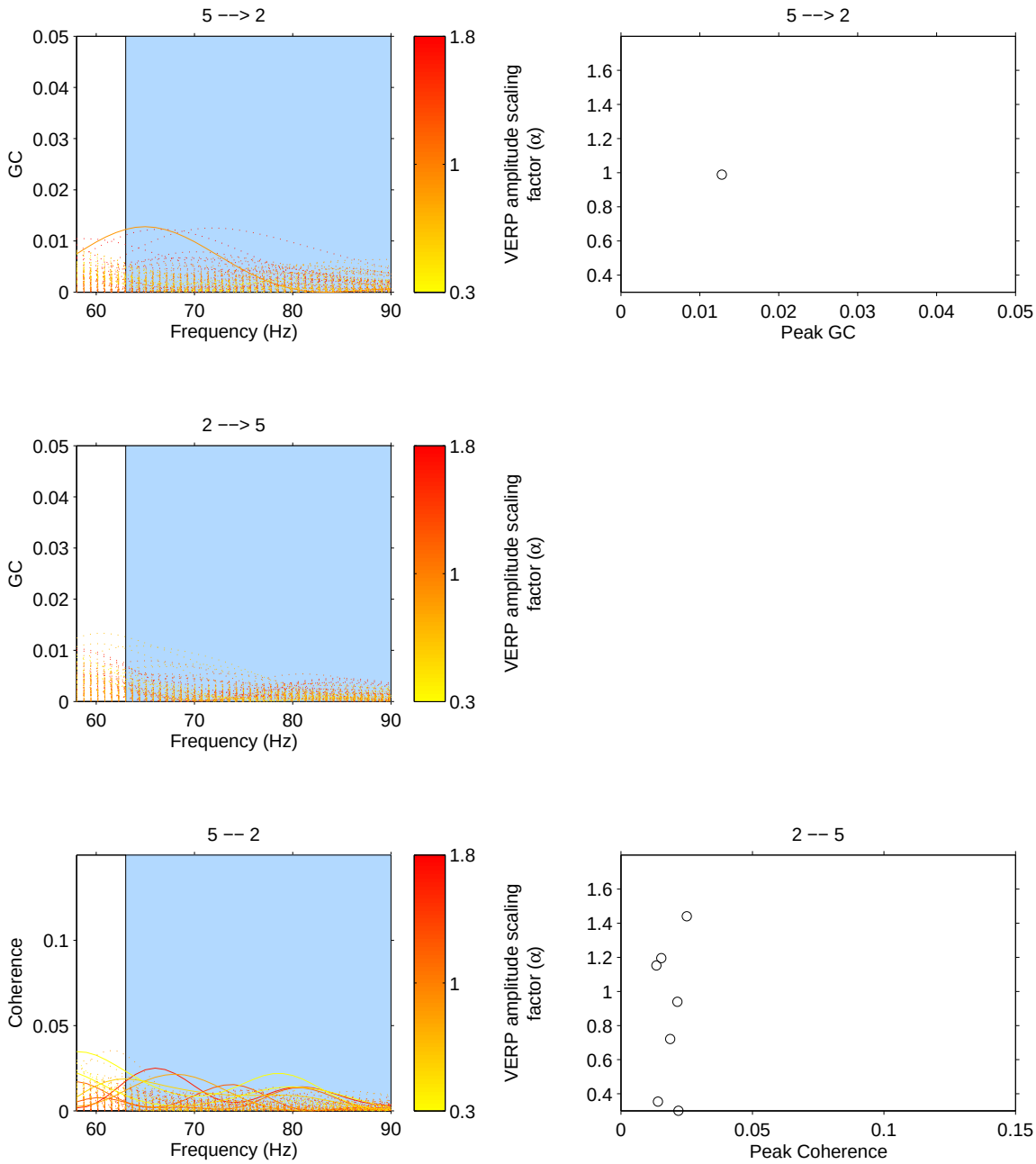

Figure A.43: Subensemble spectra for top-down and bottom-up Granger causality and coherence (left panels) and the correlations between significant high gamma-range Granger causality and coherence spectral peaks with subensemble mean striate VERP amplitude (right panels) for pair GE 5-2. Significant correlations are fit with a regression line. Spectra with significant peaks are drawn in solid lines. Spectra without significant peaks are drawn with dotted lines.

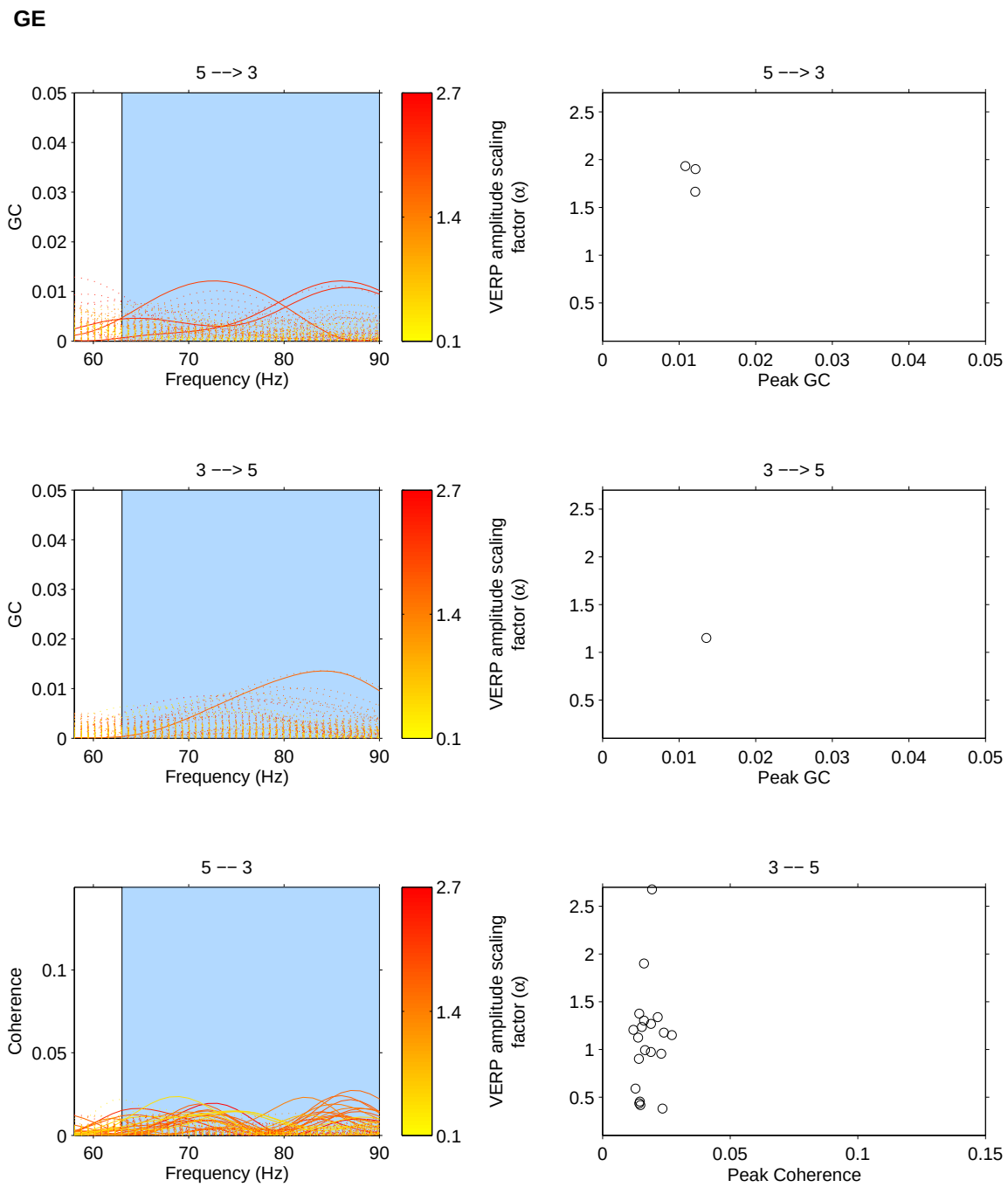

Figure A.44: Subensemble spectra for top-down and bottom-up Granger causality and coherence (left panels) and the correlations between significant high gamma-range Granger causality and coherence spectral peaks with subensemble mean striate VERP amplitude (right panels) for pair GE 5-3. Significant correlations are fit with a regression line. Spectra with significant peaks are drawn in solid lines. Spectra without significant peaks are drawn with dotted lines.

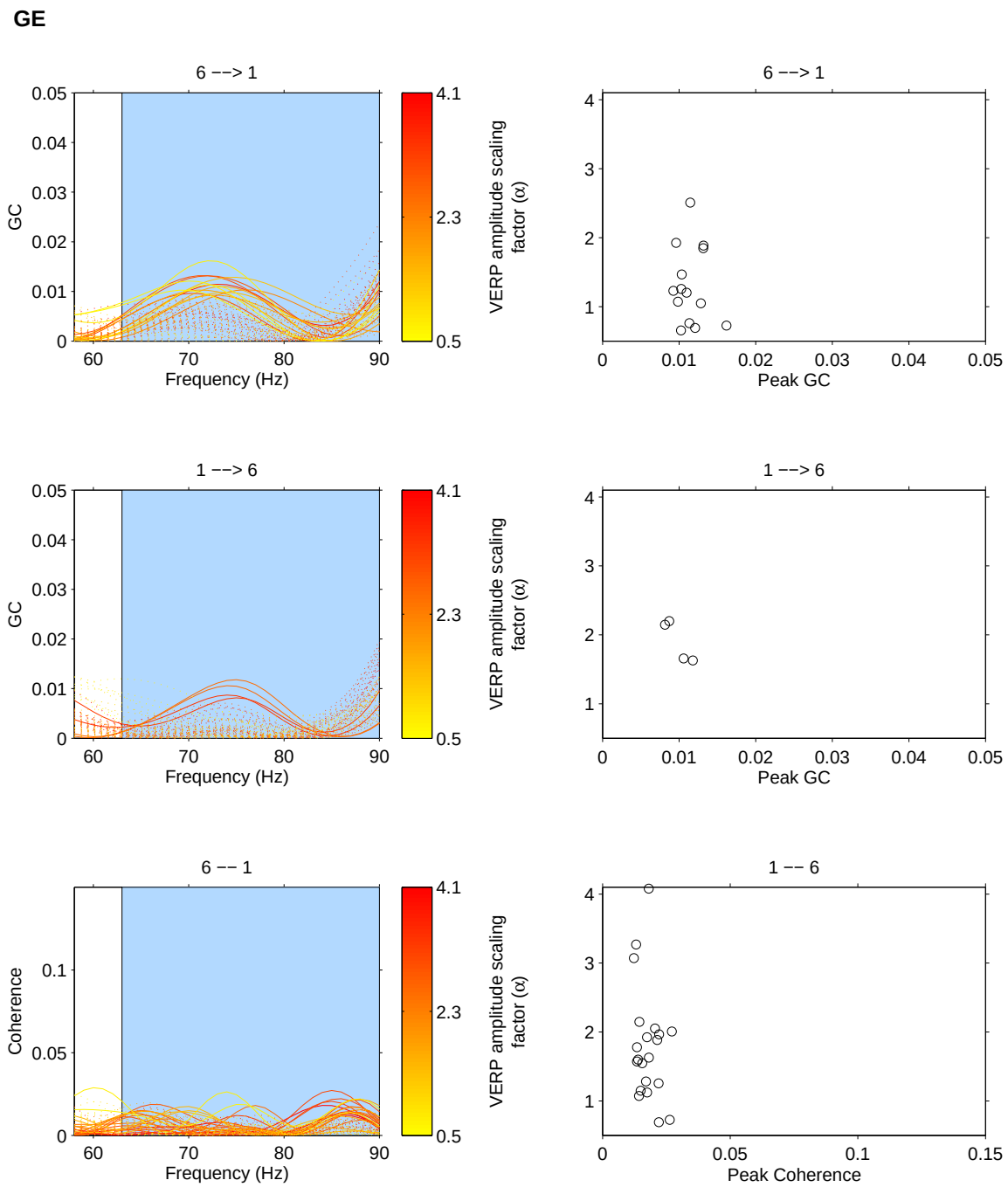

Figure A.45: Subensemble spectra for top-down and bottom-up Granger causality and coherence (left panels) and the correlations between significant high gamma-range Granger causality and coherence spectral peaks with subensemble mean striate VERP amplitude (right panels) for pair GE 6-1. Significant correlations are fit with a regression line. Spectra with significant peaks are drawn in solid lines. Spectra without significant peaks are drawn with dotted lines.

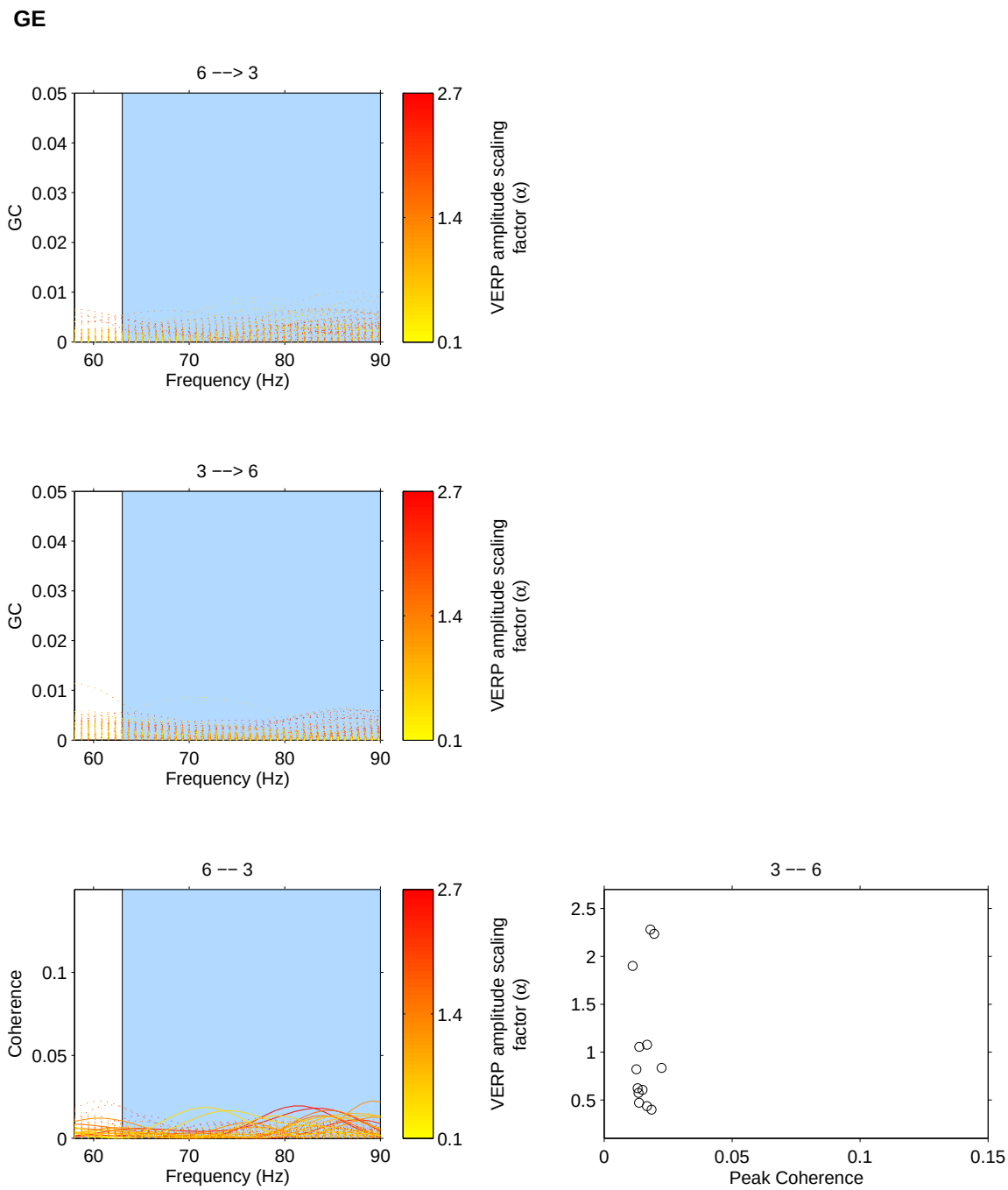

Figure A.46: Subensemble spectra for top-down and bottom-up Granger causality and coherence (left panels) and the correlations between significant high gamma-range Granger causality and coherence spectral peaks with subensemble mean striate VERP amplitude (right panels) for pair GE 6-3. Significant correlations are fit with a regression line. Spectra with significant peaks are drawn in solid lines. Spectra without significant peaks are drawn with dotted lines.

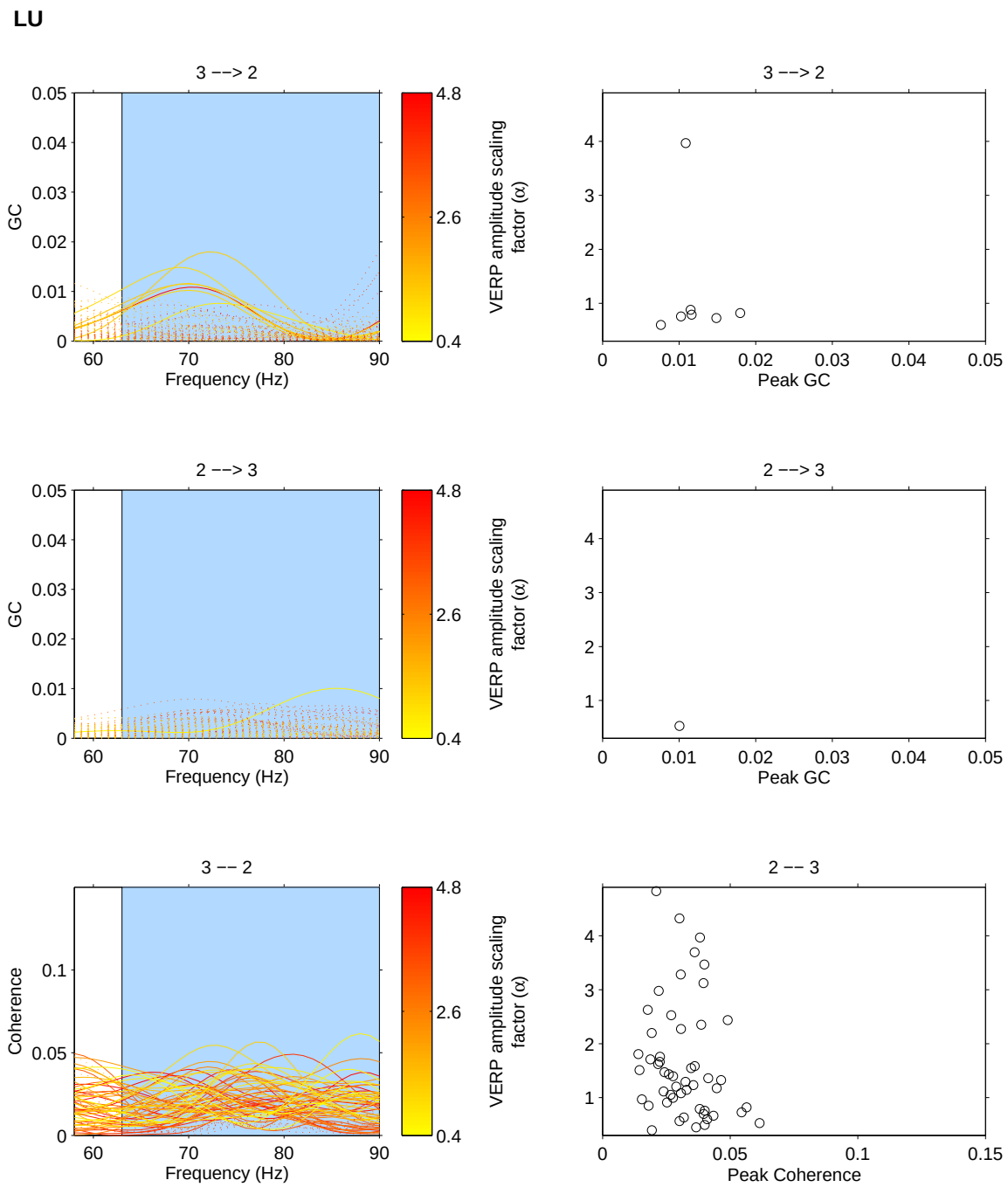

Figure A.47: Subensemble spectra for top-down and bottom-up Granger causality and coherence (left panels) and the correlations between significant high gamma-range Granger causality and coherence spectral peaks with subensemble mean striate VERP amplitude (right panels) for pair LU 3-2. Significant correlations are fit with a regression line. Spectra with significant peaks are drawn in solid lines. Spectra without significant peaks are drawn with dotted lines.

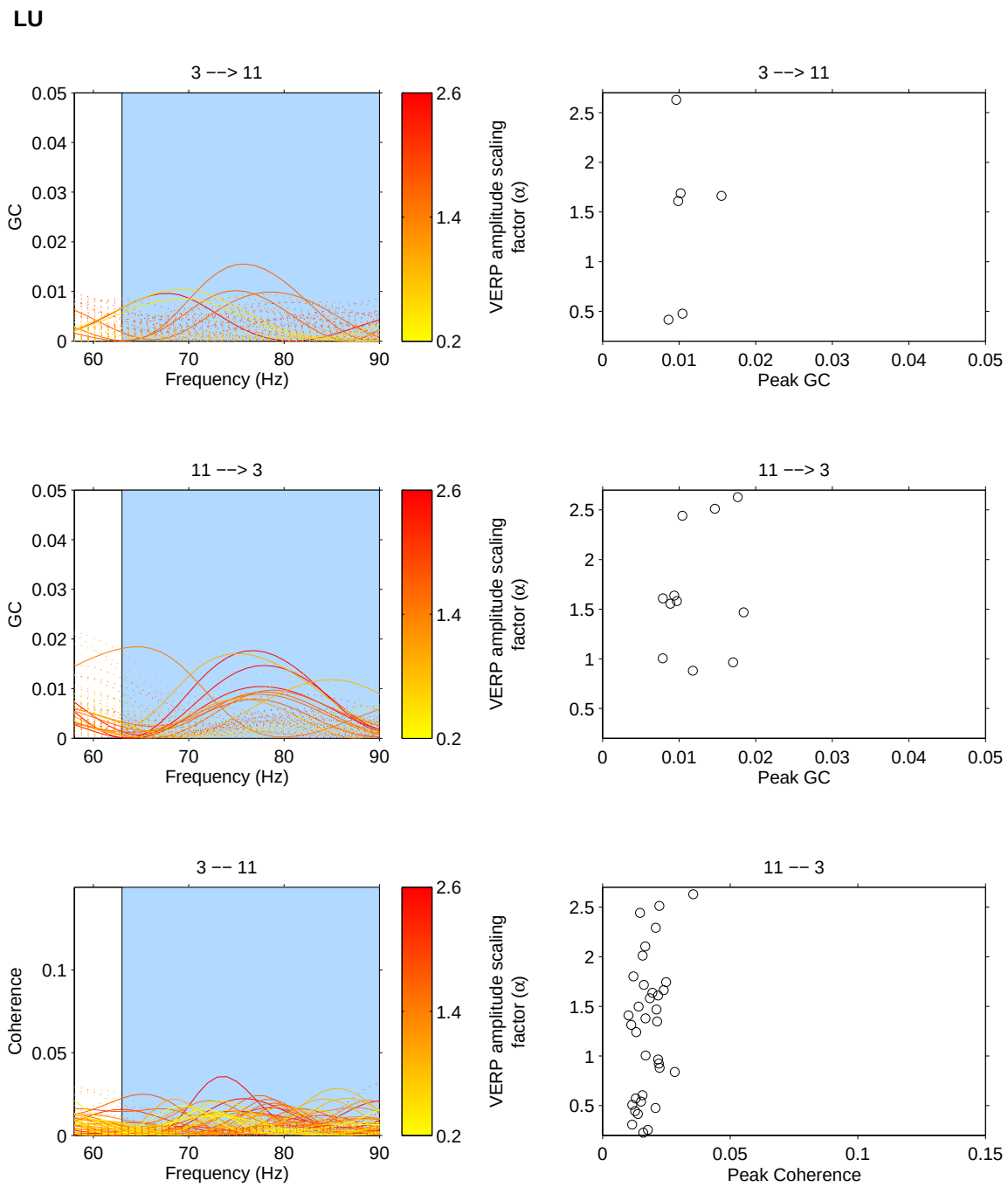

Figure A.48: Subensemble spectra for top-down and bottom-up Granger causality and coherence (left panels) and the correlations between significant high gamma-range Granger causality and coherence spectral peaks with subensemble mean striate VERP amplitude (right panels) for pair LU 3-11. Significant correlations are fit with a regression line. Spectra with significant peaks are drawn in solid lines. Spectra without significant peaks are drawn with dotted lines.

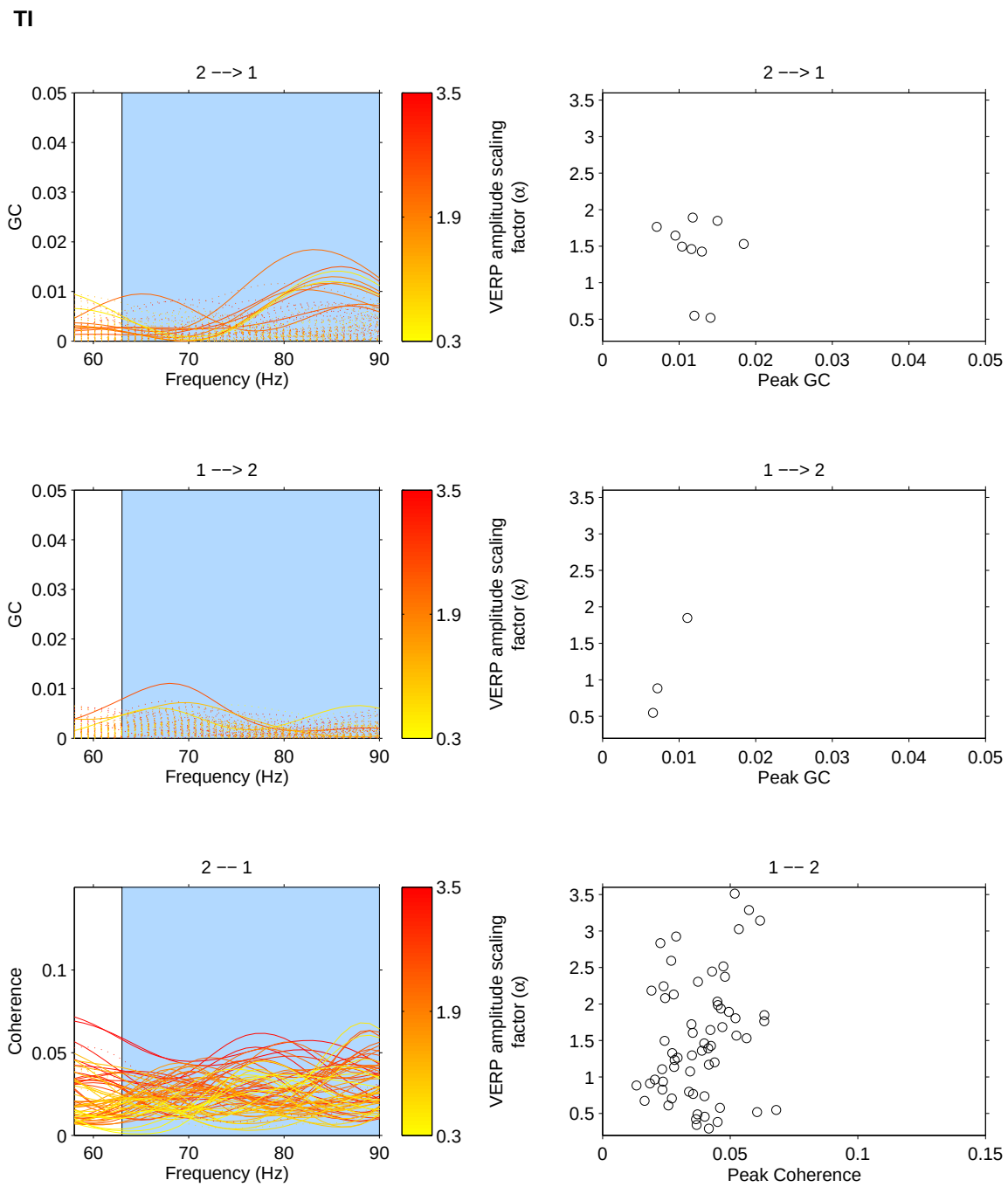

Figure A.49: Subensemble spectra for top-down and bottom-up Granger causality and coherence (left panels) and the correlations between significant high gamma-range Granger causality and coherence spectral peaks with subensemble mean striate VERP amplitude (right panels) for pair TI 2-1. Significant correlations are fit with a regression line. Spectra with significant peaks are drawn in solid lines. Spectra without significant peaks are drawn with dotted lines.

TI

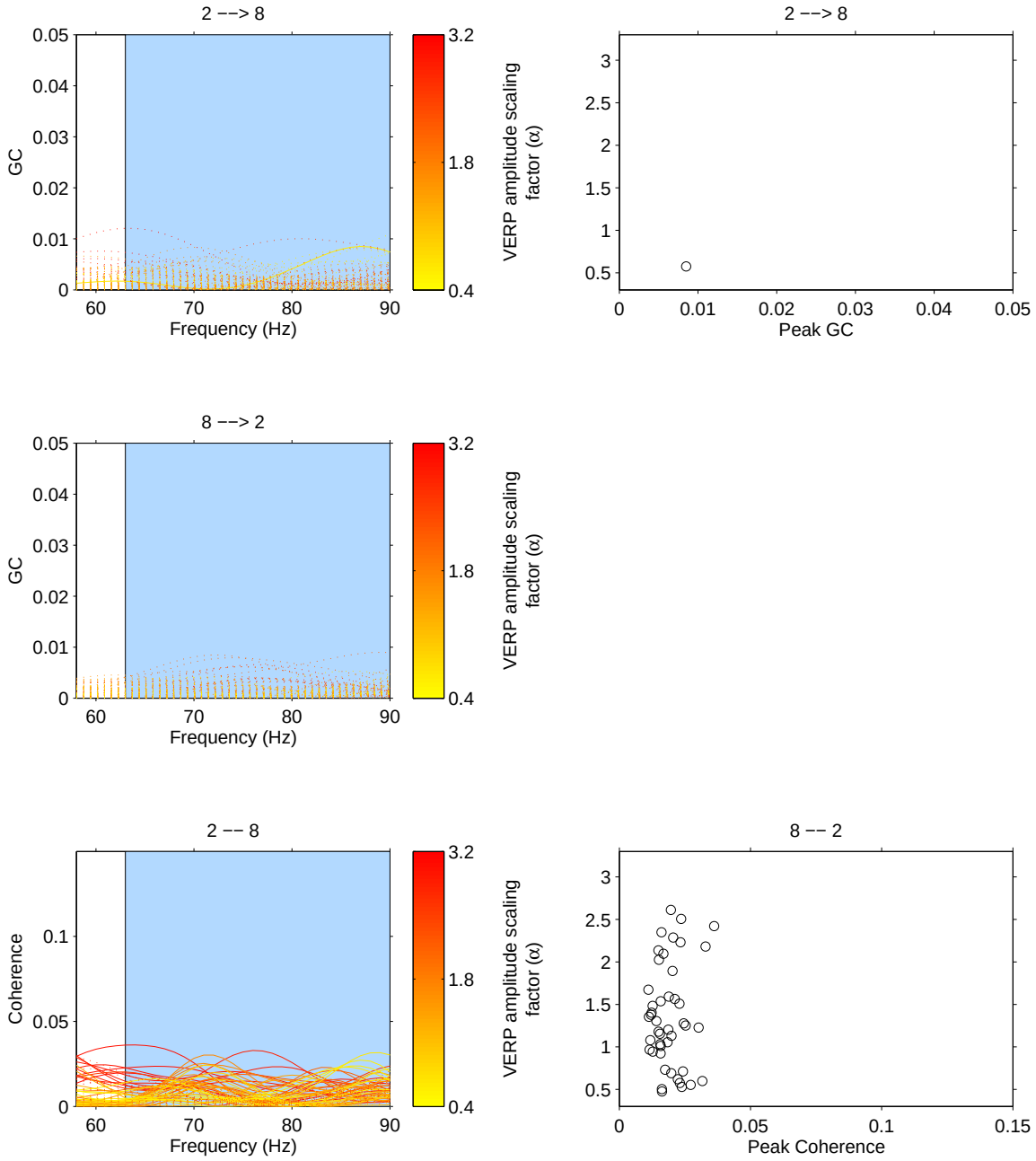

Figure A.50: Subensemble spectra for top-down and bottom-up Granger causality and coherence (left panels) and the correlations between significant high gamma-range Granger causality and coherence spectral peaks with subensemble mean striate VERP amplitude (right panels) for pair TI 2-8. Significant correlations are fit with a regression line. Spectra with significant peaks are drawn in solid lines. Spectra without significant peaks are drawn with dotted lines.

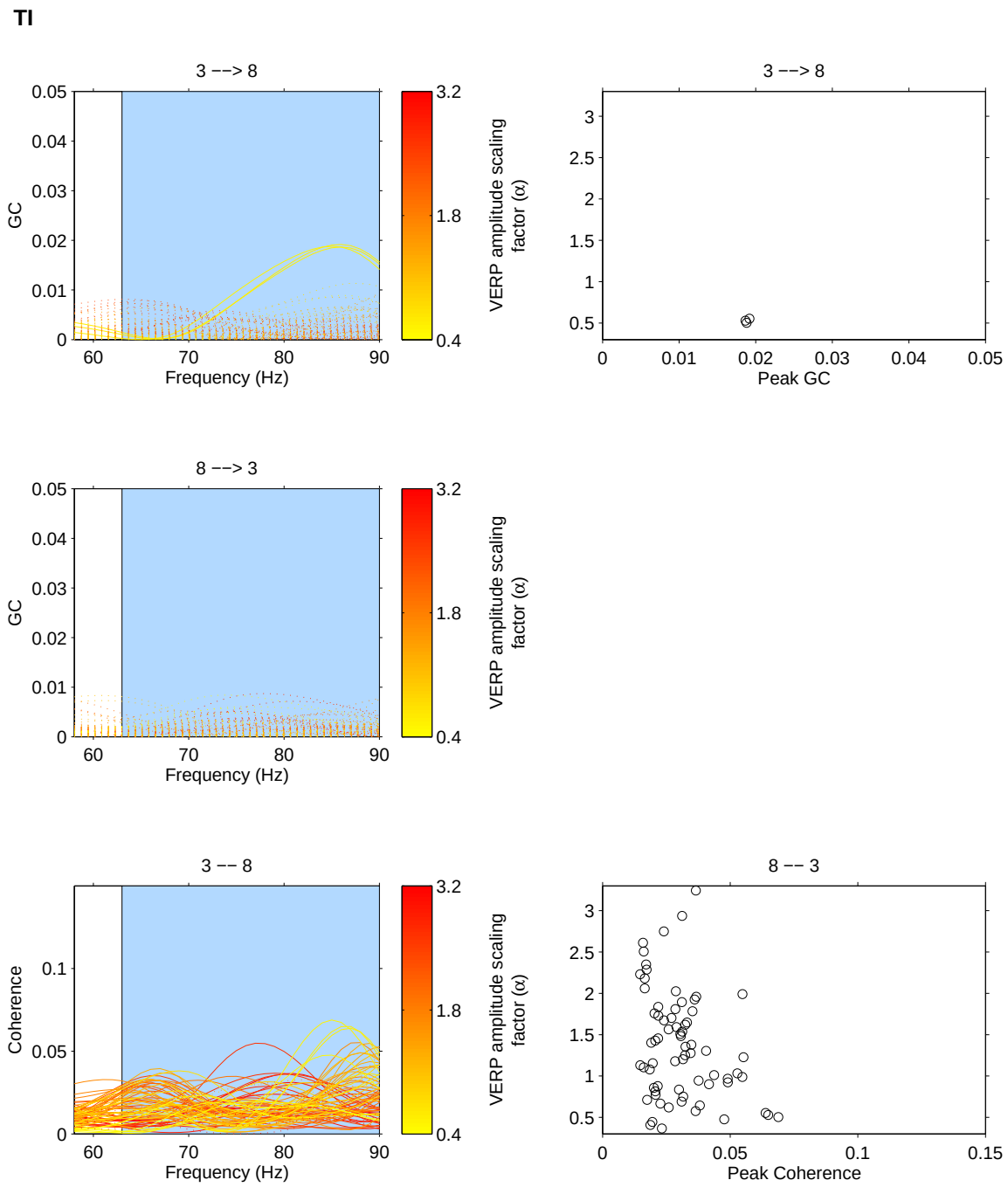

Figure A.51: Subensemble spectra for top-down and bottom-up Granger causality and coherence (left panels) and the correlations between significant high gamma-range Granger causality and coherence spectral peaks with subensemble mean striate VERP amplitude (right panels) for pair TI 3-8. Significant correlations are fit with a regression line. Spectra with significant peaks are drawn in solid lines. Spectra without significant peaks are drawn with dotted lines.

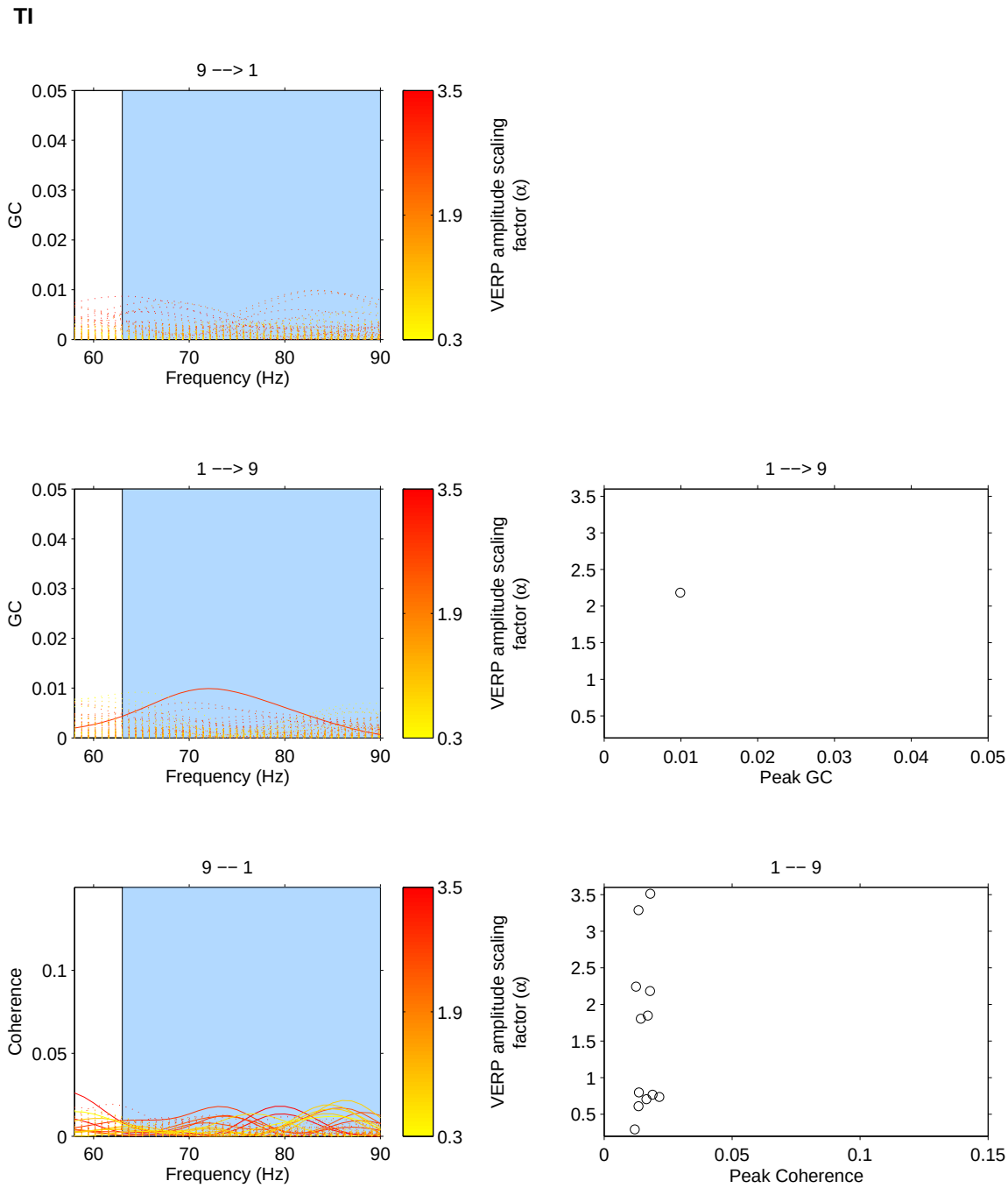

Figure A.52: Subensemble spectra for top-down and bottom-up Granger causality and coherence (left panels) and the correlations between significant high gamma-range Granger causality and coherence spectral peaks with subensemble mean striate VERP amplitude (right panels) for pair TI 9-1. Significant correlations are fit with a regression line. Spectra with significant peaks are drawn in solid lines. Spectra without significant peaks are drawn with dotted lines.

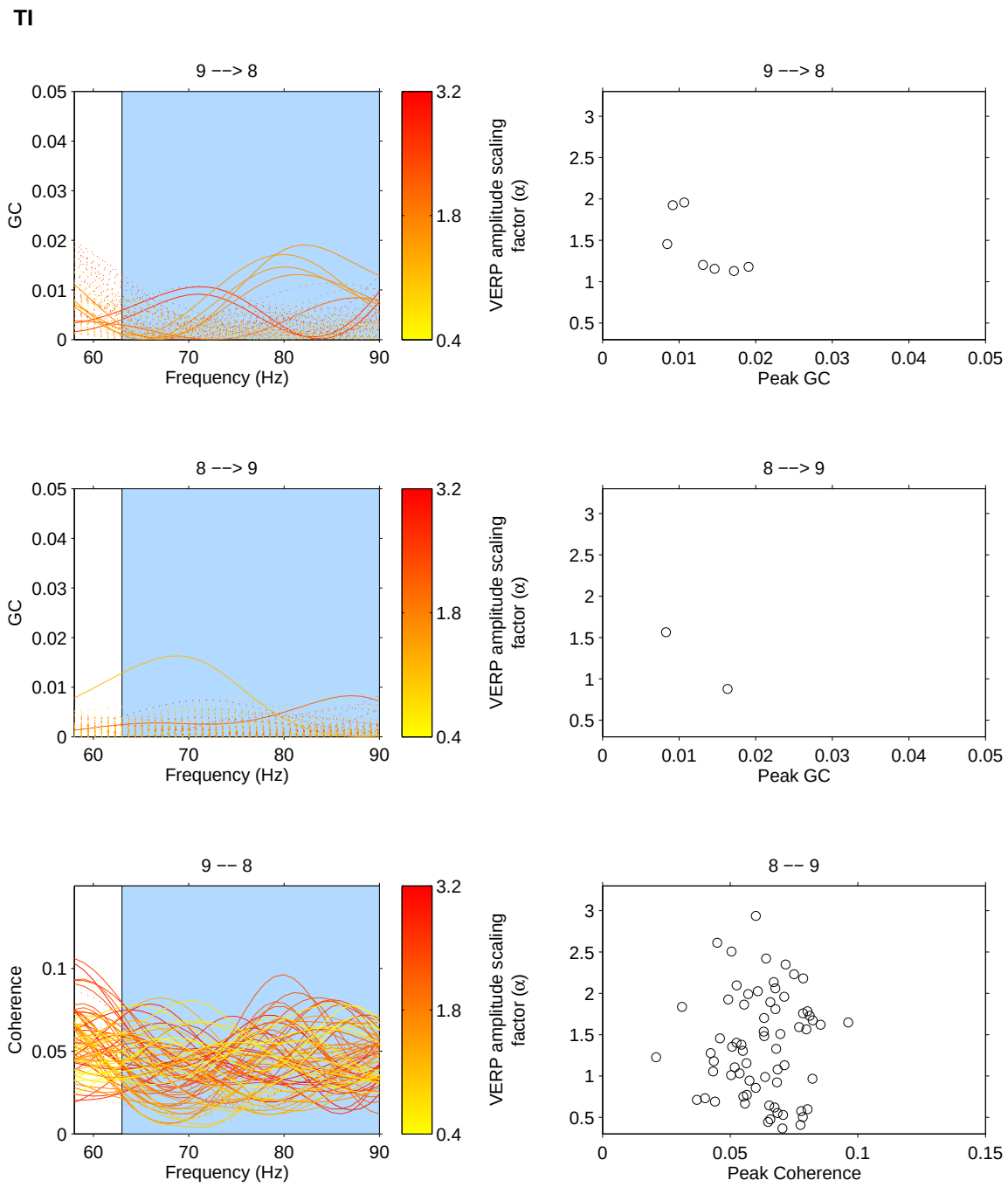

Figure A.53: Subensemble spectra for top-down and bottom-up Granger causality and coherence (left panels) and the correlations between significant high gamma-range Granger causality and coherence spectral peaks with subensemble mean striate VERP amplitude (right panels) for pair TI 9-8. Significant correlations are fit with a regression line. Spectra with significant peaks are drawn in solid lines. Spectra without significant peaks are drawn with dotted lines.

APPENDIX B

NON-SIGNIFICANT SUBSENSEMBLE COHERENCE AND GRANGER CAUSALITY VERSUS MEAN ONSET TIME CORRELATION RESULTS

GE

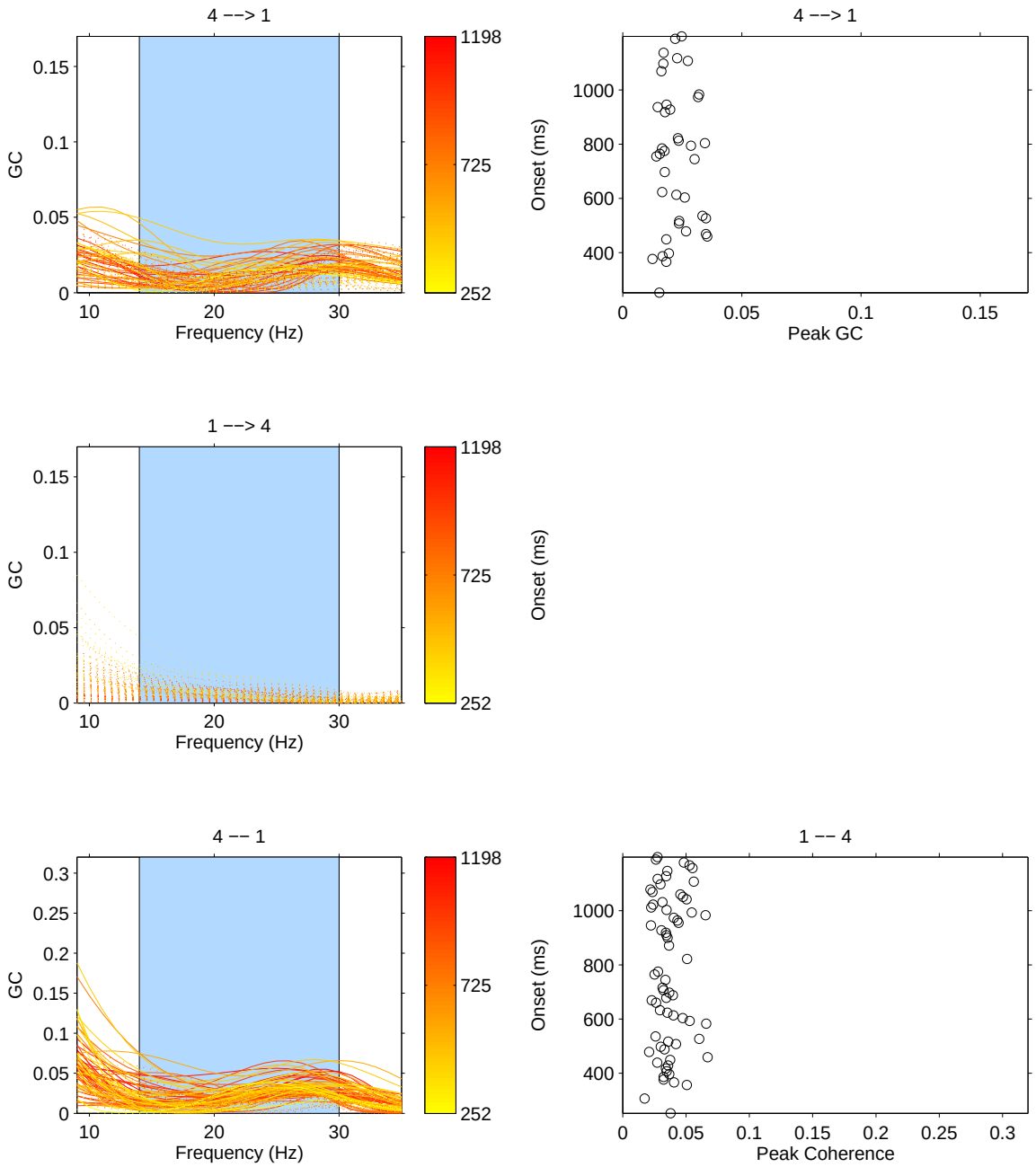

Figure B.1: Subensemble spectra for top-down and bottom-up Granger causality and coherence (left panels) and the correlations between significant beta range Granger causality and coherence spectral peaks with subensemble mean onset time (right panels) for pair GE 4-1. Significant correlations are fit with a regression line. Spectra with significant peaks are drawn in solid lines. Spectra without significant peaks are drawn with dotted lines.

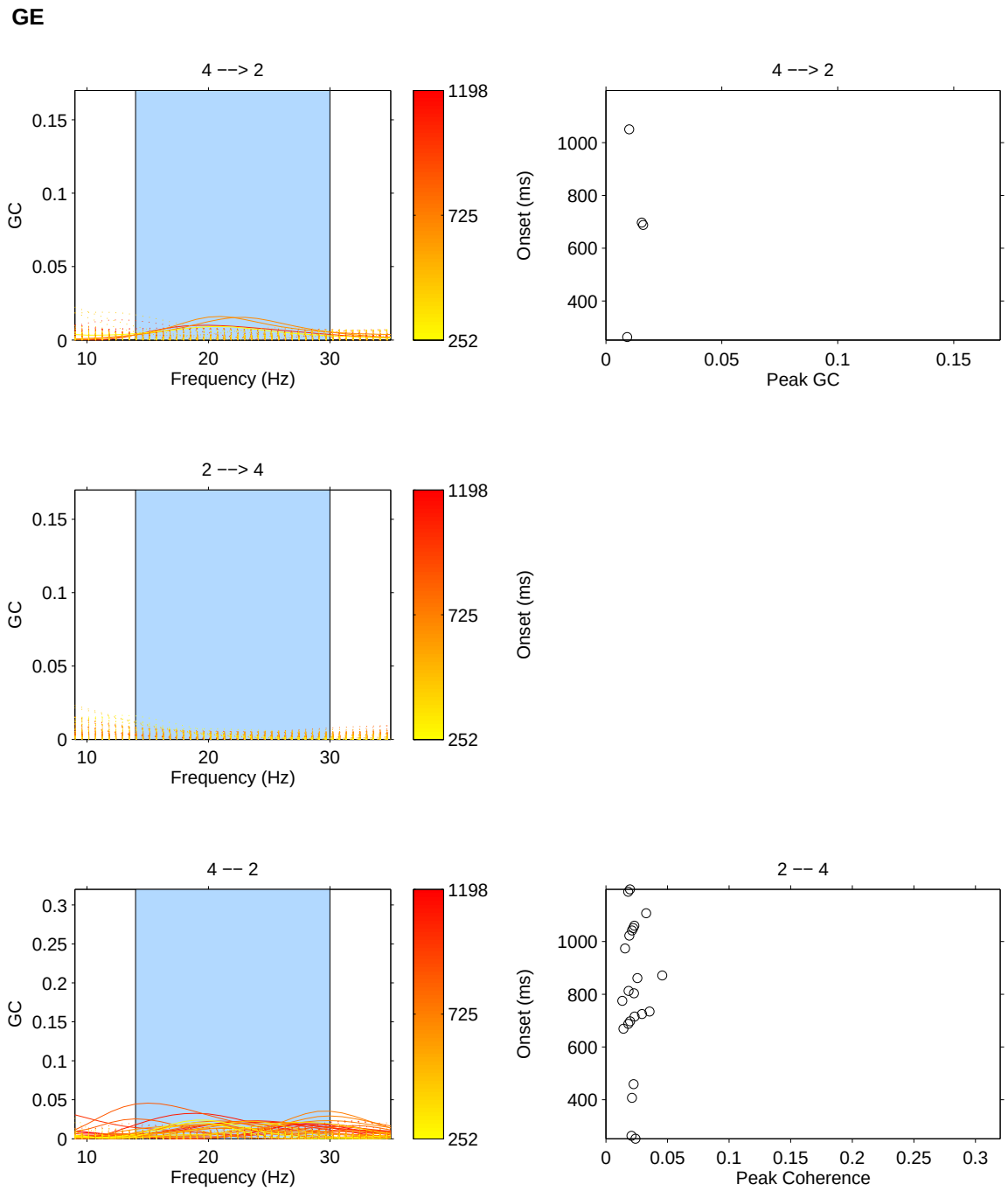

Figure B.2: Subensemble spectra for top-down and bottom-up Granger causality and coherence (left panels) and the correlations between significant beta range Granger causality and coherence spectral peaks with subensemble mean onset time (right panels) for pair GE 4-2. Significant correlations are fit with a regression line. Spectra with significant peaks are drawn in solid lines. Spectra without significant peaks are drawn with dotted lines.

GE

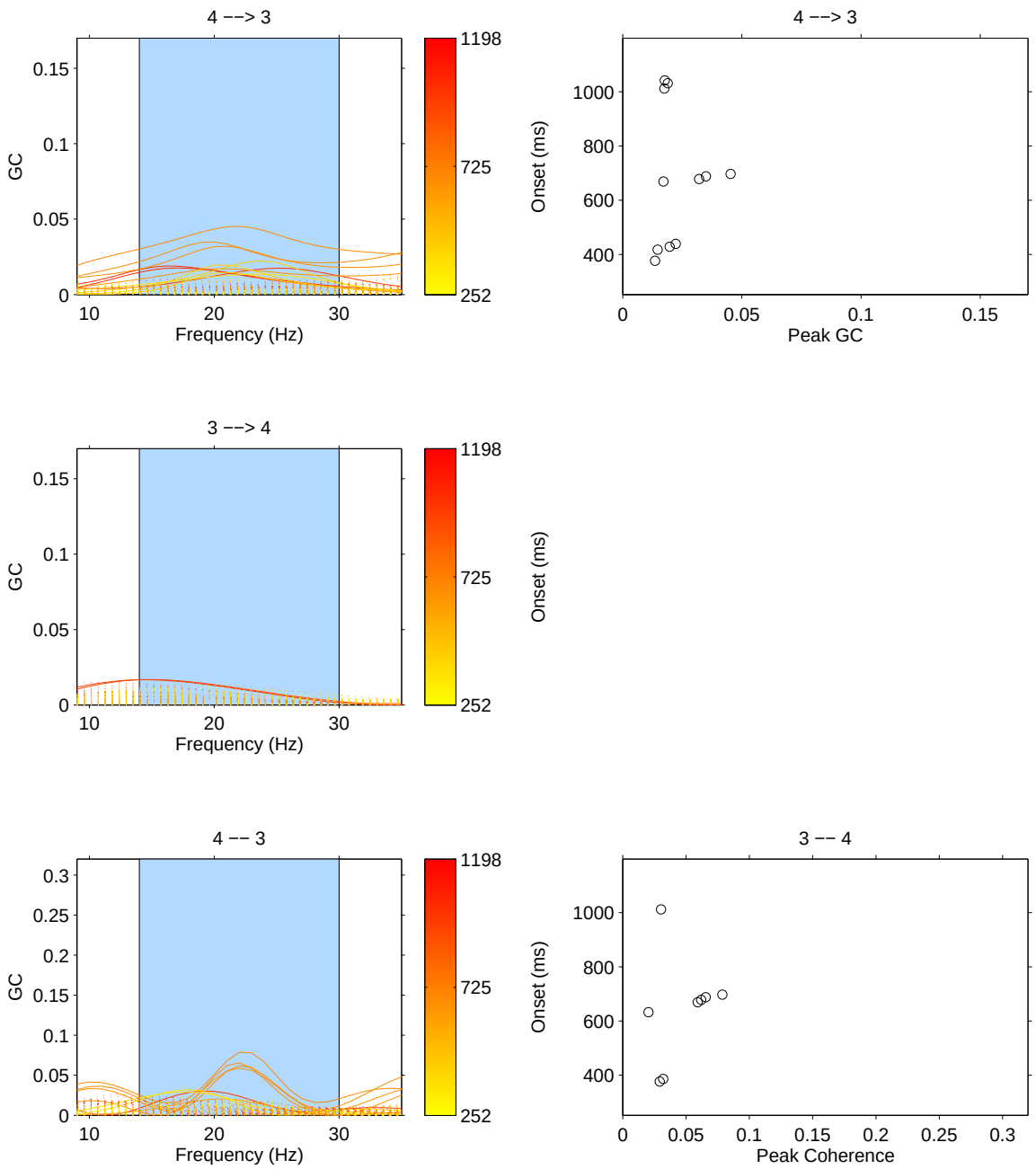

Figure B.3: Subensemble spectra for top-down and bottom-up Granger causality and coherence (left panels) and the correlations between significant beta range Granger causality and coherence spectral peaks with subensemble mean onset time (right panels) for pair GE 4-3. Significant correlations are fit with a regression line. Spectra with significant peaks are drawn in solid lines. Spectra without significant peaks are drawn with dotted lines.

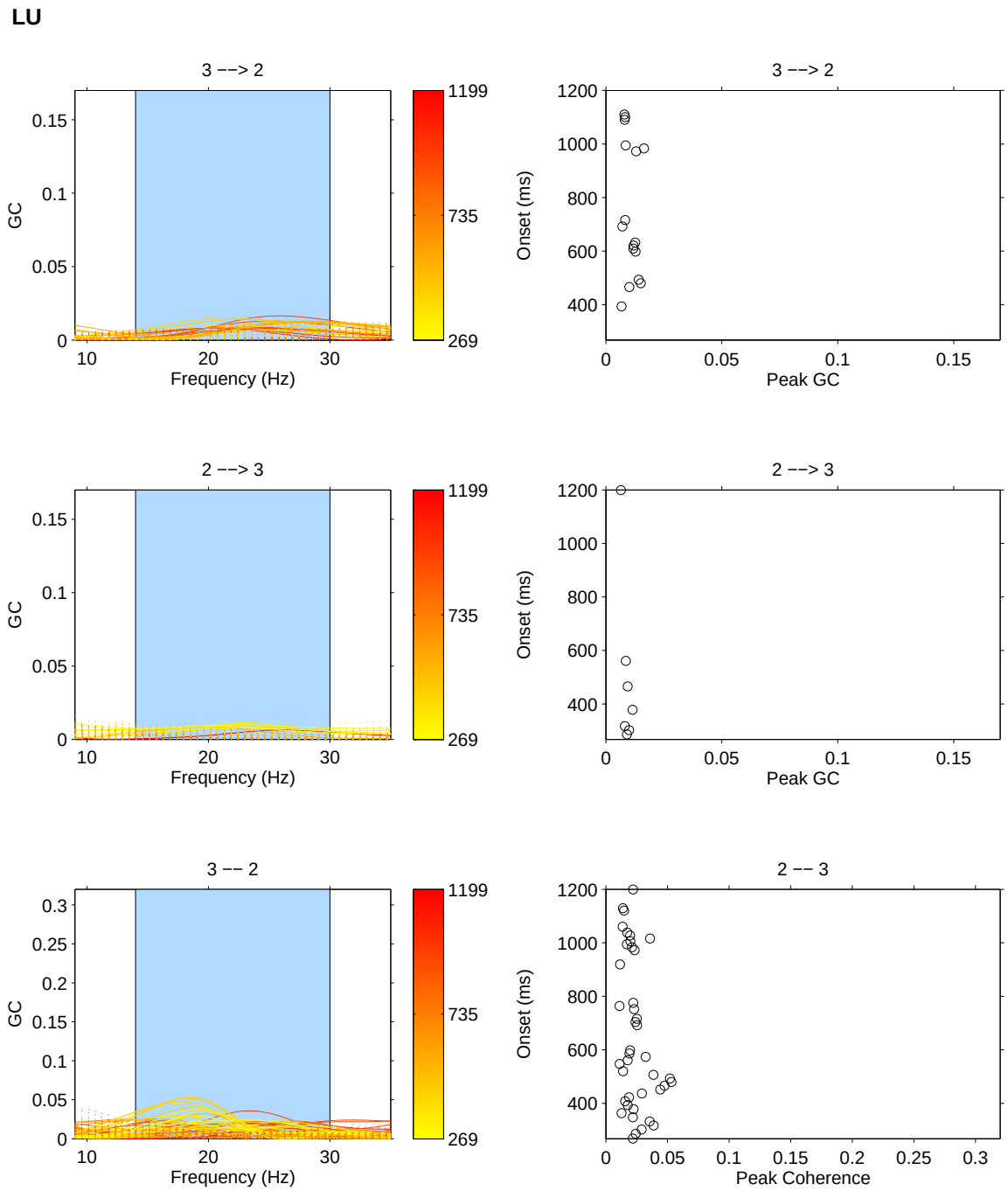

Figure B.4: Subensemble spectra for top-down and bottom-up Granger causality and coherence (left panels) and the correlations between significant beta range Granger causality and coherence spectral peaks with subensemble mean onset time (right panels) for pair LU 3-2. Significant correlations are fit with a regression line. Spectra with significant peaks are drawn in solid lines. Spectra without significant peaks are drawn with dotted lines.

TI

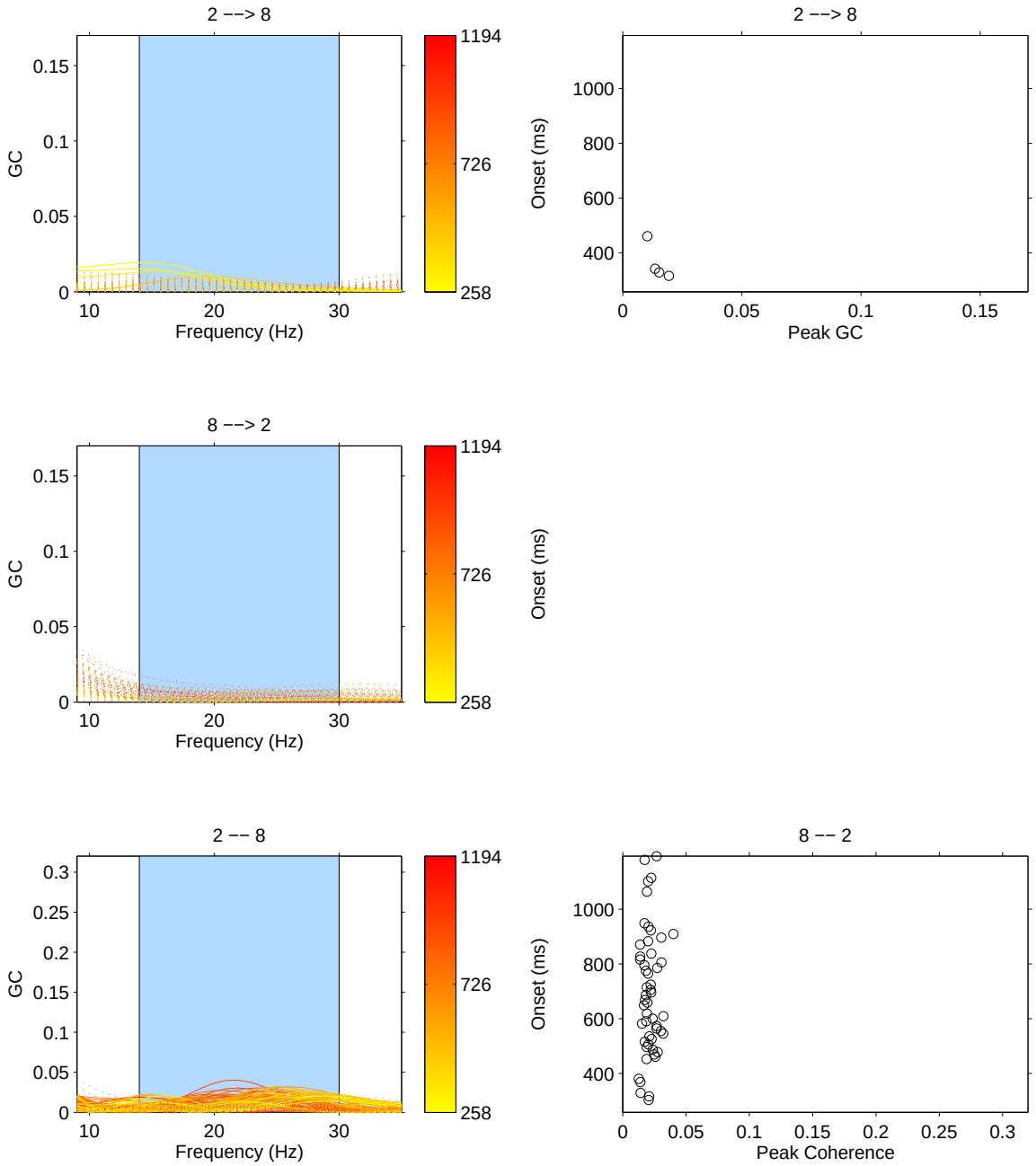

Figure B.5: Subensemble spectra for top-down and bottom-up Granger causality and coherence (left panels) and the correlations between significant beta range Granger causality and coherence spectral peaks with subensemble mean onset time (right panels) for pair TI 2-8. Significant correlations are fit with a regression line. Spectra with significant peaks are drawn in solid lines. Spectra without significant peaks are drawn with dotted lines.

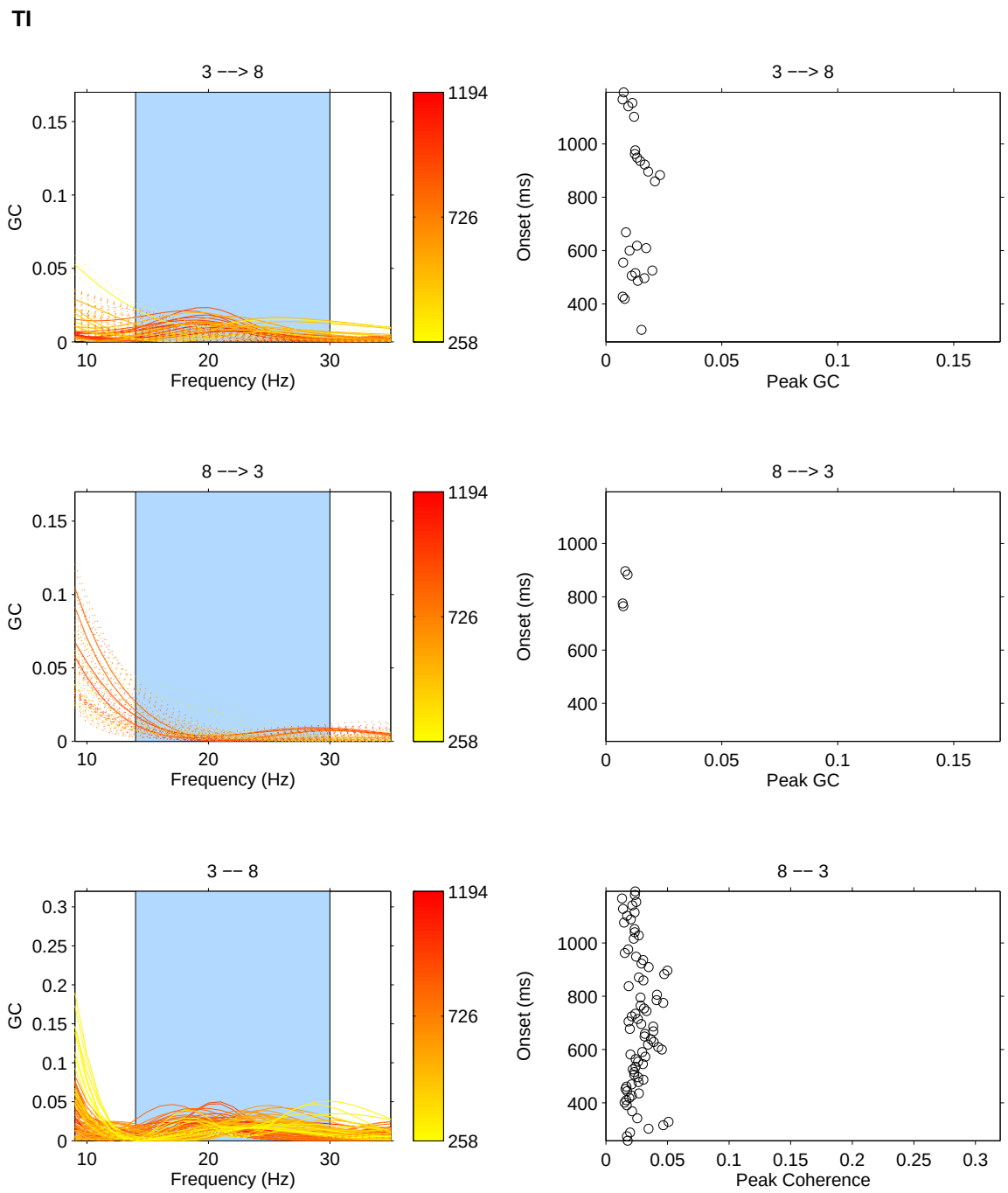

Figure B.6: Subensemble spectra for top-down and bottom-up Granger causality and coherence (left panels) and the correlations between significant beta range Granger causality and coherence spectral peaks with subensemble mean onset time (right panels) for pair TI 3-8. Significant correlations are fit with a regression line. Spectra with significant peaks are drawn in solid lines. Spectra without significant peaks are drawn with dotted lines.

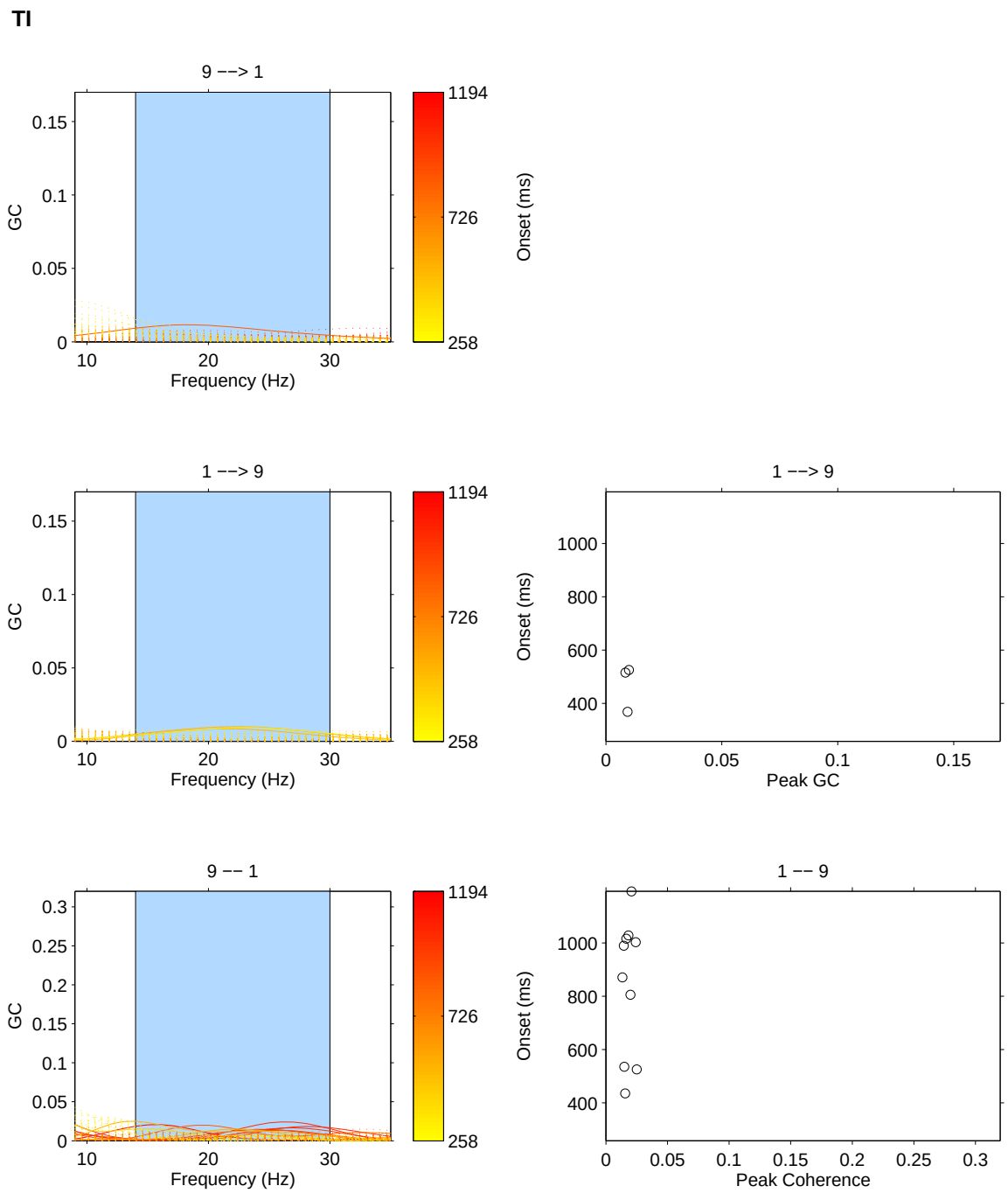

Figure B.7: Subensemble spectra for top-down and bottom-up Granger causality and coherence (left panels) and the correlations between significant beta range Granger causality and coherence spectral peaks with subensemble mean onset time (right panels) for pair TI 9-1. Significant correlations are fit with a regression line. Spectra with significant peaks are drawn in solid lines. Spectra without significant peaks are drawn with dotted lines.

BIBLIOGRAPHY

Alegre M, Gurtubay IG, Labarga A, Iriarte J, Valencia M, Artieda J (2004) Frontal and central oscillatory changes related to different aspects of the motor process: a study in go/no-go paradigms. *Experimental brain research Experimentelle Hirnforschung Expérimentation cérébrale* 159:14–22.

Arieli A, Shoham D, Hildesheim R, Grinvald A (1995) Coherent spatiotemporal patterns of ongoing activity revealed by real-time optical imaging coupled with single-unit recording in the cat visual cortex. *J Neurophysiol* 73:2072–2093.

Arieli A, Sterkin A, Grinvald A, Aertsen A (1996) Dynamics of ongoing activity: explanation of the large variability in evoked cortical responses. *Science* 273:1868–1871.

Azouz R, Gray CM (2000) Dynamic spike threshold reveals a mechanism for synaptic coincidence detection in cortical neurons in vivo. *Proc Natl Acad Sci USA* 97:8110–5.

Azouz R, Gray CM (2003) Adaptive coincidence detection and dynamic gain control in visual cortical neurons in vivo. *Neuron* 37:513–23.

Badre D, D'Esposito M (2009) Is the rostro-caudal axis of the frontal lobe hierarchical? *Nat Rev Neurosci* .

Baker SN, Kilner JM, Pinches EM, Lemon RN (1999) The role of synchrony and oscillations in the motor output. *Experimental brain research Experimentelle Hirnforschung Expérimentation cérébrale* 128:109–17.

Barbas H, Rempel-Clower N (1997) Cortical structure predicts the pattern of cortico-cortical connections. *Cereb Cortex* 7:635–46.

Bekisz M, Wróbel A (2003) Attention-dependent coupling between beta activities recorded in the cat's thalamic and cortical representations of the central visual field. *European Journal of Neuroscience* 17:421–426.

Bernasconi C, von Stein A, Chiang C, König P (2000) Bi-directional interactions between visual areas in the awake behaving cat. *Neuroreport* 11:689–692.

Bressler SL (1995) Large-scale cortical networks and cognition. *Brain Res Brain Res Rev* 20:288–304.

Bressler SL (1996) Interareal synchronization in the visual cortex. *Behav Brain Res* 76:37–49.

Bressler SL (2002) Understanding cognition through large-scale cortical networks. *Current Directions in Psychological Science* .

Bressler SL (2008) Neurocognitive networks. *Scholarpedia* 3(2):1576.

Bressler SL, Coppola R, Nakamura R (1993) Episodic multiregional cortical coherence at multiple frequencies during visual task performance. *Nature* 366:153–156.

Bressler SL, Ding M, Yang W (1999) Investigation of cooperative cortical dynamics by multivariate autoregressive modeling of event-related local field potentials. *Neuro Computing* 26-27:625–631.

Bressler SL, Kelso JAS (2001) Cortical coordination dynamics and cognition. *Trends Cogn Sci (Regul Ed)* 5:26–36.

Bressler SL, Richter CG (2009) Large-scale cortical network coordination: a proposal for the substrate of expectancy. *New Mathematics and Natural Computation* 5:47–59.

Bressler SL (2004) Inferential constraint sets in the organization of visual expectation. *Neuroinformatics* 2:227–238.

Bressler SL (2007) The formation of global neurocognitive state In Perlovsky L, Kozma R, editors, *Neurodynamics of higher-level cognition and consciousness*. Springer, Berlin ;;New York.

Bressler SL, McIntosh AR (2007) The role of neural context in Large-Scale neurocognitive network operations In Jirsa VK, McIntosh AR, editors, *Handbook of Brain Connectivity*, Understanding Complex Systems. Springer, Berlin / Heidelberg.

Bressler SL, Nakamura R (1993) Interarea synchronization in macaque neocortex during a visual pattern discrimination task In Eeckman FH, Bower JM, editors, *Computation and neural systems*, pp. 515–522. Kluwer Academic Publishers, Boston.

Bressler SL, Richter CG, Chen Y, Ding M (2007) Cortical functional network organization from autoregressive modeling of local field potential oscillations. *Stat Med* 26:3875–3885.

Bressler SL, Tognoli E (2006) Operational principles of neurocognitive networks. *Int J Psychophysiol* 60:139–148.

Broca P (1861) Remarques sur le siege de la faculté du langage articulé, suivies d'une observation d'aphemie . . . . *Bulletin de la Société Anatomique* .

Brodmann K (1909) *Vergleichende Lokalisationslehre der Grosshirnrinde in ihren Prinzipien dargestellt auf Grund des Zellenbaues* JA Barth, Leipzig.

Bronte-Stewart H, Barberini C, Koop MM, Hill BC, Henderson JM, Wingeier B (2009) The stn beta-band profile in parkinson's disease is stationary and shows prolonged attenuation after deep brain stimulation. *Exp Neurol* 215:20–8.

Brovelli A, Battaglini PP, Naranjo JR, Budai R (2002) Medium-range oscillatory network and the 20-hz sensorimotor induced potential. *Neuroimage* 16:130–41.

Brovelli A, Ding M, Ledberg A, Chen Y, Nakamura R, Bressler SL (2004) Beta oscillations in a large-scale sensorimotor cortical network: directional influences revealed by granger causality. *Proc Natl Acad Sci U S A* 101:9849–9854.

Brown P, Oliviero A, Mazzone P, Insola A, Tonali P, Lazzaro VD (2001) Dopamine dependency of oscillations between subthalamic nucleus and pallidum in parkinson's disease. *J Neurosci* 21:1033–8.

Budd JM (1998) Extrastriate feedback to primary visual cortex in primates: a quantitative analysis of connectivity. *Proc Biol Sci* 265:1037–44.

Buia CI, Tiesinga PH (2008) Role of interneuron diversity in the cortical microcircuit for attention. *J Neurophysiol* 99:2158–82.

Capotosto P, Babiloni C, Romani GL, Corbetta M (2009) Frontoparietal cortex controls spatial attention through modulation of anticipatory alpha rhythms. *J Neurosci* 29:5863–72.

Cenier T, David F, Litaudon P, Garcia S, Amat C, Buonviso N (2009) Respiration-gated formation of gamma and beta neural assemblies in the mammalian olfactory bulb. *Eur J Neurosci* 29:921–30.

Cheron G, Cebolla AM, Saedeleer CD, Bengoetxea A, Leurs F, Leroy A, Dan B (2007) Pure phase-locking of beta/gamma oscillation contributes to the n30 frontal component of somatosensory evoked potentials. *BMC neuroscience* 8:75.

Chrobak JJ, Buzsáki G (1996) High-frequency oscillations in the output networks of the hippocampal-entorhinal axis of the freely behaving rat. *J Neurosci* 16:3056–66.

Classen J, Gerloff C, Honda M, Hallett M (1998) Integrative visuomotor behavior is associated with interregionally coherent oscillations in the human brain. *J Neurophysiol* 79:1567–73.

Corbetta M, Patel G, Shulman GL (2008) The reorienting system of the human brain: from environment to theory of mind. *Neuron* 58:306–24.

Corbetta M, Shulman GL (2002) Control of goal-directed and stimulus-driven attention in the brain. *Nat Rev Neurosci* 3:201–215.

Courtemanche R, Fujii N, Graybiel AM (2003) Synchronous, focally modulated beta-band oscillations characterize local field potential activity in the striatum of awake behaving monkeys. *J Neurosci* 23:11741–52.

Deco G, Rolls ET (2005) Attention, short-term memory, and action selection: a unifying theory. *Prog Neurobiol* 76:236–56.

Dennett D (1971) Intentional systems. *The Journal of Philosophy* .

Desimone R, Duncan J (1995) Neural mechanisms of selective visual attention. *Annu Rev Neurosci* 18:193–222.

Dewey J (1896) The reflex arc concept in psychology. *Psychological Review* 3:357–370.

Ding M, Bressler SL, Yang W, Liang H (2000) Short-window spectral analysis of cortical event-related potentials by adaptive multivariate autoregressive modeling: data preprocessing, model validation, and variability assessment. *Biol Cybern* 83:35–45.

Ding M, Chen Y, Bressler SL (2006) Granger causality: Basic theory and application to neuroscience In Bjrn Schelter MW JT, editor, *Handbook of Time Series Analysis*, pp. 438–460. Wiley.

Dunn O (1961) Multiple comparisons among means. *Journal of the American Statistical Association* 56:52–64.

Düzel E, Habib R, Schott B, Schoenfeld A, Lobaugh N, McIntosh AR, Scholz M, Heinze HJ (2003) A multivariate, spatiotemporal analysis of electromagnetic time-frequency data of recognition memory. *Neuroimage* 18:185–97.

Düzel E, Richardson-Klavehn A, Neufang M, Schott BH, Scholz M, Heinze HJ (2005) Early, partly anticipatory, neural oscillations during identification set the stage for priming. *Neuroimage* 25:690–700.

Edgington E (1995) *Randomization tests* M. Dekker, New York, 3rd ed., rev. and expanded. edition.

Elul R (1971) The genesis of the eeg. *Int Rev Neurobiol* 15:227–72.

Engel A, Konig P, Kreiter A, Singer W (1991) Interhemispheric synchronization of oscillatory neuronal responses in cat visual cortex. *Science* 252:1177–1179.

Engel AK, Fries P, Singer W (2001) Dynamic predictions: oscillations and synchrony in top-down processing. *Nat Rev Neurosci* 2:704–716.

Engel AK, König P, Singer W (1991) Direct physiological evidence for scene segmentation by temporal coding. *Proc Natl Acad Sci USA* 88:9136–40.

Engel AK, Kreiter AK, König P, Singer W (1991) Synchronization of oscillatory neuronal responses between striate and extrastriate visual cortical areas of the cat. *Proc Natl Acad Sci USA* 88:6048–52.

Engel AK, Roelfsema PR, Fries P, Brecht M, Singer W (1997) Role of the temporal domain for response selection and perceptual binding. *Cereb Cortex* 7:571–82.

Ergenoglu T, Demiralp T, Bayraktaroglu Z, Ergen M, Beydagi H, Uresin Y (2004) Alpha rhythm of the eeg modulates visual detection performance in humans. *Brain Res Cogn Brain Res* 20:376–383.

Farmer S (1998) Rhythmicity, synchronization and binding in human and primate motor systems. *J Physiol (Lond)* .

Felleman DJ, Van Essen DC (1991) Distributed hierarchical processing in the primate cerebral cortex. *Cereb Cortex* 1:1–47.

Fetz EE, Chen D, Murthy VN, Matsumura M (2000) Synaptic interactions mediating synchrony and oscillations in primate sensorimotor cortex. *J Physiol Paris* 94:323–31.

Fingelkurts AA, Fingelkurts AA (2004) Making complexity simpler: multivariability and metastability in the brain. *Int J Neurosci* 114:843–62.

Fontanini A, Bower JM (2006) Slow-waves in the olfactory system: an olfactory perspective on cortical rhythms. *Trends Neurosci* 29:429–37.

Freeman W (1975) *Mass action in the nervous system : examination of the neurophysiological basis of adaptive behavior through the EEG* Academic Press, New York.

Freeman WJ (2003) The wave packet: an action potential for the 21st century. *J Integr Neurosci* 2:3–30.

Fries P, Neuenschwander S, Engel AK, Goebel R, Singer W (2001) Rapid feature selective neuronal synchronization through correlated latency shifting. *Nat Neurosci* 4:194–200.

Fries P (2005) A mechanism for cognitive dynamics: neuronal communication through neuronal coherence. *Trends Cogn Sci* 9:474–480.

Friston K (1994) Functional and effective connectivity in neuroimaging: a synthesis. *Human brain mapping* .

Friston KJ (1997) Transients, metastability, and neuronal dynamics. *Neuroimage* 5:164–71.

Friston K (2002) Functional integration and inference in the brain. *Prog Neurobiol* 68:113–43.

Fuster J (2003) Cortex and mind: Unifying cognition. *books.google.com* .

Fuster J (2006) The cognit: a network model of cortical representation. *International Journal of Psychophysiology* .

Fuster J (2008) *The prefrontal cortex* Academic Press/Elsevier, Amsterdam ;;Boston, 4th ed. edition.

Gaillard R, Dehaene S, Adam C, Clémenceau S, Hasboun D, Baulac M, Cohen L, Naccache L (2009) Converging intracranial markers of conscious access. *PLoS Biol* 7:e61.

Gerstein GL, Perkel DH (1969) Simultaneously recorded trains of action potentials: analysis and functional interpretation. *Science* 164:828–30.

Geschwind N (1970) The organization of language and the brain. *ScienceNew Series* 170:940–944.

Geweke J (1982) Measurement of linear dependence and feedback between multiple time series. *Journal of the American Statistical Association* 77:304–313.

Gilbert CD (1998) Adult cortical dynamics. *Physiol Rev* 78:467–85.

Gilbert CD, Wiesel TN (1989) Columnar specificity of intrinsic horizontal and cortico-cortical connections in cat visual cortex. *J Neurosci* 9:2432–42.

Gilbert CD, Sigman M (2007) Brain states: top-down influences in sensory processing. *Neuron* 54:677–696.

Gómez CM, Marco-Pallarés J, Grau C (2006) Location of brain rhythms and their modulation by preparatory attention estimated by current density. *Brain Res* 1107:151–60.

Gómez CM, Vaquero E, López-Mendoza D, González-Rosa J, Vázquez-Marrufo M (2004) Reduction of eeg power during expectancy periods in humans. *Acta neurobiologiae experimentalis* 64:143–51.

Gonzalez Andino SL, Michel CM, Thut G, Landis T, de Peralta RG (2005) Prediction of response speed by anticipatory high-frequency (gamma band) oscillations in the human brain. *Human brain mapping* 24:50–8.

Granger C (1969) Investigating causal relations by econometric models and cross-spectral methods. *Econometrica: Journal of the Econometric Society* .

Gray CM (1999) The temporal correlation hypothesis of visual feature integration: still alive and well. *Neuron* 24:31–47, 111–25.

Gray CM, König P, Engel AK, Singer W (1989) Oscillatory responses in cat visual cortex exhibit inter-columnar synchronization which reflects global stimulus properties. *Nature* 338:334–7.

Gregoriou GG, Gotts SJ, Zhou H, Desimone R (2009) High-frequency, long-range coupling between prefrontal and visual cortex during attention. *Science* 324:1207–10.

Grinvald A, Arieli A, Tsodyks M, Kenet T (2003) Neuronal assemblies: single cortical neurons are obedient members of a huge orchestra. *Biopolymers* 68:422–36.

Gross J, Schmitz F, Schnitzler I, Kessler K, Shapiro K, Hommel B, Schnitzler A (2004) Modulation of long-range neural synchrony reflects temporal limitations of visual attention in humans. *Proc Natl Acad Sci USA* 101:13050–5.

Haken H (1978) *Synergetics : an introduction : nonequilibrium phase transitions and self-organization in physics, chemistry, and biology* Springer-Verlag, Berlin ;;New York, 2d enl. ed. edition.

Hanslmayr S, Aslan A, Staudigl T, Klimesch W, Herrmann CS, Buml KH (2007) Prestimulus oscillations predict visual perception performance between and within subjects. *Neuroimage* 37:1465–1473.

Hanslmayr S, Klimesch W, Sauseng P, Gruber W, Doppelmayr M, Freunberger R, Pecherstorfer T (2005) Visual discrimination performance is related to decreased alpha amplitude but increased phase locking. *Neurosci Lett* 375:64–68.

Hayek F (1952) *The sensory order : an inquiry into the foundations of theoretical psychology* University of Chicago Press, Chicago Ill.

Hebb DO (1949) *The organization of behavior; a neuropsychological theory* Wiley.

Hergenhahn B (2001) *An introduction to the history of psychology* Wadsworth Thomson Learning, Belmont CA, 4th ed. edition.

Herrnstein R, Boring EG (1965) *A source book in the history of psychology,* Harvard University Press, Cambridge.

Hilgetag CC, O'Neill MA, Young MP (1996) Indeterminate organization of the visual system. *Science* 271:776–777.

Hillyard SA, Anllo-Vento L (1998) Event-related brain potentials in the study of visual selective attention. *Proc Natl Acad Sci USA* 95:781–7.

Hillyard SA, Vogel EK, Luck SJ (1998) Sensory gain control (amplification) as a mechanism of selective attention: electrophysiological and neuroimaging evidence. *Philos Trans R Soc Lond B Biol Sci* 353:1257–1270.

Hupé JM, James AC, Payne BR, Lomber SG, Girard P, Bullier J (1998) Cortical feedback improves discrimination between figure and background by v1, v2 and v3 neurons. *Nature* 394:784–7.

Ingvar DH (1985) Memory of the future: an essay on the temporal organization of conscious awareness. *Human neurobiology* 4:127–36.

Jahnke J (1997) Physiognomy, phrenology, and non-verbal communication In Bringmann WG, Luck HE, MIller R, Early CE, editors, *A pictorial history of psychology*. Quintessence Pub., Chicago.

James W (1950) *The principles of psychology.* Dover Publications, [New York], authorized ed., unabridged. edition.

Jensen O, Goel P, Kopell N, Pohja M, Hari R, Ermentrout B (2005) On the human sensorimotor-cortex beta rhythm: sources and modeling. *Neuroimage* 26:347–55.

Jung J, Hudry J, Ryvlin P, Royet JP, Bertrand O, Lachaux JP (2006) Functional significance of olfactory-induced oscillations in the human amygdala. *Cereb Cortex* 16:1–8.

Kaminski M, Ding M, Truccolo WA, Bressler SL (2001) Evaluating causal relations in neural systems: granger causality, directed transfer function and statistical assessment of significance. *Biol Cybern* 85:145–157.

Kayser C, Logothetis NK (2009) Directed interactions between auditory and superior temporal cortices and their role in sensory integration. *Frontiers in integrative neuroscience* 3:7.

Kelso J, Engstrøm DA (2008) *The complementary nature* MIT, Cambridge Mass.

Kelso JAS (1991) Behavioral and neural pattern generation: the concept of neurobehavioral dynamical systems In Koepchen HP, editor, *CardioRespiratory and Motor Coordination*. Springer-Verlag: Berlin.

Kelso JAS (1995) *Dynamic patterns : the self-organization of brain and behavior* MIT Press, Cambridge Mass., 1st MIT press paperback ed. edition.

Kelso JS, Tuller B, Bateson E, Fowler C (1984) Functionally specific articulatory cooperation following jaw perturbations during speech: Evidence for coordinative structures. *Journal of Experimental Psychology: Human Perception and Performance* 10:812–832.

Klimesch W, Sauseng P, Hanslmayr S, Gruber W, Freunberger R (2007) Event-related phase reorganization may explain evoked neural dynamics. *Neurosci Biobehav Rev* 31:1003–1016.

Koffka K (1935) *Principles of gestalt psychology* Harcourt, New York.

Köhler W (1970) *Gestalt psychology : an introduction to new concepts in modern psychology* Liveright, New York.

Kolb B, Wishaw IQ (1996) *Fundamentals of human neuropsychology* W.H. Freeman, New York N.Y., 4th ed. edition.

König P, Engel AK (1995) Correlated firing in sensory-motor systems. *Curr Opin Neurobiol* 5:511–9.

König P, Engel AK, Singer W (1996) Integrator or coincidence detector? the role of the cortical neuron revisited. *Trends Neurosci* 19:130–7.

Kopell N, Ermentrout GB, Whittington MA, Traub RD (2000) Gamma rhythms and beta rhythms have different synchronization properties. *Proc Natl Acad Sci USA* 97:1867–72.

Kranczioch C, Debener S, Maye A, Engel AK (2007) Temporal dynamics of access to consciousness in the attentional blink. *Neuroimage* 37:947–55.

Lamme VA (1995) The neurophysiology of figure-ground segregation in primary visual cortex. *J Neurosci* 15:1605–15.

Lamme VA, Supèr H, Spekreijse H (1998) Feedforward, horizontal, and feedback processing in the visual cortex. *Curr Opin Neurobiol* 8:529–35.

Larkum ME, Zhu JJ, Sakmann B (1999) A new cellular mechanism for coupling inputs arriving at different cortical layers. *Nature* 398:338–41.

Lashley K (1950) In search of the engram. . *Symposia of the Society for Experimental Biology* 4:454–482.

Ledberg A, Bressler SL, Ding M, Coppola R, Nakamura R (2007) Large-scale visuomotor integration in the cerebral cortex. *Cereb Cortex* 17:44–62.

Lee PL, Wu YT, Chen LF, Chen YS, Cheng CM, Yeh TC, Ho LT, Chang MS, Hsieh JC (2003) Ica-based spatiotemporal approach for single-trial analysis of postmovement meg beta synchronization. *Neuroimage* 20:2010–30.

Lee TS, Mumford D (2003) Hierarchical bayesian inference in the visual cortex. *Journal of the Optical Society of America A, Optics, image science, and vision* 20:1434–48.

Leopold DA, Logothetis NK (2003) Spatial patterns of spontaneous local field activity in the monkey visual cortex. *Reviews in the neurosciences* 14:195–205.

Li W, Piëch V, Gilbert CD (2004) Perceptual learning and top-down influences in primary visual cortex. *Nat Neurosci* 7:651–7.

Liang H, Bressler SL, Ding M, Truccolo WA, Nakamura R (2002) Synchronized activity in prefrontal cortex during anticipation of visuomotor processing. *Neuroreport* 13:2011–5.

Luck SJ, Chelazzi L, Hillyard SA, Desimone R (1997) Neural mechanisms of spatial selective attention in areas v1, v2, and v4 of macaque visual cortex. *J Neurophysiol* 77:24–42.

Luria AR (1973) *The working brain an introduction to neuropsychology* Basic Books, New York.

Luria AR (1980) *Higher cortical functions in man* Basic Books ;Consultants Bureau, New York, 2d ed., rev. and expanded. edition.

Makeig S, Westerfield M, Jung TP, Enghoff S, Townsend J, Courchesne E, Sejnowski TJ (2002) Dynamic brain sources of visual evoked responses. *Science* 295:690–4.

Mallet N, Pogosyan A, Márton LF, Bolam JP, Brown P, Magill PJ (2008) Parkinsonian beta oscillations in the external globus pallidus and their relationship with subthalamic nucleus activity. *J Neurosci* 28:14245–58.

Martìnez A, Anllo-Vento L, Sereno MI, Frank LR, Buxton RB, Dubowitz DJ, Wong EC, Hinrichs H, Heinze HJ, Hillyard SA (1999) Involvement of striate and extrastriate visual cortical areas in spatial attention. *Nat Neurosci* 2:364–369.

McIntosh AR (2000) Towards a network theory of cognition. *Neural networks : the official journal of the International Neural Network Society* 13:861–70.

Melloni L, Molina C, Pena M, Torres D, Singer W, Rodriguez E (2007) Synchronization of neural activity across cortical areas correlates with conscious perception. *J Neurosci* 27:2858–2865.

Melloni L, Schwiedrzik CM, Rodriguez E, Singer W (2009a) (micro)saccades, corollary activity and cortical oscillations. *Trends Cogn Sci (Regul Ed)* 13:239–45.

Melloni L, Schwiedrzik CM, Wibral M, Rodriguez E, Singer W (2009b) Response to: Yuval-greenberg et al., ”transient induced gamma-band response in eeg as a manifestation of miniature saccades.” neuron 58, 429-441. *Neuron* 62:8–10; author reply 10–12.

Mesulam MM (1990) Large-scale neurocognitive networks and distributed processing for attention, language, and memory. *Ann Neurol* 28:597–613.

Mesulam MM (1998) From sensation to cognition. *Brain* 121 (Pt 6):1013–1052.

Milner PM (1974) A model for visual shape recognition. *Psychological review* 81:521–35.

Mitra PP, Pesaran B (1999) Analysis of dynamic brain imaging data. *Biophys J* 76:691–708.

Motter BC (1993) Focal attention produces spatially selective processing in visual cortical areas v1, v2, and v4 in the presence of competing stimuli. *J Neurophysiol* 70:909–919.

Mountcastle VB (1957) Modality and topographic properties of single neurons of cat’s somatic sensory cortex. *J Neurophysiol* 20:408–34.

Mountcastle VB (1997) The columnar organization of the neocortex. *Brain* 120 (Pt 4):701–22.

Mountcastle V (1998) *Perceptual neuroscience : the cerebral cortex* Harvard University Press, Cambridge Mass.

Mountcastle VB (2003) Introduction. computation in cortical columns. *Cereb Cortex* 13:2–4.

Mumford D (1992) On the computational architecture of the neocortex. ii. the role of cortico-cortical loops. *Biological cybernetics* 66:241–51.

Murray SO (2008) The effects of spatial attention in early human visual cortex are stimulus independent. *J Vis* 8:2.1–211.

Niebur E, Hsiao SS, Johnson KO (2002) Synchrony: a neuronal mechanism for attentional selection? *Curr Opin Neurobiol* 12:190–4.

Niedermeyer E (1999) The normal eeg of the waking adult In Niedermeyer E LdSF, editor, *Electroencephalography: Basic Principles, Clinical Applications and Related Fields*, pp. 149–173. Lippincott Williams & Wilkins, Baltimore.

Nikolaev AR, Ivanitsky GA, Ivanitsky AM, Posner MI, Abdullaev YG (2001) Correlation of brain rhythms between frontal and left temporal (wernicke's) cortical areas during verbal thinking. *Neurosci Lett* 298:107–10.

Noë A (2004) *Action in perception* MIT Press, Cambridge Mass.

Nowak LG, Bullier J (1997) The timing of information transfer in the visual system In Rockland KS, Kass JH, Peters A, editors, *Cerebral Cortex: Extrastriate Cortex*, Vol. 12. Plenum Press, New York.

Nunez PL (2000) Toward a quantitative description of large-scale neocortical dynamic function and eeg. *The Behavioral and brain sciences* 23:371–98; discussion 399–437.

Ojemann GA (1991) Cortical organization of language. *J Neurosci* 11:2281–7.

Ozgören M, Başar-Eroğlu C, Başar E (2005) Beta oscillations in face recognition. *International journal of psychophysiology : official journal of the International Organization of Psychophysiology* 55:51–9.

Passingham RE, Stephan KE, Kötter R (2002) The anatomical basis of functional localization in the cortex. *Nat Rev Neurosci* 3:606–16.

Pfurtscheller G, Lopes da Silva FH (1999) Event-related eeg/meg synchronization and desynchronization: basic principles. *Clin Neurophysiol* 110:1842–57.

Ploner M, Gross J, Timmermann L, Pollok B, Schnitzler A (2006) Oscillatory activity reflects the excitability of the human somatosensory system. *Neuroimage* 32:1231–6.

Powell TP, Mountcastle VB (1959) Some aspects of the functional organization of the cortex of the postcentral gyrus of the monkey: a correlation of findings obtained in a single unit analysis with cytoarchitecture. *Bulletin of the Johns Hopkins Hospital* 105:133–62.

Riehle A, Grün S, Diesmann M, Aertsen A (1997) Spike synchronization and rate modulation differentially involved in motor cortical function. *Science* 278:1950–1953.

Rihs TA, Michel CM, Thut G (2007) Mechanisms of selective inhibition in visual spatial attention are indexed by alpha-band eeg synchronization. *Eur J Neurosci* 25:603–10.

Rihs TA, Michel CM, Thut G (2009) A bias for posterior alpha-band power suppression versus enhancement during shifting versus maintenance of spatial attention. *Neuroimage* 44:190–9.

Rockland KS (1998) Complex microstructures of sensory cortical connections. *Curr Opin Neurobiol* 8:545–51.

Rockland KS, Lund JS (1983) Intrinsic laminar lattice connections in primate visual cortex. *J Comp Neurol* 216:303–18.

Rockland KS, Pandya DN (1979) Laminar origins and terminations of cortical connections of the occipital lobe in the rhesus monkey. *Brain Res* 179:3–20.

Rodriguez E, George N, Lachaux JP, Martinerie J, Renault B, Varela FJ (1999) Perception's shadow: long-distance synchronization of human brain activity. *Nature* 397:430–3.

Roelfsema PR, Engel AK, König P, Singer W (1997) Visuomotor integration is associated with zero time-lag synchronization among cortical areas. *Nature* 385:157–61.

Roelfsema PR, Lamme VA, Spekreijse H (1998) Object-based attention in the primary visual cortex of the macaque monkey. *Nature* 395:376–381.

Roelfsema PR, Lamme VA, Spekreijse H (2000) The implementation of visual routines. *Vision Res* 40:1385–411.

Salami M, Itami C, Tsumoto T, Kimura F (2003) Change of conduction velocity by regional myelination yields constant latency irrespective of distance between thalamus and cortex. *Proc Natl Acad Sci USA* 100:6174–9.

Salazar RF, Knig P, Kayser C (2004) Directed interactions between visual areas and their role in processing image structure and expectancy. *Eur J Neurosci* 20:1391–1401.

Salmelin R, Hari R (1994) Spatiotemporal characteristics of sensorimotor neuromagnetic rhythms related to thumb movement. *Neuroscience* 60:537–50.

Sanes JN, Donoghue JP (1993) Oscillations in local field potentials of the primate motor cortex during voluntary movement. *Proc Natl Acad Sci USA* 90:4470–4.

Sauseng P, Klimesch W, Stadler W, Schabus M, Doppelmayr M, Hanslmayr S, Gruber WR, Birbaumer N (2005) A shift of visual spatial attention is selectively associated with human eeg alpha activity. *Eur J Neurosci* 22:2917–26.

Schoffelen JM, Oostenveld R, Fries P (2005) Neuronal coherence as a mechanism of effective corticospinal interaction. *Science* 308:111–3.

Schöner G, Kelso JA (1988) Dynamic pattern generation in behavioral and neural systems. *Science* 239:1513–20.

Senkowski D, Molholm S, Gomez-Ramirez M, Foxe JJ (2006) Oscillatory beta activity predicts response speed during a multisensory audiovisual reaction time task: a high-density electrical mapping study. *Cereb Cortex* 16:1556–65.

Shah AS, Bressler SL, Knuth KH, Ding M, Mehta AD, Ulbert I, Schroeder CE (2004) Neural dynamics and the fundamental mechanisms of event-related brain potentials. *Cereb Cortex* 14:476–83.

Siegel M, Krding KP, Knig P (2000) Integrating top-down and bottom-up sensory processing by somato-dendritic interactions. *J Comput Neurosci* 8:161–173.

Singer W (1993) Synchronization of cortical activity and its putative role in information processing and . . . . *Annual Review of Physiology* .

Singer W (1994) Coherence as an organizing principle of cortical functions. *Int Rev Neurobiol* 37:153–83; discussion 203–7.

Singer W (1999) Neuronal synchrony: a versatile code for the definition of relations? *Neuron* 24:49–65, 111–25.

Singer W, Engel A, Kreiter A, Munk M (1997) Neuronal assemblies: necessity, signature and detectability. *Trends Cogn Sci (Regul Ed)* .

Singer W, Gray CM (1995) Visual feature integration and the temporal correlation hypothesis. *Annu Rev Neurosci* 18:555–86.

Speckman E, Elger CE (1999) Neurophysiological basis of the EEG and of DC potentials In Niedermeyer E, Silva FLD, editors, *Electroencephalography : basic principles, clinical applications, and related fields*. Williams & Wilkins, Baltimore, 4th ed. edition.

Sporns O, Kötter R (2004) Motifs in brain networks. *PLoS Biol* 2:e369.

Spratling MW (2002) Cortical region interactions and the functional role of apical dendrites. *Behavioral and cognitive neuroscience reviews* 1:219–28.

Spratling MW, Johnson MH (2004) A feedback model of visual attention. *Journal of cognitive neuroscience* 16:219–37.

Steinmetz PN, Roy A, Fitzgerald PJ, Hsiao SS, Johnson KO, Niebur E (2000) Attention modulates synchronized neuronal firing in primate somatosensory cortex. *Nature* 404:187–190.

Steriade M (1999) Coherent oscillations and short-term plasticity in corticothalamic networks. *Trends Neurosci* 22:337–45.

Tallon-Baudry C, Kreiter A, Bertrand O (1999) Sustained and transient oscillatory responses in the gamma and beta bands in a visual short-term memory task in humans. *Vis Neurosci* 16:449–59.

Tallon-Baudry C (2003) Oscillatory synchrony and human visual cognition. *J Physiol Paris* 97:355–63.

Tononi G, Sporns O, Edelman GM (1992) Reentry and the problem of integrating multiple cortical areas: simulation of dynamic integration in the visual system. *Cereb Cortex* 2:310–35.

Treisman AM, Gelade G (1980) A feature-integration theory of attention. *Cognitive psychology* 12:97–136.

Truccolo WA, Ding M, Knuth KH, Nakamura R, Bressler SL (2002) Trial-to-trial variability of cortical evoked responses: implications for the analysis of functional connectivity. *Clin Neurophysiol* 113:206–226.

Ts'o DY, Gilbert CD, WIESEL TN (1986) Relationships between horizontal interactions and functional architecture in cat striate cortex as revealed by cross-correlation analysis. *J Neurosci* 6:1160–70.

Tsodyks MV, Markram H (1997) The neural code between neocortical pyramidal neurons depends on neurotransmitter release probability. *Proc Natl Acad Sci USA* 94:719–23.

Ullman S (1995) Sequence seeking and counter streams: a computational model for bidirectional information flow in the visual cortex. *Cereb Cortex* 5:1–11.

van Dijk H, Schoffelen JM, Oostenveld R, Jensen O (2008) Prestimulus oscillatory activity in the alpha band predicts visual discrimination ability. *J Neurosci* 28:1816–1823.

Van Essen DC, Felleman DJ (1996) On hierarchies:: Response to hilgetag et al. *Science* 271:777a.

van Wijk BCM, Daffertshofer A, Roach N, Praamstra P (2009) A role of beta oscillatory synchrony in biasing response competition? *Cereb Cortex* 19:1294–302.

Varela F, Thompson E, Rosch E (1993) The embodied mind: Cognitive science and human experience. *MIT* .

von der Malsburg C (1981) The correlation theory of brain function. *MPI Biophysical Chemistry, Internal Report 81–2* .

von der Malsburg C, Schneider W (1986) A neural cocktail-party processor. *Biological Cybernetics* 54:29–40.

von Stein A, Chiang C, Knig P (2000) Top-down processing mediated by interareal synchronization. *Proc Natl Acad Sci U S A* 97:14748–14753.

von Stein A, Rappelsberger P, Sarnthein J, Petsche H (1999) Synchronization between temporal and parietal cortex during multimodal object processing in man. *Cereb Cortex* 9:137–50.

von Stein A, Sarnthein J (2000) Different frequencies for different scales of cortical integration: from local gamma to long range alpha/theta synchronization. *International journal of psychophysiology : official journal of the International Organization of Psychophysiology* 38:301–13.

Wehr M, Laurent G (1996) Odour encoding by temporal sequences of firing in oscillating neural assemblies. *Nature* 384:162–6.

Weisstein EW (2009) Hazard function. *From MathWorld–A Wolfram Web Resource* .

Wernicke C (1874) *The aphasic Symptom-complex* Franck and Weigert: Breslau.

Whittington MA, Traub RD, Faulkner HJ, Stanford IM, Jefferys JG (1997) Recurrent excitatory postsynaptic potentials induced by synchronized fast cortical oscillations. *Proc Natl Acad Sci USA* 94:12198–203.

Wiener N (1956) The theory of prediciton In Beckenbach EF, editor, *Modern Mathematics for Engineers*, Vol. 1. McGraw-Hill.

Woody C (1967) Characterization of an adaptive filter for the analysis of variable latency neuroelectric signals. *Medical and Biological Engineering and Computing* .

Worden MS, Foxe JJ, Wang N, Simpson GV (2000) Anticipatory biasing of visuospatial attention indexed by retinotopically specific alpha-band electroencephalography increases over occipital cortex. *J Neurosci* 20:RC63.

Wróbel A (2000) Beta activity: a carrier for visual attention. *Acta neurobiologiae experimentalis* 60:247–60.

Wróbel A, Bekisz M, Kublik E, Waleszczyk W (1994) 20 hz bursting beta activity in the cortico-thalamic system of visually attending cats. *Acta neurobiologiae experimentalis* 54:95–107.

Wyart V, Tallon-Baudry C (2009) How ongoing fluctuations in human visual cortex predict perceptual awareness: baseline shift versus decision bias. *J Neurosci* 29:8715–25.

Yuval-Greenberg S, Tomer O, Keren AS, Nelken I, Deouell LY (2008) Transient induced gamma-band response in eeg as a manifestation of miniature saccades. *Neuron* 58:429–41.

Zhang Y, Chen Y, Bressler SL, Ding M (2008) Response preparation and inhibition: the role of the cortical sensorimotor beta rhythm. *Neuroscience* 156:238–46.

Zipser K, Lamme VA, Schiller PH (1996) Contextual modulation in primary visual cortex. *J Neurosci* 16:7376–7389.